Structural Performance of Mass Timber Panel-Concrete (MTPC) Composite Floor System with Inclined Self-Tapping Screws and an Insulation Layer

by

Md Abdul Hamid Mirdad

A thesis submitted in partial fulfillment of the requirements for the degree of

Doctor of Philosophy

in

Structural Engineering

Department of Civil and Environmental Engineering

University of Alberta

Abstract

Mass Timber Panels (MTP) are a new generation of engineered wood panels that are available in large plane dimensions to facilitate fast floor construction with the obvious environmental benefit of being from a renewable material. In floor construction, concrete slab or topping is often applied over the MTP panels to improve various performance attributes, including structural, acoustic and vibration serviceability. Mass Timber Panel-Concrete (MTPC) composite floor system often consists of a Mass Timber Panel (MTP) connected to the concrete layer with mechanical connectors such as Self-Tapping Screw (STS) and a sound insulation layer in between the MTP and concrete. Lack of design standards and guidelines are the most important barrier limiting wide spread use of this MTPC composite floor system.

The capacity of this type of composite system mostly depends on the strength of the interlayer connection. Also, allowable floor span is often governed by serviceability performance requirements, such as deflection and vibration, which are directly dependent on the stiffness of the interlayer connection. Usually, connection tests are performed to characterize connection strength and stiffness required for structural design. In this research, three types of MTPs with normal weight concrete, three insulation thicknesses, two screw embedment lengths and two screw angles were tested to characterize connection strength and stiffness. Test results showed that connections with screws at an insertion angle of 30° had a larger strength and stiffness than connections with screws inserted at a 45° angle. Stiffness appears to be more sensitive to the presence of an insulation layer compared to strength. Overall, 5-15% and 22-34% reduction of strength and 35-50% and 55-65% reduction of serviceability stiffness were noticed for an insulation thickness of 5 mm and 15 mm, respectively. In lieu of testing, analytical models can be developed to directly calculate connection strength and stiffness based on component properties. To that end, two analytical models each were developed for solid and layered timber, for directly predicting the stiffness and strength of a connection with inclined screws and an insulation layer. Usually, connection properties of laterally loaded connection is controlled by the dowel bearing effect of the fastener in timber, but inclined screw connection has a more complex behaviour due to the combined bearing and withdrawal action of the screw. Therefore, in the developed models, both the bearing and withdrawal actions of the screw are considered. The connection stiffness and strength model were validated with the

connection tests with wide range of parameters. It was found that the strength models are capable of predicting the mode of failure of a connection and the load-carrying capacity within 10% of the experimental value, while, the stiffness models are capable of predicting the stiffness of connection to within 18% of the experimental value.

The commonly used Gamma method to design a timber-concrete composite floor has limitations and cannot predict the load-carrying capacity, bending stiffness and failure modes of the composite floor system when there are widely spaced discrete connectors. Therefore, an analytical model has been developed considering the interlayer connector behaviour under the elastic-plastic range along with an acoustic layer between timber and concrete, to predict the capacity, bending stiffness, failure modes and load-deflection response of MTPC composite floor system. One-way acting composite floor panels were also tested under four-point bending with different configurations to investigate the influence of different parameters and to validate the developed system prediction model. It was found that the model is capable of predicting the capacity of the MTPC composite system within the range of -6% to +26%, bending stiffness within the range of -15% to +10% of the bending test values and the associated failure mode. The Gamma method cannot predict the system capacity, and it tended to over-estimate the bending stiffness on average by 43% and was found not appropriate for MTPC composite system with discrete shear connectors and MTP. This developed connection and system models for MTPC composite floors will facilitate the use of such a system in mass timber construction.

Preface

This thesis is the original work of Md Abdul Hamid Mirdad, executed under the supervision of Professor Dr. Ying Hei Chui. The identification and design of the research program was performed independently with direct supervision of Dr. Chui. Five journal papers and four conference papers related to this thesis have been published or submitted and are listed below. This thesis is organized in paper format by following the paper-based thesis guidelines and including only the journal papers.

Journal Papers:

1. **Mirdad, M. A. H.** and Chui, Y. H. (2019) "Load-slip performance of Mass Timber Panel-Concrete (MTPC) composite connection with self-tapping screws and insulation layer." Construction and Building Materials 213: 696-708 [https://doi.org/10.1016/j.conbuildmat.2019.04.117]
2. **Mirdad, M. A. H.** and Chui, Y. H. (2020) "Strength prediction of Mass Timber Panel-Concrete composite connection with inclined screws and a gap." ASCE Journal of Structural Engineering [https://doi.org/10.1061/(ASCE)ST.1943-541X.0002678]
3. **Mirdad, M. A. H.** and Chui, Y. H. (2020) "Stiffness prediction of Mass Timber Panel-Concrete composite connection with inclined screws and a gap." Engineering Structures 207: 110215 [https://doi.org/10.1016/j.engstruct.2020.110215]
4. **Mirdad, M. A. H.**, Chui, Y. H. and Tomlinson, D. " Capacity and failure mode prediction of Mass Timber Panel-Concrete composite floor system with mechanical connectors." [Submitted to a journal and under review]
5. **Mirdad, M. A. H.**, Chui, Y. H., Tomlinson, D. and Chen, Y. " Bending stiffness and load-deflection response prediction of Mass Timber Panel-Concrete Composite floor system with mechanical connectors." [Submitted to a journal and under review]

Conference Papers:

1. **Mirdad, M. A. H.** and Chui, Y. H. (2018). “Behaviour of Mass Timber Panel-Concrete connections with inclined self-tapping screws and insulation layer.” Proceedings of World Conference on Timber Engineering (WCTE), Seoul, Republic of Korea

2. Moar, F., Vanzo, S., **Mirdad, M. A. H.**, Chui, Y. H. and Steige, Y. (2019) "Influence of self-tapping screw inclination and soundproofing resilient interlayer on timber-concrete composite slab." Proceedings of 5th International Conference on Structural Health Assessment of Timber Structures (SHATiS), Guimaraes, Portugal
3. **Mirdad, M. A. H.** and Chui, Y. H. “Mass Timber Panel-Concrete composite floor behaviour with inclined self-tapping screws and insulation layer.” World Conference on Timber Engineering (WCTE) 2021, Santiago, Chile [Accepted]
4. **Mirdad, M. A. H.** and Chui, Y. H. “Development of span tables for Mass Timber Panel-Concrete composite floors.” World Conference on Timber Engineering (WCTE) 2021, Santiago, Chile [Accepted]

Acknowledgements

My heartfelt thanks to my supervisor *Professor Dr. Ying Hei Chui* for his continuous guidance and support throughout my doctoral research. *Dr. Chui* has been generous of his time in providing me with constructive feedback all the way. I also want to thank *Dr. Douglas Tomlinson* and *Dr. Yuxiang Chen* for providing constructive feedback in my research as a supervisory committee member. I am also grateful to *Dr. Samer Adeeb* for his assistance during the connection model development.

I would like to thank the Natural Sciences and Engineering Research Council of Canada (NSERC) for the financial support of this study under the Industrial Research Chair Program. Financial support was also provided by Landmark Group of Companies, FPInnovations, Canadian Wood Council, MTC Solutions, Rotho Blaas, Western Archrib, Pinkwood Ltd and Alberta Innovates. In addition, Nordic Structures, Rotho Blaas and Western Archrib provided test materials for the test program. Their contributions are gratefully acknowledged. I am also thankful to the technician *Greg Miller* and *Cameron West* of I. F. Morrison Structural Engineering Laboratory for their assistant during the test programs.

I am entirely grateful to my late mother *Farida Akter* for her inspiration from my childhood to reach at this stage and my father *Md Musa Mirdad* for his support throughout my life. I am grateful to my wife, *Samira Fairuz*, for her encouragement, and patience in this journey of becoming a doctorate.

Most of all, I am thankful to almighty *Allah*, whose grandeur and creative design are full of awe and wonder.

Table of Contents

List of Tables

List of Figures

Chapter 1. Introduction

1.1 Mass Timber Panel-Concrete Composite System

Timber construction has gained attention over the last two decades due to global interest in reducing green house gas (GHG) emissions in construction on one hand, and on the other hand due to the evolution of the building codes, the emergence of new engineered wood products, tools, and mechanical fasteners, which broaden the range of timber construction possibilities. The construction of modern multi-storey timber structure is therefore rapidly increasing and Timber Concrete Composite (TCC) floor is a preferred choice now-a-days by designers due to its higher strength and stiffness to weight ratio, larger span to total depth ratio, higher in-plane rigidity, better acoustics, damping, thermal and fire performances along with the possibility of pre-manufacturing (Ceccotti, 2002) (Yeoh, et al., 2011) (Dias, 2005) (Frangi & Fontana, 2003). TCC is a structural technique in which timber beam or deck/panel is connected to a reinforced concrete slab with mechanical fasteners as connectors where the timber primarily resists tensile stress while the concrete slab resists compressive stress generated by out-of-plane bending action.

In modern timber construction, mass timber construction is a great prospect where traditional or contemporary engineered wood products are used as the primary structural members. Mass timber construction is approximately 25 % faster than similar on-site concrete construction. It also requires 90 % less construction traffic and 75 % fewer workers which yields a much quieter job site (Kremor & Symmons, 2015). Nowadays, using timber deck/panel instead of a timber beam is getting popular because of the high demand for building mid- to high-rise timber structure. This timber deck/panel is known as Mass Timber Panel (MTP). MTP is a construction form typically characterized by the use of large solid wood panels for a wall, floor, and roof construction. Because of its strength and dimensional stability, mass timber offers a low-carbon alternative to steel, concrete, and masonry for many applications (Think Wood, 2019). Some popular MTP are Cross Laminated Timber (CLT), Nail Laminated Timber (NLT), Glue Laminated Timber (GLT) and Dowel laminated Timber (DLT). Using Mass Timber Panel instead of a timber beam in TCC yields a longer span which also reduces the floor height, because the panel with concrete will support the floor load without any beams. Usually, MTP acts in one-way

direction but if these panels are connected together side by side with proper connection, they will act as a two-way plate.

The Mass Timber Panel-Concrete (MTPC) composite system considered in this paper consists of a Mass Timber Panel (MTP) connected to a reinforced concrete slab by mechanical fasteners. In floors under out-of-plane bending situations, the MTP primarily resist tensile stress while the concrete slab resists compressive stress. An insulation layer is commonly sandwiched between the timber panel and concrete slab which provides better acoustic and thermal performance. The mechanical connectors such as Self-Tapping Screw (STS) which penetrate all three components, allow for partial shear transfer and therefore partial composite behaviour between the components. The structural efficiency of this composite system mostly depends on the performance of this interlayer connection and by avoiding failures in the connections, it is possible to maximize the load-carrying capacity and increase the effective bending stiffness of the composite system. *Figure 1.1* illustrates a MTPC composite floor system with its components.

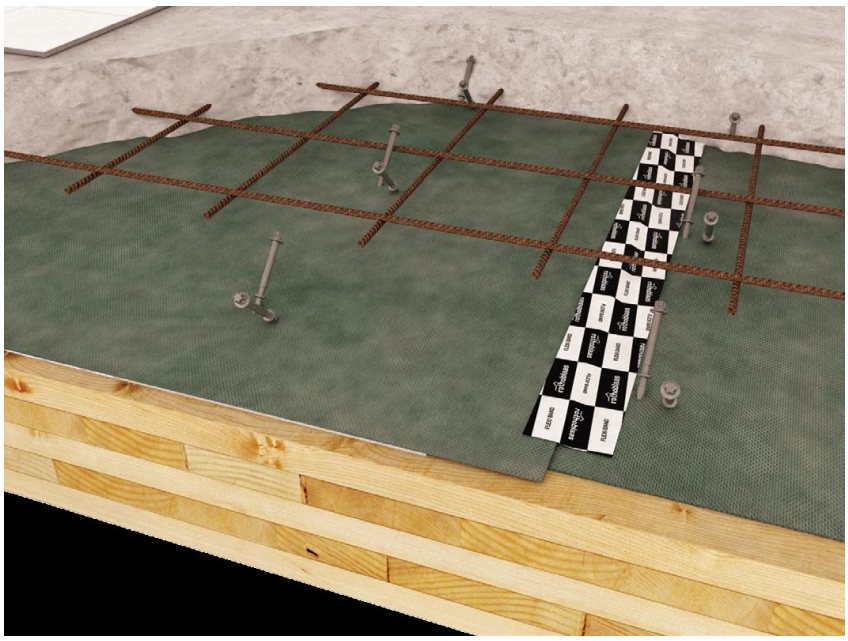

Figure 1.1 : Mass Timber Panel Concrete (MTPC) composite floor system (RothoBlaas, 2019a)

In the modern timber structures either for the residential or commercial purpose, acoustic comfort is really important as one of the major serviceability limit state requirements and therefore, an insulation layer is required in between timber panel and concrete layer. The purpose of the insulation is to absorb the noise

and vibration induced by foot traffic from the upper level of the floor and give acoustic comfort to the residence beneath the floor. The insulation layer may also act as a thermal barrier where the hydronic heating system is concealed in the concrete slab. But, the presence of this interlayer might have a negative impact on the mechanical performance of connections namely ultimate load and slip modulus as this interlayer acts as a gap in between timber and concrete surface. The influence of an insulation layer in this composite floor system was not well investigated before, especially in MTP floor system.

1.2 Connection Design

Screws, bolts and dowels are examples of dowel-type fasteners, with their lateral strengths mostly governed by the dowel-bearing or embedment strength of timber elements and the yield moment of the fastener and may be calculated based on Johansen's yield theory. According to Johansen (Johansen, 1949), the strength of a connection containing dowel-type fasteners is dependent on the fastener resistance to bending (yield moment) and the resistance of the wood to crushing (dowel-bearing or embedment). Self-Tapping Screw (STS) are widely used modern timber connectors which were developed as an improved threaded fastener for the application in large-scale timber structures. This type of screw mostly features a continuous thread over the whole length (fully-thread) which leads to a more uniform load transfer between the screw and the wood material under axial or withdrawal action (Dietsch & Brandner, 2015). In addition many experimental and numerical studies (Tomasi, et al., 2010) (Bejtka & Blass, 2001) (Kevarinmäki, 2002) (Bejtka & Blass, 2002) (Blass, et al., 2006) (Closen, 2012) (Jockwer, et al., 2014) have concluded that there is a substantial increase in the strength and stiffness of a STS connection if the screw is installed at an angle (e.g., 45° or 30°) to the surface of the wood member, instead of normal (90°) to the surface. In the application of timber concrete composite, fully threaded screw with wide countersank head is beneficial as full thread gives better load transfer in timber and better bonding with concrete, while the countersank head gives pullout resistance in concrete. Also, this screw is specially made for structural application as full thread provides resistance proportional to the entire thread length. This screw provides limited slip and higher rigidity. In the application of axial direction and cross-pairs, this fully thread screw is more suitable compared to partially threaded screw for full shear transfer.

Joints fabricated with inclined screws have a more complex behaviour because, the load transfer mechanism involves not only the bending of the screw and the embedment of the wood but also the withdrawal resistance of the fasteners as well as the friction between the elements. In an inclined position, the screw is subjected to a combined axial and lateral loading condition. According to Eurocode 5 (EN 1995-1-1, 2009), a quadratic combination of the axial and lateral loading ratios can be used to predict the capacity of a connection with fasteners at an inclined position. However, the EC5 method underestimates the strength of the modern screw type connection (e.g., self-tapping screw). On the other hand, according to Eurocode 5 (EN 1995-1-1, 2009), the slip modulus or connection stiffness of a laterally loaded single screw can be calculated based on timber properties such as density and fastener diameter. Similar to strength, EC5 method also underestimate the stiffness of a connection with inclined screws by a large margin due to the lack of consideration of contribution from the withdrawal action. Therefore, in order to characterize the strength and stiffness of the fasteners, often tests are performed according to standardized procedure such as EN 26891:1991 (EN 26891, 1991). In addition to testing, the properties of self-tapping screw connection can be estimated using mechanics-based model that accounts for component properties such as lateral (embedment) and withdrawal action of the screw and other factors such as friction.

The strength model of inclined screws in timber-to-timber joints has been addressed by a few researchers (Tomasi, et al., 2010) (Kevarinmäki, 2002) (Bejtka & Blass, 2002) and strength model of inclined screws in concrete-to-timber joints extending Johansen's yield theory has been addressed by others (Kavaliauskas, et al., 2007) (Marchi, et al., 2017) (Symons, et al., 2010). So far, no analytical model has been presented for concrete-to-timber joints that consider inclined screws, insulation layer gap and layered structure of the timber member. Besides, stiffness modeling of inclined screws in timber-to-timber joints has been addressed by a few researchers (Tomasi, et al., 2010) (Blass, et al., 2006) (Kevarinmäki, 2002) (Girhammar, et al., 2017) and of inclined screws in concrete-to-timber joints by others (Marchi, et al., 2017) (Symons, et al., 2010) (Moshiri, et al., 2014). So far, no analytical model has been presented for concrete-to-timber joints that consider inclined screws, insulation layer gap and layered structure of the timber member. These factors necessitate the simultaneous consideration of the timber bearing, withdrawal and flexural rigidity of the screw.

1.3 System Design

Serviceability performance requirements such as deflection and vibration often govern the allowable span for this type of MTPC composite floor system. Therefore, system effective bending stiffness is an important property in structural design. Due to the semi-rigid nature of the mechanical behaviour of the shear connector, a relative slip occurs between the bottom fibre of concrete and the top fibre of timber under shear transfer which violates the Euler-Bernoulli assumption of plane section remain plane. Therefore, the method of the transformed section from the conventional principle of structural analysis for determining composite bending stiffness and stress distribution widely used for steel-concrete cannot be used in design.

The majority of timber design standards around the world do not address the design of this type of MTPC composite floor system, with the exception of Eurocode 5 (EN 1995-1-1, 2009) where the so-called Gamma method (Ceccotti, 2002) is adopted. Gamma method can only predict elastic bending stiffness more accurately for stiff notched timber, mechanical and glued connections but, inappropriate in the case of flexible connectors (COST, 2018). Also, the Gamma method cannot be applied to predict the ultimate load-carrying capacity and complete load-deflection response due to onset of inherent elasto-plastic behaviour of the interlayer connection even at relatively low load levels.

The frozen shear force model by Van der Linden (Van der Linden, 1999) partially considers the ductility of the connection by modifying the Gamma method with the assumption of an elastic-plastic load-slip relationship for the connection. Once the applied load approaches the elastic limit load, the connectors close to the supports with the highest load yield first and at this point, the model assumes the entire system has yielded. This approach overestimates the load-carrying capacity of composite system significantly, because all the interior connectors still remain elastic at the point of first yield (Zhang, 2013). On the other hand, the model by Frangi and Fontana (Frangi & Fontana, 2003) was based on a rigid perfectly plastic load-slip relationship for all connectors by neglecting the connector stiffness. As most types of connectors are not inherently stiff, assuming a rigid behavior of the connection in the elastic state also overestimates the structural performance of the composite system at service and ultimate load level. A nonlinear model for timber-concrete composite beam was developed directly from the mechanical

properties of the members and laterally loaded dowels by Cuerrier-Auclair (Cuerrier-Auclair, et al., 2016) by extending the Winkler model of a beam on an elastic foundation and composite beam theory. In that model, there are different levels of calculation to generate the load-deflection responses of composite beams directly from the material properties of the components. Initially, the moment-curvature relationship is drawn from the dowel's uniaxial stress-strain relationship. Then the shear force-slip relationship is drawn for the dowel considering the properties of concrete and timber from moment-curvature relation. Therefore, the structural load-deflection response of the composite beam can be drawn but, this method is complicated for general use and limited to only laterally loaded dowel's inserted at 90° angle.

To better predict the capacity, effective bending stiffness and plot load-deflection response, Zhang (Zhang, 2013) developed a model for timber-concrete composite beam considering linear-elastic perfectly plastic load-slip relationship of the connection based on progressive yielding under increasingly applied load. Zhang's model (Zhang, 2013) was developed for timber beam and concrete slab type composite where, soft insulation layer was not considered. Therefore, a model extending Zhang's model (Zhang, 2013) can be developed to consider the soft sandwich insulation layer and to better predict the expected failure modes, capacity and effective bending stiffness of MTPC composite floor system.

1.4 Research Needs

As massive timber structures are getting more popular all over the world, MTPC composite floor system is under serious consideration. Research on MTPC composite is going on all over the world especially in Europe and North America, but lack of design standard and guidelines is the main barrier to widespread use of this system in North America. Also, without insulation, this composite cannot be a complete system for widespread use in the residential and commercial application. No such research has been performed so far considering insulation in the MTPC system. Insulation will have a major influence on the design of connection as well as a whole composite system as this interlayer insulation will behave like a gap which might reduce the stiffness and strength of the system significantly. As an innovative product, Self-Tapping Screw (STS) has a growing popularity in timber construction because of its high yield strength and withdrawal strength in wood. Due to its high withdrawal strength, self-tapping screws are often used in an inclined orientation relative to the surface of the jointing member in a laterally loaded connection. The

behavior of concrete-timber connection containing self-tapping screws inserted in an inclined orientation and an insulation layer between the components is an important and timely research area, as designers seek to use timber floor systems that are capable of spanning a long distance. Once the behaviour of this connection is well understood, then the development of the design method for MTPC composite floor systems can be achieved.

1.5 Research Objectives and Scope

From the literature review, it is clear that the design of timber-concrete composite structure must satisfy for both ultimate (ULS) and serviceability limit state (SLS) in short and long-term. Although long-term behavior such as creep, mechano-sorptive creep, shrinkage/swelling, and thermal strain may occur in the extended service period of the composite system, it is beyond the scope of this research. Fire and vibration performance is another important aspect of a timber-concrete composite system which is also beyond the scope. Here the focus will be on the short-term structural performance of the connections and composite system under one-way behaviour. Therefore, the main objective of this research is to:

1) Evaluate the influence of connection and insulation on the structural behavior of the MTPC composite floor system.
2) Develop and validate analytical model to predict the strength of connection containing insulation layer and inclined screws.
3) Develop and validate analytical model to predict the stiffness of connection containing insulation layer and inclined screws.
4) Extend and validate analytical model to predict the capacity and failure modes of MTPC composite floor system containing insulation layer.
5) Extend and validate analytical model to predict the effective bending stiffness and load-deflection response of MTPC composite floor system containing insulation layer.

1.6 Thesis Outline

The research has been sub-divided into two parts such as, connection and system. In the connection part, analytical models for prediction strength and stiffness of connection in concrete-to-solid timber and concrete-to-layered timber were developed and validated with wide range of connection test data. In the

system part, extended analytical models for predicting capacity, bending stiffness and failure modes were developed and validated with bending test data. The thesis is organized into seven chapters with five journal articles in five chapters besides introduction and conclusion.

Chapter 1: Introduction – Provides the basic background knowledge of MTPC composite with the research needs, scopes and objectives.

Chapter 2: Connection Test – Presents, connection test results and discussions of 32 different configurations. This connection test results are used to validate the developed connection strength and stiffness prediction models in Chapter 3 and Chapter 4. This Chapter belongs to journal paper #1. Part of this chapter was presented in conference papers #1 and #2.

Chapter 3: Connection Strength Prediction Model – Presents, two analytical model for predicting strength of connection into solid and layered timber, and validation with the connection test results from Chapter 2. This Chapter belongs to journal paper #2.

Chapter 4: Connection Stiffness Prediction Model – Presents, two analytical model for predicting stiffness of connection into solid and layered timber, and validation with the connection test results from Chapter 2. This Chapter belongs to journal paper #3.

Chapter 5: System Capacity and Failure Mode Prediction Model – Presents, extended analytical model for predicting system capacity and failure modes of MTPC composite, and validation with the bending test results. The input parameters of the connection in the model are based on Chapter 3 and Chapter 4. This Chapter belongs to journal paper #4. Part of this chapter was presented in conference papers #3 and #4.

Chapter 6: System Bending Stiffness and Load-Deflection Prediction Model – Presents, extended analytical model for predicting system effective bending stiffness and load-deflection response of MTPC composite, and validation with the bending test results. The input parameters of the connection in the model are based on Chapter 3 and Chapter 4. This Chapter belongs to journal paper #5. Part of this chapter was presented in conference papers #3 and #4.

Chapter 7: Conclusion – Summarizes the key results observed from preceding chapters with research contributions and future recommendations.

Chapter 2. Connection Test

Journal Paper #1

Load-Slip Performance of Mass Timber Panel-Concrete (MTPC) Composite Connection with Self-Tapping Screws and Insulation Layer

by Md Abdul Hamid Mirdad and Ying Hei Chui

Published in Construction and Building Materials, 2019

Abstract:

The Mass Timber Panel-Concrete (MTPC) composite floor systems are often encountered in mass timber buildings. Such a floor system consists of a Mass Timber Panel (MTP) connected to a reinforced concrete slab with Self-Tapping Screw (STS) connector and a sound insulation layer in between. In this study three types of MTPs with normal weight concrete, three insulation thicknesses, two screw embedment lengths and two screw angles were tested to characterize connection stiffness and strength. The main goal of this connection test program was to provide preliminary test data to assist in the development of an analytical model to predict connection lateral stiffness and strength considering the insulation layer in the MTPC system. Test results showed that connections with screws at an insertion angle of 30° had a larger stiffness and strength than connections with screws inserted at a 45° angle. Stiffness appears to be more sensitive to the presence of an insulation layer compared to strength. Overall, 35-50% and 55-65% reduction of serviceability stiffness, and 5-15% and 22-34% reduction of strength were noticed for an insulation thickness of 5 mm and 15 mm, respectively. Screws in Cross Laminated Timber (CLT) showed higher strength while screws in Glue Laminated Timber (GLT) showed higher stiffness, but the difference is insignificant in all three MTP products with different failure modes.

2.1 Introduction

The Mass Timber Panel-Concrete (MTPC) composite system considered in this paper consists of a Mass Timber Panel (MTP) connected to a reinforced concrete slab by mechanical fasteners. In floors under out-of-plane bending action, the MTP primarily resists tensile stress while the concrete slab resists compressive stress. An insulation layer is sandwiched between the timber panel and concrete slab which provides better acoustic and thermal performance. The mechanical fasteners, which penetrate all three components, allow for partial shear transfer and therefore partial composite behavior between the components. *Figure 2.1* illustrates the type of MTPC composite system considered in this study. The advantages of this MTPC composite system are high strength and stiffness to weight ratios, large span to total depth ratio, high in-plane rigidity, and better acoustics, damping, thermal, and fire performances (Yeoh, et al., 2011) (Ceccotti, 2002). This type of floor system is intended for mid-to-high rise building applications as well as long-span flooring construction. Since the structural performance of this type of composite floor system is influenced greatly by the connection properties, a connection test program was conducted first to evaluate the influence of component characteristics on stiffness and strength of the connections, which will aid the subsequent development of construction details and design approach for this type of floor system.

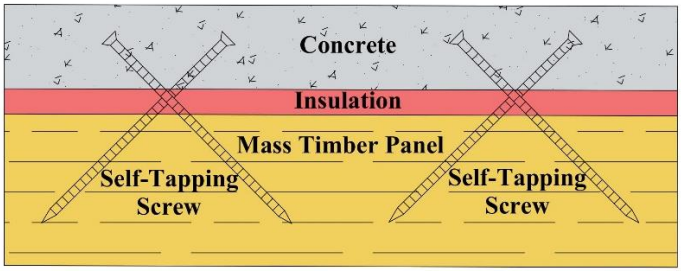

Figure 2.1: Typical Mass Timber Panel Concrete (MTPC) composite

2.2 Background

Timber construction has gained attention over the last two decades due to global interest in reducing green house gas (GHG) emissions in construction on one hand, and on the other hand due to the evolution of the building codes, the emergence of new engineered wood products, tools, and mechanical fasteners, which broaden the range of timber construction possibilities (Jacquier, 2015). The construction of modern multi-storey timber structure is therefore rapidly increasing, and Timber-Concrete Composite

(TCC) floor is often a preferred choice by designers due to its capacity to span longer distances, and provide good sound and fire performance, compared with using timber alone. TCC system has been investigated for nearly 80 years. After the two world wars, there was a shortage of steel for reinforcement in concrete, which initiated the development of TCC system in Europe in the use of rehabilitation and new flooring system (Yeoh, et al., 2011). TCC is a structural technique in which timber beam or deck/panel is connected to a reinforced concrete slab with mechanical fasteners as connectors where the timber primarily resists tensile stress while the concrete slab resists compressive stress generated by out-of-plane bending action.

In modern timber construction, mass timber construction is a great prospect where traditional or contemporary engineered wood products are used as the primary structural members. Mass timber construction is approximately 25 % faster than similar on-site concrete construction. It also requires 90 % less construction traffic and 75 % fewer workers which yields a much quieter job site (Kremor & Symmons, 2015). Nowadays, using timber deck/panel instead of a timber beam is getting popular because of the high demand for building mid- to high-rise timber structure. This timber deck/panel is known as Mass Timber Panel (MTP). MTP is a construction form typically characterized by the use of large solid wood panels for a wall, floor, and roof construction. Because of its strength and dimensional stability, mass timber offers a low-carbon alternative to steel, concrete, and masonry for many applications (Think Wood, 2019). Using Mass Timber Panel instead of a timber beam in TCC yields a longer span which also reduces the floor height, because the panel with concrete will support the floor load without any beams. Usually, MTP acts in one-way direction but if these panels are connected together side by side with proper connection, they will act as a two-way plate.

In modern timber structures either for the residential or commercial purposes, acoustic comfort is of major importance. To enhance acoustic performance of timber-concrete composite floor, an insulation layer is commonly inserted between timber and concrete layers. The purpose of the insulation is to absorb the noise induced by foot traffic from the upper level of the floor and give acoustic comfort to the occupants beneath the floor. The insulation layer may also be present to act as a thermal barrier where a hydronic heating system is concealed in the concrete slab, which keeps the floor warm.

The role of the mechanical fasteners (or shear connectors) in a composite structure is to transfer shearing forces between the different members, thereby providing a certain level of composite action. The structural efficiency of a TCC highly depends on the stiffness of this interlayer connection. The stiffer the connection, the higher the level of composite action and therefore, the lower the vertical deformation of the floor structure under transverse loading. The connection should ideally exhibit ductile behavior as both concrete and timber are essentially brittle materials (Deam, et al., 2008).

In order to characterize Timber-Concrete Composite (TCC) systems, tests are often performed on connection specimens. EN 26891:1991 (EN 26891, 1991) provides a standardized procedure for such a test where the load-displacement curve is produced to determine the strength and stiffness of the connection. Load-carrying capacity (strength), slip modulus (stiffness) and ultimate deformation capacity (ductility) are the most important mechanical properties of the connection. The load-slip modulus of the connection represents the relative displacement between the timber and concrete under an applied shear force. The ultimate deformation capacity of the connection would be that where the ultimate slip of the connection is not reached before the failure of the connection (Dias, et al., 2010) (Dias & Jorge, 2011) (Dias, et al., 2007). By avoiding failures in the connections in the timber-concrete composite system, it is possible to maximize the load-carrying capacity and increase the ultimate deformation capacity of the system.

The use of different concrete grades has a very limited influence on the behavior of the timber-concrete connection and therefore floor systems. Use of lightweight concrete instead of normal weight concrete reduces the dead load of the floor by up to 15%, and high strength concrete gives the option to reduce the thickness of the concrete slab (Dias, et al., 2007). Load-carrying capacity of the connection slightly increases with the increase of compressive strength of concrete but, normal weight concrete shows higher stiffness followed by lightweight concrete and high strength concrete (Dias, et al., 2010) (Marchi, et al., 2017). Overall, the best choice is to use normal weight concrete considering the cost, stiffness and strength. Also, it is well known that presence of interlayer decreases the mechanical performance of connections namely ultimate load and load-slip modulus, as this interlayer acts as a gap in between timber and concrete surface (Van der Linden, 1999) (Gelfi, et al., 2002). Van dar Linden (Van der Linden,

1999) reported a decrease of 30% in ultimate load-carrying capacity and 50% in the load-slip modulus for an axially loaded (45° angle) screw with a 19 mm thick particleboard interlayer compared to the same construction without an interlayer. His results matched with those from Timmermann (Timmerman & Meierhofer, 1993) who used a 20 mm interlayer while, Dias (Dias, et al., 2010) (Dias, et al., 2007) found a decrease of 35% in load-slip modulus and 8% in strength with a 20 mm thick particleboard interlayer for laterally loaded (90° angle) screws. The influence of an insulation layer in the composite floor system was not well investigated before, especially in MTP floor system. The main focus of this study was to evaluate the influence of this insulation and connection properties on the MTPC composite floor system.

2.3 Methodology

The connection test program presented in this paper was carried out at the I. F. Morrison Structural Engineering Laboratory of the University of Alberta in Canada. In total, 96 shear connection tests with 32 different configurations were performed.

2.3.1 Materials

2.3.1.1 Self-Tapping Screw

Self-tapping screws were developed as an improved threaded fastener and are now widely used in mass timber structures. These screws often feature a continuous thread over the whole length (fully-thread), which leads to a more uniform load transfer between the screw and the wood material as well as a considerably enhanced withdrawal resistance (Dietsch P., 2015). If these screws are inserted at an angle, usually at 30° to 45°, in a laterally loaded connection the high withdrawal strength and stiffness of the screws can lead to higher lateral strength and stiffness when compared to an insertion angle of 90°. Because of their self-drilling tip, no pre-drilling is required. However, at the application of temperature below zero degrees, pre-drilling may be required to prevent splitting of the timber, which becomes more brittle at these temperatures (Pirnbacher, et al., 2009). Fully threaded self-tapping screw (Rothoblaas, 2019b) of 11 mm diameter was used in this research, with a countersunk head and self-drilling tip, which is made of carbon steel and white galvanic zinc coating. The head diameter, nominal diameter and shank diameter are 19.3 mm, 11 mm and 7.7 mm respectively. Two lengths of 150 mm and 200 mm were used for achieving different embedment lengths into MTP. The modulus of elasticity of the screw was reported

to be 210 GPa (ETA-Danmark, 2016). In the application of timber concrete composite, fully threaded screw with wide countersank head is beneficial as full thread gives better load transfer in timber and better bonding with concrete, while the countersank head gives pullout resistance in concrete. Also, this screw is specially made for structural application as full thread provides resistance proportional to the entire thread length. This screw provides limited slip and higher rigidity. In the application of axial direction and cross-pairs, this fully thread screw is more suitable compared to partially threaded screw for full shear transfer.

Table 2.1: Mechanical properties of 11 mm diameter Self-Tapping Screw

Mechanical Properties	**Symbol, Unit**	**Characteristic** (Rothoblaas, 2019b)	**Measured**
Yield Moment	$M_{y,k}$, kN.mm	45.91	80.58
Tensile Strength	$f_{tens,k,}$ kN	38	42.85
Yield Strength	$f_{y,k,}$ N/mm^2	1000	1059.1

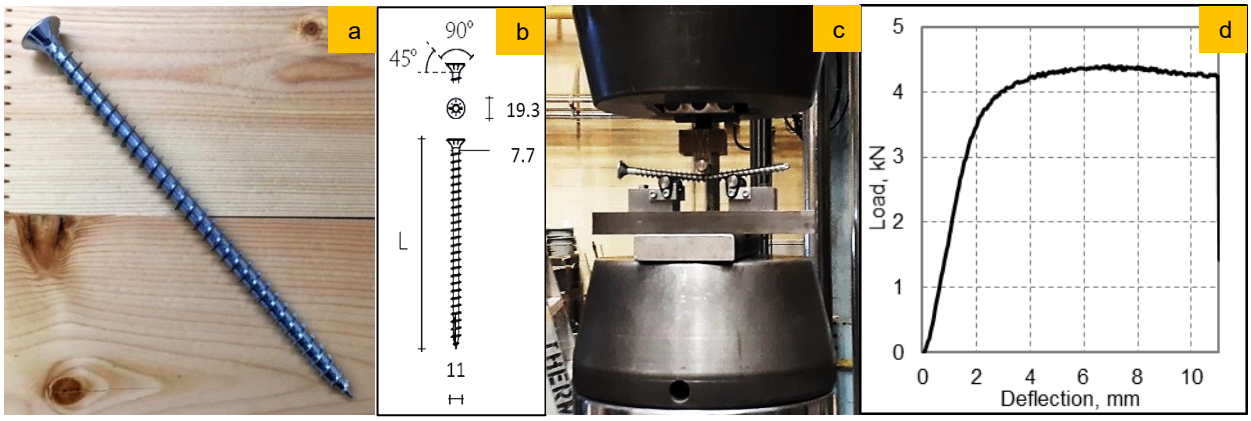

Figure 2.2: a) Fully threaded screw, b) geometry (Rothoblaas, 2019b) in mm, c) yield moment test, and d) load-deflection curve of yield moment test

The mechanical characteristic and measured properties of this 11 mm diameter self-tapping screw are shown in *Table 2.1*. The characteristic values were quoted from (Rothoblaas, 2019b) while the measured values were obtained by performing yield moment test in the laboratory according to ASTM F1575-17 (ASTM, 2017). In *Figure 2.2*, the self-tapping screw is shown along with its geometry and bending yield moment test set-up and a typical load-deflection response.

2.3.1.2 Mass Timber Panels

Three types of Mass Timber Panel (MTP), namely Cross Laminated Timber (CLT), Glue Laminated Timber (GLT) and Composite Laminated Panel (CLP) were used in the tests. CLT, a widely used mass timber panel consists of layers of dimension lumber oriented at a right angle to one another and face glued. Five-ply E1 grade CLT (Nordic Structures, 2019) with a 175 mm total thickness was used in this study, which has 1950f_b-1.7E Spruce-Pine-Fir (S-P-F) MSR lumber in longitudinal and No. 3/Stud S-P-F lumber in transverse layers. The unit weight of the panel is 89.9 kg/m^2. The reported density of the wood was 515 kg/m^3, and the measured average density of the test CLT was 504.4 kg/m^3. The average moisture content of the wood during the test was found to be 8.3%.

GLT is made of lumber glued in a parallel direction on the edge where, the grain of all laminations runs parallel to the length of the member. In this research, standard profile GLT (Western Archrib, 2019) was used which was 175 mm thick and made of # 2-grade S-P-F lumber. The reported density of the wood was 440 kg/m^3 and measured density was 454.8 kg/m^3 with an average moisture content of 8.3%.

CLP (Niederwestberg, et al., 2018) is a new type of mass timber panel made with lumber and Structural Composite Lumber (SCL) panels and is under development. It can be produced with various lay-ups with alternating layer orientation or all layers being parallel to each other. In the present study, 5-layer CLP panels of 185 mm thickness with #2 grade S-P-F lumber in the outer layers and laminated strand lumber (LSL) in the inner layer was used. Both component products were oriented with their major strength axis in the direction along the length of the member. CLP has improved rolling shear and stiffness over CLT. The measured density of S-P-F lumber and LSL was 470 kg/m^3 and 644 kg/m^3 with a moisture content of 7.4% and 3.4% respectively.

2.3.1.3 Acoustic material

The acoustic material (RothoBlaas, 2019a) used in this study was a sound-proofing layer made of polyester felt and elasto-plastomer bitumen, designed as an acoustic insulating material for absorbing noise and vibrations resulting from foot traffic. The acoustic material creates an elastic separation between stiff elements, slabs and walls, dampening vibrations due to foot traffic, and to the various sound

sources in the rooms. This material is 5 mm thick which has the dynamic stiffness of 7 MN/m^3 and can absorb vibrations from impact noise up to 26 dB (RothoBlaas, 2019a).

2.3.1.4 Concrete

Normal weight concrete of 75 mm thickness with 19 mm aggregate size was used. Laboratory tests on cylinder specimens prepared from the same concrete batch revealed that it has an average compressive strength of 39 MPa after 28 days with a modulus of elasticity of 29.4 GPa, and a density of 2345 kg/m^3. Stucco steel wire mesh was used to limit crack propagation in concrete in order to maintain the integrity of the connection.

2.3.2 Test Setup

The MTP elements had a length of 400 mm and a width of 200 mm. Normal weight concrete of 75 mm thickness was used. Insulation thicknesses studied were 0 mm (no insulation), 5 mm (1 layer) and 15 mm (3 layers). Plastic separation sheets were placed between the concrete and timber surface when there was no insulation to remove any bond at the interface, which increases the load-slip modulus at low load levels (Lukaszewka, 2009). The symmetric test setup with single shear plane was selected since, the asymmetrical shear test setup leads to a slight overestimation of the shear strength and load-slip modulus (Van der Linden, 1999). Among the different setups, it seems that concrete-timber-concrete specimens provide more representative results than timber-concrete-timber setup. In the case of timber-concrete-timber, the concrete member at the center is stressed under the directly applied load leading to an increased probability of premature concrete failure (Carvalho & Carrasco, 2010). Monteiro et al. (Monteira, et al., 2013) concluded that the results are not significantly affected by the chosen test setup by comparing numerical and experimental results from different studies with different setups on connection tests.

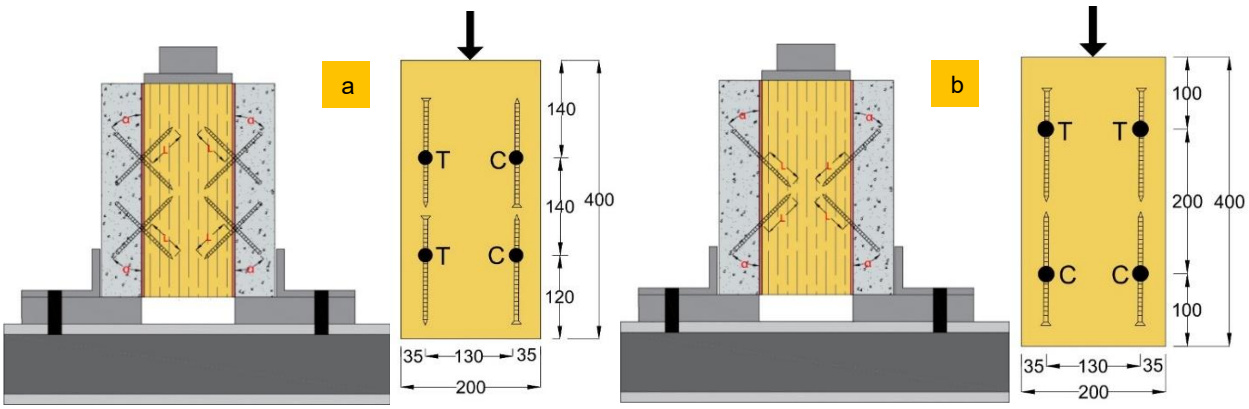

Figure 2.3: a) Screw orientation with horizontal cross-pair and configuration in timber shear plane (mm), and b) screw orientation with vertical cross-pair and configuration in timber shear plane (mm)

Only one screw diameter (11 mm) was included in this study. Two angles of insertion relative to timber grain (30° and 45°) were tested. Based on a review of the literature (Marchi, et al., 2017) (Gerber, 2016), the horizontal cross-pair of screws was selected initially, *Figure 2.3(a)*. Initially, in the CLP and CLT specimens, the screws were installed cross-wise in horizontal pair (per pair, one screw each in tension and compression). In this arrangement, tension and compression force cancel each other and eliminate friction (Tomasi, et al., 2010) (Bejtka & Blaß, 2001) (Marchi, et al., 2017). Two horizontal cross-wise pairs (4 screws total) per shear plane with two in tension (T) and two in compression (C) were installed as shown in *Figure 2.3(a)*. It was subsequently found that for specimens with a thick insulation (15 mm), the horizontal cross-wise arrangement led to substantial in-plane rotation of the side member's relative to the center member due to the unsymmetrical configuration. As a result, the specimens in the subsequent tests were all conducted with the vertical cross-pair arrangement. Therefore, in all GLT specimens along with CLP and CLT specimens with 15 mm insulation, the screws were installed in vertical pair cross-wise (per pair, one screw each in tension and compression). Two vertical cross-wise pairs (4 screws total) per shear plane with two in tension (T) and two in compression (C) were installed as shown in *Figure 2.3 (b)*. The spacing of the self-tapping screw in timber was based on European Technical Approval ETA (ETA-Danmark, 2016) to avoid interaction effect and is shown in *Figure 2.3*. In horizontal cross-pair, screws are located at a 3d distance from the parallel edge, 11d in the unloaded edge, and 13d in the loaded edge, and in vertical cross-pair, screws are located at a 3d distance from the parallel edge, 9d in both unloaded,

and loaded edge to accommodate all the screws, where d is the diameter of the screw. Acoustic insulation was inserted between concrete and MTP. A typical connection test setup is shown in *Figure 2.4*. Here, the bottom steel plate along with L shape angles was clamped to a steel beam to avoid the lateral movement of the specimen. The top steel plate was used to distribute the applied load evenly into the specimens. Linear Variable Differential Transformers (LVDT's) were used on both sides of shear planes to measure the relative slip between wood-based material and concrete. Average values measured from the two LVDT's were used in the calculation.

A total of 36 configurations (3 MTP x 2 screw angles x 2 embedment lengths x 3 insulation thicknesses x 1 concrete thickness x 1 screw diameter) with three replicates each leading to a total of 108 connection specimens were planned to test. However, the groups of 100 mm embedment length into CLT and CLP with 15 mm insulation for two angles were not tested. Therefore, only a total 32 configurations were tested with 96 specimens. The investigated parameters are listed in *Table 2.2*. There were 12 major screw configurations tested for all MTP. The specifications of the screws in each composite material for different configuration are shown in *Table 2.3*, where L# refers to the embedment length of the screw into MTP, I# refers to the insulation thickness, and #° refers to the insertion angle of the screw to the timber grain. Screw length was adjusted in concrete to achieve the 80 and 100 mm embedment length in wood.

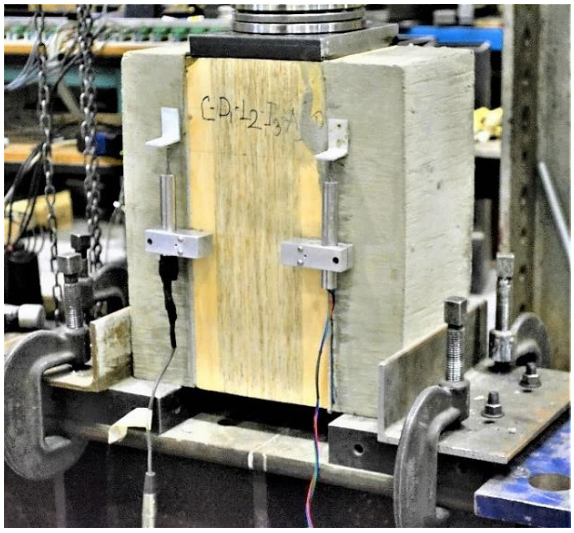

Figure 2.4: Typical connection test setup of CLP specimen

Table 2.2: Investigation parameters

Material	Parameter
Mass Timber Panel (MTP)	Cross Laminated Timber (CLT)
	Glue Laminated Timber (GLT)
	Composite Laminated Panel (CLP)
Insulation Thickness	0 mm (no insulation)
	5 mm (1 layer)
	15 mm (3 layers)
Screw Angle	30° (cross-pair)
	45° (cross-pair)
Screw Embedment Length	80 mm
	100 mm
Screw Diameter	11 mm
Concrete Thickness	75 mm

Table 2.3: Construction details of connection specimens

Configuration	MTP	Screw Length, mm	Screw in Concrete, mm	Screw in Insulation, mm	Screw in MTP, mm
L80-I0-45°	CLT, CLP, GLT	150	70	0	80
L80-I5-45°	CLT, CLP, GLT	150	62.9	7.1	80
L80-I15-45°	CLT, CLP, GLT	150	48.8	21.2	80
L80-I0-30°	CLT, CLP, GLT	150	70	0	80
L80-I5-30°	CLT, CLP, GLT	150	60	10	80
L80-I15-30°	CLT, CLP, GLT	150	40	30	80
L100-I0-45°	CLT, CLP, GLT	200	100	0	100
L100-I5-45°	CLT, CLP, GLT	200	92.9	7.1	100
L100-I15-45°	GLT	200	78.8	21.2	100
L100-I0-30°	CLT, CLP, GLT	200	100	0	100
L100-I5-30°	CLT, CLP, GLT	200	90	10	100
L100-I15-30°	GLT	200	70	30	100

The specimens were prepared by inserting the screws into the MTP block with proper orientation specified in *Table 2.3*, therefore casting a normal weight concrete on both sides of the MTP in the laboratory. After casting the concrete, specimens were kept in normal laboratory temperature with plastic sheets at the top for 7 days and left in the laboratory for at least another 21 days before testing. Concrete cylinder samples were prepared, and were tested at 28 days to obtain the compressive strength and modulus of elasticity of concrete. In *Figure 2.5*, pictures of the specimen preparation before the connection test are shown.

Figure 2.5: Specimen preparation; a) insertion of screw at 30° angle in horizontal cross-pair b) insertion of screw at 45° angle in vertical cross-pair, c) screwed MTP are ready for putting into forms, d) specimens are ready for casting, and e) specimens are ready for testing

2.3.3 Test Procedure

The loading protocol according to EN 26891:1991 (EN 26891, 1991) which was initially developed for timber-timber connection and later implemented in timber-concrete connection was followed, where the specimen was loaded initially up to 40% of the estimated failure load (F_{est}), then the loading was stopped for 30 seconds, unloaded to 10% and stopped for 30 seconds. Finally, the specimen was loaded to failure. The loading was stopped just after the specimen failed and there was a drop in the measured load. The reason for the unloading step was to allow the specimen to settle and to eliminate the internal friction between timber and concrete, and to ensure that the connection does not fail due to initial slip or slack (Khorsandnia, et al., 2012). The estimated failure load (F_{est}) was found from the trial test with different configurations. However, during the execution of the tests, if the maximum load obtained deviated by more than 20% from the F_{est}, then F_{est} was adjusted in the subsequent tests of the same

configuration. Because, the influence of the estimated failure load on the load-slip modulus is significant (Dias, 2012). The load was applied at a loading rate of 5 mm/min. The maximum allowable slip level was chosen to be 15 mm in accordance with EN 26891:1991 (EN 26891, 1991), although all the specimens failed before this limit.

The connection strength was defined as the maximum load before failure of the specimen (peak load) or the load at 15 mm slip, whichever is lower, and can be obtained directly from the load-slip curve. The stiffness was quantified by the load-slip modulus at three different load levels (40% of F_{est}, 80% of F_{est} and F_{max}) corresponding to Serviceability Limit State (SLS), Ultimate Limit State (ULS), and Collapse Load Level (CLL) respectively (Gerber, 2016). *Figure 2.6* shows the applied loading procedure, and an idealized load-slip curve. The initial stiffness of the connection (k_i) represents the first slope of the load-slip behavior. The slip modulus $k_{0.4}$ corresponds to the slope of the load-slip curve between 10% and 40% of the failure load, which is usually used for serviceability stiffness. Since the serviceability stiffness based on the first loading cycle normally shows inconsistent results, the second reloading cycle was considered to check for consistency. The next phase of this research will focus on development of an analytical model for these types of 3-member connection. For the purpose of validating the connection stiffness predicted by the analytical model, stiffness based on the first loading cycle will be more appropriate. Therefore, in this paper, serviceability stiffness based on both the first and second loading cycle along with initial stiffness are shown. The initial stiffness (k_i), SLS stiffness ($k_{0.4}$) considering first and second loading cycle, ULS stiffness ($k_{0.8}$), and CLL stiffness (k_{CLL}) were calculated using the equations shown below. Equations [2] and [3] represent the serviceability stiffness considering the first and second loading cycle respectively, while Equation [4] considers the ultimate stiffness.

$$k_i = \frac{0.4F_{est}}{v_{04}} \quad [1]$$

$$k_{(0.4)_1} = \frac{0.4F_{est}}{4/3(v_{04} - v_{01})} \quad [2]$$

$$k_{(0.4)_2} = \frac{0.4F_{est}}{4/3(v_{24} - v_{21})} \quad [3]$$

$$k_{0.8} = \frac{0.8F_{est}}{(v_{28} - v_{24}) + 4/3(v_{04} - v_{01})} \quad [4]$$

$$k_{CLL} = \frac{F_{max}}{v_{ult}} \quad [5]$$

Here, F_{est} is the estimated failure load, F_{max} is the maximum load at failure, and υ refers to the relative slip at specified points shown in *Figure 2.6*.

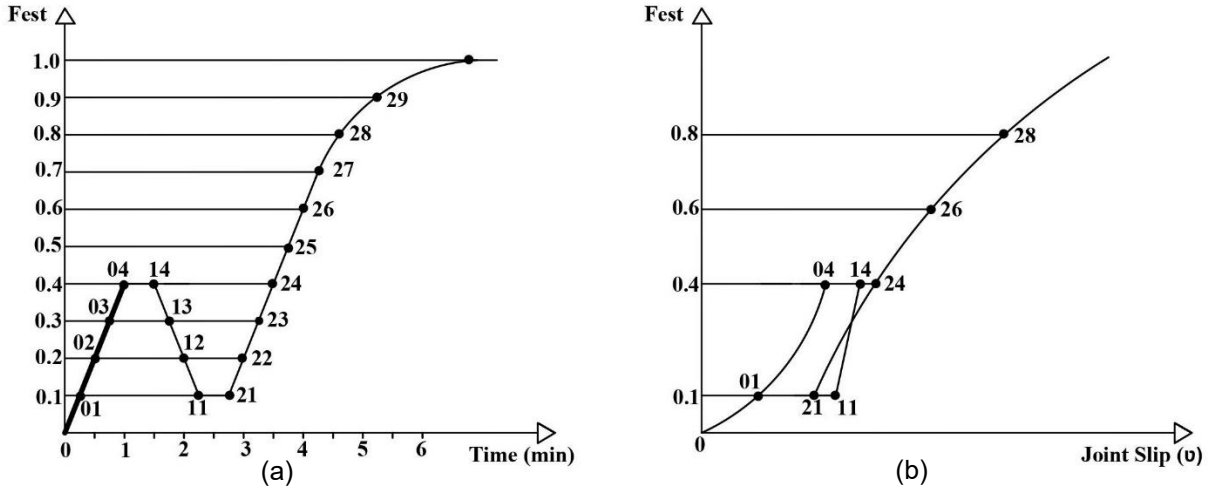

Figure 2.6: a) Loading procedure and b) idealized load slip curves; based on EN 26891

2.4 Results and Discussion

The load-slip curves were obtained by taking the average displacement of four LVDTs and applied load on the specimen recorded by the load cell, and selected specimen from each configuration is presented in *Figures 2.7, 2.8 and 2.9* for CLP, CLT, and GLT specimen respectively. The solid lines represent the specimens without insulation, small dotted lines represent the specimens with 5 mm insulation, and large dotted lines represent the specimens with 15 mm insulation. It can be seen clearly that stiffness is reduced significantly with the inclusion of an insulation layer between concrete and MTP. Overall connection test results for all configurations per pair of screws are shown in *Table 2.4*. In *Table 2.4* screw orientation, ultimate strength, stiffness at initial, SLS, ULS, and collapse load level, and reduction percentage in strength and stiffness per pair of screws due to the presence of an insulation layer are included. Here, H-X refers to a horizontal cross-pair and V-X refers to a vertical cross-pair. Also, to investigate the influence of the screw angle, screw embedment length, insulation thickness, MTP, and loading cycle, a comparison chart was drawn for strength and stiffness at SLS level separately, and discussed in the following section. Since the results in CLP and CLT are almost the same, the comparison chart for CLP is not shown.

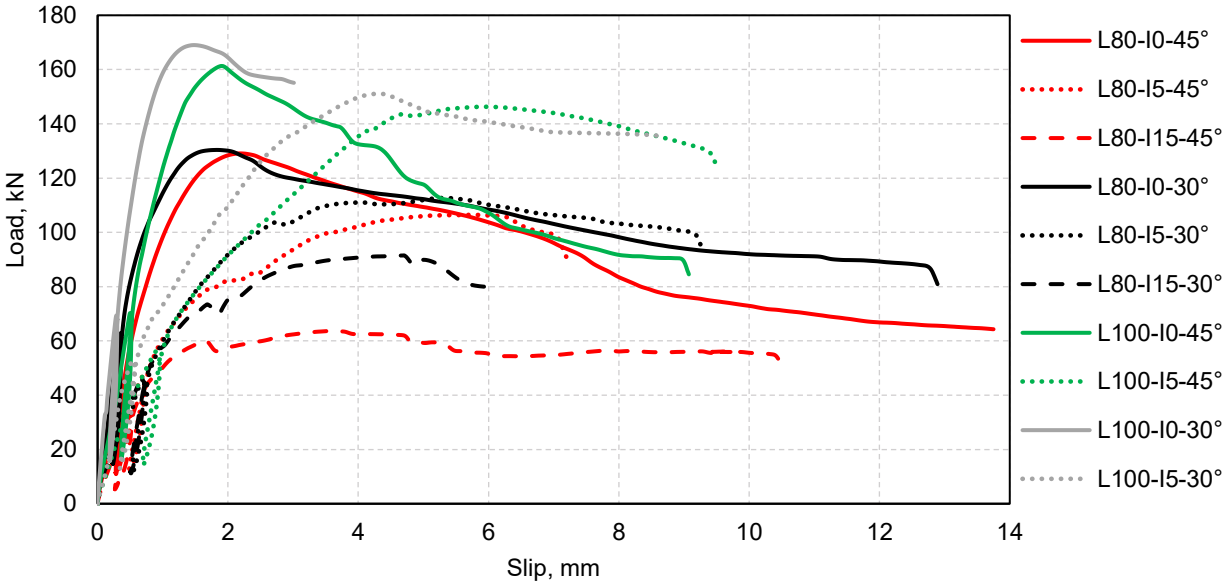

Figure 2.7: Load-slip curve of CLP specimen

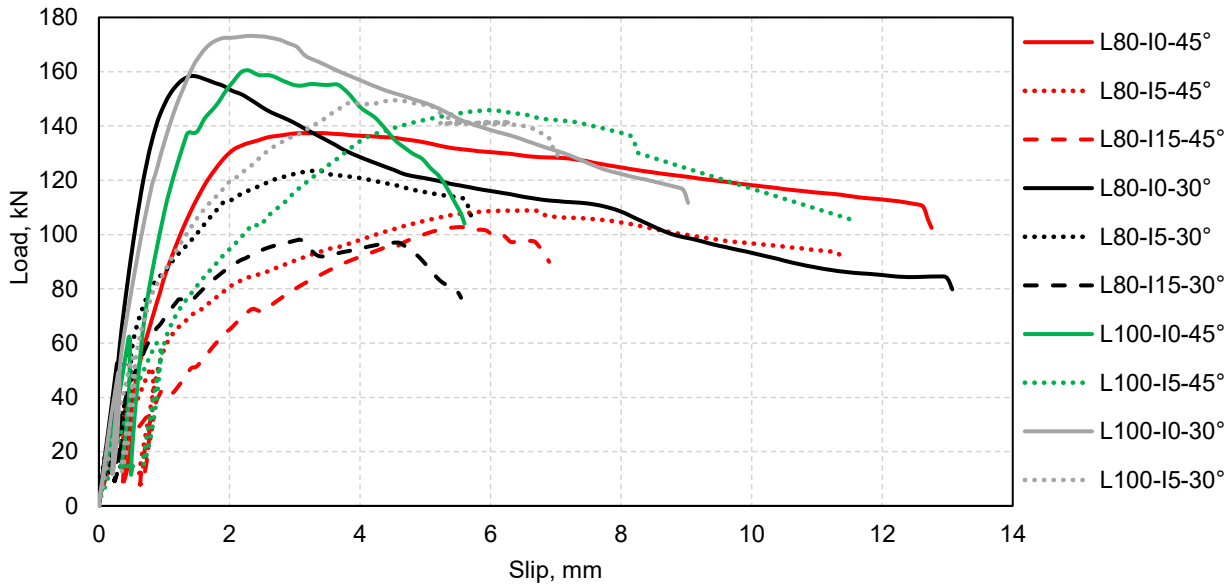

Figure 2.8: Load-slip curve of CLT specimens

2.4.1 Influence of Insertion Angle

From the connection test result, it can be seen that the ultimate load-carrying capacity of the connection increases with the increase of insertion angle of connection along the timber grain. This statement is valid for the connections in all three MTP as well as in both embedment lengths in MTP. From the test result, it was found that strength and stiffness in CLT and CLP are almost the same. From *Figure 2.10(a)* for CLT, a significant increase in strength can be noted when there was no insulation, except the case of

100 mm embedment length. In CLT, the configuration L100-I0-30° had weaker concrete compared to other batches, which explains why the strength was lower than L100-45°. However, in all other cases with 5 mm and 15 mm insulation, the influence of insertion angle was insignificant, although the strength was higher (average 8%) in 30° insertion angle. In CLT and CLP, L100-I15-30° and L100-I15-45° configurations were not tested. In case of GLT, from *Figure 2.10(b)* it can be observed that a similar pattern of results as CLT was obtained, where the strength of connection is higher in 30° compared to 45° angle (average 12%) in all three insulation thicknesses and two embedment lengths. However, when one compares the result of serviceability stiffness in CLT in *Figure 2.11(a)* and *Figure 2.12(a),* a significant increase (average 38%) of stiffness for the 30° insertion angle compared to 45° angle in all configurations can be observed. In case of GLT, from *Figure 2.11(b)* and *Figure 2.12(b),* a significant stiffness increase (average 47%) for 30° angled screw compared to 45° angle is observed for all configurations. In case of CLP, the strength (8%) and stiffness (32%) increase percent values are almost the same as CLT. As the angle of inclination of the screw with surface grain increases, the withdrawal strength and stiffness of screw also increase, and that is the reason for higher strength and stiffness in case of 30° angle compared to 45° angle. Overall, stiffness of connection is more sensitive to the angle of insertion than strength.

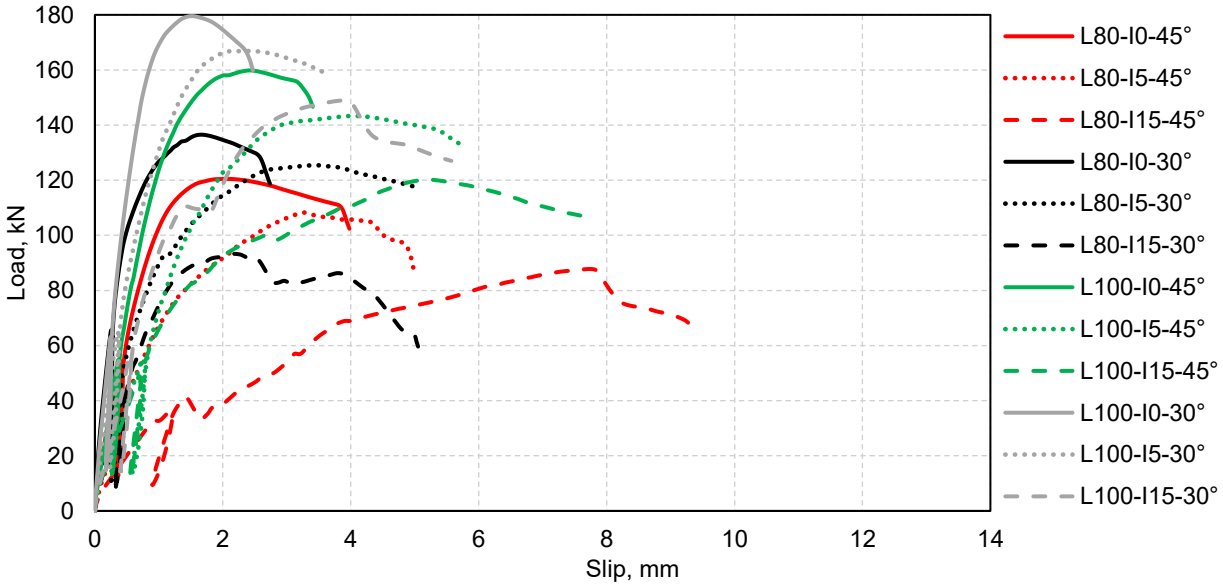

Figure 2.9: Load-slip curve of GLT specimens

Table 2.4: Connection test results per pair of screws

Specimen	Orient -ation	F_{ult}, kN	Strength Reduce	$k_{(0.4)1}$, kN/mm	Stiffness Reduce	$k_{(0.4)2}$, kN/ mm	Stiffness Reduce	k_i, kN/mm	$k_{0.8}$, kN/mm	k_{CLL}, kN/mm	Failure[1]
CLP-L80-I0-45°	H-X	30.26	0%	34.74	0%	53.66	0%	35.30	25.58	13.97	W C + C C
CLP-L80-I5-45°	H-X	27.36	10%	14.88	57%	26.36	51%	17.93	9.04	5.10	W C
CLP-L80-I15-45°	V-X	19.61	35%	12.09	65%	20.88	61%	12.37	7.68	2.95	W C + C C
CLP-L80-I0-30°	H-X	34.96	0%	56.31	0%	92.72	0%	56.78	40.31	21.34	W C
CLP-L80-I5-30°	H-X	29.04	17%	20.03	64%	39.99	57%	20.87	14.70	6.87	W C
CLP-L80-I15-30°	V-X	23.17	34%	19.32	66%	36.63	60%	18.77	12.85	6.51	W C
CLP-L100-I0-45°	H-X	41.86	0%	45.79	0%	89.79	0%	41.62	36.43	22.26	W C + C C
CLP-L100-I5-45°	H-X	36.97	12%	16.64	64%	36.07	60%	14.09	10.18	7.01	W C
CLP-L100-I15-45°	--	--	--	--	--	--	--	--	--	--	--
CLP-L100-I0-30°	H-X	42.09	0%	59.74	0%	92.90	0%	63.52	47.96	26.05	W C
CLP-L100-I5-30°	H-X	38.64	8%	26.31	56%	37.68	59%	28.60	17.54	9.85	W C
CLP-L100-I15-30°	--	--	--	--	--	--	--	--	--	--	--
CLT-L80-I0-45°	H-X	33.61	0%	24.71	0%	56.35	0%	24.92	22.07	12.39	W C + C C
CLT-L80-I5-45°	H-X	28.70	15%	14.70	41%	31.78	44%	15.99	7.29	4.60	W C
CLT-L80-I15-45°	V-X	24.27	28%	11.05	55%	25.89	54%	13.04	6.74	4.30	W C + C C
CLT-L80-I0-30°	H-X	41.88	0%	45.76	0%	92.76	0%	46.05	45.05	28.21	W C
CLT-L80-I5-30°	H-X	31.55	25%	25.88	43%	52.49	43%	27.41	15.21	9.63	W C
CLT-L80-I15-30°	V-X	25.04	40%	18.02	61%	43.79	53%	20.46	13.51	6.60	W C
CLT-L100-I0-45°	H-X	44.23	0%	36.57	0%	80.45	0%	37.94	27.05	15.92	W C + C C
CLT-L100-I5-45°	H-X	35.85	19%	17.21	53%	38.42	52%	16.13	10.01	6.50	W C
CLT-L100-I15-45°	--	--	--	--	--	--	--	--	--	--	--
CLT-L100-I0-30°	H-X	39.66	0%	47.37	0%	83.27	0%	42.77	31.33	17.56	W C
CLT-L100-I5-30°	H-X	36.07	9%	27.31	42%	53.15	36%	27.93	18.00	8.53	W C
CLT-L100-I15-30°	--	---	--	--	--	--	--	--	--	--	--
GLT-L80-I0-45°	V-X	28.37	0%	27.88	0%	74.00	0%	32.71	21.21	12.79	W C
GLT-L80-I5-45°	V-X	26.84	5%	17.18	38%	49.77	33%	20.49	14.92	7.71	W C + C C
GLT-L80-I15-45°	V-X	22.32	21%	9.42	66%	24.55	67%	9.07	6.06	2.91	W C + C C
GLT-L80-I0-30°	V-X	32.42	0%	53.69	0	128.48	0%	60.94	33.57	20.41	W C
GLT-L80-I5-30°	V-X	31.11	4%	26.68	50%	65.61	49%	30.08	21.77	10.87	W C
GLT-L80-I15-30°	V-X	22.47	31%	21.89	59%	52.87	59%	22.93	14.08	8.66	W C
GLT-L100-I0-45°	V-X	37.31	0%	35.84	0%	87.24	0%	38.35	29.06	14.93	W C
GLT-L100-I5-45°	V-X	34.84	7%	18.20	49%	51.49	41%	20.31	17.36	8.68	W C + C C
GLT-100-I15-45°	V-X	30.69	18%	12.19	66%	39.57	55%	13.16	9.01	5.75	W C + C C
GLT-L100-I0-30°	V-X	43.27	0%	62.41	0%	139.48	0%	67.42	56.59	29.64	W C
GLT-L100-I5-30°	V-X	40.83	6%	35.56	43%	70.60	49%	35.62	26.59	16.78	W C
GLT-L100-I15-30°	V-X	36.16	16%	23.17	63%	61.03	56%	25.08	16.15	10.51	W C

[1] WC: Wood Crush; CC: Concrete Cracking

2.4.2 *Influence of Embedment Length*

As expected for all MTP, the connection strength (average 23%) and serviceability stiffness (average 15%) increase with any increase in embedment length of connection into MTP. In CLT and GLT, the influence of embedment length on serviceability stiffness was significant in all the cases of specimens with and without insulation. All these results can be seen in *Figures 2.10, 2.11 and 2.12*. The reason for the increase of strength and stiffness with the increase of embedment length is obviously related to the extra embedment length. Also, in an attempt to vary the embedment length of the screw into MTP, the length in concrete was in turn affected but, this did not have any influence on the failure mode. Configurations of L80-I5-30° and L100-I5-30° had a screw length of 63 mm and 93 mm in concrete but, the failure modes for both configurations were the same, although L100-I5-30° had a larger length in concrete. Similarly, in all other cases where the length of screw varied in concrete showed the same failure mode. The failure mode varied from the specimen with and without insulation as well as screw orientation. Overall, strength of connection is more sensitive to embedment length than stiffness.

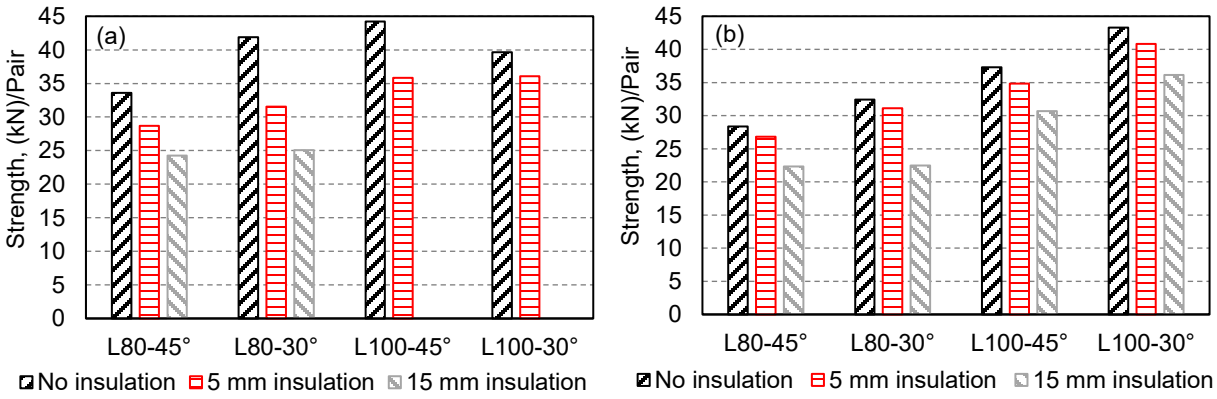

Figure 2.10: Strength per pair of screws; a) in CLT specimen and b) in GLT specimen

2.4.3 *Influence of Insulation Thickness*

Insulation thickness is expected to reduce the strength and stiffness of the connection because of its low stiffness. In *Table 2.4*, the connection test results per pair of screws are shown with the reduction percentage due to the presence of an insulation layer. In case of GLT, approximately a 5% decrease in strength for 5 mm insulation and a 22% decrease for 15 mm insulation are observed while in case of CLT, 17% strength reduction for 5 mm insulation and 34% decrease for 15 mm insulation are noted. In case of CLP, a 12% decrease for 5 mm insulation and 34% decrease for 15 mm insulation are found. So, the

insulation thickness has a significant effect on the strength of the connections. However, if we consider the serviceability stiffness of the connection in GLT, 35-50% reduction for 5 mm insulation and 55-65% reduction for 15 mm insulation are obtained considering both first and second loading cycle. In case of serviceability stiffness of connection in CLP and CLT, almost the same 35-50% reduction for 5 mm insulation and 55-60% reduction for 15 mm insulation are detected. These results show that connection stiffness is more sensitive to changes in insulation thickness than connection strength. The percent reduction of connection strength and stiffness with change in insulation thickness follows the trends with the previous study using particleboard interlayer conducted by Dias (Dias, et al., 2010) (Dias, et al., 2007), Van dar Linden (Van der Linden, 1999) and Timmermann (Timmerman & Meierhofer, 1993), although there were some differences in experimental details between the present and these studies, and direct comparison is not appropriate. In the previous studies, particleboard was used as an interlayer which also works as formwork for concrete and contribute in the mechanical properties of connection. In the present study, the interlayer is a relatively soft acoustic material that does not contribute to the mechanical properties of connection.

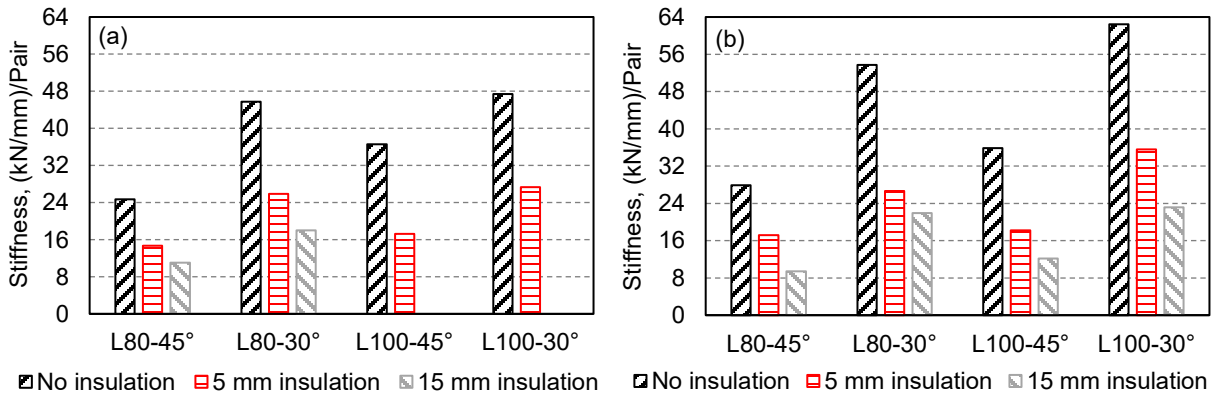

Figure 2.11: Serviceability stiffness per pair of screws for 1st loading cycle; a) in CLT specimen and b) in GLT specimen

For the serviceability stiffness, both the first and second loading cycle showed almost the same percentage of reduction due to the insulation thickness in all MTP but, it was more consistent in CLT compared to GLT. Also, the initial stiffness is almost the same as serviceability stiffness considering the first loading cycle. This percent reduction followed the same trend in terms of ultimate stiffness as well as collapse load level stiffness. The stiffness of the connection seemed more influenced by the insertion

angle of the screw when there was no insulation. However, in the presence of an insulation layer, the insertion angle and embedment length did not appear to have a significant influence on strength and stiffness of these connections. This can be seen on both *Figure 2.11 and Figure 2.12*. After a certain embedment length of the screw into MTP, the stiffness and strength are less affected because, for larger embedment length, bending of the screw becomes more dominant than the withdrawal strength. This was found when the wood member was cut after the tests and discussed in Section 2.2.4.6 (Failure Modes).

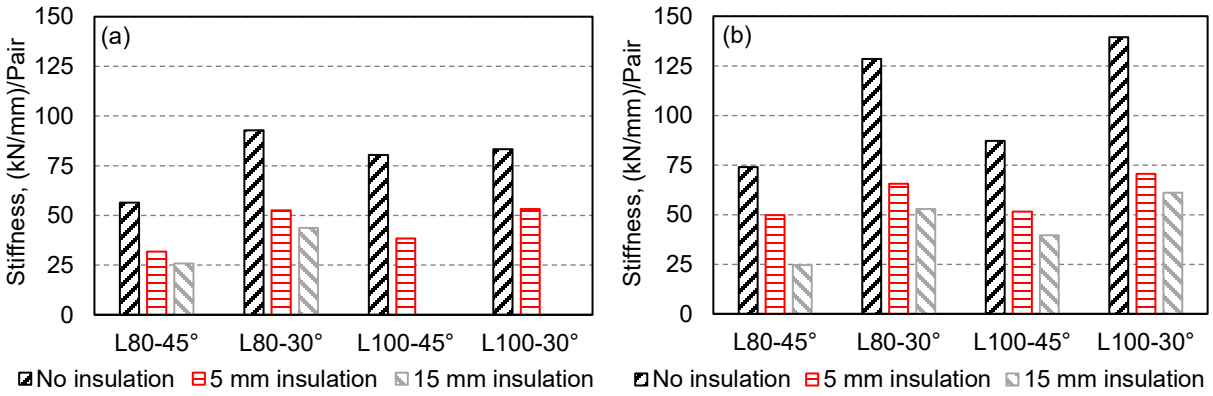

Figure 2.12: Serviceability stiffness per pair of screws for 2nd loading cycle; a) in CLT specimen and b) in GLT specimen

2.4.4 Influence of MTP

As discussed earlier in section 2.2.3.2 (test setup), horizontal cross-pair was used in CLP and CLT while vertical cross-pair was used in GLT along with 15 mm insulation in CLT and CLP. In the case of horizontal cross-pair, the screw orientation was not symmetric. Because of the non-symmetric screw setup, when insulation thickness is large (15 mm), an obvious in-plane rotation of the side members was observed during the test. As a result, the screw arrangement was changed to a vertical cross pair thereafter. In the cases of specimens with no insulation and 5 mm insulation, no such side member rotation was observed. The highest connection strength was found in CLT but connection stiffness was observed significantly higher in GLT in both loading cycles. Although there was different screw orientation in the MTP, especially in GLT where all configurations were in vertical cross pairs, the percent reduction of strength and stiffness was noticed to be similar in all MTP due to the insulation layer. Even though a same trend was found in the test results for both screw orientations, different failure mode was observed which are

described in section 2.2.4.6 (Failure modes). This difference in failure mode indicates that the screw orientation has some influence on the result although this influence is not significant.

2.4.5 Influence of Loading Cycle

The initial stiffness calculated by Equation [1] was found nearly the same as the serviceability stiffness calculate by Equation [2] using the first loading cycle in all the configurations of the three MTP. The serviceability stiffness calculated by Equation [3] using the second loading cycle was found to be 55% higher compared to the serviceability stiffness considering the first loading cycle for all configurations. However, percent stiffness reduction values for the connection with an insulation layer using first and second loading cycles were similar and can be seen in *Table 2.4*. In the second loading cycle, the materials settled down and any friction between timber and concrete is stabilized. Therefore, a more consistent stiffness can be found compared with the first loading cycle. In the ultimate stiffness, percent reduction due to insulation thickness remains the same as serviceability stiffness. Also, the collapse load level stiffness reduces by 59% compared to the serviceability stiffness.

2.4.6 Failure Modes

After the connection test, selected specimens from all the configurations were cut opened to examine the deformed shape of the screw. General failure modes for all the tested configurations are noted in *Table 2.4* where, WC means wood crushing which includes the embedment of screws in timber and CC means concrete cracking. With the inclined cross-pairs of screws, the observed possible failures were partial pull-out of screws, significant destruction of wood near screws with embedment in wood, deformation of screws and concrete crushing. The wood crushing was due to the embedment of screws in wood, often after the formation of plastic hinges in the screws. Concrete cracking was found only in the specimens where the screw was installed at 45° angle. This cracking was neither a uniform cracking nor a local cracking due to non-uniform bearing of the concrete on the support. The failure of concrete was likely due to the higher angle of the screw to the surface of concrete, leading to 'lifting' of concrete when the side member was under load. In *Figure 2.13*, failure modes of CLT and CLP specimen are shown. For the CLT, the failure modes in the cases without insulation were a combination of a plastic hinge formed in the screw within the MTP and wood embedment and concrete cracking (only when screws were at 45°

angle). This is because the stresses acting on concrete are higher when there is no insulation and cracking of concrete was dominant. This mode is shown in *Figure 2.13(a)*. Tension and compression screws tend to oppose the load applied but the direct contact between timber and concrete leads to higher stresses in concrete. In the cases with insulation, failure occurred due to wood embedment and plastic hinges formation in the MTP. This is because; the insulation does not contribute to the system stiffness and strength and behaves like a gap. When there is a gap, the stress on timber is more compared to the stress in concrete due to the additional lever arm in bending as shown in *Figure 2.13(b) and (c)*. Also, the cross-grain of lumber in CLT likely contributes to this difference in failure mode, compred with GLT. The single hinge was observed in the case of 5 mm insulation while double hinges were found in the case of 15 mm insulation, as shown in *Figure 2.13(d), (e) and (f)* respectively. The failure modes in CLP were found to be exactly the same as in CLT.

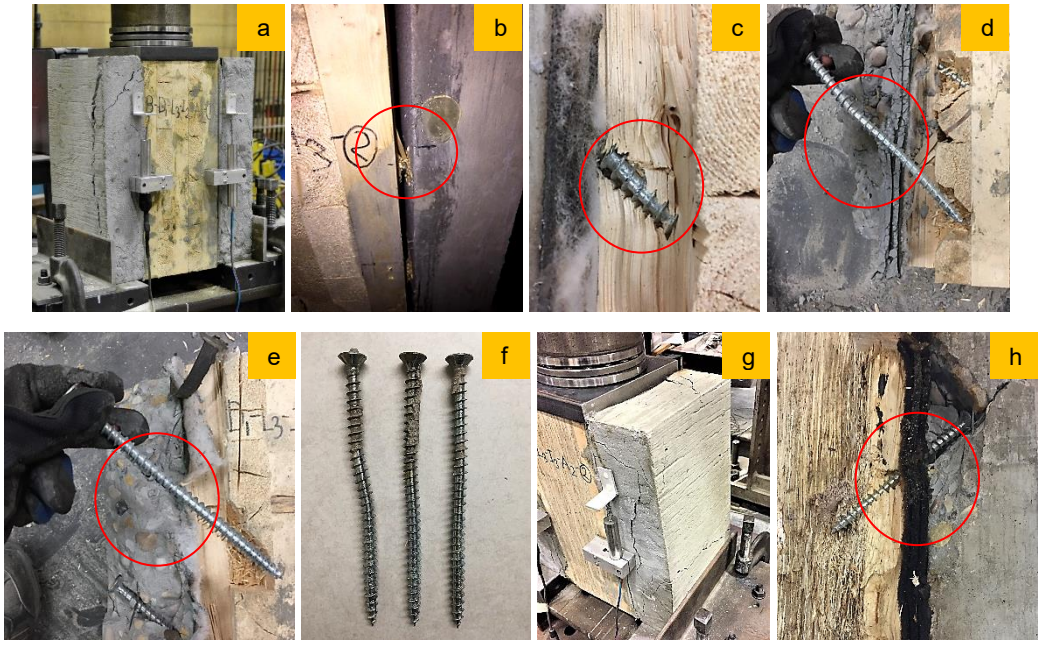

Figure 2.13: Failure mode in CLT; a) concrete cracking in the specimen without insulation, b) wood crush, c) wood embedment, d) double plastic hinges with 15 mm insulation, e) single plastic hinge with 5 mm insulation, f) plastic hinge in screws and failure mode in CLP; g) concrete cracking, and h) plastic hinge.

Similar to CLT, for GLT wood embedment and plastic hinges of the screw were observed in the cases without insulation as shown in *Figure 2.14(b) and (c).* Plastic hinge along with concrete cracking (when

screws were at 45° angle) was observed in the cases with insulation. This is because, due to the longer level arm tension screw tends to pull out from the timber while the compression screw tends to resist the load and the stresses at the bottom of concrete become higher which leads to the cracking of concrete as shown in *Figure 2.14(a*). The single hinge was observed in the case of 5 mm insulation while double hinges were found in the case of 15 mm insulation as shown in *Figure 2.14(d), (e) and (f)* respectively.

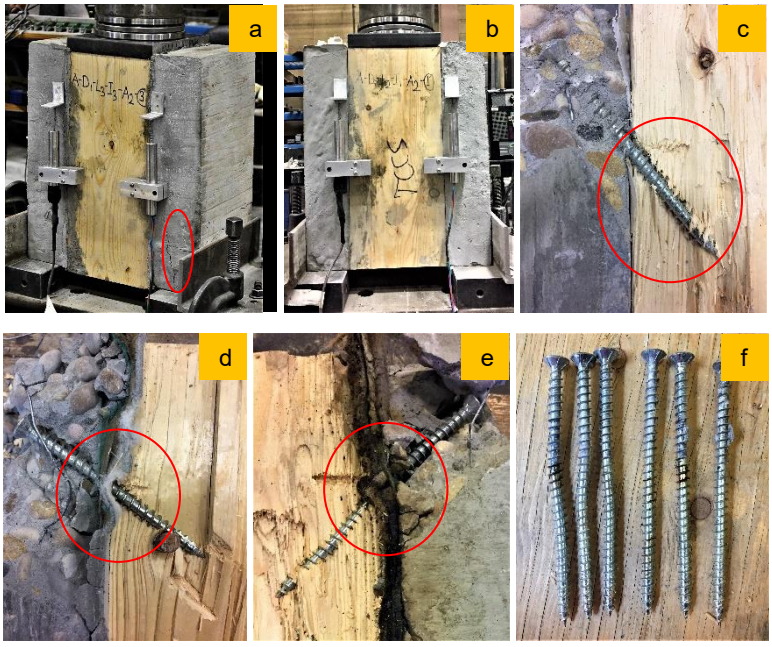

Figure 2.14: Failure modes in GLT; a) Concrete cracking at the bottom of the specimen in the presence of insulation, b) specimen after failure without insulation has no concrete cracking, c) embedment of wood in opened specimen without insulation, d) single plastic hinge with 5 mm insulation, e) double plastic hinges with 15 mm insulation, and f) plastic hinges in screw.

Overall, initially, the screw connections were fully rigid followed by bond failure where the load was transferred to the less stiff screw and therefore, the screws started to pick up an additional load before failure in either tension or withdrawal. The cracking of the concrete is not desirable and can only be suppressed by increasing the thickness of concrete. This issue was not considered in the present study but may be studied in a future phase of the research. Observations of failure modes will be useful when evaluating the validity of any prediction analytical model for connection strength (Marchi, et al., 2017) (Kavaliauskas, et al., 2007).

2.5 Conclusions

One of the major aims of this study was to evaluate the impacts of an insulation layer and inclined self-tapping screws on strength, stiffness and failure modes of MTPC connections to help in the development and validation of analytical models for predicting stiffness and strength of this type of connection with an intermediate insulation layer.

The stiffness of the connections appears to be strongly influenced by the insulation layer in this study. The use of an insulation layer resulted in a significant reduction in stiffness even for very small insulation thickness. When the insulation thickness increased to a certain limit, the stiffness reduced by almost 65%. The strength seems to be less affected with a maximum of 35% reduction. Further, 30° angled screws relative to the timber grain showed higher strength and stiffness compared to 45° angled ones. The influence of insertion angle was found to be more significant in the stiffness of specimens without insulation compared to the specimens with insulation. A larger embedment length of screw into MTP showed a higher stiffness and strength but it was less significant in the presence of an insulation layer. Also, strength of connection is more sensitive to embedment length of screws while stiffness is more sensitive to the insertion angle of screws. Test values in terms of strength and stiffness were similar for CLP, CLT and GLT. Despite this, different failure modes were found in the MTP, and the percent reduction due to insulation thickness was found to be similar. Therefore, it can be concluded that the connection properties are heavily influenced by the insulation thickness compared to the insertion angle, embedment length, and orientation of screws. Special consideration is required while designing MTPC composite floors that have an insulation layer between timber and concrete.

Chapter 3. Connection Strength Prediction Model

Journal Paper #2

Strength Prediction of Mass Timber Panel-Concrete Composite Connection with Inclined Screws and a Gap

by Md Abdul Hamid Mirdad and Ying Hei Chui

Published in ASCE Journal of Structural Engineering, 2020

Abstract:

Mass Timber Panels (MTP) are a new generation of engineered wood panels that are available in large plane dimensions to facilitate fast floor construction with the obvious environmental benefit of being from a renewable material. In floor construction, concrete slab or topping is often applied over the MTPs to improve various performance attributes, including structural, acoustic and vibration serviceability. Mass Timber Panel-Concrete (MTPC) composite floor system often consists of a Mass Timber Panel (MTP) connected to the concrete layer with mechanical fasteners and a sound insulation layer in between. The capacity of this type of composite system mostly depends on the strength of the connection, and often tests are performed in order to characterize connection properties required for structural design. In lieu of testing, analytical models can be developed to calculate connection properties based on component properties. To that end, two analytical models were developed for solid and layered timber by characterizing all possible kinematical failure modes, for directly predicting the strength of a connection with inclined screws and an insulation layer. According to Johansen's yield theory, the strength of laterally loaded connection is controlled by the dowel-bearing effect of the fastener in timber, but joints with inclined screw have a more complex behaviour due to the combined bearing and withdrawal action of the screw. In the developed models, both the dowel-bearing and withdrawal action of the screw are considered along with the bending capacity of the screw and friction between the members. Both models were experimentally validated with a wide range of material properties. It was found that the models are capable of predicting the mode of failure of a connection and the load-carrying capacity within 10% of the experimental value.

3.1 Introduction

Mass timber construction has gained attention over the last two decades due to global interest in reducing environmental footprints of building construction. At the same time, changes in building codes, the emergence of a new generation of engineered wood products, availability of sophisticated design tools, and innovative fastening systems, has helped to broaden the range of timber construction possibilities (Jacquier, 2015). The construction of modern multi-storey timber structure is therefore rapidly increasing. Mass Timber Panel-Concrete (MTPC) composite floor is often a preferred choice by designers due to its higher strength and stiffness to weight ratios, larger span to total depth ratio, higher in-plane rigidity, and better acoustics, thermal and fire performances (Ceccotti, 2002) (Yeoh, et al., 2011). Mass Timber Panel-Concrete (MTPC) composite floor generally consists of a Mass Timber Panel (MTP) [e.g., Cross Laminated Timber (CLT), Glue Laminated Timber (GLT), Nail Laminated Timber (NLT) and Dowel Laminated Timber (DLT)], connected to a concrete slab by mechanical fasteners. Such a system is structurally efficient in that the MTP primarily resists tensile stress while the concrete slab resists compressive stress generated by out-of-plane bending action, and the mechanical fasteners allow for partial shear transfer and therefore partial composite action between the components. An insulation layer is often sandwiched between the timber panel and concrete slab to provide better acoustics, vibration and thermal performance. Practically this insulation layer will not contribute to the composite action and have a negative impact on the strength of the connection by acting as a gap (Mirdad & Chui, 2019). The structural efficiency of this composite system mostly depends on the performance of this interlayer connection and by avoiding failures in the connections, it is possible to maximize the load-carrying capacity and increase the ultimate deformation capacity of the composite system.

Screws, bolts and dowels are examples of dowel-type fasteners, with their lateral strengths mostly governed by the dowel-bearing or embedment strength of timber elements and the yield moment of the fastener and may be calculated based on Johansen's yield theory. According to Johansen (Johansen, 1949), the strength of a connection containing dowel-type fasteners is dependent on the fastener resistance to bending (yield moment) and the resistance of the wood to crushing (dowel-bearing or embedment). Self-Tapping Screws (STS) are widely used modern fasteners which were developed as an improved threaded fastener for the application in large-scale timber structures. This type of screw mostly

features a continuous thread over the whole length (fully-thread) which leads to a more uniform load transfer between the screw and the wood material under axial or withdrawal action (Dietsch & Brandner, 2015). In addition many experimental and numerical studies (Tomasi, et al., 2010) (Bejtka & Blass, 2001) (Kevarinmäki, 2002) (Bejtka & Blass, 2002) (Blass, et al., 2006) (Closen, 2012) (Jockwer, et al., 2014) have concluded that there is a substantial increase in the strength and stiffness of a STS connection if the screw is installed at an angle to the surface of the wood member, instead of normal to the surface.

Joints fabricated with inclined screws have a more complex behaviour because, the load transfer mechanism involves not only the bending of the screw and the embedment of the wood but also the withdrawal resistance of the fasteners as well as the friction between the elements. In an inclined position, the screw is subjected to a combined axial and lateral loading condition. According to Eurocode 5 (EN 1995-1-1, 2009), a quadratic combination of the axial and lateral loading ratios can be used to predict the capacity of a connection with fasteners at an inclined position. However, the EC5 method underestimates the strength of the modern screw type connection (e.g. self-tapping screw). Therefore, in order to characterize the strength of the fasteners, often tests are performed according to standardized procedure such as EN 26891:1991 (EN 26891, 1991). In addition to testing, the properties of self-tapping screw connection can also be estimated using mechanics-based model that accounts for component properties and other factors such as friction. The strength model of inclined screws in timber-to-timber joints has been addressed by a few researchers (Tomasi, et al., 2010) (Kevarinmäki, 2002) (Bejtka & Blass, 2002) and strength model of inclined screws in concrete-to-timber joints extending Johansen's yield theory has been addressed by others (Kavaliauskas, et al., 2007) (Marchi, et al., 2017) (Symons, et al., 2010). So far, no analytical model has been presented for concrete-to-timber joints that consider inclined screws, insulation layer gap and layered structure of the timber member.

The aim of this research work is to introduce and experimentally validate the analytical modeling approach for predicting the strength of a connection with an inclined screw and insulation layer gap. Two different analytical models are presented for inclined screws in solid and layered timber respectively. In a layered timber member, the mechanical properties of the layers differ. Also, different connection strength parameters are presented from material tests to predict the strength of the connection from the models.

This prediction from the models are compared and validated with data from short-term connection test (Mirdad & Chui, 2019) with brief conclusions. These models will facilitate the design approach for the MTPC composite floor system with or without an insulation gap. Also, the analytical models can be used for single screw in tension, single screw in compression and cross-paired screw (one screw in tension and one screw in compression).

3.2 Analytical Models for Predicting Strength of Inclined Screws

An analytical model for predicting the strength of inclined screws in concrete-to-timber connection can be developed extending Johansen's yield theory (Johansen, 1949), by considering withdrawal resistance of the screws as well as the friction in the contact surface. One of the basic assumptions in Johansen's yield theory is an idealized rigid-plastic material behaviour of the timber and of the fastener. In the extension of Johansen's theory for inclined screws, the withdrawal capacity of the screw needs to be taken into account as well as the friction between contact interfaces of concrete and timber. Depending on the axial displacement of the screw at the ultimate capacity of the connection, the screw may or may not have reached its withdrawal strength before reaching full embedment capacity and vice versa (Bejtka & Blass, 2002). Therefore, a ratio of embedment and withdrawal strength can be used for the progressive failure. To develop the analytical models for strength prediction of inclined screws in concrete-to-timber (either solid or layered MTP) based on the hypotheses of (Kavaliauskas, et al., 2007), the following assumptions can be considered: a) single screw model in tension, b) idealized rigid-plastic behaviour of timber in bearing, c) idealized rigid-plastic behaviour of screw in bending, d) screw part in concrete is rigid and fixed so that no deformation appears, e) friction between contact surfaces contributes to resistance when there is no insulation gap, f) both embedment and withdrawal resistances of the screw contribute to the lateral strength, and g) the timber layer can have up to 3 layers of different properties through which the screw penetrates.

As the screw part in concrete is assumed rigid and fixed, therefore, according to Johansen's yield theory, only the following 3 kinematic failure modes can occur out of 6 failure modes:

Mode 1) Embedment of screw in timber due to a rigid translation of screw,

Mode 2) Single plastic hinge and embedment of the screw, and

Mode 3) Double plastic hinge and embedment of the screw.

For layered timber, Mode 1 will be the same in each layer because of the rigid translation of the screw and the ultimate load will be reached when the wood yields plastically along the screw shank. Mode 2 will be realized when the plastic hinge at the interface between timber and concrete is formed and the screw rotates as a stiff member which generates embedment in timber. Mode 3 will be realized when an additional plastic hinge in the timber is formed along with the one at the interface and the screw rotates as a rigid member resulting in embedment in timber. Modes 2 and 3 will have more failure components as the embedment of the screw can extend to each of the penetrated layers. Therefore, there will be Mode 2(a, b, c) and 3(a, b, c) stating embedment in 1st, 2nd and 3rd layers respectively with a plastic hinge as the screw is assumed to penetrate three layers. As the screw part in concrete is assumed rigid and fixed, the plastic hinge will develop at the edge of the concrete surface. The input parameters for the models are insulation gap thickness (g), insertion angle of screw with respect to timber grain (α), outer thread diameter of screw (d), screw embedment length in timber (l_i), screw embedment length in insulation gap (l_g) which can be written as ($g/sin\alpha$), withdrawal strength of screw in timber ($f_{ax,i}$), embedment strength of screw in timber ($f_{h,i}$), bending yield moment capacity of the screw (M_y) and, friction between concrete and timber surface (μ). These parameters are defined as in *Figure 3.1, 3.2, 3.3 and 3.4* respectively for different failure modes.

The ultimate load-carrying capacity can be calculated as the sum of internal forces based on the equilibrium in the non-deformed state. The ultimate connection load will increase if the deformed shape of the fastener is taken into account (Bejtka & Blass, 2002). Due to the assumed rigid behaviour of the screw in concrete, at the concrete and timber interface point O, resultant axial force (F_{ax}), resultant lateral force (F_{lat}) and, the moment due to the bending of the screw (M_y) develop. Also, due to the tensile effect of the screw, a tensile force (H) acts perpendicular to the concrete surface and a resultant force (μH) acts along with the interface. Therefore, based on the equilibrium of forces at the interface between timber and concrete point O, the ultimate load for all the cases can be written as:

$$F_{un,(s,l)} = F_{ax}\cos\alpha + F_{lat}\sin\alpha + \mu(F_{ax}\,sin\,\alpha - F_{lat}\cos\alpha) = F_{ax}(\cos\alpha + \mu.sin\,\alpha) + F_{lat}(\sin\alpha - \mu.\cos\alpha) \quad [1]$$

3.2.1 *Model for Inclined Screw in Solid Timber*

In *Figure 3.1*, three possible failure modes are shown for inclined screw in solid timber with stress distribution for embedment (f_h) and withdrawal (f_{ax}). The ultimate loads for all three failure modes in solid timber are derived as shown below.

Considering the ratio (φ) of embedment and withdrawal strength as both failure modes do not occur at the same time, the axial force will be,

$$F_{ax} = f_{ax}.d.l.\varphi \quad [2]$$

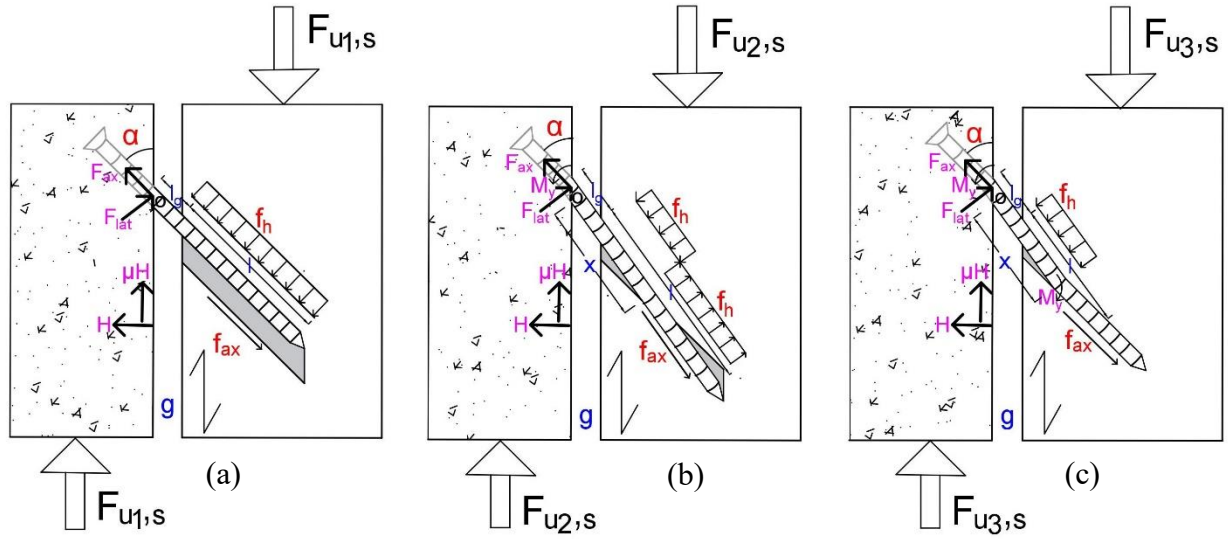

Figure 3.1: Stress distributions and forces in concrete-to-solid timber connection with an inclined screw for failure a) Mode 1, b) Mode 2, and c) Mode 3

3.2.1.1 *Mode 1: Embedment of Screw*

$$F_{lat} = f_h.d.l \quad [3]$$

Substituting equations [2] and [3] into equation [1], the ultimate load for Mode 1 is,

$$\boldsymbol{F_{u1,s}} = f_{ax}.d.l.\varphi(\cos\alpha + \mu.sin\,\alpha) + f_h.d.l(\sin\alpha - \mu.\cos\alpha) \quad [4]$$

3.2.1.2 *Mode 2: Single Plastic Hinge and Embedment of Screw*

Using the equilibrium of force and moment at point O,

$$M_y = f_h.d(x - l_g)\left(\frac{x - l_g}{2} + l_g\right) - f_h.d(l - x + l_g)\left(x + \frac{l - x + l_g}{2}\right) \quad [5]$$

Therefore, $x = \frac{1}{\sqrt{2}}\sqrt{\frac{2M_y}{f_h.d} + l_g^2 + \left(l + l_g\right)^2}$ [6]

$$F_{lat} = f_h.d\left(x - l_g\right) - f_h.d\left(l - x + l_g\right) = f_h.d\left[\sqrt{2}.\sqrt{\frac{2M_y}{f_h.d} + l_g^2 + \left(l + l_g\right)^2} - 2l_g - l\right] \quad [7]$$

Substituting equations [2] and [7] into equation [1], the ultimate load for Mode 2 is,

$$\boldsymbol{F_{u2,s}} = f_{ax}.d.l.\varphi\ (\cos\alpha + \mu.sin\,\alpha) + f_h.d(\sin\alpha - \mu.\cos\alpha)\left[\sqrt{2}.\sqrt{\frac{2M_y}{f_h.d} + l_g^2 + \left(l + l_g\right)^2} - 2l_g - l\right] \quad [8]$$

3.2.1.3 Mode 3: Double Plastic Hinge and Embedment of Screw

In the same way as the previous mode, using the equilibrium of force and moment at point O,

$$2M_y = f_h.d\left(x - l_g\right)\left(\frac{x - l_g}{2} + l_g\right) \quad [9]$$

Therefore, $x = \sqrt{\frac{4M_y}{f_h.d} + l_g^2}$ [10]

$$F_{lat} = f_h.d\left(x - l_g\right) = f_h.d\left[\sqrt{\frac{4M_y}{f_h.d} + l_g^2} - \ l_g\right] \quad [11]$$

Substituting equation [2] and [11] into equation [1], the ultimate load for Mode 3 is,

$$\boldsymbol{F_{u3,s}} = f_{ax}.d.l.\varphi\ (\cos\alpha + \mu.sin\,\alpha) + f_h.d(\sin\alpha - \mu.\cos\alpha)\left[\sqrt{\frac{4M_y}{f_h.d} + l_g^2} - \ l_g\right] \quad [12]$$

Therefore, the load-carrying capacity for the connection in solid timber will be the minimum of the ultimate loads given in equations [4], [8] and [12], ie.

$$\boldsymbol{F_{u,s} = min\{F_{u1,s}, F_{u2,s}, F_{u3,s}\}} \quad [13]$$

3.2.2 Model for Inclined Screw in Layered Timber

This model for inclined screw in concrete-to-layered timber is based on (Uibel & Blaß, 2006), where models for predicting strengths of connections containing dowel-type fastener in steel-to-layered timber were developed. In *Figure 3.2, 3.3 and 3.4,* three possible failure modes in layered timber are shown respectively. In layered timber, Mode 1 will be the same for all three penetrated layers because of the pure embedment for the stiff screw which is shown in *Figure 3.2*. However, when bending occurs in the screw, there are three sub-failure modes in the three penetrated layers for both single and double plastic hinge. It means, due to the plastic hinges, the embedment can extend to each penetrated layer as shown

in *Figure 3.3* for the single plastic hinge and in *Figure 3.4* for the double plastic hinge. The ultimate loads for all three failure modes in layered timber are derived as shown below. Considering the ratio (φ_i) of embedment and withdrawal strength as both the failure modes do not occur at the same time, the axial force will be,

$$F_{ax} = d(\varphi_1 . f_{ax1} . l_1 + \varphi_2 . f_{ax2} . l_2 + \varphi_3 . f_{ax3} . l_3) \quad [14]$$

3.2.2.1 Mode 1: Embedment of Screw

$$F_{lat} = f_{h1} . d . l_1 + f_{h2} . d . l_2 + f_{h3} . d . l_3 \quad [15]$$

Substituting equations [14] and [15] into equation [1], the ultimate load for Mode 1 is,

$$\boldsymbol{F_{u1,3l}} = d(\cos\alpha + \mu . sin\,\alpha)(\varphi_1 . f_{ax1} . l_1 + \varphi_2 . f_{ax2} . l_2 + \varphi_3 . f_{ax3} . l_3) + d(\sin\alpha - \mu . \cos\alpha)(f_{h1} . l_1 + f_{h2} . l_2 + f_{h3} . l_3) \quad [16]$$

If the screw penetrates two layers of MTP then this equation becomes,

$$\boldsymbol{F_{u1,2l}} = d(\cos\alpha + \mu . sin\,\alpha)(\varphi_1 . f_{ax1} . l_1 + \varphi_2 . f_{ax2} . l_2) + d(\sin\alpha - \mu . \cos\alpha)(f_{h1} . l_1 + f_{h2} . l_2) \quad [17]$$

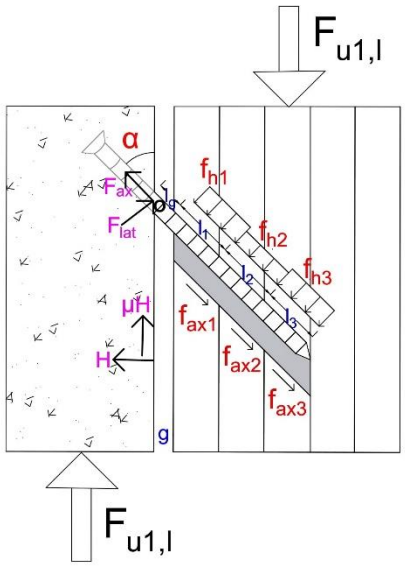

Figure 3.2: Stress distributions and forces in concrete-to-layered timber connection with an inclined screw for failure Mode 1

3.2.2.2 Mode 2a: Single Plastic Hinge and Embedment of Screw in 1st Layer

Using the equilibrium of force and moment at point O,

$$M_y = f_{h1}.d(x-l_g)\left(\frac{x-l_g}{2}+l_g\right) - f_{h1}.d(l_1-x+l_g)\left(x+\frac{l_1-x+l_g}{2}\right) - f_{h2}.d.l_2\left(\frac{l_2}{2}+l_1+l_g\right) - f_{h3}.d.l_3\left(\frac{l_3}{2}+l_1+l_2+l_g\right) \quad [18]$$

$$x = \frac{1}{\sqrt{2}}\sqrt{\frac{2M_y}{f_{h1}.d}+l_g^2+\left(l_1+l_g\right)^2+\psi_{2,1}.l_2\left(l_2+2l_1+2l_g\right)+\psi_{3,1}.l_3\left(l_3+2l_1+2l_2+2l_g\right)} \quad [19]$$

Here, $\psi_{2,1} = f_{h2}/f_{h1}$ and $\psi_{3,1} = f_{h3}/f_{h1}$

$$F_{lat} = f_{h1}.d(x-l_g) - f_{h1}.d(l-x+l_g) - f_{h2}.d.l_2 - f_{h3}.d.l_3$$

$$= f_{h1}.d\left[\sqrt{2\left[\frac{2M_y}{f_{h1}.d}+l_g^2+\left(l_1+l_g\right)^2+\psi_{2,1}.l_2\left(l_2+2l_1+2l_g\right)+\psi_{3,1}.l_3\left(l_3+2l_1+2l_2+2l_g\right)\right]}-2l_g-l_1\right] - f_{h2}.d.l_2 - f_{h3}.d.l_3 \quad [20]$$

Substituting equations [14] and [20] into equation [1], the ultimate load for Mode 2a is,

$$\boldsymbol{F_{u2a,3l}} = d(\cos\alpha+\mu.sin\,\alpha)(\varphi_1.f_{ax1}.l_1+\varphi_2.f_{ax2}.l_2+\varphi_3.f_{ax3}.l_3)+d(\sin\alpha-\mu.\cos\alpha)$$

$$\left[f_{h1}\left[\sqrt{2\left[\frac{2M_y}{f_{h1}.d}+l_g^2+\left(l_1+l_g\right)^2+\psi_{2,1}.l_2\left(l_2+2l_1+2l_g\right)+\psi_{3,1}.l_3\left(l_3+2l_1+2l_2+2l_g\right)\right]}-2l_g-l_1\right] - f_{h2}.l_2 - f_{h3}.l_3\right] \quad [21]$$

If the screw penetrates two layers of timber then the ultimate load becomes,

$$\boldsymbol{F_{u2a,2l}} = d(\cos\alpha+\mu.sin\,\alpha)(\varphi_1.f_{ax1}.l_1+\varphi_2.f_{ax2}.l_2)+d(\sin\alpha-$$

$$\mu.\cos\alpha)\left[f_{h1}\left[\sqrt{2\left[\frac{2M_y}{f_{h1}.d}+l_g^2+\left(l_1+l_g\right)^2+\psi_{2,1}.l_2\left(l_2+2l_1+2l_g\right)\right]}-2l_g-l_1\right]-f_{h2}.l_2\right] \quad [22]$$

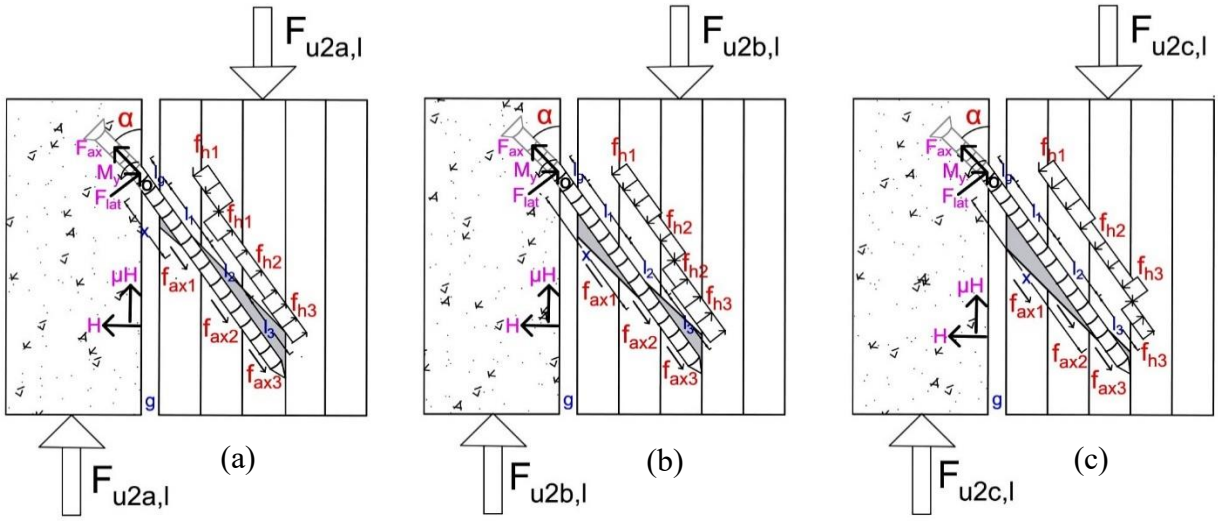

Figure 3.3: Stress distributions and forces in concrete-to-layered timber connection with an inclined screw for failure Mode 2; a) embedment in the first layer, b) embedment in the second layer and, c) embedment in the third layer due to the single plastic hinge.

3.2.2.3 *Mode 2b: Single Plastic Hinge and Embedment of Screw in 2nd Layer*

Using the equilibrium of force and moment at point O,

$$M_y = f_{h1}.d.l_1\left(\frac{l_1}{2}+l_g\right)+f_{h2}.d\left(x-l_1-l_g\right)\left(\frac{x-l_1-l_g}{2}+l_1+l_g\right)-f_{h2}.d\left(l_2-x+l_1+l_g\right)\left(x+\frac{l_2-x+l_1+l_g}{2}\right)-f_{h3}.d.l_3\left(\frac{l_3}{2}+l_1+l_2+l_g\right) \quad [23]$$

$$x=\frac{1}{\sqrt{2}}\sqrt{\frac{2M_y}{f_{h2}.d}+(l_1+l_g)^2+\left(l_2+l_1+l_g\right)^2-\psi_{1,2}.l_1\left(l_1+2l_g\right)+\psi_{3,2}.l_3\left(l_3+2l_1+2l_2+2l_g\right)} \quad [24]$$

Here, $\psi_{1,2} = f_{h1}/f_{h2}$ and $\psi_{3,2} = f_{h3}/f_{h2}$

$$F_{lat} = f_{h1}.d.l_1+f_{h2}.d\left(x-l_1-l_g\right)-f_{h2}.d\left(l_2-x+l_1+l_g\right)-f_{h3}.d.l_3$$

$$= f_{h1}.d.l_1-f_{h3}.d.l_3+ f_{h2}.d\left[\sqrt{2\left[\frac{2M_y}{f_{h2}.d}+(l_1+l_g)^2+\left(l_2+l_1+l_g\right)^2-\psi_{1,2}.l_1\left(l_1+2l_g\right)+\psi_{3,2}.l_3\left(l_3+2l_1+2l_2+2l_g\right)\right]}-2l_1-2l_g-l_2\right] \quad [25]$$

Substituting equations [14] and [25] into equation [1], the ultimate load for Mode 2b is,

$$\boldsymbol{F_{u2b,3l}} = d(\cos\alpha+\mu.sin\,\alpha)(\varphi_1.f_{ax1}.l_1+\varphi_2.f_{ax2}.l_2+\varphi_3.f_{ax3}.l_3)+d(\sin\alpha-\mu.\cos\alpha)$$

$$\left[f_{h2}\left[\sqrt{2\left[\frac{2M_y}{f_{h2}.d}+(l_1+l_g)^2+\left(l_2+l_1+l_g\right)^2-\psi_{1,2}.l_1\left(l_1+2l_g\right)+\psi_{3,2}.l_3\left(l_3+2l_1+2l_2+2l_g\right)\right]}-2l_1-2l_g-l_2\right]+f_{h1}.l_1-f_{h3}.l_3\right] \quad [26]$$

If the screw penetrates two layers of timber then the ultimate load becomes,

$$\boldsymbol{F_{u2b,2l}} = d(\cos\alpha+\mu.sin\,\alpha)(\varphi_1.f_{ax1}.l_1+\varphi_2.f_{ax2}.l_2)+d(\sin\alpha-\mu.\cos\alpha)\left[f_{h2}\left[\sqrt{2\left[\frac{2M_y}{f_{h2}.d}+(l_1+l_g)^2+\left(l_2+l_1+l_g\right)^2-\psi_{1,2}.l_1\left(l_1+2l_g\right)\right]}-2l_1-2l_g-l_2\right]+f_{h1}.l_1\right] \quad [27]$$

3.2.2.4 *Mode 2c: Single Plastic Hinge and Embedment of Screw in 3rd Layer*

Using the equilibrium of force and moment at point O,

$$M_y = f_{h1}.d.l_1\left(\frac{l_1}{2}+l_g\right)+f_{h2}.d.l_2\left(\frac{l_2}{2}+l_1+l_g\right)+f_{h3}.d\left(x-l_2-l_1-l_g\right)\left(\frac{x-l_2-l_1-l_g}{2}+l_1+l_2+l_g\right)-f_{h3}.d\left(l_3-x+l_1+l_2+l_g\right)\left(x+\frac{l_3-x+l_1+l_2+l_g}{2}\right) \quad [28]$$

$$x=\frac{1}{\sqrt{2}}\sqrt{\frac{2M_y}{f_{h3}.d}+(l_1+l_2+l_g)^2+\left(l_1+l_2+l_3+l_g\right)^2-\psi_{1,3}.l_1\left(l_1+2l_g\right)+\psi_{2,3}.l_2\left(l_2+2l_1+2l_g\right)} \quad [29]$$

Here, $\psi_{1,3} = f_{h1}/f_{h3}$ and $\psi_{2,3} = f_{h2}/f_{h3}$

$$F_{lat} = f_{h1}.d.l_1+f_{h2}.d.l_2+f_{h3}.d\left(x-l_2-l_1-l_g\right)-f_{h3}.d\left(l_3-x+l_1+l_2+l_g\right)$$

$$= f_{h1}.d.l_1 + f_{h2}.d.l_2 +$$
$$f_{h3}.d\left[\sqrt{2\left[\frac{2M_y}{f_{h3}.d}+(l_1+l_2+l_g)^2+\left(l_1+l_2+l_3+l_g\right)^2-\psi_{1,3}.l_1\left(l_1+2l_g\right)+\psi_{2,3}.l_2\left(l_2+2l_1+2l_g\right)\right]}-2l_1-\right.$$
$$\left.2l_2-2l_g-l_3\right] \quad [30]$$

Substituting equations [14] and [30] into equation [1], the ultimate load for Mode 2c is,

$$\boldsymbol{F_{u2c,3l}} = d(\cos\alpha+\mu.sin\,\alpha)(\varphi_1.f_{ax1}.l_1+\varphi_2.f_{ax2}.l_2+\varphi_3.f_{ax3}.l_3)+d(\sin\alpha-\mu.\cos\alpha)$$
$$\left[f_{h3}\left[\sqrt{2\left[\frac{2M_y}{f_{h3}.d}+(l_1+l_2+l_g)^2+\left(l_1+l_2+l_3+l_g\right)^2-\psi_{1,3}.l_1\left(l_1+2l_g\right)+\psi_{2,3}.l_2\left(l_2+2l_1+2l_g\right)\right]}-2l_1-\right.\right.$$
$$\left.\left.2l_2-2l_g-l_3\right]+f_{h1}.l_1+f_{h2}.l_2\right] \quad [31]$$

If the screw penetrates only two layers of timber, then this mode would not occur.

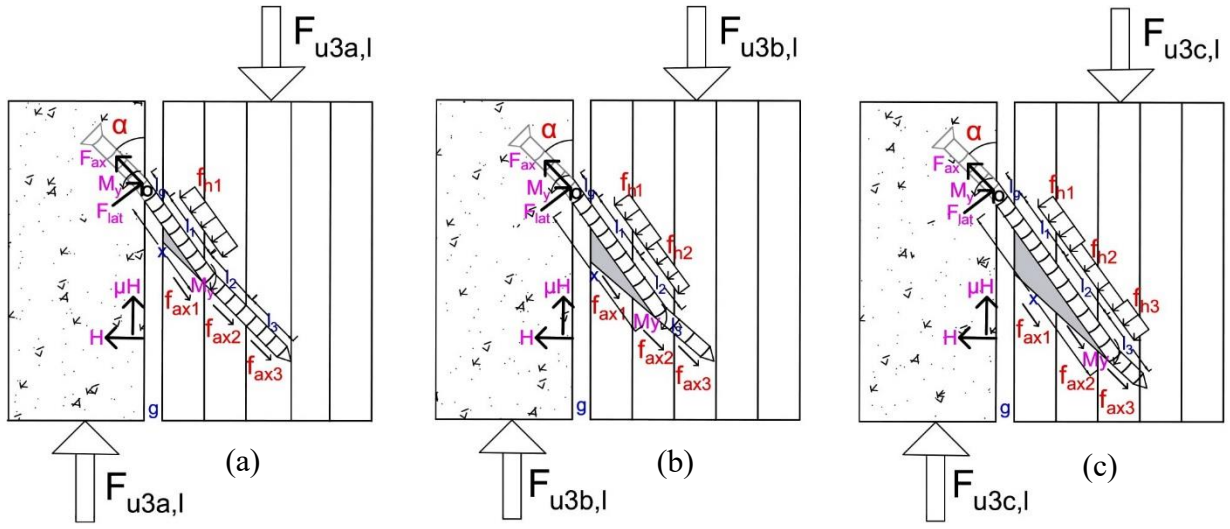

Figure 3.4: Stress distributions and forces in concrete-to-layered timber connection with an inclined screw for failure Mode 3; a) embedment in the first layer, b) embedment in the second layer and, c) embedment in the third layer due to the double plastic hinge.

3.2.2.5 *Mode 3a: Double Plastic Hinge and Embedment of Screw in 1st Layer*

In the same way as the previous mode, using the equilibrium of force and moment at point O,

$$2M_y = f_{h1}.d(x-l_g)\left(\frac{x-l_g}{2}+l_g\right) \quad [32]$$

Therefore, $x = \sqrt{\frac{4M_y}{f_{h1}.d}+l_g^2}$ [33]

$$F_{lat} = f_{h1}.d(x-l_g) = f_{h1}.d\left[\sqrt{\frac{4M_y}{f_{h1}.d}+l_g^2}-\ l_g\right] \quad [34]$$

Substituting equations [14] and [34] into equation [1], the ultimate load for Mode 3a is,

$$\boldsymbol{F_{u3a,3l}} = d(\cos\alpha + \mu.sin\,\alpha)(\varphi_1.f_{ax1}.l_1 + \varphi_2.f_{ax2}.l_2 + \varphi_3.f_{ax3}.l_3) + f_{h1}.d(\sin\alpha - \mu.\cos\alpha)\left[\sqrt{\frac{4M_y}{f_{h1}.d} + l_g^2} - l_g\right] \quad [35]$$

If the screw penetrates two layers of timber, then the ultimate load becomes,

$$\boldsymbol{F_{u3a,2l}} = d(\cos\alpha + \mu.sin\,\alpha)(\varphi_1.f_{ax1}.l_1 + \varphi_2.f_{ax2}.l_2) + f_{h1}.d(\sin\alpha - \mu.\cos\alpha)\left[\sqrt{\frac{4M_y}{f_{h1}.d} + l_g^2} - l_g\right] \quad [36]$$

3.2.2.6 Mode 3b: Double Plastic Hinge and Embedment of Screw in 2nd Layer

Again, using the equilibrium of force and moment at point O,

$$2M_y = f_{h1}.d.l_1\left(\frac{l_1}{2} + l_g\right) + f_{h2}.d(x - l_1 - l_g)\left(\frac{x - l_1 - l_g}{2} + l_1 + l_g\right) \quad [37]$$

Therefore, $x = \sqrt{\frac{4M_y}{f_{h2}.d} + (l_1 + l_g)^2 - \psi_{1,2}.l_1(l_1 + 2l_g)}$ [38]

$$F_{lat} = f_{h1}.d.l_1 + f_{h2}.d(x - l_1 - l_g) = f_{h1}.d.l_1 + f_{h2}.d\left[\sqrt{\frac{4M_y}{f_{h2}.d} + (l_1 + l_g)^2 - \psi_{1,2}.l_1(l_1 + 2l_g)} - l_1 - l_g\right] \quad [39]$$

Substituting equation [14] and [39] into equation [1], the ultimate load for Mode 3b is,

$$\boldsymbol{F_{u3b,3l}} = d(\cos\alpha + \mu.sin\,\alpha)(\varphi_1.f_{ax1}.l_1 + \varphi_2.f_{ax2}.l_2 + \varphi_3.f_{ax3}.l_3) + d(\sin\alpha - \mu.\cos\alpha)\left[f_{h1}.l_1 + f_{h2}.\left[\sqrt{\frac{4M_y}{f_{h2}.d} + (l_1 + l_g)^2 - \psi_{1,2}.l_1(l_1 + 2l_g)} - l_1 - l_g\right]\right] \quad [40]$$

If the screw penetrates two layers of timber, then the ultimate load becomes,

$$\boldsymbol{F_{u3b,2l}} = d(\cos\alpha + \mu.sin\,\alpha)(\varphi_1.f_{ax1}.l_1 + \varphi_2.f_{ax2}.l_2) + d(\sin\alpha - \mu.\cos\alpha)\left[f_{h1}.l_1 + f_{h2}.\left[\sqrt{\frac{4M_y}{f_{h2}.d} + (l_1 + l_g)^2 - \psi_{1,2}.l_1(l_1 + 2l_g)} - l_1 - l_g\right]\right] \quad [41]$$

3.2.2.7 Mode 3c: Double Plastic Hinge and Embedment of Screw in 3rd Layer

Again, using the equilibrium of force and moment at point O,

$$2M_y = f_{h1}.d.l_1\left(\tfrac{l_1}{2} + l_g\right) + f_{h2}.d.l_2\left(\tfrac{l_2}{2} + l_1 + l_g\right) + f_{h3}.d(x - l_1 - l_2 - l_g)\left(\tfrac{x - l_1 - l_2 - l_g}{2} + l_1 + l_2 + l_g\right) \quad [42]$$

Therefore, $x = \sqrt{\frac{4M_y}{f_{h3}.d} + (l_1 + l_2 + l_g)^2 - \psi_{1,3}.l_1(l_1 + 2l_g) - \psi_{2,3}.l_2(l_2 + 2l_1 + 2l_g)}$ [43]

$$F_{lat} = f_{h1}.d.l_1 + f_{h2}.d.l_2 + f_{h3}.d(x - l_1 - l_2 - l_g)$$

$$= f_{h3}.d\left[\sqrt{\frac{4M_y}{f_{h3}.d} + (l_1 + l_2 + l_g)^2 - \psi_{1,3}.l_1(l_1 + 2l_g) - \psi_{2,3}.l_2(l_2 + 2l_1 + 2l_g)} - l_1 - l_2 - l_g\right] + f_{h1}.d.l_1 + f_{h2}.d.l_2 \quad [44]$$

Substituting equations [14] and [44] into equation [1], the ultimate load for Mode 3c is,

$$\boldsymbol{F_{u3c,3l}} = d(\cos\alpha + \mu.sin\,\alpha)(\varphi_1.f_{ax1}.l_1 + \varphi_2.f_{ax2}.l_2 + \varphi_3.f_{ax3}.l_3) +$$

$$d(\sin\alpha - \mu.\cos\alpha)\left[f_{h3}\left[\sqrt{\frac{4M_y}{f_{h3}.d} + (l_1 + l_2 + l_g)^2 - \psi_{1,3}.l_1(l_1 + 2l_g) - \psi_{2,3}.l_2(l_2 + 2l_1 + 2l_g)} - l_1 - l_2 - l_g\right] + f_{h1}.l_1 + f_{h2}.l_2\right] \quad [45]$$

If the screw penetrates only two layers, this mode will not occur.

Therefore, the load-carrying capacity for the screw penetrating three layers of timber will be,

$$\boldsymbol{F_{u,3l} = min\{F_{u1,3l}, F_{u2a,3l}, F_{u2b,3l}, F_{u2c,3l}, F_{u3a,3l}, F_{u3b,3l}, F_{u3c,3l}\}} \quad [46]$$

And, the load-carrying capacity for the screw penetrating two layers of timber will be,

$$\boldsymbol{F_{u,2l} = min\{F_{u1,2l}, F_{u2a,2l}, F_{u2b,2l}, F_{u3a,2l}, F_{u3b,2l}\}} \quad [47]$$

In case of connections where screw pairs are crosswise applied, one loaded in tension and one in compression, so far no detailed approach was developed. As there is no significant difference between tension and compression (Bejtka, 2005), the capacity of one screw can be doubled, while any friction in the contact surface can be neglected. This is because in the cross-pair arrangement, tension and compression forces cancel each other and technically eliminate friction (Tomasi, et al., 2010) (Bejtka & Blass, 2001) (Marchi, et al., 2017).

3.3 Validation of Analytical Model

Material tests such as embedment of the screw in timber, withdrawal of the screw from timber, yield moment of the screw, tensile strength of the screw, and withdrawal of the screw from concrete are presented in this section, to provide material property input into the developed analytical models. The prediction results are then compared with the connection test results (Mirdad & Chui, 2019), as a mean to validate the models.

3.3.1 Material Test

3.3.1.1 Embedment Test

Wood embedment tests of the screw at various angles to the wood grain were performed according to the half-hole test procedure in ASTM D5764-97a (ASTM , 2013), to evaluate the embedment strength. Fully-threaded self-tapping screw of 11 mm diameter (Rothoblaas, 2019b) was tested in five different angles (0°, 30°, 45°, 60° and 90°) relative to the timber grain with 5 replicates each. The dimensions of the wood specimens were 50 mm x 50 mm x 50 mm according to the minimum specification in ASTM D5764-97a (ASTM , 2013). These pieces were cut from the same source of laminated timber used in the connection tests, ie. Spruce-Pine-Fir (S-P-F) lumber. The tests were conducted at a constant displacement rate of 1.0 mm/min. The load and displacement were recorded during the tests and acquired data were analyzed in accordance with ASTM D5764-97a (ASTM , 2013). The bearing yield load was determined by establishing the stiffness by linear regression. The linear regression line was then shifted by a deformation equal to 5% of the screw diameter. The bearing yield load can be found at the intersection of the shifted stiffness regression line and the actual load-deformation curve. If the shifted stiffness regression line does not intersect with the load-deformation curve the maximum load was used as the yield load. The mean density of the wood was 424 kg/m^3 and the mean moisture content was 9.4%.

Table 3.1: Embedment strength of SPF timber under 11mm diameter screw

Angle	Mean Strength, N/mm^2	CoV, %
0°	8.83	20.5
30°	11.49	11.4
45°	13.45	8.0
60°	14.75	14.3
90°	15.61	5.4

The embedment strength according to (Kennedy, 2014) was calculated using the following equation,

$$f_{h,k} = \frac{F_{yield}}{d.t} \quad [48]$$

where F_{yield} is the yield load, d is the outer diameter of screw and t is the width of the specimen. Tested embedment strength is shown in *Table 3.1*, where embedment strength increases with the increase of grain angle. The Coefficient of Variation (CoV) for test strength is within a range of 5-20%.

3.3.1.2 Withdrawal Test

Withdrawal test of the screw into the timber at a various angle to the grain was performed according to the procedure in EN 1382 (EN 1382, 1999), to evaluate the withdrawal strength. Fully-threaded self-tapping screw with 11 mm diameter (Rothoblaas, 2019b) was tested in five different angles (0°, 30°, 45°, 60° and 90°) relative to the timber grain and two penetration length (80 mm and 100 mm) with 5 replicates each. The dimensions of the wood specimens were 450 mm x 150 mm x 150 mm according to the minimum specification stated in EN 1382 (EN 1382, 1999), where three screws were placed on one side at 10d spacing and two on the opposite side. These pieces were cut from the same source of laminated timber used in the connection tests. The tests were conducted at a constant displacement rate of 1.5 mm/min. The load and displacement were recorded during the tests and the maximum load was taken from the curve to calculate the withdrawal strength. The mean density of the wood was 429 kg/m^3 and the mean moisture content was 8.3%.

Table 3.2: Withdrawal strengths of 11mm diameter screw from SPF timber

Angle	Penetration Length, mm	Mean Strength, N/mm^2	CoV, %
0°	80	5.74	7.0
30°	80	6.16	8.1
45°	80	7.06	5.2
60°	80	6.19	3.8
90°	80	6.42	17.1
0°	100	5.68	11.3
30°	100	6.38	13.8
45°	100	6.92	3.2
60°	100	6.89	3.1
90°	100	6.51	5.4

The withdrawal strength according to (Ringhofer, 2017) was calculated using the following equation,

$$f_{ax,k} = \frac{F_{max}}{\pi.d.l_{ef}} \quad [49]$$

where F_{max} is the maximum load, d is the thread diameter of the screw and l_{ef} is the effective penetration length which is equal to (L – 10 mm) according to (ETA-Danmark, 2016).

Tested withdrawal strengths are shown in *Table 3.2*, where, higher strength can be seen at 45° angle to the grain in both penetration lengths. The Coefficient of Variation (CoV) for the test strength is within a range of 3-17%.

3.3.1.3 Screw Yield Moment Test

Yield moment of a fastener is defined as the moment at which the entire cross-section has reached its yield stress. This is theoretically the maximum bending moment that the section can resist. When this point is reached, a plastic hinge is formed and any load beyond this point will result in theoretically infinite plastic deformation. Bending yield moment test was performed on the 11 mm diameter (Rothoblaas, 2019b) self-tapping screw with 5 replicates according to ASTM F1575 (ASTM , 2017). The tests were conducted at a constant displacement rate of 1.5 mm/min. The load and displacement were recorded during the tests and acquired data were analyzed in accordance with ASTM F1575 (ASTM , 2017). The bending yield moment is determined by fitting a straight line to the initial linear portion of the load-deformation curve, offsetting this line by a deformation equal to 5% of the screw diameter, and selecting the load at which the offset line intersects the load-deformation curve. According to ASTM F1575 (ASTM , 2017), the yield moment and yield strength are calculated using the following equations,

$$M_y = \frac{P.s_{bp}}{4} \quad [50]$$

$$F_{yb} = \frac{6M_y}{d^3} \quad [51]$$

where, P is the yield load, s_{bp} is cylindrical bearing point spacing equal to 11.5d, and d is core diameter of the screw.

The calculated yield moment, as well as yield strength, are shown in *Table 3.3*.

Table 3.3: Mechanical properties of 11 mm diameter Self-Tapping Screw

Property	Symbol, Unit	Mean	COV, %
Yield Moment	$M_{y,k,}$ kN.mm	80.58	7.7
Yield Strength	$f_{y,k,}$ N/mm^2	1059	7.7
Tensile Strength	$f_{tens,k,}$ N/mm^2	451.1	0.5

3.3.1.4 Tension Test

Tension test of the self-tapping screw was performed to obtain the tensile strength of the screw according to ASTM E8/E8M-16a (ASTM , 2016). The tests were conducted at a constant displacement rate of 0.5 mm/min. The load and displacement were recorded during the test and the peak load per cross-sectional area was taken as the tensile strength of the screw which is shown in *Table 3.*3. The modulus of elasticity

of the screw was reported to be 210 GPa (ETA-Danmark, 2016). Tensile failure of the screw will not govern in the case with inclined timber-concrete joint because of dominant withdrawal force from wood. Here, the tensile strength for 11 mm diameter self-tapping screw is significantly higher than the withdrawal strength of screw in timber and therefore, tensile failure of the screw will not govern.

3.3.1.5 Withdrawal Test in Concrete

Withdrawal test of the screw in concrete was performed to check the concrete cone effect based on Concrete Capacity Method (CCM) for 30° cone (Hlavicˇka & Lublóy, 2018) (Shirvani, 1998) (ACI, 1985) (CSA , 2014) (ACI, 2008) which may influence the concrete cracking behaviour. According to CSA A23.3 (CSA , 2014), concrete breakout resistance of screw in tension for a single screw can be checked with the following equation,

$$N_{cc} = \left(\frac{A_{Nc}}{A_{Nco}}\right) k_c . \lambda_a . \sqrt{f_c'} . h_{ef}^{1.5} . R . \varphi_{ed,N} . \varphi_{c,N} . \varphi_{cp,N} \text{ (kN)} \quad [52]$$

where, k_c is 1 for cast in headed screw, λ_a is 1 for normal weight concrete, R is 1 for no supplementary reinforcement, f'_c is concrete compressive strength, h_{ef} is the effective height of screw in concrete. A_{Nco} is equal to $9h_{ef}^2$ which is the projected concrete failure area of a single anchor with an edge distance equal to or greater than $1.5h_{ef}$. A_{Nc} is 1 for $c_{a,min}$ greater than $1.5h_{ef}$ and, actual area for $c_{a,min}$ smaller than $1.5h_{ef}$, which is the projected concrete failure area of a single anchor for calculation of resistance in tension. Here, $c_{a,min}$ is the minimum distance from centre of an anchor shaft to the edge of concrete. $\varphi_{cp,N}$ is 1 for cast in headed screws and $\varphi_{c,N}$ is 1.25 for no cracking at service load at cast in headed screw. $\varphi_{ed,N}$ is 1 for $c_{a,min}$ greater than $1.5h_{ef}$ and $[0.7+0.3(c_{a,min}/1.5h_{ef})]$ for $c_{a,min}$ smaller than $1.5h_{ef}$.

For the cast in headed screw of 70 mm embedment in 39 MPa concrete (150 mm x 130 mm) block, the withdrawal strength using equation [52] was found to be 17.91 kN and the mean withdrawal strength for 3 replicates was found to be 17.8 kN. Similarly, the penetration length of the screw in the concrete portion was checked carefully to prevent breaking of concrete in the specimen before casting as well as during the validation of the models. If the withdrawal strength of screw in concrete is lower than the withdrawal strength in timber, then concrete will crack. The cracking of concrete check is shown in *Table 3.6*.

3.3.2 Connection Test

Lateral load tests (Mirdad & Chui, 2019) were conducted on 24 groups of connection specimens with 3 replicates for each. The 24 combinations covered different timber member, screw angle of insertion, screw penetration length and insulation thickness while keeping the screw diameter and concrete thickness constant. The investigation parameters have been described in (Mirdad & Chui, 2019). Standard profile Glue Laminated Timber (GLT) (Western Archrib, 2019) was used which was 175 mm thick and made of # 2-grade Spruce-Pine-Fir (S-P-F) lumber. The measured density was 455 kg/m^3 with an average moisture content of 8.3%. Five-ply E1 grade Cross Laminated Timber (CLT) (Nordic Structures, 2019) with a 175 mm total thickness was used in this study, which has 1950f_b-1.7E S-P-F machine stress rated (MSR) lumber in longitudinal and No. 3/Stud S-P-F lumber in transverse layers. The measured average density of the CLT was 504 kg/m^3. The average moisture content of the wood during the test was found to be 8.3%. Fully threaded self-tapping screw (Rothoblaas, 2019b) of 11 mm diameter was used in the shear test, with a countersunk head and self-drilling tip. The acoustic material (RothoBlaas, 2019a) used in this study was a sound-proofing layer made of polyester felt and elasto-plastomer bitumen. Normal weight concrete of 75 mm thickness with an average compressive strength of 39 MPa at 28 days was used. The test procedure was according to EN 26891:1991 (EN 26891, 1991) and the test setup is shown in *Figure 3.5*.

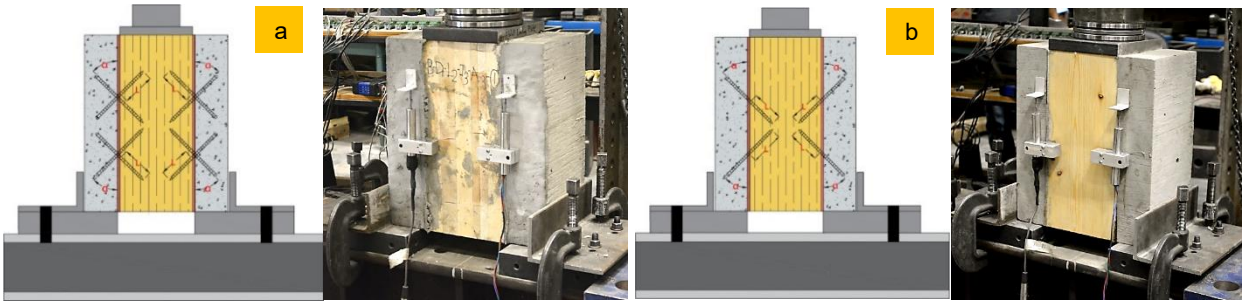

Figure 3.5: a) Screw orientation with horizontal cross-pair (H-X) and typical test setup of CLT specimen with H-X, and b) Screw orientation with vertical cross-pair (V-X) and typical test setup of GLT specimen with V-X

3.3.3 Model Validation

The mean connection test results are shown in *Figure 3.6 and Figure 3.7* for screws in GLT and CLT respectively. In the coding of the test groups, L# refers to the penetration length of the screw into MTP, I# refers to the insulation thickness, and #° refers to the insertion angle of the screw to the timber grain, which can be seen in *Figure 3.5*. The connection test result shows that screws at an insertion angle of 30° have a higher strength along with a larger penetration length compared to the screws at a 45° angle and smaller penetration length. Overall, 5-15% and 22-34% reduction in strength were noticed for an insulation thickness of 5 mm and 15 mm respectively. Screws in CLT showed higher strength than GLT with different failure modes in the presence of an insulation layer.

The analytical models were validated using the material properties data shown in *Table 3.1, Table 3.2 and Table 3.3*. These calculated material properties were used to validate the analytical models described in Section 3.2. In Figure 3.6 and Figure 3.7, the predictions from analytical models are compared to connection test data from (Mirdad & Chui, 2019). In GLT, where the screw penetrates as in solid timber, equation [13] was used and compared with connection test data. Also, in the connection test where screw penetrates in CLT which is a layered timber, equation [47] was used because screw penetrates only two layers. In the connection test, crossed-pairs of the screw was used in the horizontal and vertical direction which are shown in *Figure 3.5* and therefore, the ultimate load-carrying capacity of the single screw was multiplied by 2, to obtain the strength in cross-pair and any friction in the contact surface was ignored according to (Bejtka, 2005). For 30° angled screw, the embedment and withdrawal properties of 60° was used because the screw was actually at 60° to the wood grain. In the case of CLT, when screw penetrates in the transverse layer, the embedment and withdrawal properties of 90° was used for a similar reason as stated before. Also, the ability of the developed models to predict accurately the failure modes in GLT and CLT connections can be seen in *Table 3.4 and Table 3.5* respectively. In the tables, SH refers to single hinge, DH refers to double hinge and CC refers to concrete crushing.

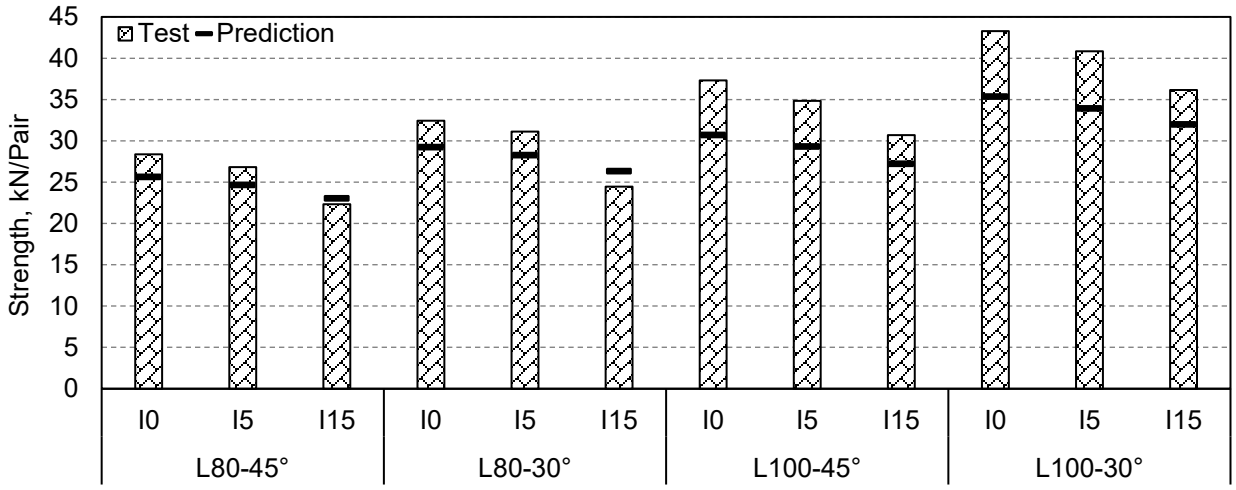

Figure 3.6: Comparison of GLT connection test strengths with predicted strengths using material property testing

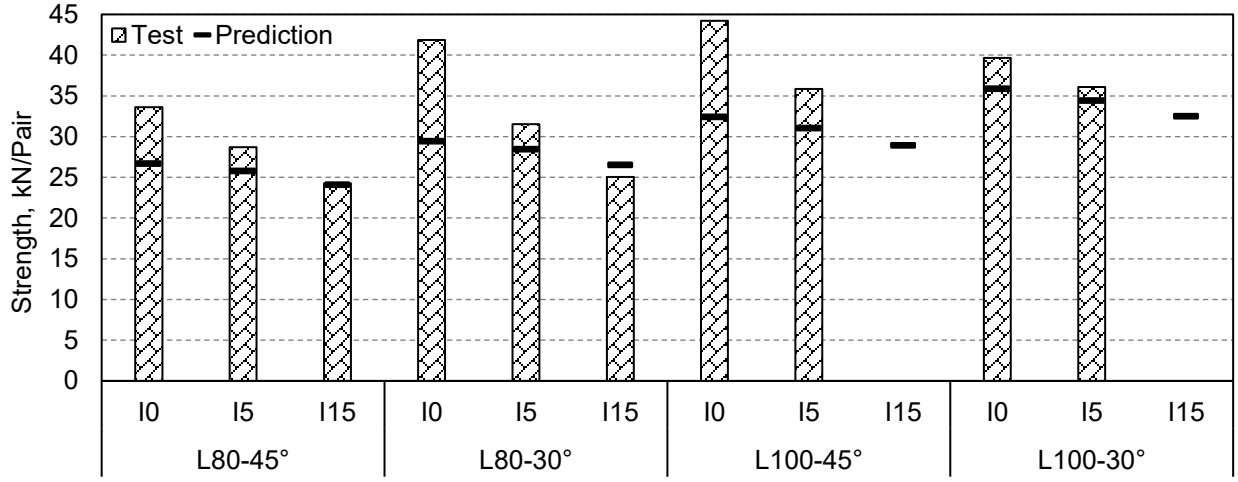

Figure 3.7: Comparison of CLT connection test strengths with predicted strengths using material property testing

As can be seen in *Figure 3.6*, with test material properties, the predicted connection strength in GLT was found to be 14% less when there was no insulation, 13% less for 5 mm insulation and 3% less for 15 mm insulation respectively. Overall, for GLT, it can be concluded that the analytical model can predict on average within 10% of the test strength. For CLT the predicted connection strength was found to be 22% less for no insulation, 10% for 5 mm insulation, and 2% more in 15 mm insulation using tested material properties, as can be seen in *Figure 3.7*. On average the predicted strength is within about 12% of the

test strength. In general, the model predictions agree better with test strength for GLT than for CLT. In addition, the discrepancy gets smaller as the insulation gap size increases.

Table 3.4: Connection strength comparison in GLT

Configuration in GLT	F_u/pair, kN	Failure Mode[a]	F_u/Screw, kN	$F_{u1,s}$, kN	$F_{u2,s}$, kN	$F_{u3,s}$, kN	$F_{u,s}$, kN	Error
L80-I0-45°	28.37	SH	14.18	16.73	**12.80**	13.25	12.80	+10%
L80-I5-45°	26.84	SH + CC	13.42	16.73	**12.33**	12.57	12.33	+8%
L80-I15-45°	22.32	DH + CC	11.16	16.73	11.62	**11.51**	11.51	-3%
L80-I0-30°	32.42	SH	16.21	17.73	**14.62**	14.86	14.62	+10%
L80-I5-30°	31.11	SH	15.56	17.73	**14.13**	14.14	14.13	+9%
L80-I15-30°	24.47	DH	12.23	17.73	13.46	**13.17**	13.17	-8%
L100-I0-45°	37.31	DH	18.66	20.92	15.58	**15.34**	15.34	+18%
L100-I5-45°	34.84	DH + CC	17.42	20.92	15.13	**14.66**	14.66	+16%
L100-I15-45°	30.69	DH + CC	15.34	20.92	14.41	**13.60**	13.60	+11%
L100-I0-30°	43.27	DH	21.64	22.17	17.97	**17.67**	17.67	+18%
L100-I5-30°	40.83	DH	20.42	22.17	17.50	**16.95**	16.95	+17%
L100-I15-30°	36.16	DH	18.08	22.17	16.80	**15.98**	15.98	+12%

[a] SH: Single Hinge; DH: Double Hinge; CC: Concrete Crushing; Bold: Governing Values

Table 3.5: Connection strength comparison in CLT

Configuration in CLT	F_u/pair, kN	Failure Mode[a]	F_u/Screw, kN	$F_{u1,2l}$, kN	$F_{u2a,2l}$, kN	$F_{u2b,2l}$, kN	$F_{u3a,2l}$, kN	$F_{u3b,2l}$, kN	$F_{u,2l}$, kN	Error
L80-I0-45°	33.61	SH + CC	16.81	17.76	**13.33**	14.15	13.76	13.76	13.33	+21%
L80-I5-45°	28.70	SH	14.35	17.76	**12.88**	13.83	13.08	13.09	12.88	+10%
L80-I15-45°	24.27	DH + CC	12.14	17.76	12.18	13.33	**12.03**	12.08	12.03	+1%
L80-I0-30°	41.88	SH	20.94	17.86	**14.71**	17.19	14.94	14.97	14.71	+30%
L80-I5-30°	31.55	SH	15.77	17.86	**14.22**	17.07	14.23	14.27	14.22	+10%
L80-I15-30°	25.04	DH	12.52	17.86	13.55	16.91	**13.25**	13.33	13.25	-6%
L100-I0-45°	44.23	DH + CC	22.12	22.62	16.41	16.54	**16.19**	16.19	16.19	+27%
L100-I5-45°	35.85	DH	17.93	22.62	15.98	16.07	**15.51**	15.52	15.51	+13%
L100-I15-45°	----	----	----	22.62	15.29	15.33	**14.45**	14.51	14.45	----
L100-I0-30°	39.66	DH	19.83	22.56	18.24	19.68	**17.92**	17.95	17.92	+10%
L100-I5-30°	36.07	DH	18.04	22.56	17.77	19.45	**17.19**	17.25	17.19	+5%
L100-I15-30°	----	----	----	22.56	17.07	19.10	**16.22**	16.31	16.22	----

[a] SH: Single Hinge; DH: Double Hinge; CC: Concrete Crushing; Bold: Governing Values

During the validation, it was found that the actual failure modes in the connection tests matched with the failure modes predicted by the analytical models. In the connection test with 80 mm penetration length, the single plastic hinge was observed in 0 mm and 5 mm insulation, while double plastic hinge was noticed in 15 mm insulation, *Figure 3.8*. From *Table 3.4 and Table 3.5*, the double plastic hinge failure mode occurred in all connections with 100mm penetration length for both GLT and CLT. Therefore, using the matched material properties determined from testing, the developed models are capable of predicting the failure modes accurately. The percent reduction in strength due to the insulation gap also shows

consistent results with the models. Also, the influence of friction in the cross-pair screw connections seemed minor and can be ignored in the analytical model.

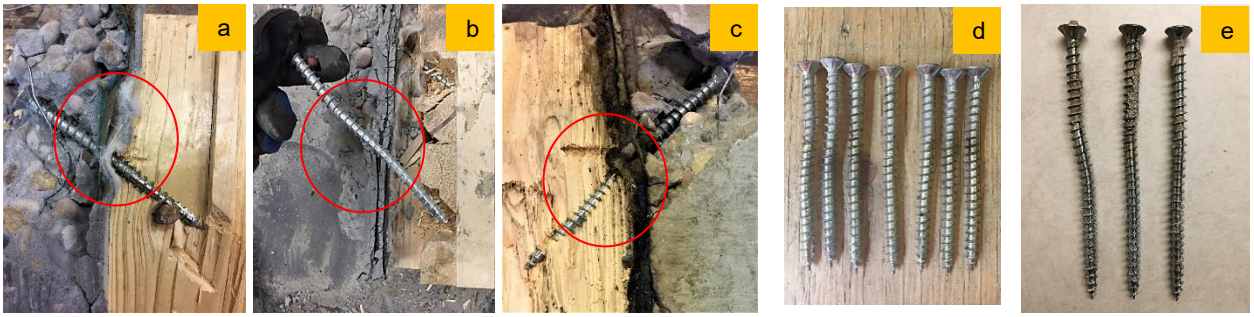

Figure 3.8: Failure modes in tested specimen; a) single plastic hinge in GLT with 80 mm embedment, b) double plastic hinge in CLT with 100 mm embedment, c) double plastic hinge in GLT with 100 mm embedment, d) single and double hinge in 80 mm embedded screw, and e) double hinge in 100 mm embedded screw

Table 3.6: Concrete breakout resistance

Configuration	Effective Length, mm	Breakout Resistance, N/mm²	Withdrawal Strength, N/mm²
L80-I0-45°	70.0	9.84	7.06
L80-I5-45°	62.9	9.96	7.06
L80-I15-45°	48.8	9.84	7.06
L80-I0-30°	70.0	9.84	6.19
L80-I5-30°	60.0	9.92	6.19
L80-I15-30°	40.0	9.90	6.19
L100-I0-45°	100.0	7.97	6.92
L100-I5-45°	92.9	8.58	6.92
L100-I15-45°	78.8	9.46	6.92
L100-I0-30°	100.0	7.97	6.89
L100-I5-30°	90.0	8.87	6.89
L100-I15-30°	70.0	9.84	6.89

In the connection test, concrete failure governed in 7 configurations out of total 24 configurations with 45° angle, which are shown in *Table 3.4 and Table 3.5*. The cracking was neither a uniform crack nor a local crack due to the non-uniform bearing of concrete on the support. In the analytical model, if the tensile strength of screw in concrete is lower than the withdrawal strength of the screw in timber, then concrete failure would govern. Although, the embedment of screw in the concrete was checked carefully during designing of the specimens to control concrete pull-out (cone effect), crushing occurred due to the higher shear angle (45°) of the screw to the surface of concrete, leading to 'lifting' (pull-push situation of cross-pair screws) of concrete when the side member was under load. In cross-pair, one screw was in shear

tension while another screw was in shear compression. The tension screw pulled the screw from concrete while the compression screw pushed concrete. If the screw was only in tension, the cracking would not govern with the penetration length used in the tests, which was checked for the cone effect and shown in *Table 3.6*. For the screw in compression at a larger shear angle (45°), the concrete cracking would likely occur due to the pushing of screw to concrete. In *Table 3.6*, concrete breakout resistance check has been shown using equation [52] and compared with the withdrawal strength of screw in timber. From the result, it can be found that the concrete pull-out resistance in all configuration is higher than the withdrawal strength of the screw in timber, and therefore, the effective length is enough for resisting pull-out of concrete. As a result, using the concrete breakout resistance formula described earlier, cannot predict concrete failure accurately. Although, the effective penetration length of the screw in concrete might be sufficient to resist the pull-out of the concrete, but cracking can happen due to the pushing of concrete by the compression screw when cross-pair screws are used, which can only be controlled by increasing the concrete thickness.

3.4 Conclusions

Analytical models for predicting timber-to-concrete connection strength with inclined screws and an insulation gap are presented in this study for solid and layered timber based on the extended Johansen's yield theory. The models are sub-divided with all possible failure modes. An extensive range of material test data is presented. These material properties were used as input into the developed models to predict the strengths of self-tapping screw connections tested in an earlier study. The predictive capability of the developed models is evaluated by comparing the predictions with connection test results.

It was found that on average, the developed models predict within 10% of connection strengths for solid timber and 12% for layered timber. The failure modes were also accurately predicted by the models except the cracking of the concrete, which was not an input parameter in the models and special care is required to mitigate this cracking during test. As was observed by previous researchers, the strengths of connections with inclined screws are influenced significantly by the screw withdrawal and embedment strengths. Also, the contribution of interfacial friction in cross-pair configuration seemed insignificant.

Chapter 4. Connection Stiffness Prediction Model

Journal Paper #3

Stiffness Prediction of Mass Timber Panel-Concrete Composite Connection with Inclined Screws and a Gap

by Md Abdul Hamid Mirdad and Ying Hei Chui

Published in Engineering Structures, 2020

Abstract:

An increasingly popular wood composite floor system consists of a Mass Timber Panel (MTP) connected to a concrete slab or topping with mechanical connectors such as Self-Tapping Screw (STS) with a sound insulation layer in between the MTP and concrete. Allowable floor span for this type of MTP-concrete composite system is often governed by serviceability performance requirements, such as deflection and vibration, which are directly dependent on the stiffness of the interlayer connection. Often tests are performed to characterize connection stiffness required for structural design. In lieu of testing, analytical models can be developed to calculate connection stiffness based on component properties. To that end, two analytical models were developed for solid and layered timber, for directly predicting the stiffness of a connection with inclined screws and an insulation layer. Usually, stiffness of laterally loaded connection is controlled by the dowel bearing effect of the fastener in timber, but inclined screw connection has a more complex behaviour due to the combined bearing and withdrawal action of the screw. In the developed models, both the bearing and withdrawal actions of the screw are considered along with the bending stiffness of the screw by applying a theoretically derived correction factor for the embedment stiffness modulus based on the beam on elastic foundation and friction between the concrete and MTP. Both models were experimentally validated with a wide range of material properties. It was found that the models are capable of predicting the stiffness of the MTP-concrete connection to within 18% of the experimental value. It was also noted that the model for solid timber panel is simpler in form and can be adopted for layered timber panel such as CLT with a small difference in solutions. Friction was found to be notable when there was no insulation gap in between timber and concrete.

4.1 Introduction

Mass Timber Panel-Concrete (MTPC) composite floor is often a preferred choice by designers in the construction of modern multi-storey mass timber buildings, due to its desirable strength and stiffness to weight ratios, span to total depth ratio, in-plane rigidity, and acoustics, thermal and fire performances, when compared with more conventional systems (Ceccotti, 2002) (Yeoh, et al., 2011). Mass Timber Panel-Concrete (MTPC) composite floor system consists of a Mass Timber Panel (MTP) connected to a reinforced concrete slab by mechanical fasteners. Such a system is structurally efficient in that the MTP primarily resists tensile stress while the concrete slab resists compressive stress generated by out-of-plane bending action, and the mechanical fasteners allow for a partial shear transfer and therefore partial composite action between the components. An insulation layer sandwiched between the timber panel and concrete slab is often provided to enhance acoustic, vibration and thermal performances. Practically this insulation layer serves as a gap and as such has a negative impact on the stiffness of the connection (Mirdad & Chui, 2019). Design and efficiency of this type of composite system are mostly governed by floor vibration serviceability performance which is largely influenced by the stiffness of this interlayer connection.

Self-Tapping Screws (STS) are widely used modern dowel-type fasteners which were developed as an improved threaded fastener for the application in large-scale timber structures as well as in the composite system such as MTPC composite. This type of screw mostly features a continuous thread over the whole length (fully-thread) which leads to a more uniform load transfer between the screw and the wood material (Dietsch & Brandner, 2015). In addition many experimental and numerical studies (Tomasi, et al., 2010) (Bejtka & Blass, 2001) (Kevarinmäki, 2002) (Bejtka & Blass, 2002) (Blass, et al., 2006) (Jockwer, et al., 2014) (Closen, 2012) have concluded that there is a substantial increase in the strength and stiffness of the STS connection if the screw is installed at an angle to the surface of the wood member, instead of normal to the surface. Laterally loaded dowel-type connections with fasteners inserted normal to member face are mostly governed by the embedment (i.e. dowel bearing) of the fastener in timber and fastener resistance to bending (yield moment) according to Johansen's yield theory (Johansen, 1949), but connections with inclined threaded fasteners have a more complex behaviour due to the combined lateral

and withdrawal action of the screw at small displacement. Laterally loaded screw connections show ductile behaviour at large displacement and low stiffness compared to axially loaded screw connection.

According to Eurocode 5 (EN 1995-1-1, 2009), the slip modulus or connection stiffness of a laterally loaded single screw joint depends on the timber properties, e.g.; mean density, ρ_m [kg/m^3], fastener diameter, d [mm], and can be expressed as,

$$k_{ser} = \rho_m^{1.5} \, d/23 \, (\mathrm{N/mm}) \qquad [1]$$

Equation [1] is valid for timber-to-timber connection and may be multiplied by 2.0 for concrete-to-timber connection according to (EN 1995-1-1, 2009). Also, this equation only considers the bearing action of the screw and therefore would underestimate the stiffness of a connection with inclined screws by a large margin due to the lack of consideration of contribution from the withdrawal action. Therefore, in order to characterize the stiffness of a connection, often testing is performed according to a standardized procedure such as EN 26891:1991 (EN 26891, 1991).

In lieu of testing, the properties of self-tapping screw connection can be estimated using mechanics-based model that accounts for component properties such as lateral (embedment) and withdrawal action of the screw and other factors such as friction and the flexibility of the screw in timber by applying a theoretically derived correction factor for the embedment stiffness modulus based on beam on elastic foundation (Hetenyi, 1983). As most types of connections are not inherently stiff, assuming a rigid behaviour of the connection in the elastic state would overestimate the performance of the composite system at service load levels (Zhang, 2013). Also, a model that only considers bearing action without friction and withdrawal properties of the screw was found to underestimate the stiffness by a large margin (Symons, et al., 2010). A model based on linear elastic beam-on-elastic foundation approach over a similar non-linear model is simpler and practical in the design application. Stiffness modeling of inclined screws in timber-to-timber joints has been addressed by a few researchers (Tomasi, et al., 2010) (Blass, et al., 2006) (Kevarinmäki, 2002) (Girhammar, et al., 2017) and of inclined screws in concrete-to-timber joints by others (Marchi, et al., 2017) (Symons, et al., 2010) (Moshiri, et al., 2014). So far, no analytical model has been presented for concrete-to-timber joints that consider inclined screws, insulation layer gap

and layered structure of the timber member. These factors necessitate the simultaneous consideration of the timber bearing, withdrawal and flexural rigidity of the screw. Earlier, two different analytical models (Mirdad & Chui, 2020a) for inclined screws in solid and layered timber with insulation layer gap were developed and experimentally validated for predicting the strength of a connection in MTPC composite system.

The aim of this research work is to introduce and experimentally validate the analytical modeling approach for predicting the stiffness of a timber-concrete connection with an inclined screw and insulation layer gap. Two different analytical models are presented for inclined screws in solid timber (where the properties of laminations are similar with similar orientation) and layered timber (where the properties of laminations are different with similar or different orientation). Also, different connection stiffness parameters are presented from material tests to predict the stiffness of the connection from the models. The model predictions are compared and validated with data from short-term connection test (Mirdad & Chui, 2019) with brief conclusions. The proposed analytical modeling approach can be applied to single screw in tension, single screw in compression and cross-paired screws (one screw in tension and one screw in compression) in the serviceability limit state and is valid when all materials are in the linear elastic range and the deformations are small. These models will facilitate the serviceability design of MTPC composite floor system with or without an insulation gap.

4.2 Analytical Models for Predicting Connection Stiffness

An analytical model for predicting the stiffness of concrete-to-timber connection with an inclined screw can be developed by accounting for the embedment, withdrawal and flexural rigidity of the screw in timber member as well as the friction at the contact surface. To develop the analytical models based on the hypotheses of (Girhammar, et al., 2017), the following assumptions can be considered: a) single screw model in shear-tension where screws are principally loaded in tension in the timber member and in shear at the connection point of timber and concrete, b) joint is under approximate linear-elastic condition at the serviceability limit state, c) screw part in concrete is rigid and fixed so that no deformation occurs, d) after applied load, screw bends as a cantilever and rotates elastically in the fixing point at the shear plane, e) flexibility of screw is considered in timber based on beam-on-elastic foundation but extensibility of screw

is neglected, f) friction between contact surfaces contributes to stiffness when there is no insulation gap, g) both embedment and withdrawal actions of the screw contribute to the stiffness, h) axial and lateral displacement of the screw in timber is considered, i) the timber layer can have up to 3 layers of different properties through which the screw penetrates, and j) additional displacement due to the gap is considered by assuming the segment of screw within the gap as a "rigid link".

After application of the loads in serviceability limit state, screw starts to bend and rotate elastically. In the presence of the gap, the initial and final positions of screw intersect each other in timber at a distance x from concrete edge. Therefore, stress distribution under embedment will be a triangular shape as shown in the *Figures 4.1-4.4*. For the layered timber, the screw intersection point in timber can be in the 1st, 2nd or 3rd penetrated layers. The input parameters for the models are insulation gap thickness (g), insertion angle of screw with respect to timber grain (α), outer thread diameter of screw (d), screw embedment length in timber (l_i), embedment stiffness ($K_{h,i}$), axial stiffness ($K_{ax,i}$), screw embedment length in insulation gap (l_g) which can be written as ($g/\sin\alpha$) and, friction between concrete and timber surface (μ).
The embedment force per unit length in each penetrated layer can be written as,

$$q_{h,i} = k_{h,i}\delta_{lat} = K_{h,i} d \delta_{lat} \quad [2]$$

where, $k_{h,i}$ [N/mm^2] is the embedment stiffness of the timber per unit length, δ_{lat} is the displacement of the screw at the surface of the timber member perpendicular to its axis and $K_{h,i}$ [N/mm^3] is the corresponding embedment stiffness per unit area. The stiffness is expressed as $k_{h,i}$ or $K_{h,i}.d$, where $K_{h,i}$ is assumed proportional to the diameter d. The embedment force per unit length is a function of embedment stiffness of the timber per unit length and the displacement of the screw perpendicular to its axis. Embedment stiffness of the timber per unit length is a constant for a given material at a certain angle. The displacement of the screw perpendicular to its axis is linear to its length or position on the screw and therefore, the embedment force per unit length has a triangular shape in *Figure 4.1-4.4*.

Similarly, the axial withdrawal force of the screw per unit length in each penetrated layer can be written as,

$$q_{ax,i} = k_{ax,i}\delta_{ax} = K_{ax,i} \pi d \delta_{ax} \quad [3]$$

where, $k_{ax,i}$ [N/mm^2] is the axial withdrawal stiffness of the screw per unit length, δ_{ax} is the displacement of the screw parallel to its axis and $K_{ax,i}$ [N/mm^3] is the corresponding effective axial withdrawal stiffness of the screw per unit area. The stiffness is thus expressed as $k_{ax,i}$ or $K_{ax,i}.\pi d$, where $K_{ax,i}$ is assumed proportional to the circumference πd. These parameters are defined as in *Figure 4.1-4.4* for different modes.

The force acting on the screw in the interface of components can be divided into axial force (F_{ax}) (withdrawal of screw) and lateral force (F_{lat}) (embedment in timber). The stiffness can be calculated as the sum of internal forces at serviceability limit state based on the equilibrium in the undeformed state. Due to the assumed rigid behaviour of the screw in concrete, at the concrete and timber interface point A, resultant axial force (F_{ax}), resultant lateral force (F_{lat}) and, the moment due to the elastic bending of the screw (M) develops. Also, due to the tensile effect of the screw, a tensile force (H) acts perpendicular to the concrete surface and a resultant force (μH) acts along with the interface. Therefore, based on the equilibrium of forces at the interface between timber and concrete point A, the serviceable load at the level of serviceability limit state for all the cases can be written as,

$$F_{n(s,l)} = F_{ax}\cos\alpha + F_{lat}\sin\alpha + \mu(F_{ax}\,sin\,\alpha - F_{lat}\cos\alpha) = F_{ax}(\cos\alpha + \mu sin\,\alpha) + F_{lat}(\sin\alpha - \mu\cos\alpha) \qquad [4]$$

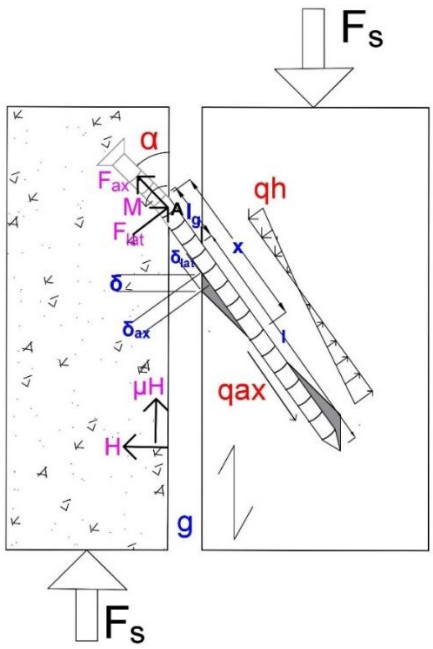

Figure 4.1: Stress distributions and forces in concrete-to-solid timber connection with an inclined screw

4.2.1 Model for Inclined Screw in Solid Timber

In *Figure 4.1*, stress distributions along with the displacement in the lateral and axial direction are shown for solid timber. Considering a ratio (φ) of embedment and withdrawal stiffness and equation [3], the axial force is expressed in equation [5],

$$F_{ax} = q_{ax} l\varphi = \ (k_{ax}\delta_{ax}) l\varphi = \ (K_{ax}\pi d)\delta_{ax} l\varphi \quad [5]$$

Because of the rigidity of screw in concrete and moment equilibrium at point A,

$$M_A = \frac{1}{2} q_h (x - l_g)\left(\frac{x - l_g}{3} + l_g\right) - \frac{1}{2} q_h \frac{(l - x + l_g)^2}{(x - l_g)}\left(x + \frac{2(l - x + l_g)}{3}\right) = 0 \quad [6]$$

Therefore, solving equation [6] to obtain

$$x = \left(\frac{6ll_g + 6l_g^2 + 2l^2}{3l + 6l_g}\right) \quad [7]$$

Applying force equilibrium perpendicular to the screw axis using equation [2],

$$F_{lat} = \frac{1}{2} q_h (x - l_g) - \frac{1}{2} q_h \frac{(l - x + l_g)^2}{(x - l_g)} = \frac{1}{2} K_h d\delta_{lat}\left(\frac{l^2}{3l_g + 2l}\right) \quad [8]$$

The relationship between the lateral displacement and axial displacement with the slip in each component can be written as follows,

$$\delta_{ax} = \delta cos\alpha \quad [9]$$

$$\delta_{lat} = \delta sin\alpha \quad [10]$$

Now, substituting equation [9] and [10] into equation [5] and [8], equation [4] can be rewritten as,

$$F_s = K_{ax}\pi dl\delta\varphi cos\alpha(\cos\alpha + \mu si\,n\,\alpha) + \frac{1}{2} K_h d\delta sin\alpha(\sin\alpha - \mu\cos\alpha)\left(\frac{l^2}{3l_g + 2l}\right) \quad [11]$$

The stiffness of the screw in concrete-to-solid timber can be expressed as,

$$\boldsymbol{k} = \frac{F_s}{\delta + \delta(l_g) sin\alpha} \quad [12]$$

Here, $\delta(l_g)$ is the additional displacement due to the presence of the gap assuming a fastener as a rigid link and can be written as,

$$\delta(l_g) = \frac{F_{lat} l_g^3}{3EI} \quad [13]$$

Where, *EI* is the effective bending stiffness of the screws in timber.

Therefore, the stiffness of the concrete-to-solid timber connection can be written as,

$$\boldsymbol{k_s} = \frac{3EId[2(3l_g + 2l)K_{ax}\pi l\varphi(cos^2\alpha + 0.5\mu si\,n\,2\alpha) + K_h l^2(sin^2\alpha - 0.5\mu si\,n\,2\alpha)]}{[6EI(3l_g + 2l) + K_h d l^2 l_g^3 sin^2\alpha]} \quad [14]$$

To account for the flexibility of the screw, the embedment stiffness K_h can be replaced by the equivalent embedment stiffness according to the equation from Appendix A,

$$K_h^{eq} = (2K_h)\frac{sinh^2(\omega l) - sin^2(\omega l)}{\omega l[sinh(\omega l)\,cosh(\omega l) - sin(\omega l)cos(\omega l)]}\ where,\ \omega = \sqrt[4]{[K_h d/(4EI)]} \quad [15]$$

4.2.2 Model for Inclined Screw in Layered Timber

As stated earlier, in layered timber, the screw intersection point in timber due to rotation can happen in one of the penetrated layers. Therefore, according to the assumption, we need to calculate three stiffness equations for possible rotation in each of the penetrated layers (*Figure 4.2, Figure 4.3 and Figure 4.4*) and the minimum will govern as the stiffness of the joint. To account for the material properties in each layer, the analytical models for stiffness prediction in layered timber will not be as straight forward as the one in solid timber. Considering a ratio (φ_i) of embedment and withdrawal stiffness in each layer to balance the joint at the presence and absence of the gap, the axial force for all three cases is obtained using equation [3],

$$F_{ax} = K_{ax1}\pi d\delta_{ax} l_1\varphi_1 + K_{ax2}\pi d\delta_{ax} l_2\varphi_2 + K_{ax3}\pi d\delta_{ax} l_3\varphi_3 \quad [16]$$

4.2.2.1 Mode 1: Rotation of Screw in 1st layer

In *Figure 4.2*, stress distributions along with the displacement in the lateral and axial direction are shown for the screw rotation in 1st layer. Similar to the previous model, the moment equilibrium at point A is as follows:

$$\begin{aligned} M_A = {} & \frac{q_{h1}}{2}(x - l_g)\left(\frac{x - l_g}{3} + l_g\right) - \frac{q_{h1}}{2}\frac{(l_1 - x + l_g)^2}{(x - l_g)}\left(x + \frac{2(l_1 - x + l_g)}{3}\right) \\ & - \frac{q_{h2}.\,l_2}{2}\frac{(2l_1 + l_2 - 2x + 2l_g)}{(x - l_g)}\left(l_1 + l_g + \frac{l_2(3l_1 + l_2 - 3x + 3l_g)}{3(2l_1 + l_2 - 2x + 2l_g)}\right) \\ & - \frac{q_{h3}.\,l_3}{2}\frac{(2l_1 + 2l_2 + l_3 - 2x + 2l_g)}{(x - l_g)}\left(l_1 + l_2 + l_g + \frac{l_3(3l_1 + 3l_2 + l_3 - 3x + 3l_g)}{2(2l_1 + 2l_2 + l_3 - 2x + 2l_g)}\right) = 0 \end{aligned} \quad [17]$$

The force equilibrium perpendicular to the screw axis is as follows:

$$F_{lat} = \frac{1}{2}q_{h1}(x - l_g) - \frac{1}{2}q_{h1}\frac{(l_1 - x + l_g)^2}{(x - l_g)} - \frac{1}{2}q_{h2}l_2\frac{(2l_1 + l_2 - 2x + 2l_g)}{(x - l_g)} - \frac{1}{2}q_{h3}l_3\frac{(2l_1 + 2l_2 + l_3 - 2x + 2l_g)}{(x - l_g)} \quad [18]$$

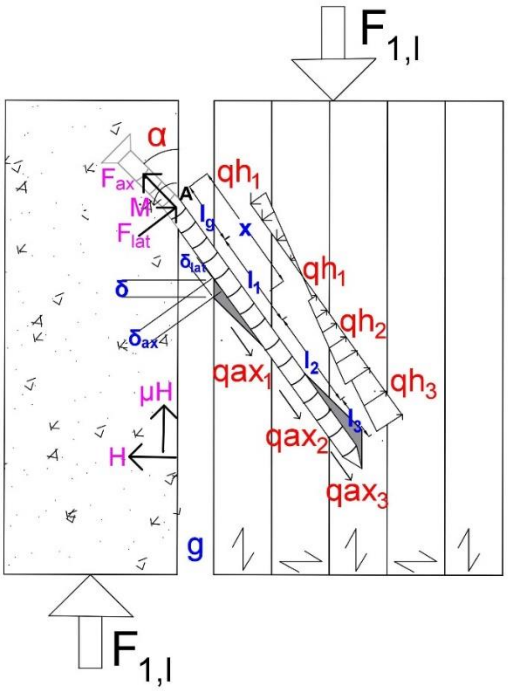

Figure 4.2: Stress distributions and forces in concrete-to-layered timber connection for rotation in 1st layer

After solving equation [17], the value of *x* can be found and using this *x* value in equation [18] F_{lat} is calculated as follows,

$$F_{lat} = \frac{d\delta_{lat}\{A\}}{\{B\}} \quad [19]$$

where,

$$\{A\}_{1\_3} = \left[l_1^4 {K_{h1}}^2 - {l_2}^4 {K_{h2}}^2 + l_3^4 {K_{h3}}^2 + \left(4{l_3}^3 l_2 + 6{l_1}^2 {l_2}^2 + 2l_1 {l_2}^3\right)K_{h1}K_{h2} - \left(4{l_1}^3 + 6l_1 {l_2}^2 + 12{l_1}^2 l_2 + 6{l_1}^2 l_3 + 6{l_1}^2 l_g + 6l_1 l_2 l_3 + 12l_1 l_2 l_g + l_1 {l_3}^2 + 6l_1 l_3 l_g\right)2l_3 K_{h1}K_{h3} - \left({l_2}^2 + l_2 l_3\right)\left(6l_1 + 5l_2 + l_3 + 6l_g\right)2l_3 K_{h2}K_{h3}\right] \quad [19.1]$$

$$\{B\}_{1\_3} = 2\left[\left(2{l_1}^3 + 3{l_1}^2 l_g\right)K_{h1} + \left(6l_1 {l_2}^2 + 6l_1 l_2 l_g + {l_2}^3 + 3l_g {l_2}^2 + 6{l_1}^2 l_2\right)K_{h2} - \left(12l_1 l_2 l_3 + 6l_1 {l_3}^2 + 6l_1 l_3 l_g + 6{l_2}^2 l_3 + 6l_2 {l_3}^2 + 6l_2 l_g l_3 + {l_3}^3 + 3{l_3}^2 l_g - 6{l_1}^2 l_3\right)K_{h3}\right] \quad [19.2]$$

If screw penetrates only two layers of timber, then the properties of third layer will vanish. Then A and B will be,

$$\{A\}_{1\_2} = \left[{l_1}^4 {K_{h1}}^2 + 2l_1 l_2 (2l_1^2 + 3l_1 l_2 + l_2^2) K_{h1} K_{h2} - {l_2}^4 {K_{h2}}^2\right] \quad [19.3]$$

$$\{B\}_{1\_2} = [2{l_1}^2 (2l_1 + 3l_g) K_{h1} + 2l_2 (6l_1^2 + 6l_1 l_2 + 6l_1 l_g + l_2^2 + 3l_2 l_g) K_{h2}] \quad [19.4]$$

Using equation [12], [13], [16] & [19], the stiffness of concrete-to-layered timber connection can be written as,

$$\boldsymbol{k_{1,l}} = \frac{F_{1,l}}{\delta + \delta(l_g) sin\alpha} = \frac{F_{ax}(\cos\alpha + \mu sin\,\alpha) + F_{lat}(\sin\alpha - \mu\cos\alpha)}{\delta + \frac{F_{lat} l_g^3}{3EI} sin\alpha}$$

$$= \frac{3EId[\pi(K_{ax1} l_1 \varphi_1 + K_{ax2} l_2 \varphi_2 + K_{ax3} l_3 \varphi_3)(cos^2\alpha + 0.5\mu \sin 2\alpha)\{B\}_{1\_r} + (sin^2\alpha - 0.5\mu \sin 2\alpha)\{A\}_{1\_r}]}{\left[3EI\{B\}_{1\_r} + d\{A\}_{1\_r} l_g^3 sin^2\alpha\right]} \quad [20]$$

Where r = 2, if the screw penetrates two layers and r = 3, if the screw penetrates 3 layers of timber. To account for the flexibility of the screw, the embedment stiffness K_h can be replaced by the equivalent embedment stiffness K_h^{eq} according to the equation [A4] from Appendix A.

4.2.2.2 Mode 2: Rotation of Screw in 2nd layer

In *Figure 4.3*, stress distributions along with the displacement in the lateral and axial direction are shown for the screw rotation in 2nd layer. Similar to the previous model, the moment equilibrium at point A is as follows:

$$M_A = \frac{q_{h1} l_1}{2} \frac{(2x - 2l_g - l_1)}{(x - l_g)} \left(l_g + \frac{l_1(3x - 3l_g - 2l_1)}{3(2x - 2l_g - l_1)}\right) + \frac{q_{h2}}{2} \frac{(x - l_1 - l_g)^2}{(x - l_g)} \left(l_1 + l_g + \frac{(x - l_1 - l_g)}{3}\right)$$

$$- \frac{q_{h2}}{2} \frac{(l_2 + l_1 - x + l_g)^2}{(x - l_g)} \left(x + \frac{2(l_2 + l_1 - x + l_g)}{3}\right)$$

$$- \frac{q_{h3} l_3}{2} \frac{(2l_1 + 2l_2 + l_3 - 2x + 2l_g)}{(x - l_g)} \left(l_1 + l_2 + l_g + \frac{l_3(3l_1 + 3l_2 + l_3 - 3x + 3l_g)}{3(2l_1 + 2l_2 + l_3 - 2x + 2l_g)}\right) = 0 \quad [21]$$

The force equilibrium perpendicular to the screw axis is as follows:

$$F_{lat} = \frac{q_{h1} l_1}{2} \frac{(2x - 2l_g - l_1)}{(x - l_g)} + \frac{q_{h2}}{2} \frac{(x - l_1 - l_g)^2}{(x - l_g)} - \frac{q_{h2}}{2} \frac{(l_2 + l_1 - x + l_g)^2}{(x - l_g)}$$

$$- \frac{q_{h3} l_3}{2} \frac{(2l_1 + 2l_2 + l_3 - 2x + 2l_g)}{(x - l_g)} \quad [22]$$

After solving equation [21], the value of *x* can be found and using this *x* value in equation [22] F_{lat} is obtained as follows,

$$F_{lat} = \frac{d\delta_{lat}\{A\}}{\{B\}} \quad [23]$$

where,

$$\{A\}_{2\_3} = \left[l_1{}^4 K_{h1}{}^2 + l_2{}^4 K_{h2}{}^2 - l_3{}^4 K_{h3}{}^2 + \left(4l_1{}^3 l_2 + 6l_1{}^2 l_2{}^2 + 4l_1 l_2{}^3\right) K_{h1} K_{h2}\right.$$
$$+ \left(2l_1{}^3 + 6l_1 l_2{}^2 + 6l_1 l_2 l_3 + l_1 l_3{}^2 + 6l_1{}^2 l_2 + 3l_1{}^2 l_3\right) 2l_3 K_{h1} K_{h3}$$
$$\left. + \left(l_2{}^2 + l_2 l_3\right)(2l_2 + l_3) 2l_3 K_{h2} K_{h3}\right] \quad [23.1]$$

$$\{B\}_{2\_3} = 2\left[\left(2l_1{}^3 + 3l_1{}^2 l_g\right) K_{h1} + (2l_2{}^3 + 3l_g l_2{}^2 + 6l_1 l_2{}^2 + 6l_1 l_2 l_g + 6l_1{}^2 l_2) K_{h2} + (6l_2{}^2 l_3 + 6l_2 l_3{}^2 + 6l_2 l_g l_3\right.$$
$$\left. + l_3{}^3 + 3l_3{}^2 l_g + 12 l_1 l_2 l_3 + 6l_1 l_3{}^2 + 6l_1 l_3 l_g + 6l_1{}^2 l_3) K_{h3}\right] \quad [23.2]$$

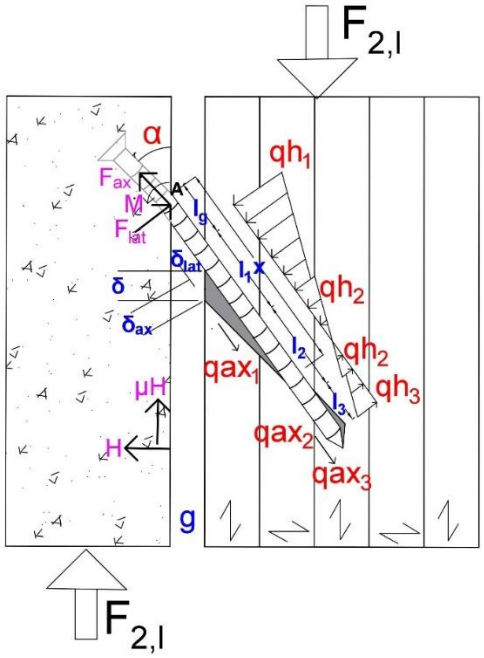

Figure 4.3: Stress distributions and forces in concrete-to-layered timber connection for rotation in 2nd layer

If screw penetrates only two layers of timber, then the properties of third layer will vanish, and A and B will be,

$$\{A\}_{2\_2} = \left[l_1{}^4 K_{h1}{}^2 + 2l_1 l_2 \left(2l_1{}^2 + 3l_1 l_2 + 2l_2{}^2\right) K_{h1} K_{h2} + l_2{}^4 K_{h2}{}^2\right] \quad [23.3]$$

$$\{B\}_{2\_2} = \left[2l_1{}^2 \left(2l_1 + 3l_g\right) K_{h1} + 2l_2 \left(6l_1^2 + 6l_1 l_2 + 6l_1 l_g + 2l_2^2 + 3l_2 l_g\right) K_{h2}\right] \quad [23.4]$$

Using equations [12], [13], [16] and [23], the stiffness of concrete-to-layered timber connection can be written as,

$\boldsymbol{k_{2,l}}$

$$= \frac{3EId[\pi(K_{ax1}l_1\varphi_1 + K_{ax2}l_2\varphi_2 + K_{ax3}l_3\varphi_3)(cos^2\alpha + 0.5\mu \sin 2\alpha)\{B\}_{2\_r} + (sin^2\alpha - 0.5\mu \sin 2\alpha)\{A\}_{2\_r}]}{\left[3EI\{B\}_{2\_r} + d\{A\}_{2\_r}l_g^3 sin^2\alpha\right]} \quad [24]$$

Where r = 2, if the screw penetrates two layers and r = 3, if the screw penetrates 3 layers of timber. To account for the flexibility of the screw, the embedment stiffness K_h can be replaced by the equivalent embedment stiffness K_h^{eq} according to the equation [A4] from Appendix A.

4.2.2.3 Mode 3: Rotation of Screw in 3rd layer

In *Figure 4.4*, stress distributions along with the displacement in the lateral and axial direction are shown for the screw rotation in 3rd layer. Similar to the previous model, the moment equilibrium at point A is as follows:

$$\begin{aligned} M_A = {} & \frac{q_{h1}l_1}{2}\frac{(2x - 2l_g - l_1)}{(x - l_g)}\left(l_g + \frac{l_1(3x - 3l_g - 2l_1)}{3(2x - 2l_g - l_1)}\right) \\ & + \frac{q_{h2}l_2}{2}\frac{(2x - 2l_g - 2l_1 - l_2)}{(x - l_g)}\left(l_1 + l_g + \frac{l_2(3x - 3l_g - 3l_1 - 2l_2)}{3(2x - 2l_g - 2l_1 - l_2)}\right) \\ & + \frac{q_{h3}}{2}\frac{(x - l_1 - l_2 - l_g)^2}{(x - l_g)}\left(l_1 + l_2 + l_g + \frac{-l_1 - l_2 - l_g}{3}\right) \\ & - \frac{q_{h3}}{2}\frac{(l_1 + l_2 + l_3 - x + l_g)^2}{(x - l_g)}\left(x + \frac{2(l_1 + l_2 + l_3 - x + l_g)}{3}\right) = 0 \end{aligned} \quad [25]$$

The force equilibrium perpendicular to the screw axis is as follows:

$$\begin{aligned} F_{lat} = {} & \frac{q_{h1}l_1}{2}\frac{(2x - 2l_g - l_1)}{(x - l_g)} + \frac{q_{h2}l_2}{2}\frac{(2x - 2l_g - 2l_1 - l_2)}{(x - l_g)} + \frac{q_{h3}}{2}\frac{(x - l_1 - l_2 - l_g)^2}{(x - l_g)} \\ & - \frac{q_{h3}}{2}\frac{(l_1 + l_2 + l_3 - x + l_g)^2}{(x - l_g)} \end{aligned} \quad [26]$$

After solving equation [25], the value of *x* can be found and using this *x* value in equation [26] F_{lat} is obtained**,**

$$F_{lat} = \frac{d\delta_{lat}\{A\}}{\{B\}} \quad [27]$$

where,

$$\begin{aligned} \{A\}_{3\_3} = {} & \left[{l_1}^4{K_{h1}}^2 + {l_2}^4{K_{h2}}^2 + {l_3}^4{K_{h3}}^2 + \left(4{l_1}^3l_2 + 6{l_1}^2{l_2}^2 + 4l_1{l_2}^3\right)K_{h1}K_{h2}\right. \\ & + \left(4{l_2}^3l_3 + 6{l_2}^2{l_3}^2 + 4l_2{l_3}^3\right)K_{h2}K_{h3} \\ & \left. + \left(4{l_1}^3l_3 + 12{l_1}^2l_2l_3 + 6{l_1}^2{l_3}^2 + 12l_1{l_2}^2l_3 + 12l_1l_2{l_3}^2 + 4l_1{l_3}^3\right)K_{h1}K_{h3}\right] \end{aligned} \quad [27.1]$$

$$\{B\}_{3\_3} = 2\big[\big(2{l_1}^3 + 3{l_1}^2 l_g\big)K_{h1} + (2{l_2}^3 + 3l_g{l_2}^2 + 6l_1{l_2}^2 + 6l_1 l_2 l_g + 6{l_1}^2 l_2)K_{h2} + (6{l_2}^2 l_3 + 6l_2{l_3}^2 + 6l_2 l_g l_3$$
$$+ 2{l_3}^3 + 3{l_3}^2 l_g + 12l_1 l_2 l_3 + 6l_1{l_3}^2 + 6l_1 l_3 l_g + 6{l_1}^2 l_3)K_{h3}\big] \quad [27.2]$$

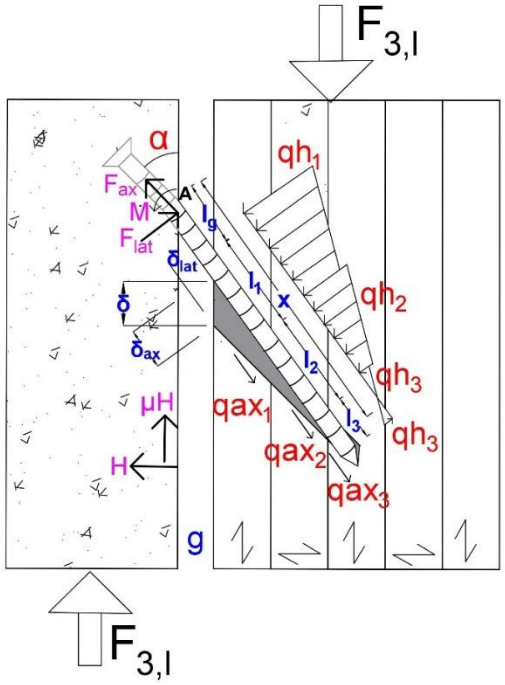

Figure 4.4: Stress distributions and forces in concrete-to-layered timber connection for rotation in 3rd layer

Therefore, using equations [12], [13], [16] and [27], the stiffness of the concrete-to-layered timber connection can be written as,

$$\boldsymbol{k_{3,l}} = \frac{3EId[\pi(K_{ax1}l_1\varphi_1 + K_{ax2}l_2\varphi_2 + K_{ax3}l_3\varphi_3)(cos^2\alpha + 0.5\mu\sin 2\alpha)\{B\}_{3\_3} + (sin^2\alpha - 0.5\mu\sin 2\alpha)\{A\}_{3\_3}]}{\big[3EI\{B\}_{3\_3} + d\{A\}_{3\_3}l_g^3 sin^2\alpha\big]} \quad [28]$$

To account for the flexibility of the screw, the embedment stiffness K_h can be replaced by the equivalent embedment stiffness K_h^{eq} according to the equation [A4] from Appendix A.

If screw penetrates only the first two layers of timber, this mode will not occur.

Therefore, using equations [19.1], [19.2], [23.1], [23.2], [27.1] and [27.2], the stiffness for the connection with the screw penetrating all three layers of timber will be,

$$\boldsymbol{k_{l\_3} = min\{k_{1,l}, k_{2,l}, k_{3,l}\}} \quad [29]$$

And, using equation [19.3], [19.4], [23.3] and [23.4], the stiffness for the screw penetrating two layers of timber will be,

$$\boldsymbol{k_{l\_2} = min\{k_{1,l}, k_{2,l}\}} \quad [30]$$

In case of connection where screw pairs are crosswise applied, with one loaded in tension and the other in compression, so far no detailed approach has been developed. As testing has shown that there was no noticeable difference between the tension and compression cases (Bejtka, 2005), the stiffness of the connection with crosswire pair can be obtained by doubling the values calculated using the single-screw models presented above.

4.3 Validation of Analytical Models

Material tests such as embedment of the screw in timber, withdrawal of the screw from timber, and friction between concrete and timber surface are presented in this section, to provide material property input into the developed analytical models. The prediction results are then compared with the connection test results (Mirdad & Chui, 2019), as a mean to validate the models.

4.3.1 Material Test

4.3.1.1 Embedment Test

Wood embedment tests of the screw at various angles to the wood grain were performed according to the half-hole test procedure in ASTM D5764-97a (ASTM, 2013), to evaluate the embedment strength. The fully-threaded self-tapping screw of 11 mm diameter (Rothoblaas, 2019b) was tested in five different angles (0°, 30°, 45°, 60° and 90°) relative to the timber grain with 5 replicates each. The dimensions of the wood specimens were 50 mm x 50 mm x 50 mm according to the minimum specification in ASTM D5764-97a (ASTM, 2013). These pieces were cut from the same source of laminated timber used in the connection tests, ie. Spruce-Pine-Fir (S-P-F) lumber. The tests were conducted at a constant displacement rate of 1.0 mm/min. The load and displacement were recorded during the tests and the acquired data were analyzed in accordance with ASTM D5764-97a (ASTM, 2013). Stiffness was calculated by taking the slope of the load-displacement response at 10-40% of maximum load. The mean density of the wood was 424 kg/m^3 with a COV of 4.7% and the mean moisture content was 9.4% based on oven-dry method. The embedment stiffness [N/mm^3] is calculated using the following equation,

$$K_h = \frac{S}{dt} \left(\mathrm{N}/\mathrm{mm}^3\right) \quad [31]$$

Where, *S* is the slope at 10-40%, *d* is the outer diameter of screw and *t* is the width of the specimen. Test results are shown in *Table 4.1* where stiffness was highest at about 45° angle. The Coefficient of Variation (CoV) for test stiffness is within a range of 9-20%. Embedment test set-up at 45° grain angles is shown in *Figure 4.5(a)*.

Table 4.1: Embedment stiffness of SPF timber under 11mm diameter screw.

Angle	Mean Stiffness, N/mm^3	CoV, %	Mean Density, kg/m^3	CoV, %
0°	5.28	18.3	426	4.4
30°	4.90	20.2	435	1.8
45°	6.52	9.2	419	4.9
60°	6.19	19.1	408	7.7
90°	4.43	9.8	431	4.6

4.3.1.2 Withdrawal Test

Withdrawal tests of the screw into the timber at various angles to the grain were performed according to the procedure in EN 1382 (EN 1382, 1999), to evaluate the withdrawal stiffness. Fully-threaded self-tapping screw with 11 mm diameter (Rothoblaas, 2019b) was tested in five different angles (0°, 30°, 45°, 60° and 90°) relative to the timber grain and two penetration length (80 mm and 100 mm) with 5 replicates each. The dimensions of the wood specimens were 450 mm x 150 mm x 150 mm according to the minimum specification stated in (ETA-Denmark, 2016), where three screws were placed on one side at 10d spacing and two on the opposite side. These pieces were cut from the same source of laminated timber used in the connection tests. The tests were conducted at a constant displacement rate of 1.5 mm/min. The load and displacement were recorded during the tests and the slope at 10-40% of the maximum load were taken from the curve to calculate the withdrawal stiffness. The mean density of the wood was 429 kg/m^3 and the mean moisture content was 8.3% based on oven-dry method. The withdrawal stiffness was calculated using the following equation,

$$K_{ax} = \frac{S}{\pi d l_{ef}} \left(\mathrm{N}/\mathrm{mm}^3\right) \quad [32]$$

where, *S* is the slope at 10-40%, *d* is the thread diameter of the screw and l_{ef} is the effective penetration length which is equal to (*L*-10mm) according to (ETA-Denmark, 2016).

Test results are summarized in *Table 4.2*, where higher stiffness can be seen at 60° angle to the grain for both penetration lengths. The stiffness per unit area was found nearly similar for both penetration lengths. The Coefficient of Variation (CoV) for the test stiffness is within a range of 5-21%. Withdrawal test at 60° grain angle is shown in *Figure 4.5(b)*.

Table 4.2: Withdrawal stiffness of 11mm diameter screw from SPF timber.

Angle	Penetration Length, mm	Mean Stiffness, N/mm^3	CoV, %	Density, kg/m^3
0°	80	4.79	21.2	436
30°	80	4.05	17.5	421
45°	80	4.01	15.8	401
60°	80	4.57	5.5	443
90°	80	3.46	15.1	443
0°	100	4.82	11.5	452
30°	100	3.89	11.1	413
45°	100	3.82	11.0	402
60°	100	4.69	11.8	421
90°	100	3.59	14.4	456

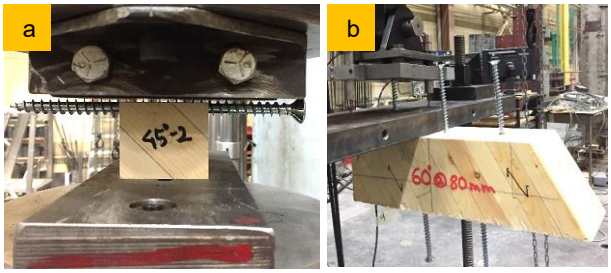

Figure 4.5: a) Embedment test of the screw in timber at 45° angle to the grain and b) withdrawal test of screws at 60° angle to the timber grain

4.3.1.3 Friction Test

Friction coefficient at the contact surface between timber and concrete was measured without and with a plastic sheet, according to ASTM D1894 (ASTM , 2014). The friction coefficient was used in the stiffness prediction models of connection when there was no insulation gap. The friction test was performed, with a loading rate of 150 mm/min. For timber-concrete surface, static coefficient of friction is important and valid which is the ratio of the force required to move one surface over another to the total force applied normal to those surfaces at the instant motion starts and can be written as,

$$\mu_k = \frac{F_f}{N} = \frac{Friction\ Force}{Normal\ Force} \quad [33]$$

A concrete block of 200 mm x 200 mm with known weight was dragged over a timber surface with and without a plastic sheet, and 5 replicates each to get the friction coefficient as shown in *Figure 4.6*. According to ASTM D1894 (ASTM , 2014), the static friction coefficient in timber-concrete surface is 0.62 without plastic sheet. In the present study measured friction coefficient with and without plastic along with the Coefficient of Variation (CoV) is shown in *Table 4.3*.

Table 4.3: Coefficient of friction

Configuration	Coefficient of Friction (μ)	CoV, %
Without Plastic	0.65	4.2
With Plastic	0.45	5.5

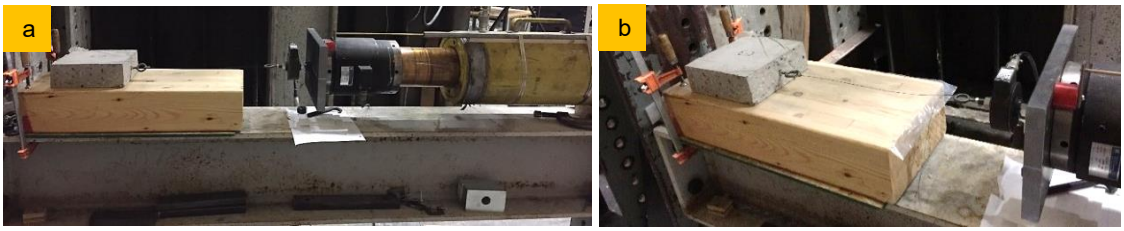

Figure 4.6: Friction test; a) without plastic sheet and b) with plastic sheet

4.3.2 Connection Test

Lateral load tests (Mirdad & Chui, 2019) were conducted on 24 groups of connection specimens with 3 replicates each. The 24 combinations covered different timber member, screw angle of insertion, screw penetration length and insulation thickness while keeping the screw diameter and concrete thickness constant. The investigation parameters have been described in (Mirdad & Chui, 2019). Standard profile Glue Laminated Timber (GLT) (Western Archrib, 2019) was used which was 175 mm thick and made of # 2-grade spruce and lodgepole pine lumber. The measured density was 455 kg/m^3 with an average moisture content of 8.3%. Five-ply E1 grade Cross Laminated Timber (CLT) (Nordic Structures, 2019) with a 175 mm total thickness was used in this study, which has 1950f$_b$-1.7E S-P-F machine stress rated (MSR) lumber in longitudinal and No. 3/Stud S-P-F lumber in transverse layers. The measured average density of the CLT was 504 kg/m^3. The average moisture content of the wood during the test was found to be 8.3%. Fully threaded self-tapping screw (Rothoblaas, 2019b) of 11 mm diameter was used in the shear test, with a countersunk head and self-drilling tip. The acoustic material (RothoBlaas, 2019a) used in this study was a sound-proofing layer made of polyester felt and elasto-plastomer bitumen. Normal

weight concrete of 75 mm thickness with an average measured compressive strength of 39 MPa at 28 days was used. The test procedure was according to EN 26891:1991 (EN 26891, 1991) and the test setup is shown in *Figure 4.7*.

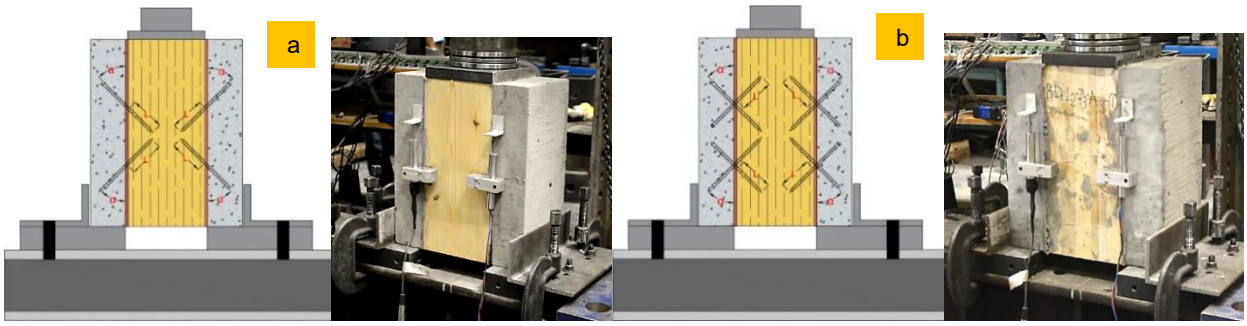

Figure 4.7: a) Screw orientation with vertical cross-pair (V-H) and typical test setup of GLT specimen with V-X, and b) Screw orientation with horizontal cross-pair (H-X) and typical test setup of CLT specimen with H-X

4.3.3 Model Validation

The mean connection test results are shown in *Figure 4.8 and Figure 4.9* for screws in GLT and CLT respectively. In the coding of the test groups, L# refers to the penetration length of the screw into MTP, I# refers to the insulation thickness, and #° refers to the insertion angle of the screw to the timber grain, which can be seen in *Figure 4.7*. The connection test results show that screws at an insertion angle of 30° have a higher stiffness along with a larger penetration length compared to the screws at a 45° angle and smaller penetration length. Overall, 35-50% and 55-60% reduction in stiffness were noticed for an insulation thickness of 5 mm and 15 mm respectively. Screws in GLT showed higher stiffness than CLT in the presence of an insulation layer (Mirdad & Chui, 2019).

The analytical models were validated using the material properties data shown in *Table 4.1*, *Table 4.2* and *Table 4.3*. These material properties were used to validate the analytical models described earlier. In *Figure 4.8* and *Figure 4.9*, the predictions from analytical models are compared to connection test data from (Mirdad & Chui, 2019). In GLT, where the screw penetrates as in solid timber, equation [14] was used and compared with connection test data. In the connection test where screw penetrates in CLT which is a layered timber, equation [30] was used because screw penetrates only two layers. In the

connection tests, crossed-pairs of the screws were used in the horizontal and vertical directions which are shown in *Figure 4.7* and therefore, the stiffness of the single screw was multiplied by 2.0, to obtain the stiffness of the cross-pair. For 30° angled screws, the embedment and withdrawal properties of 60° were used because the screws were at 60° to the wood grain. In the case of CLT, when screw penetrates in the transverse layer, the embedment and withdrawal properties of 90° were used for a similar reason as stated before.

Table 4.4: Connection stiffness comparison in GLT

Configuration in GLT	$k_{0.4}$/Pair, kN/mm	$k_{0.4}$/Screw, kN/mm	K_h^{eq}, kN/mm^3	φ	k_s, kN/mm	Relative Error
L80-I0-45°	27.88	13.94	6.24	1.56	12.89	+8%
L80-I5-45°	17.18	8.59	6.24	1.00	6.14	+29%
L80-I15-45°	10.34	5.17	6.24	1.00	5.97	-15%
L80-I0-30°	53.69	26.85	5.93	1.30	15.58	+42%
L80-I5-30°	26.68	13.34	5.93	1.00	9.75	+27%
L80-I15-30°	21.89	10.94	5.93	1.00	9.57	+13%
L100-I0-45°	35.84	17.92	5.90	1.54	15.24	+15%
L100-I5-45°	18.20	9.10	5.90	1.00	7.34	+19%
L100-I15-45°	12.19	6.09	5.90	1.00	7.13	-17%
L100-I0-30°	62.41	31.21	5.63	1.20	18.46	+41%
L100-I5-30°	35.56	17.78	5.63	1.00	12.50	+30%
L100-I15-30°	23.17	11.58	5.63	1.00	12.24	-6%

The ability of the developed models (solid and layered) to predict the stiffness in GLT and CLT connections can be seen in *Table 4.4* and *Table 4.5* respectively. Also, the stiffness predictions in CLT connection using the solid timber model by taking the average timber properties of the layers are shown in *Table 4.6*. For the cross-pair arrangement, the friction can be neglected as tension and compression forces cancel each other and technically eliminate friction (Tomasi, et al., 2010) (Bejtka & Blass, 2001) (Marchi, et al., 2017). In the case of stiffness at service load level, the effect of friction can be significant when there was no insulation, *Table 4.7*.

As can be seen in *Figure 4.8*, with material properties, the predicted connection stiffness in GLT was found to be 26% less when there was no insulation, 26% less for 5 mm insulation and 13% more for 15 mm insulation respectively. Overall, for GLT, it can be concluded that the solid timber analytical model

can predict on average within 22% of the test stiffness and shown individually for each configuration in *Table 4.4*. The embedment /withdrawal stiffness ratio was implemented only when there was no insulation gap. With the gap, the ratio was assumed as unity. This is because the assumption for the model was considering a gap in between concrete and timber. When there is no gap, the actual mode might differ than the one assumed and therefore, the ratio was introduced to mitigate this situation.

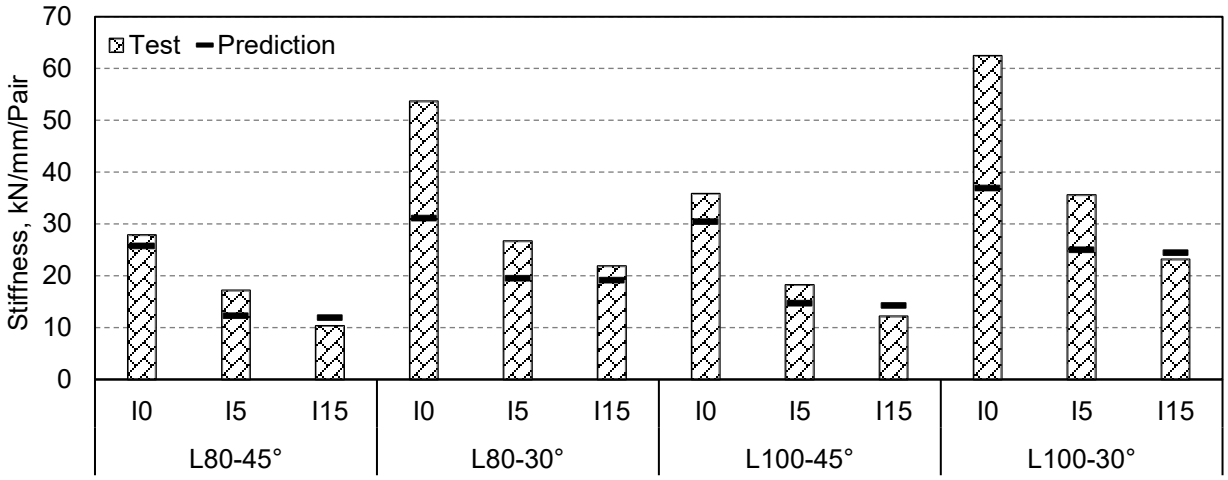

Figure 4.8: Comparison of GLT connection test stiffness with predicted stiffness using material property testing

For CLT using the layered timber model, the predicted connection stiffness was found to be 21% less for no insulation, 20% less for 5 mm insulation, and neutral in 15 mm insulation, using tested material properties, as can be seen in *Figure 4.9*. On average the predicted stiffness is within about 14% of the test stiffness which is shown in *Table 4.5* for individual configuration. In addition, the solid timber model was applied to CLT by taking the average layer properties and the result can be seen in *Table 4.6*. In this case, the predicted connection stiffness was found to be 25% less for no insulation, 23% less for 5 mm insulation, and 3% less in 15 mm insulation, using material properties. On average the predicted stiffness is within about 17% of the test stiffness. Overall, for CLT it can be concluded that the use of the solid timber model may be accepted as a compromise between calculation complexity and accuracy as the additional discrepancy is only about 3%. In addition, the discrepancy gets smaller as the insulation gap size increases.

Table 4.5: Connection stiffness comparison in CLT using layered timber model

Configuration in CLT	$k_{0.4}$/Pair, kN/mm	$k_{0.4}$ /Screw, kN/mm	K_{h1}^{eq}, kN/mm^3	K_{h2}^{eq}, kN/mm^3	φ_1	φ_2	$k_{1,l}$, kN/mm	$k_{2,l}$, kN/mm	$k_{l,2}$, kN/mm	Relative Error
L80-I0-45°	24.71	12.35	6.48	4.42	1.62	1.28	**11.76**	11.79	11.76	+5%
L80-I5-45°	14.70	7.35	6.48	4.42	1.00	1.00	**5.80**	5.84	5.80	+21%
L80-I15-45°	11.05	5.52	6.48	4.42	1.00	1.00	**5.59**	5.62	5.59	-1%
L80-I0-30°	45.76	22.88	6.04	4.43	1.32	1.28	**15.31**	15.31	15.31	+33%
L80-I5-30°	25.88	12.94	6.04	4.43	1.00	1.00	**9.44**	9.44	9.44	+27%
L80-I15-30°	18.02	9.01	6.04	4.43	1.00	1.00	**8.96**	8.96	8.96	+1%
L100-I0-45°	36.57	18.29	6.48	4.40	1.69	1.23	**14.00**	14.07	14.00	+23%
L100-I5-45°	17.21	8.61	6.48	4.40	1.00	1.00	**7.03**	7.16	7.03	+18%
L100-I15-45°	----	----	6.48	4.40	1.00	1.00	**6.77**	6.85	6.77	----
L100-I0-30°	47.37	23.69	6.04	4.42	1.29	1.23	**18.21**	18.22	18.21	+23%
L100-I5-30°	27.31	13.66	6.04	4.42	1.00	1.00	**11.61**	11.62	11.61	+15%
L100-I15-30°	----	----	6.04	4.42	1.00	1.00	10.89	**10.87**	10.87	----

Table 4.6: Connection stiffness comparison in CLT using solid timber model

Configuration in CLT	$k_{0.4}$/Pair, kN/mm	$k_{0.4}$ /Screw, kN/mm	$K_h^{eq(avg)}$, kN/mm^3	$K_{ax}^{eq(avg)}$, kN/mm^3	φ_{avg}	k_s, kN/mm	Relative Error
L80-I0-45°	24.71	12.35	5.45	3.73	1.46	11.25	+9%
L80-I5-45°	14.70	7.35	5.45	3.73	1.00	5.69	+23%
L80-I15-45°	11.05	5.52	5.45	3.73	1.00	5.54	0%
L80-I0-30°	45.76	22.88	5.23	4.01	1.30	13.73	+40%
L80-I5-30°	25.88	12.94	5.23	4.01	1.00	8.56	+34%
L80-I15-30°	18.02	9.01	5.23	4.01	1.00	8.41	+7%
L100-I0-45°	36.57	18.29	5.44	3.71	1.47	14.04	+23%
L100-I5-45°	17.21	8.61	5.44	3.71	1.00	7.07	+18%
L100-I15-45°	----	----	5.44	3.71	1.00	6.89	----
L100-I0-30°	47.37	23.69	5.23	4.14	1.26	17.15	+28%
L100-I5-30°	27.31	13.66	5.23	4.14	1.00	11.04	+19%
L100-I15-30°	----	----	5.23	4.14	1.00	11.00	----

The influence of friction in the cross-pair screw connections at the serviceability limit state may be significant and cannot be ignored in the analytical models when there is no insulation gap. To validate the analytical models, friction value of 0.45 from *Table 4.3* was used as in the connection test, a plastic sheet was inserted in between concrete and timber when there was no insulation. A general comparison of the influence of friction can be seen in *Table 4.7.* The influence of friction can be significant in 45° angled screws with an average difference of 24.25% and less dominant in 30° angled screws with an average

difference of 12.5% in both GLT and CLT. This is because the contribution from the withdrawal action is dominant for smaller inclination (e.g. 30°) angle than larger inclination.

Table 4.7: Influence of friction in the connection stiffness prediction without insulation

Configuration	$k_{0.4}$/Screw, kN/mm	k with friction, kN/mm	Relative Error	k without friction, kN/mm	Relative Error	Difference
GLT-L80-I0-45°	13.94	12.89	8%	9.31	33%	25%
GLT-L80-I0-30°	26.85	15.58	42%	12.63	53%	11%
GLT-L100-I0-45°	17.92	15.24	15%	11.01	39%	24%
GLT-L100-I0-30°	31.21	18.46	41%	14.97	52%	11%
CLT-L80-I0-45°	12.35	11.76	5%	8.51	31%	26%
CLT-L80-I0-30°	22.88	15.31	33%	12.42	46%	13%
CLT-L100-I0-45°	18.29	14.00	23%	10.09	45%	22%
CLT-L100-I0-30°	23.69	18.21	23%	14.78	38%	15%

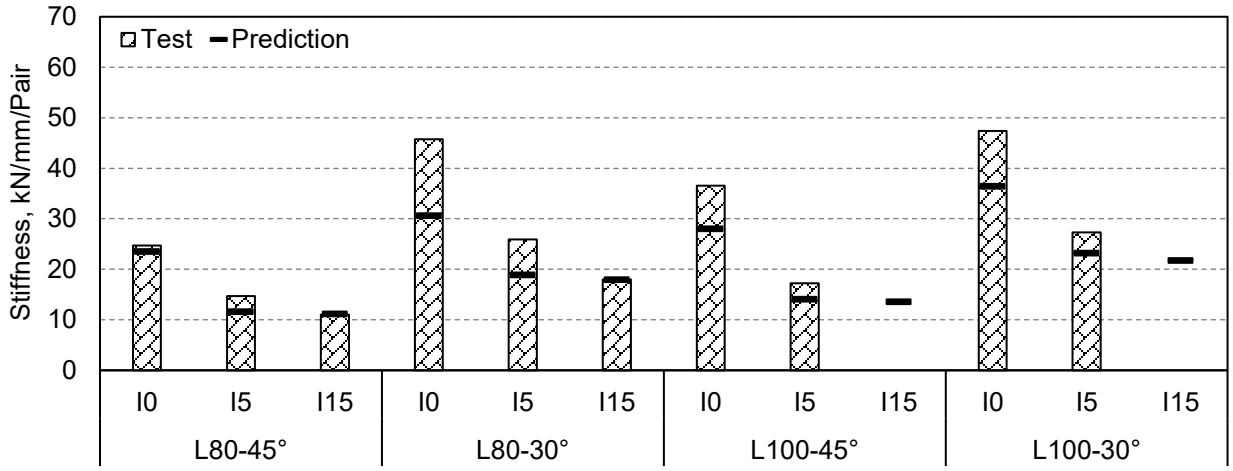

Figure 4.9: Comparison of CLT connection test stiffness with predicted stiffness using material property testing

4.4 Conclusions

Analytical models for predicting timber-to-concrete connection stiffness with inclined screws and an insulation gap are presented in this study for solid and layered timber. An extensive range of material test data is presented. These material properties were used as input into the developed models to predict the stiffness of self-tapping screw connections tested in an earlier study. The predictive capability of the developed models is evaluated by comparing the predictions with connection test results.

It was found that on average, the developed models predict within 22% of connection stiffness for solid timber and 14% for layered timber. In addition, when the solid timber model was used for the layered timber connection by taking average properties of each layer, it resulted in only a further 3% reduction in prediction accuracy. The contribution of interfacial friction to the connection stiffness was considerable and more dominant in large inclination.

Chapter 5. System Capacity and Failure Mode Prediction Model

Journal Paper #4

Capacity and Failure Mode Prediction of Mass Timber Panel-Concrete Composite Floor System with Mechanical Connectors

by Md Abdul Hamid Mirdad, Ying Hei Chui and Douglas Tomlinson

Submitted to a journal and under review

Abstract:

Lack of design standards and guidelines are the most important barrier limiting wide spread use of Mass Timber Panel-Concrete (MTPC) composite floor systems, a preferred choice by designers in modern multi-storey mass timber construction. The commonly used Gamma method to design timber-concrete composite floor has some limitations and cannot predict the load-carrying capacity and failure modes of the composite floor system. Therefore, an analytical model has been developed considering the interlayer connector behaviour under the elastic-plastic range along with an acoustic layer between timber and concrete, to accurately predict the capacity and failure modes of MTPC composite floor system. One-way acting composite floor panels were tested under four-point bending with different configurations to investigate the influence of different parameters and to validate the developed capacity prediction model. It was found that the model is capable of predicting the capacity of the MTPC composite system within the range of -6% to +26% of the experimental value and the associated failure mode. This developed capacity prediction model for MTPC composite floors will facilitate the use of these system in mass timber construction.

5.1 Introduction

Mass timber composite floor systems consisting of a Mass Timber Panel (MTP) connected to a concrete slab or topping with ductile mechanical connectors such as Self-Tapping Screw (STS) and a sound insulation layer sandwiched between the MTP and concrete, have attracted the attention of structural engineers. This system is promoted by designers in the construction of modern multi-storey mass timber buildings due to its desirable strength and stiffness to weight ratios, in-plane rigidity, acoustics, thermal and fire performances, when compared with a more conventional timber only system (Ceccotti, 2002) (Yeoh, et al., 2011). Allowable floor spans for this type of MTP-Concrete (MTPC) composite system are often governed by serviceability performance requirements, such as deflection and vibration, which are dependent on the stiffness of the interlayer connection but could also be governed by bending moment capacity. The sandwiched insulation layer between the timber panel and concrete slab is often provided to enhance acoustic and thermal performances. Due to its soft nature, this insulation layer practically serves as a gap and as such has a negative impact on the strength and stiffness of the connection (Mirdad & Chui, 2019). Also, it was experimentally (Mirdad & Chui, 2019), and later analytically (Mirdad & Chui, 2020a) (Mirdad & Chui, 2020b), proven that there is a significant increase in strength and stiffness of STS connection when the screws are inserted at 30° angle to the surface of wood member compared to 45° angle.

Due to the semi-rigid interlayer mechanical shear connector, relative slip between the bottom fiber of concrete and the top fiber of timber will occur which violates the Euler-Bernoulli assumption of plane sections remaining plane. Therefore, the transformed section method from the conventional principle of structural analysis for determining composite bending stiffness and stress distribution widely used for reinforced concrete cannot be used in design. Also, in the partial composite system like this, concrete and timber components does not act as a whole which yields two neutral axis. The composite action as well as the failure of the system mostly depends on this neutral axis. Therefore, the system needs to be designed in such a way that the concrete remains in pure compression while the timber in pure tension. The majority of timber standards around the world do not address the design of MTPC, with the exception of Eurocode 5 (EN 1995-1-1, 2009), where the so-called Gamma method (Ceccotti, 2002) is adopted.

This method can only predict elastic bending stiffness and cannot predict the load-carrying capacity and failure modes beyond elastic limit because of the linear elasticity assumption for the connection by ignoring the ductility.

The frozen shear force model by Van der Linden (Van der Linden, 1999) partially considers the ductility of the connection by modifying the Gamma method with the assumption of an elastic-plastic load-slip relationship for the connection. Once the applied load approaches the elastic limit load, the connectors close to the supports with the highest load yield first and at this point, the model assumes the entire system has yielded. This approach overestimate the load-carrying capacity of composite system significantly, because all the interior connectors still remain elastic at the point of first yield (Zhang, 2013). On the other hand, the model by Frangi and Fontana (Frangi & Fontana, 2003) was based on a rigid perfectly plastic load-slip relationship for all connectors by neglecting the connector stiffness. As most types of connectors are not inherently stiff, assuming a rigid behavior of the connection in the elastic state also overestimates the structural performance of the composite system at service and ultimate load level.

To mitigate all these issues, Zhang (Zhang, 2013) developed a model to predict connection strength of a timber-concrete composite beam with a partial failure considering linear elastic perfectly plastic load-slip relationship of the connection based on progressive yielding under increasingly applied load. In this paper, an analytical model was developed by extending Zhang's model (Zhang, 2013), to consider the soft sandwich insulation layer and to better predict the expected failure modes and bending moment capacity of MTPC composite floor system. Also, the model was validated by test data from four-point bending tests on MTPC composite floor strip panels containing STS and an insulation layer with construction parameters (e.g., MTP, concrete thickness, insulation thickness, span, STS angle and spacing).

5.2 Analytical Model

The structural system for the analytical model is defined by the following conditions: a) the panel is simply-supported in one-way action, b) gravity load is applied uniformly to the system, so that a single cross-section (panel segment) can be extracted from the system and analyzed as a single panel with per meter width, which is the same approach used in the design of typical one-way reinforced concrete slabs,

c) the cross-section of the panel consists of MTP below and concrete slab at the top, d) possible presence of soft insulation layer between timber and concrete, e) the uncracked concrete and timber exhibit linear behaviour for simplification and remain in contact at all points along the panel with the shear connectors, and f) the horizontal load transfer between timber and concrete is entirely by the means of linear elastic perfectly plastic mechanical connectors which are arranged symmetrically from the mid-span and in the vertical direction the connection is assumed rigid. The structural system considered is shown in *Figure 5.1*. The primary geometric and material parameters are defined as follows, *h:* depth, *A:* cross-sectional area, *I:* moment of inertia, *E:* modulus of elasticity, and *b:* width of the cross-section of concrete, insulation and MTP with the subscript *c*, *i* and *t* respectively. Initially in this model, behavior of connector is analyzed assuming linear elastic and then extended for the case of linear-perfectly plastic behavior.

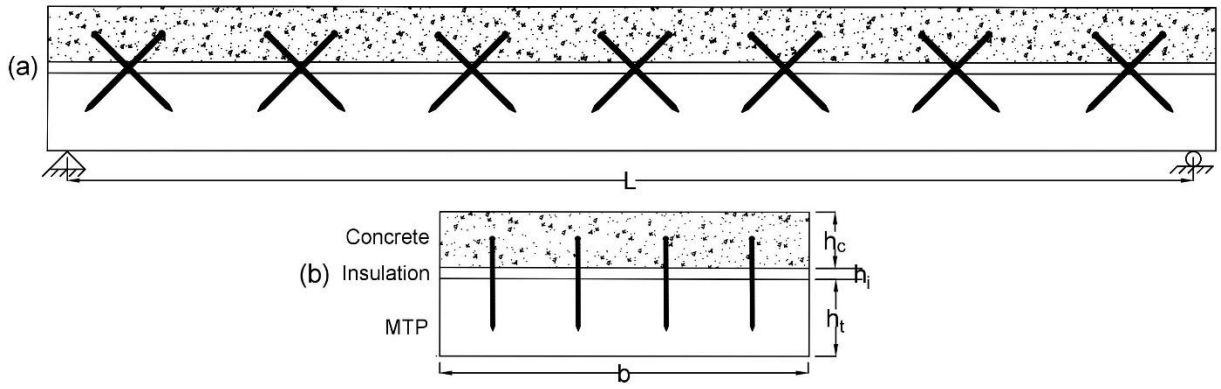

Figure 5.1: a) Longitudinal section and, b) cross-section of MTPC composite system considered.

5.2.1 Linear-Elastic Connectors

The connection shear force demand is less than its yield strength in the linear-elastic stage of the composite panel. In this analytical approach, superposition and compatibility conditions are used to determine the redundant shear forces in the connectors of the composite system. This approach, inspired by (Tommola & Jutila, 2001), can be applicable to any composite beam with discrete connectors of linear stiffness. According to (Zhang, 2013), the simplified compatibility condition for timber-concrete composite systems are, 1) at any cross section, the curvature of concrete and timber must be equal although, in reality, both the components might not bend at the same time due to the presence of an insulation gap and, 2) longitudinal interfacial slip at any connector cross-section must sum to zero. According to the

superposition method, the simply supported panel is subdivided into two Sub-Systems under uniform load. In Sub-System 1, the connection is released and the unconnected (i.e. fully non-composite) panel is analyzed under a uniform applied load. In Sub-System 2, the connectors are replaced by redundant shear force that acts opposite to the slip caused by the first Sub-System. The unknown force being transferred between concrete and MTP is found by applying the compatibility condition when the two sub-systems are combined. The Sub-Systems are shown in *Figure 5.2*. Here, a uniform load *w* is applied over span *L* and the distance between the connectors is *n*.

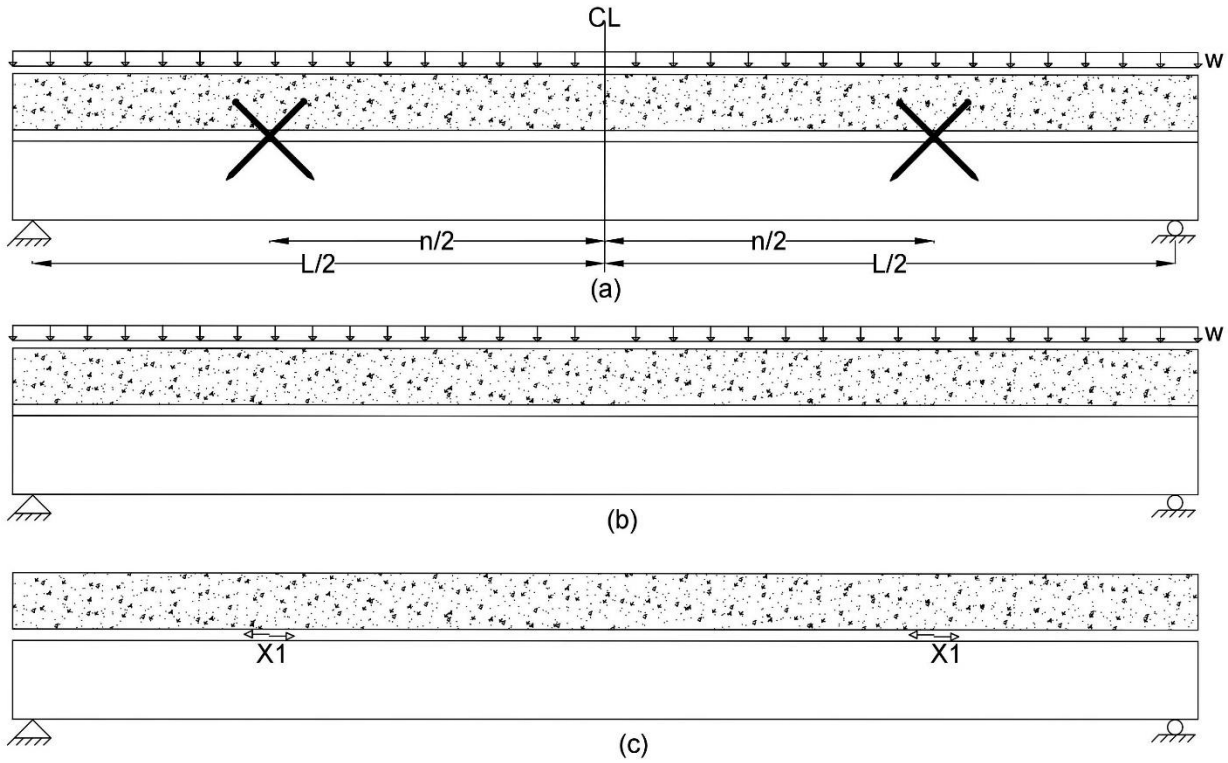

Figure 5.2: a) Primary system with uniform load, b) Sub-System 1 with released connection and c) Sub-System 2 with unknown redundant force

In Sub-System 1, the condition is equivalent to the pure bending of the members with equal curvature along the span under the applied uniformly distributed load, *w*. Therefore, initial slip at the interlayer surface due to the bending can be calculated. The total applied bending moment *M(x)* due to the load *w* at a given point *x* along the span can be written as,

$$M(x) = M_c(x) + M_i(x) + M_t(x) \quad [1]$$

According to the compatibility condition, the curvature at each member at a distance "*x*" along the beam should be equal. Therefore,

$$\frac{M_c(x)}{E_c I_c} = \frac{M_i(x)}{E_i I_i} = \frac{M_t(x)}{E_t I_t} \quad [2]$$

Combining Equations [1] and [2] yields the following expressions for M_c, M_i and M_t respectively.

$$M_c(x) = M(x)\frac{E_c I_c}{E_c I_c + E_i I_i + E_t I_t} \quad [3]$$

$$M_i(x) = M(x)\frac{E_i I_i}{E_c I_c + E_i I_i + E_t I_t} \quad [4]$$

$$M_t(x) = M(x)\frac{E_t I_t}{E_c I_c + E_i I_i + E_t I_t} \quad [5]$$

Therefore, total strain at the concrete-insulation interface is expressed as,

$$\varepsilon_0(x) = \varepsilon_{0,c}(x) - \{\varepsilon_{0,t}(x) + \varepsilon_{0,i}(x)\} = \frac{M_c(x)h_c}{2E_c I_c} + \frac{M_i(x)h_i}{2E_i I_i} + \frac{M_t(x)h_t}{2E_t I_t} \quad [6]$$

where, $\varepsilon_{0,c}$ is the bottom fiber strain in the concrete slab, $\varepsilon_{0,i}$ is the top fiber strain in insulation and $\varepsilon_{0,t}$ is the top fiber strain in timber. In the case of a soft insulation, $E_i I_i$ is small compared with those of concrete and timber and can be ignore. Therefore, the initial slip due to the pure bending at the location of the connector between timber and concrete can be written as,

$$\delta_{1,0} = \int_{(L/2)-(n/2)}^{L/2} \varepsilon_0(x)dx = \frac{h_c + h_i + h_t}{2(E_c I_c + E_t I_t)} \int_{(L/2)-(n/2)}^{L/2} M(x)dx \quad [7]$$

In Sub-System 2, the redundant force X_1 at a given cross-section of connector location is directly proportional to the connector stiffness, *k*. The force acting on the connectors at timber and concrete members will be equal and opposite. In *Figure 5.3*, the eccentrically applied redundant force X_1 is shifted vertically relative to the centroid of the concrete and timber with new eccentricity called e_c and e_t. This results in a bending moment in both components between the two connectors, which can be written as $M_{Nc} = (X_1.e_c)$ and $M_{Nt} = (X_1.e_t)$. The equilibrium requires the two forces act along the same line of action as shown in *Figure 5.3(b)*. Therefore, with the combination of equation [2], the eccentricity can be stated as follows,

$$e_c + e_t = \frac{h_c + h_t + 2h_i}{2} \quad [8]$$

$$e_c = \frac{h_c + h_t + 2h_i}{2} \cdot \frac{E_c I_c}{E_c I_c + E_t I_t} \quad [9]$$

$$e_t = \frac{h_c + h_t + 2h_i}{2} \cdot \frac{E_t I_t}{E_c I_c + E_t I_t} \quad [10]$$

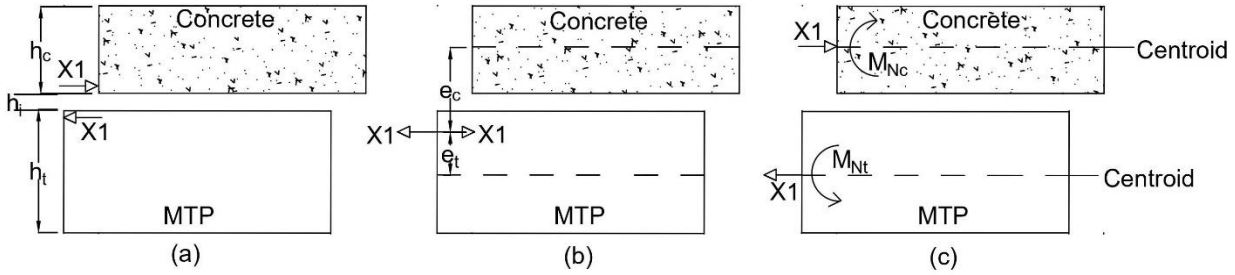

Figure 5.3: a) Eccentric axial force, b) Location of eccentric axial force and, c) Equivalent concentric axial force and moment

The extreme fiber strains at the member interface (bottom of concrete and top of timber) due to the axial force and moment resultants are,

$$\varepsilon_{1,c} = \frac{X_1}{E_c A_c} + \frac{X_1 e_c}{E_c S_c} \quad [11]$$

$$\varepsilon_{1,t} = -\frac{X_1}{E_t A_t} - \frac{X_1 e_t}{E_t S_t} \quad [12]$$

Here, $\varepsilon_{1,c}$ is the combined axial and bending strain at the bottom fiber of concrete and $\varepsilon_{1,t}$ is the combined axial and bending strain at the top fiber of timber. Sign convention for tensile and compressive strain is (+ve) and (-ve) respectively. The strain difference at the interface is constant between connectors and can be expressed as,

$$\varepsilon_1 = \varepsilon_{1,c} - \varepsilon_{1,t} = X_1 \left(\frac{1}{E_c A_c} + \frac{e_c h_c}{2E_c I_c} + \frac{1}{E_t A_t} + \frac{e_t h_t}{2E_t I_t} \right) \quad [13]$$

The relative slip at the location of the connector for $X_1 = 1$ can be calculated as follows,

$$\delta_{1,1} = \int_{(L/2)-(n/2)}^{L/2} \varepsilon_1 dx = \left(\frac{1}{E_c A_c} + \frac{e_c h_c}{2E_c I_c} + \frac{1}{E_t A_t} + \frac{e_t h_t}{2E_t I_t} \right) \cdot \frac{n}{2} \quad [14]$$

According to the force method, the connector displacement $\delta_{1,c}$ is the product of the flexibility of the connector, $f = 1/k$ and redundant force X_1. Here, k is the stiffness of the shear connector. A negative sign is required for the consistency of the compatibility equation and can be expressed as,

$$\delta_{1,c} = -X_1 f \quad [15]$$

According to the second compatibility condition, at any connector cross section, the longitudinal interlayer slips must sum to zero. Therefore, the unknown shear force X_1 in the connector can be solved based on the following compatibility equation,

$$\delta_{1,0} + X_1\delta_{1,1} = \delta_{1,c} = -X_1 f \quad [16]$$

$$\delta_{1,0} + (\delta_{1,0} + f)X_1 = 0 \quad [17]$$

The unknown redundant force X_1 for one pair of shear connector can be calculated using equation [17].

Now, for more than one pair of connectors over a span L, there are r pairs of shear connectors arranged symmetrically from the mid-span. The outermost pair of connectors can be assigned as index 1 and the index will increase with the decrease of the connector distance from the mid-span. With r number of connectors, the unknown redundant shear force will be X_r, which can be calculated based on the following matrix expression extending equation [17].

$$\begin{Bmatrix} \delta_{1,0} \\ \delta_{2,0} \\ \vdots \\ \delta_{r,0} \end{Bmatrix} + \left[\begin{pmatrix} \delta_{1,1} & \delta_{1,2} & \dots & \delta_{1,r} \\ \delta_{2,1} & \delta_{2,2} & \dots & \delta_{2,r} \\ \vdots & \vdots & \ddots & \vdots \\ \delta_{r,1} & \delta_{r,2} & \dots & \delta_{r,r} \end{pmatrix} + \begin{pmatrix} f & 0 & \dots & 0 \\ 0 & f & \dots & 0 \\ \vdots & \vdots & \ddots & \vdots \\ 0 & 0 & \dots & f \end{pmatrix} \right] \begin{Bmatrix} X_1 \\ X_2 \\ \vdots \\ X_r \end{Bmatrix} = 0 \quad [18]$$

where, $\delta_{i,0}$ for Sub-System 1 can be calculated from equation [7] and $\delta_{i,r}$ for Sub-System 2 can be calculated from equation [14]. Flexibility of the connection is the reciprocal of the connection stiffness k. From the equation [18], unknown redundant force in each connector can be calculated.

5.2.2 Linear-Perfectly Plastic Connectors

The equations presented in the previous section are extended to the case of linear-perfectly plastic behavior of connectors considering its ductility based on (Zhang, 2013). Due to the external applied load, the interface shear force must be carried by all connectors between the point of maximum moment to the support. Therefore, the connectors near the support will reach their yield strength first due to the high

shear forces. Once the connector near the support yields, the load will be redistributed to the remaining elastic connectors until the next connector yields. This redistribution process of shear forces can be considered as a progressive yield mechanism which will lead to the elastic-plastic analysis for the entire system. The redistribution due to the yielding of each connector will affect the structural behavior by reducing the system bending stiffness and increasing stresses in the members. The progressive yielding mechanism is shown in the *Figure 5.4*. As per *Figure 5.4*, the concrete and MTP is connected by 3 pairs of symmetric shear connectors. The load-slip diagram of a connector is elastic-perfectly plastic as shown in the *Figure 5.4*. The connection yield strength F_y can be calculated from the connection strength model (Mirdad & Chui, 2020a) and connection stiffness *k* can be calculated from the connection stiffness model (Mirdad & Chui, 2020b) where, the contribution from insulation gap in the shear behavior of connection was considered. A monotonically increasing uniform load *w* is applied to the composite beam. Here, load w_i refers to the load corresponding to the onset of yielding in connectors *i*L and *i*R. In *Figure 5.4*, forces in the shear connectors are shown as follows,

1) For $w \leq w_1$, all connectors are elastic, although forces are higher in the outer connectors 1L and 1R.
2) For $w_1 < w \leq w_2$, the connectors 1L and 1R have yielded while the remaining connectors are still elastic.
3) For $w_2 < w \leq w_3$, connectors 1L, 1E, 2L and 2R have yielded and connectors 3 are still elastic.
4) For $w_3 < w$, all connectors have yielded and therefore, there will be no more additional composite action and system will reach its capacity.

After yielding of a connector, it does not contribute to resisting load greater than its yield load, which provides the basis for an incremental method to calculate the shear force in the concrete-MTP connection. The analysis procedure for the incremental method is illustrated below, for a panel with six connectors under uniform load. $F_i(w)$ is the force in connector *i* when load *w* is applied to the panel counting for any connector yielding. $X_i^{(r)}(w)$ is the force in connector *i* when load *w* is applied to the panel calculated based on equation [18]. The superscript *(r)* refers to the increment numbers used in the model for the calculation. The connection force can be calculated as follows,

1) For $w \leq w_1$ in *Figure 5.4(a)*,

$$F_1(w) = X_1^{(0)}(w) < F_y; \quad F_2(w) = X_2^{(0)}(w) < F_y; \quad F_3(w) = X_3^{(0)}(w) < F_y \qquad [19]$$

Here, the forces $X_i^{(0)}(w)$ are the solution of the system with three linear equations and three unknowns but, first connector has not yielded.

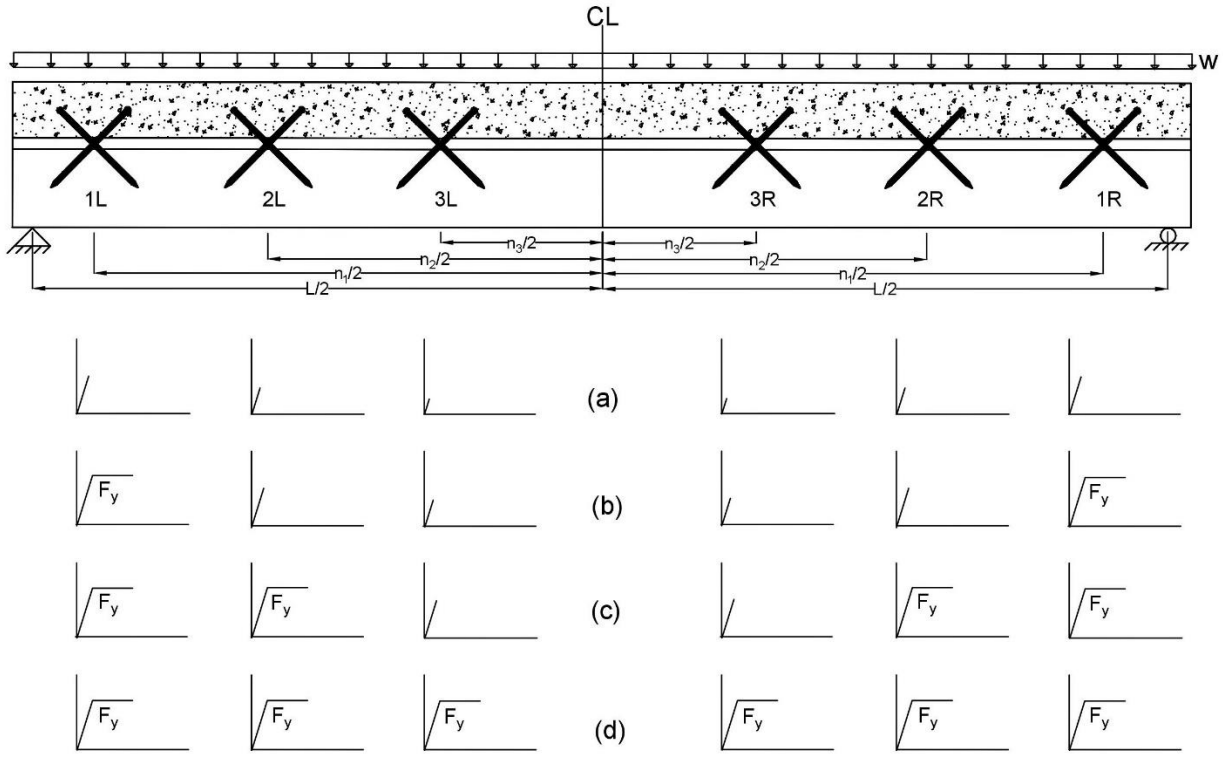

Figure 5.4: Progressive yielding of the connectors under incremental load in MTPC composite

2) For $w_1 < w \leq w_2$ in *Figure 5.4(b)*,

$$F_1(w) = X_1^{(0)}(w_1) = F_y; \quad F_2(w) = X_2^{(0)}(w_1) < F_y; \quad F_3(w) = X_3^{(0)}(w_1) < F_y \qquad [20]$$

Here, the forces $X_i^{(0)}(w_1)$ are the solution of the system with three linear equations and three unknowns like equation [19] but, first connector yielded for w_1 which can be called as w_e for the first yielding.

3) For $w_2 < w \leq w_3$ in *Figure 5.4(c)*, as connectors 1L and 1R have yielded, therefore system of two linear equations with two unknowns can be solved for the load increment of $\Delta w_1 = (w - w_2)$

$$F_1(w) = X_1^{(0)}(w_1) + 0 = F_y$$

$$F_2(w) = X_2^{(0)}(w_1) + X_2^{(1)}(\Delta w_1) = F_y$$

$$F_3(w) = X_3^{(0)}(w_1) + X_3^{(1)}(\Delta w_1) < F_y \qquad [21]$$

4) For $w_3 < w$ in *Figure 5.4(d)*, as connectors 1L, 1R, 2L and 2R have yielded, a system with one linear equation and 1 unknown can be solved for the load increment of $\Delta w_2 = (w - w_3)$

$$F_1(w) = X_1^{(0)}(w_1) + 0 + 0 = F_y$$

$$F_2(w) = X_2^{(0)}(w_1) + X_2^{(1)}(\Delta w_1) + 0 = F_y$$

$$F_3(w) = X_3^{(0)}(w_1) + X_3^{(1)}(\Delta w_1) + X_3^{(2)}(\Delta w_2) = F_y \quad [22]$$

In equations [19] – [22], each of the connection force components is obtained by solving the system of linear equations. Therefore, combining the linear calculation with incremental load, the non-linear calculation for the connector force can be performed easily. The final load after summing all the load increments will be the capacity of the composite system which can be written as,

$$w_u = w_e + \sum_{i=1}^{a} \Delta w_i \quad [23]$$

where, *a* is the maximum load increments until failure of the composite components.

5.2.3 Stresses in Concrete and Timber

After yielding of a connector, the stresses in concrete and timber are checked to determine if either of them fails (e.g., concrete compression, timber tension and/or shear) before yielding of the next connector. This approach allows designers to determine if the design ultimate limit state is either first yielding of connector or material failure in either the concrete or timber. As illustrated in *Figure 5.5*, the total stress at each position in a cross section can be calculated by summing the axial stress in the released Sub-System 1 (*Figure 5.2(b)*) due to the bending moment, and the axial stress in the redundant subsystem 2 (*Figure 5.2(c)*) due to the normal force and the bending moment caused by the longitudinal shear force in the connection. The calculation of these axial stress components is described in the following section.

5.2.3.1 Axial stress caused by normal forces in Sub-System 2:

According to the equilibrium condition, the resultant normal force applied in the timber and concrete at a given cross section is equal to the sum of shear forces in all the connections between the zero bending moment and the cross-section location. Therefore, the resultant normal force at the mid-span cross-section and axial stress in the members are,

$$N_t = N_c = \sum_{i=1}^{r} X_i \quad [24]$$

$$\sigma_{t,N} = \frac{N_t}{A_t} \quad \& \quad \sigma_{c,N} = \frac{N_c}{A_c} \quad [25]$$

Here, *r* is the number of connections between point of zero bending moment and the cross-section location, $\sigma_{m,N}$ is the axial stress and A_m is the cross-sectional area of the member.

5.2.3.2 Axial stress due to bending in Sub-Systems 1 and 2

The resultant axial stress due to bending at a position in the cross section is the sum of the bending stresses obtained from the two Sub-Systems as shown below,

$$\sigma_{t,B} = \sigma_{1,t} + \sigma_{2,t}$$

$$\sigma_{c,B} = \sigma_{1,c} + \sigma_{2,c} \quad [26]$$

Here, $\sigma_{1,m}$ is the stress of the member in Sub-System 1 and $\sigma_{2,m}$ is the stress of the member in Sub-System 2 due to bending, and $\sigma_{m,B}$ is the resultant stress. In Sub-System 1, the axial stress in the members is caused by the bending moment assuming the concrete and timber are unconnected while in Sub-System 2 it is caused by the bending moment induced by the eccentric normal force. The stresses can be written as,

$$\sigma_{1,t} = \frac{M_t}{S_t} \quad \& \quad \sigma_{1,c} = \frac{M_c}{S_c} \quad [27]$$

$$\sigma_{2,t} = \frac{N_t e_t}{S_t} \quad \& \quad \sigma_{2,c} = \frac{N_c e_c}{S_c} \quad [28]$$

Here, M_m is the component bending moment from equation [3] and [5] and, S_m is the section modulus of the components.

5.2.3.3 Total axial stress

The total axial stress for the member is the sum of the stresses in the subsystems and can be written as,

$$\sigma_{t,z} = \sigma_{t,N} + \sigma_{t,B} \quad \& \quad \sigma_{c,z} = \sigma_{c,N} + \sigma_{c,B} \quad [29]$$

Here, $\sigma_{t,z}$ represents the total tensile stress $\sigma_{t,t}$ or total compressive stress of timber $\sigma_{t,c}$. On the other hand, $\sigma_{c,i}$ represents the total tensile stress $\sigma_{c,t}$ or total compressive stress of concrete $\sigma_{c,c}$. From this stress distribution, the neutral axis of each member can be found and as the degree of composite action

decreases, the neutral axes move further apart from each other and toward the respective member centroid. Also, once the concrete starts to crack, the neutral axis moves towards the geometric centroid of the cross section, therefore, contribution of concrete to the system bending stiffness decreases and deflection increases (Cuerrier-Auclair, et al., 2016). For simplification, the concrete cracking behaviour has been ignored in this model. Total stress distribution in a MTPC is as shown in *Figure 5.5*.

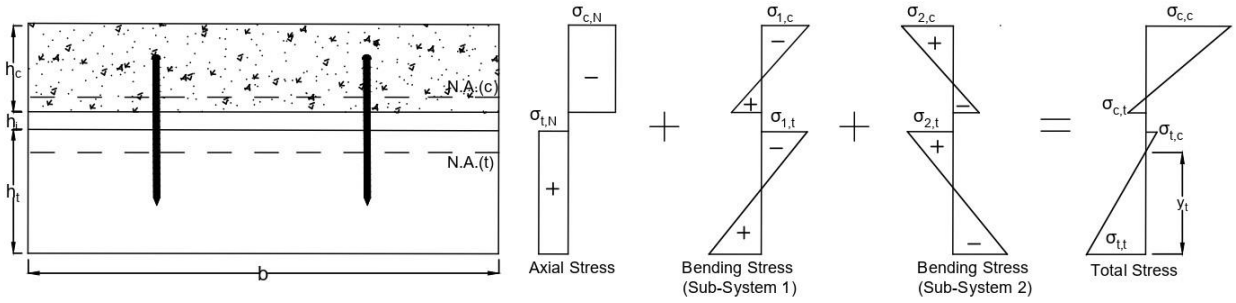

Figure 5.5: Total stress distribution in MTPC composite

5.2.3.4 Shear Stress

The shear stress is most critical in the timber member and the maximum stress happens at the neutral axis of timber member where flexural stress is zero. The shear stress of the concrete was also considered but, it did not govern in this case. The shear stress can be calculated from the following equation using the neutral axis of timber,

$$\tau_{max} = \frac{{y_t}^2 E_t V}{2EI_{eff}} \qquad with, \quad y_t = \frac{h_t\,(\sigma_{t,N}+\sigma_{t,B})}{2\sigma_{t,B}} \qquad [30]$$

Here, V is the applied shear force at the connector location due to the external load, y_t is the neutral axis of timber, E_t is the modulus of elasticity of timber and EI_{eff} is the effective bending stiffness of the beam. The effective bending stiffness can be calculated based on the procedure in Chapter 6 where, a procedure of developing composite load-displacement curve under linear elastic perfectly plastic connector behavior has been discussed. In the Appendix B, calculation procedure of a composite panel is shown in detail for better understanding the full capacity prediction model.

5.3 Verification Test Program

A bending test program was conducted to verify the developed model presented earlier. In total, 12 MTPC strip panel specimens with different configurations were tested in bending.

5.3.1 Materials

5.3.1.1 Mass Timber Panel (MTP):

Two types of Mass Timber Panel (MTP), namely Cross Laminated Timber (CLT) and Glue Laminated Timber (GLT) were used in the tests. GLT is made by face-gluing lumber in vertical lamination where the grain of all laminations runs parallel to the length of the panel. In this research, standard profile GLT (Western Archrib, 2019) was used which was 130 mm thick and made of No. 2 grade Spruce-Pine-Fir (S-P-F) lumber. The measured mean density at test of the wood was 455 kg/m^3. CLT consists of layers of dimension lumber oriented at right angle to one another and face glued. The total thickness of CLT is 105 mm and CLT grade is E1, which has 1950F$_b$-1.7E grade S-P-F lumber in longitudinal and No. 3/Stud S-P-F lumber in transverse layer (Nordic Structures, 2019). The measured average density at test was 504 kg/m^3. The mean material properties of the lamination of GLT and transverse layers of CLT made of no 2 grade and 1950F$_b$-1.7E grade S-P-F lumber are presented in *Table 5.1*. For GLT, the data was extracted from the Canadian lumber properties (Barrett & Lau, 1994) by interpolating 2x4 and 2x8 lumber data to achieve the required thickness of GLT equivalent to 2x6 lumber. In case of CLT, the material properties of transverse layer were also extracted from the Canadian lumber properties (Barrett & Lau, 1994) for 1950Fb-1.7E grade S-P-F lumber. Timber-concrete composite is a partial composite system and therefore, the timber and concrete member will neither be in pure bending nor be in pure tension due to the applied loads. In view of the stress distribution shown in *Figure 5.5* it is felt that using the mean lumber tensile strength would be more appropriate than using mean bending strength for model validation purpose. A similar approach of using tensile strength was adopted for determining moment capacity of wood I-joist in ASTM D5055-19e1 (ASTM, 2019). Moreover, the model validation purpose, use of mean instead of lower tail characteristic properties would be more appropriate.

Table 5.1: Mean material properties of the lamination of MTP

Properties	**Symbol, Unit**	**GLT**	**CLT**
Tensile Stress	f_t, MPa	21.4	19.9
Longitudinal Shear	f_v, MPa	1.3	1.5
Rolling Shear	f_s, MPa	----	0.75
Modulus of Elasticity	E, MPa	9500	11700

5.3.1.2 Self-Tapping Screw

Fully threaded self-tapping screws (Rothoblaas, 2019b) with diameters of 11 mm were used in this research, with countersunk head and self-drilling tip which is made of carbon steel and white galvanic zinc coating. The head diameter, nominal diameter and shank diameter are 19.3 mm, 11 mm and 7.7 mm respectively. One length of 200 mm was used with a penetration length of 100 mm into the MTP. In the application of timber concrete composite, fully threaded self-tapping screw with wide countersank head is beneficial as full thread provides better load transfer in timber and better bonding with concrete, while the countersank head gives pullout resistance in concrete (Mirdad & Chui, 2019). The characteristic and measured average mechanical properties of this 11 mm diameter screw are shown in *Table 5.2*.

Table 5.2: Mechanical properties of Self-Tapping Screw

Mechanical Properties	Symbol, Unit	Characteristic	Measured	CoV, %
Yield Moment	$M_{y,k}$, kN.mm	45.9	80.6	7.7
Tensile Strength	$f_{tens,k}$, kN	38	42.9	0.5
Yield Strength	$f_{y,k}$, N/mm^2	1000	1059	7.7

5.3.1.3 Acoustic material

A sound-proofing layer (RothoBlaas, 2019a) made of polyester felt and elasto-plastomer bitumen, designed as an acoustic insulating material for absorbing noise and vibrations resulting from foot traffic is used in this study. The acoustic material creates an elastic separation between stiff elements of slab and dampening vibrations due to foot traffic. This material is 5 mm thick which has the dynamic stiffness of 7 MN/m^3 and can absorb vibrations from impact noise up to 26 dB (RothoBlaas, 2019a).

5.3.1.4 Concrete

Normal density ready-mix concrete with 13 mm nominal aggregate size was used. The concrete was reinforced with smooth steel welded wire reinforcement with a diameter of 6.35 mm and a grid size of 100 mm x 100 mm was used at mid-depth of concrete to limit crack propagation in concrete due to shrinkage and temperature changes. The 28-day design strength class of the concrete was C35/45 but tests on 100 mm diameter and 200 mm tall cylinders showed that the actual compressive strength was 55.8 MPa on

average after 60 days. Cylinder tests were performed according to ASTM C39/C39M-18 (ASTM, 2018) and ASTM C469/C469M-14 (ASTM, 2014) before the large-scale composite panel tests. The results from the concrete cylinder tests are summarized in *Table 5.3* with the Coefficient of Variation (CoV).

Table 5.3: Mean material properties from concrete cylinder testing

Compressive Strength, MPa (CoV)	Young's Modulus, MPa (CoV)	Poisson's Ratio (CoV)	Number of tests	Cylinder age at testing in days
55.8 (3%)	23480 (5%)	0.142 (11%)	10	60

5.3.2 Composite Beam Tests

Two types of Mass Timber Panel (MTP), namely Cross Laminated Timber (CLT) and Glue Laminated Timber (GLT) were used in the tests. The CLT and GLT panel had a length varied from 4.5 m to 6 m with a constant width of 600 mm. Normal weight concrete of 75 mm and 100 mm thickness was used. Insulation thicknesses studied were 0 mm (no insulation), 5 mm (1 layer) and 15 mm (3 layers). Plastic separation sheets were used between the concrete and timber surface to remove any adhesion bonding at the interface which increases the load-slip modulus at low load levels (Lukaszewka, 2009). One screw diameter (11 mm) with two angles of insertion relative to timber grain (30° and 45°) was tested at 250 mm and 500 mm spacing in cross-pairs. The selected spacing of the self-tapping screws in timber was based on European Technical Approval ETA (ETA-Danmark, 2016) to avoid group effect. Acoustic insulation was inserted between the concrete and MTP. A total of 12 specimens with different configurations were tested. Basic specimens of 6 m and 4.5 m length with 250 mm and 500 mm screw spacings were included. The construction parameters that were changed for CLT and GLT were: concrete thickness (h_c), insulation thickness (h_i), screw angle and screw spacing. Two cross-pairs of screw (2 in shear-tension and 2 in shear-compression) were used in the 600 mm width specimen. Screws were located 75 mm from the edge and spaced 150 mm in the width direction. The construction details of all bending specimens with different configurations are shown in *Table 5.4*. The intension of the configurations were to cover a number of potential failure modes, including timber fracture, concrete crushing and rolling shear.

The specimens were prepared by placing the acoustic layer over MTP and inserting the screws into the MTP with the depths given in *Table 5.4.* Formwork was installed to the top of the MTP to ensure the

appropriate concrete thickness was achieved. The next step was to cast normal weight concrete on top of the MTP. After casting the concrete, specimens were kept under normal shop temperature and covered with plastic sheets for 7 days. Then the specimens were stacked outside and wrapped with tarps for a total 28 days before testing. After 28 days, the specimens were shipped to the laboratory for testing.

Table 5.4: Construction details of bending test specimens

Specimen		MTP	Length, m	Concrete Thickness, mm	Insulation Thickness, mm	Screw Angle	Screw Spacing, mm	Screw #	Screw Row from Midspan
#	Code								
1	GLT6-C100-I0-45°-S250	GLT	6	100	0	45°	250	96	12
2	GLT6-C75-I0-30°-S500	GLT	6	75	0	30°	500	48	6
3	GLT6-C75-I5-30°-S500	GLT	6	75	5	30°	500	48	6
4	GLT6-C75-I15-30°-S250	GLT	6	75	15	30°	250	96	12
5	CLT6-C75-I5-45°-S500	CLT	6	75	5	45°	500	48	6
6	CLT6-C75-I15-30°-S500	CLT	6	75	15	30°	500	48	6
7	GLT4.5-C100-I5-45°-S500	GLT	4.5	100	5	45°	500	36	4
8	GLT4.5-C100-I15-45°-S250	GLT	4.5	100	15	45°	250	72	9
9	GLT4.5-C100-I5-30°-S250	GLT	4.5	100	5	30°	250	72	9
10	GLT4.5-C75-I15-45°-S500	GLT	4.5	75	15	45°	500	36	4
11	CLT4.5-C100-I5-45°-S250	CLT	4.5	100	5	45°	250	72	9
12	CLT4.5-C100-I0-30°-S250	CLT	4.5	100	0	30°	250	72	9

5.3.3 Test Setup and Loading Procedure

The focus of the testing is determining the capacity and failure modes of the specimens though stiffness was also determined. The bending test setup is shown schematically in *Figure 5.6* and a typical test setup of a specimen is shown in *Figure 5.7(c)*. As a four-point bending test, the shear spans were 1400 mm and 1900 mm respectively for 4.5 m and 6 m specimens. One end of the support was a roller over a pivot (*Figure 5.7(a)*) while the other support was allowed to rotate but not sliding by placing wedges. The specimen was loaded through horizontal needle roller bearings placed at third points along the span. A steel spreader beam with a design capacity of 420 kN was placed over the loading points. The needle roller bearing at loading point is shown in *Figure 5.7(b).* Four horizontal Linear Variable Displacement Transducers (LVDT's) were placed at four corners of the specimen to measure relative slip between timber and the concrete which can be seen in *Figure 5.7(c)*. In the mid-span, cable transducer was placed to measure the midspan displacement and can be seen in *Figure 5.7(c)*. Load was applied over the steel

spreader beam by a hydraulic actuator with a capacity of 521 kN and recorded using a calibrated load cell. The loading was monotonic with a constant rate of 5 mm/minutes until failure. The loading was stopped just after the specimen failed and there was a significant drop in the measured load. The load-carrying capacity of the composite specimen was defined as the maximum load achieved before failure.

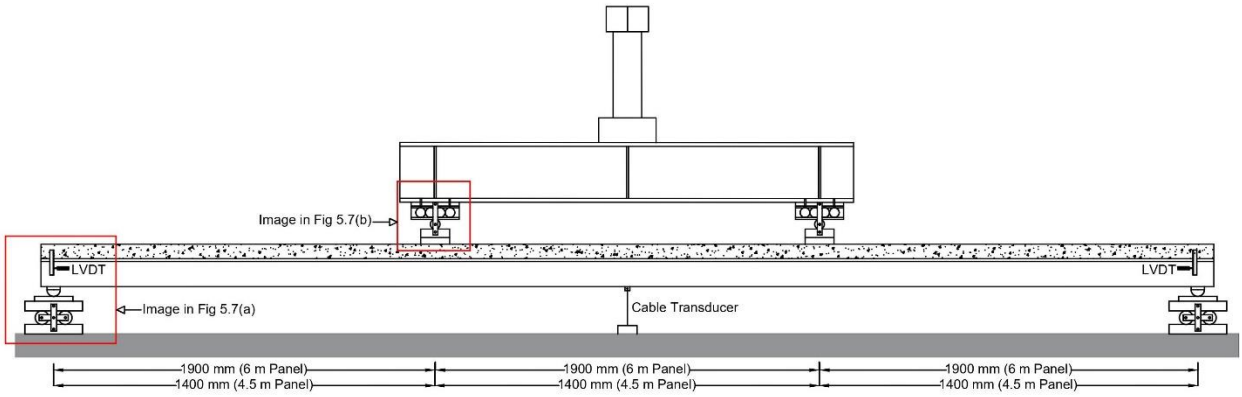

Figure 5.6: Bending test setup and instrumentation

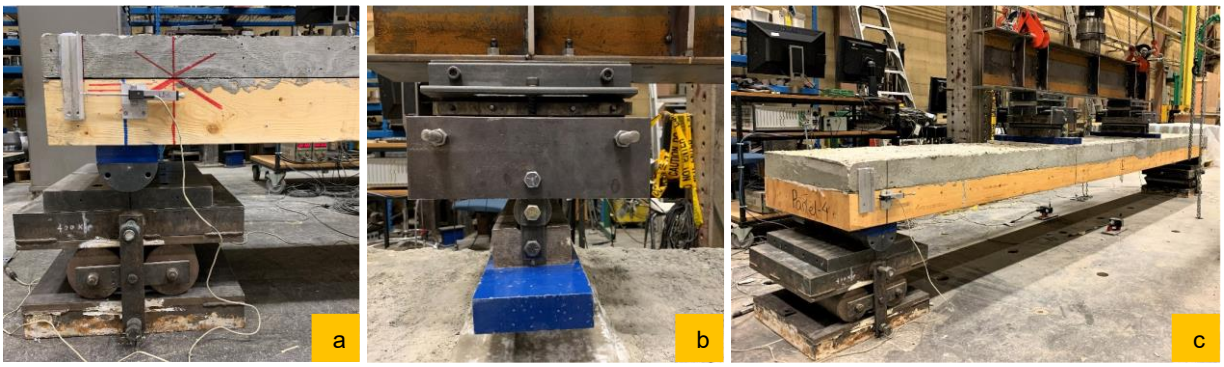

Figure 5.7: Bending test setup; a) roller support, b) distributed beam connected to needle roller bearing and, c) typical bending test setup of one specimen

5.4 Model Validation

The load-deflection curves were obtained by taking the average mid-span displacement from the cable transducer and the applied load on the specimen recorded by the calibrated load cell and is presented in *Figure 5.8* and *Figure 5.9* for 6 m and 4.5 m specimens respectively. The specimen with CLT showed lower capacity compared to the GLT specimen because of the higher thickness in GLT as well as the weak transverse layer present in the CLT. When the screws were closely spaced (e.g. 250 mm), the capacity increases significantly when compared with 500 mm spacing. Also, the specimens with 30°

angled screw showed higher capacity compared to 45° angled screw, as was determined in the connection tests conducted earlier (Mirdad & Chui, 2019). When comparing the results of specimen (#5) CLT6-C75-I5-45°-S500 and (#6) CLT6-C75-I15-30°-S500, it can be seen that with 30° angled screw, the capacity of specimen (#6) CLT6-C75-I15-30°-S500 is nearly the same as that of specimen (#5) CLT6-C75-I5-45°-S500, even though its insulation thickness is larger. This also applies to specimens (#8) GLT4.5-C100-I15-45°-S250 and (#9) GLT4.5-C100-I5-30°-S250. During the fabrication process, the concrete thickness was kept higher in 45° angled screw to mitigate the crushing failure of concrete at this angle observed in the connection tests (Mirdad & Chui, 2019). Otherwise, increasing concrete thickness does not help much in the capacity of the system unless the thickness of the MTP is larger. Also, the capacity reduces significantly in the presence of insulation layer as can be seen in specimen (#7) GLT4.5-C100-I5-45°-S500 and specimen (#10) GLT4.5-C75-I15-45°-S500 and observed from the connection tests (Mirdad & Chui, 2019).

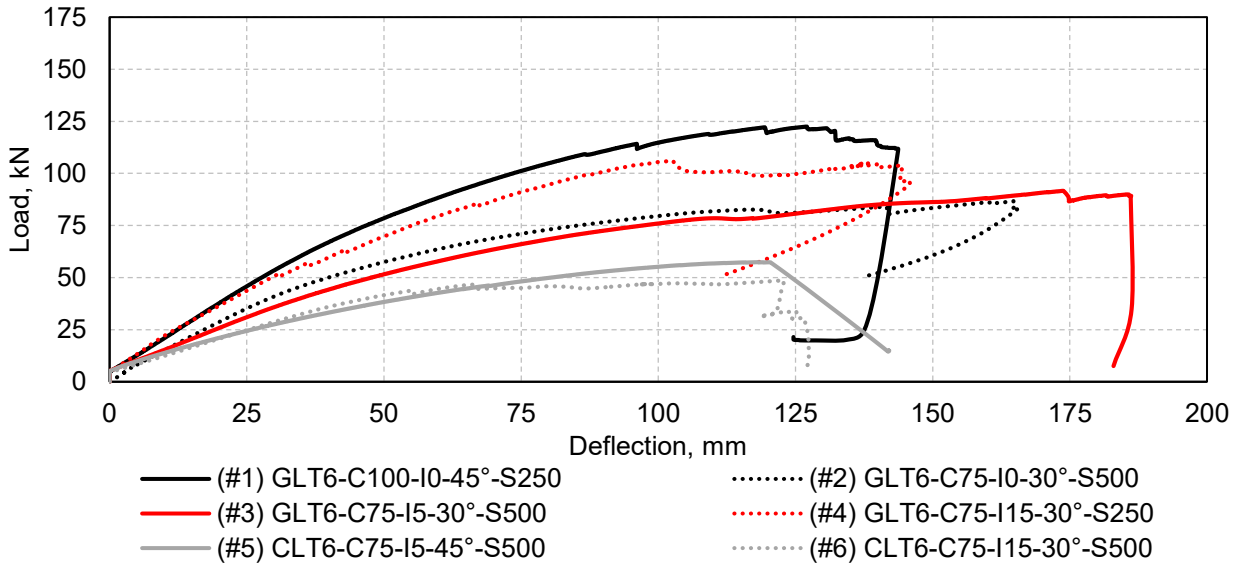

Figure 5.8: Load-deflection responses of 6.0 m specimen

The comparison between test and predicted results is shown in *Figure 5.10* with detailed numerical values given in *Table 5.5*. For the 6 m long specimens, the model prediction is within -2% to +26% of tested values which means, the model overpredicts the capacity by up to 26% and for 4.5 m long specimen, the range is from -6% to +21%. Overall, the model overpredicts the capacity by 13% on average. The capacity prediction in CLT specimen was found to be close compared to the GLT specimen.

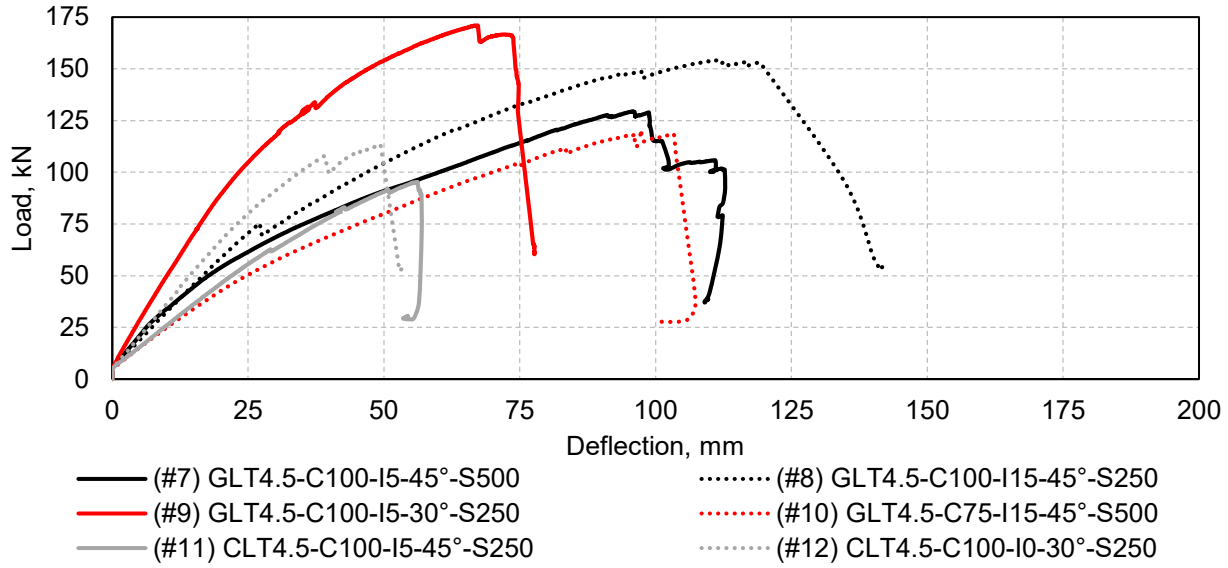

Figure 5.9: Load-deflection responses of 4.5 m specimen

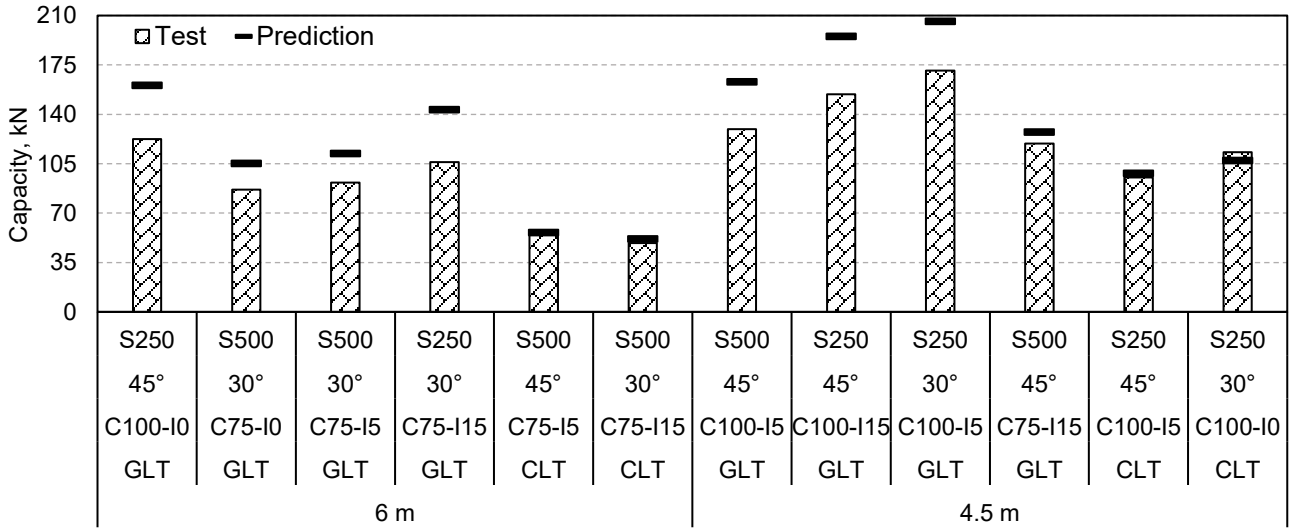

Figure 5.10: Test capacity compared to predicted capacity for each specimen.

In all the GLT specimens, the predictions are higher than bending test values. The overprediction is mainly due to the ignorance of the cracking behaviour of concrete in the model. In the post elastic region after yielding of the first connector, the concrete started to crack and at some point, reached its tensile stress limit. Due to the ignorance of cracking behaviour, the model assumes the concrete is uncracked until the failure of the specimens which resulted in higher capacity prediction than the tested capacity. The observed failure modes from the four-point bending test are presented in *Table 5.5,* which match well the failure mode predictions from the analytical model. All the specimens with GLT failed in timber fracture

while with CLT, rolling shear (*Figure 5.11 (e)*) was found dominant. No concrete crushing in compression was found because of the higher strength (55.8 MPa) concrete supplied by the ready-mix company compared to the order strength (35 MPa). Concrete cracking in the tension zone was observed in specimen (#7) GLT4.5-C100-I5-45°-S500, (#8) GLT4.5-C100-I15-45°-S250, (#9) GLT4.5-C100-I5-30°-S250 and (#10) GLT4.5-C75-I15-45°-S500 (*Figure 5.11 (f)*) where, tensile stress limit of concrete was found exceeded from the model. Although the concrete tensile crack was observed in the midspan of 4.5 m long specimens, they were still able to take the applied load until reaching the timber tensile stress limit. This tensile crack of concrete might also be due to the thicker concrete. Withdrawal and bending of the STS was also observed in 6 m long specimens, especially in the presence of an insulation layer because of the soft nature of the insulation leading to a gap and can be seen in *Figure 5.11 (c) and (d).* This withdrawal and bending of the screw was already considered in the connection model (Mirdad & Chui, 2020a) (Mirdad & Chui, 2020b), to get the connection properties.

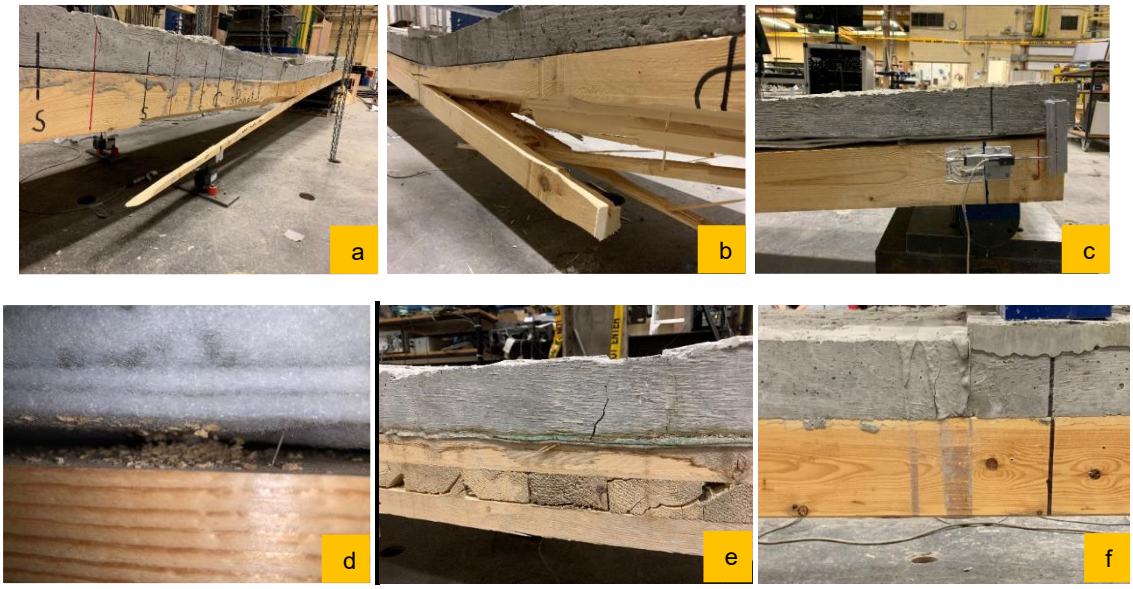

Figure 5.11: Failure modes: a) timber fracture at the presence of slope of grain in the bending zone of specimen (#1) GLT6-C100-I0-45°-S250 ; b) timber fracture at the presence of knot in specimen (#4) GLT6-C75-I15-30°-S250; c) big gap due to the withdrawal of screws at the presence of 15 mm insulation; d) withdrawal of screws at the presence of 15 mm insulation; e) rolling shear in specimen (#12) CLT4.5-C100-I0-30°-S250 with CLT; and, f) concrete tensile crack in specimen (#10) GLT4.5-C75-I15-45°-S500

Table 5.5: Bending test results comparison with prediction

Specimen	MC, %	Predicted Capacity, kN	Test Capacity, kN	Error	Predicted Yield Row	Predicted Stress in Timber, MPa	Predicted Stress in Concrete, MPa	Predicted Shear Stress, MPa	Predicted Failure Mode[a]	Test Failure Mode[a]
GLT6-C100-I0-45°-S250	8.0	160.5	122.5	24%	9/12	**21.4**	-36.2	0.4	TF	TF
GLT6-C75-I0-30°-S500	10.5	105.3	86.7	18%	5/6	**21.4**	-32.0	0.1	TF	TF
GLT6-C75-I5-30°-S500	8.3	112.2	91.7	18%	5/6	**21.4**	-31.9	0.1	TF	TF
GLT6-C75-I15-30°-S250	7.5	143.2	106.2	26%	9/12	**21.4**	-32.9	0.6	TF	TF
CLT6-C75-I5-45°-S500	7.0	56.3	57.4	-2%	1/6	5.9	-8.5	**0.75**	RS	RS
CLT6-C75-I15-30°-S500	6.3	48.5	48.7	0%	2/6	3.9	-5.5	**0.75**	RS	RS
GLT4.5-C100-I5-45°-S500	6.5	163.0	129.5	21%	3/4	**21.4**	-38.9	0.3	TF	TF
GLT4.5-C100-I15-45°-S250	7.5	195.2	154.1	21%	6/9	**21.4**	-37.8	0.6	TF	TF
GLT4.5-C100-I5-30°-S250	8.5	206.0	170.9	17%	6/9	**21.4**	-37.1	0.7	TF	TF
GLT4.5-C75-I15-45°-S500	7.5	127.3	119.3	6%	3/4	**21.4**	-31.3	0.2	TF	TF
CLT4.5-C100-I5-45°-S250	6.3	96.8	95.3	2%	1/9	1.1	-1.5	**0.75**	RS	RS
CLT4.5-C100-I0-30°-S250	6.3	107.2	113.2	-6%	2/9	4.0	-5.8	**0.75**	RS	RS

[a] TF: Timber Fracture; RS: Rolling Shear; Bold: Maximum Stress at Failure

The stress levels in extreme edge of timber (bottom tension) and concrete (top compression) were calculated using the analytical model for predicting the proper failure modes. After yielding of each connector, stresses in concrete and MTP were checked separately to evaluate if failure would occur in timber or concrete members at that load level. In *Figure 5.12 and Figure 5.13*, the extreme stresses in timber and concrete calculated from the model for 6 m and 4.5 m GLT specimens at the maximum applied load level are presented. The numerical results are also shown in *Table 5.5*. In all GLT specimens, the bottom stress of timber reaches its tensile stress limit of 21.4 MPa before reaching the concrete compressive stress limit of 55.8 MPa and therefore, timber fracture happened in the bending zone. Although concrete tensile crack at the bottom was also observed, especially in 4.5 m long specimens with 100 mm thick concrete, this will not lead to the entire system failure and instead the system stress distribution will be affected leading to a reduced capacity. In 6 m specimens, the concrete stress reached around 32 MPa at the point of timber failure while in 4.5 m specimens, it reached around 38 MPa. From *Figures 5.12* and *5.13*, it can be seen that the stresses in concrete and timber remain low until a certain load level within the linear elastic stage. As the load increases from zero, the stresses in these components increase based on the incremental load until the failure of the composite system. The

stress distribution depends on the bending stiffness and connection shear force which are a function of applied loads. At a low load level in the linear stage, the bending stiffness and connection shear force depend on the yield strength of the first connector that reaches its yield capacity. With the progressive yielding mechanism, this shear force starts to increase due to the force redistributions in the connectors and bending stiffness starts to decrease. This is reflected in the stress distribution patterns shown in *Figure 5.12* and *Figure 5.13*.

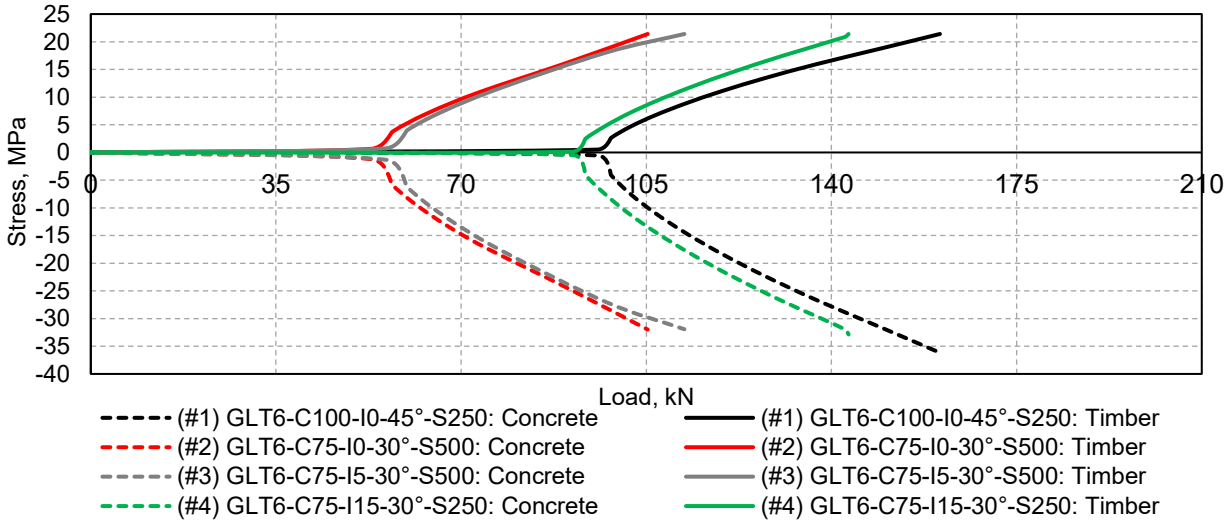

Figure 5.12: Concrete and timber stresses in the 6.0 m specimens from the model

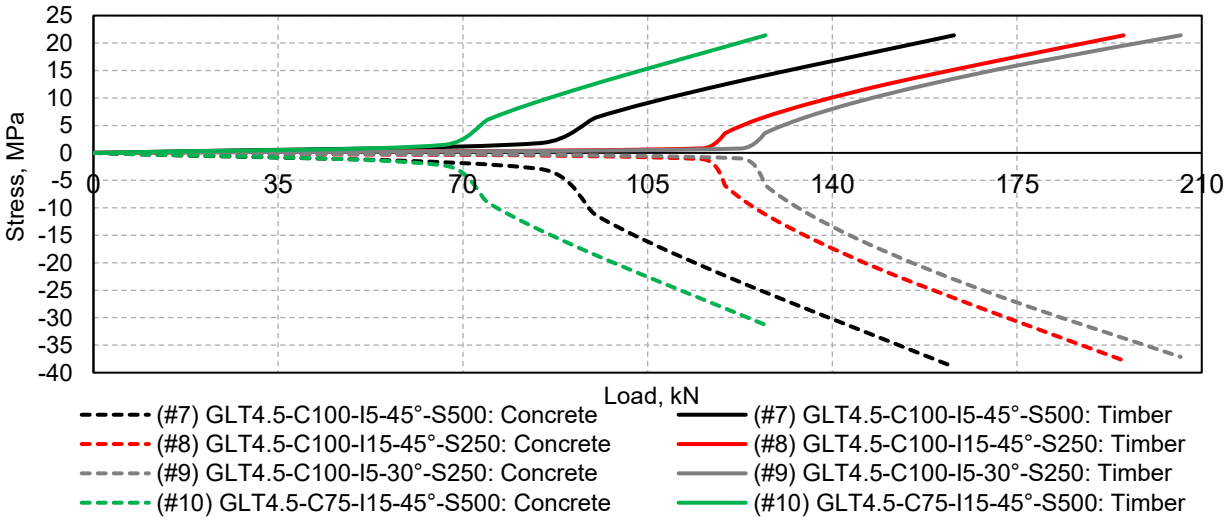

Figure 5.13: Concrete and timber stresses in the 4.5 m specimens from the model

The failure modes could be different if the GLT thickness was higher and the concrete strength was lower. Initially, the concrete was designed for 35 MPa to achieve concrete crushing in some of the specimens but, due to the supplied higher strength, there was no crushing occurring in compression which can be seen in *Figure 5.13*. In *Figure 5.13*, three of the specimens except specimen (#10) GLT4.5-C75-I15-45°-S500, reached stress level of 35 MPa in concrete which means, those three specimens were supposed to fail by concrete crushing in compression if the strength of concrete was 35 MPa as designed. In all the GLT specimens, the shear stresses were within the limit of 1.3 MPa, but in the CLT specimens, the rolling shear stress limit of 0.75 MPa was exceeded after yielding of first or second screw row, which was also observed in the test. The reason of observing rolling shear in the CLT specimen was, due to the composite action, the stress level in the transverse layer gets higher along with the progressive yielding of the screws. This propagates the rolling shear at the middle third of the specimen instead of near the support region. In all the specimens except the CLT, all the screw row yielded until it reaches the middle third portion. The moisture content of the specimens were also measured following the electrical resistance method before the test and presented in *Table 5.5*.

5.5 Conclusions

The major aim of this study was to develop a rational analytical model to predict the capacity and failure modes of MTPC composite system considering the strength, stiffness and ductility of the interlayer connection. MTPC composite panel test specimens with various construction parameters, including an insulation layer and inclined self-tapping screws, were tested to validate the developed capacity model.

An analytical model for predicting the load-carrying capacity of MTPC composite panel with inclined screws and an insulation gap was developed in this study, by extending the model by Zhang (Zhang, 2013). Initially the model predicts the linear elastic behaviour of the system. Once first yielding of the highest stressed connector occurs, linear perfectly plastic behaviour is considered, leading to progressive yielding of the remaining connectors. Material stresses in timber and concrete can then be checked to evaluate if failure of the system, which is defined as material failure in either timber or concrete, has occurred. The predictive capability of the developed models was evaluated by comparing the predictions with bending test results. It was found that on average, the developed models predict composite capacity

within the range from -6% to +26% of tested values. The overestimation of the capacity was due to the ignorance of the cracking behaviour of concrete. The failure modes were also accurately predicted by the model. Similar to the connection behaviour reported earlier (Mirdad & Chui, 2019), the capacity of the composite panel is influenced significantly by the screw inclination and insulation thickness. The influence of screw spacing on system capacity was found to be significant and can be used to mitigate the reduction in capacity due to the presence of an insulation layer. On the other hand, concrete thickness had less influence on the system capacity.

Chapter 6. System Bending Stiffness and Load-Deflection Prediction Model

Journal Paper #5

Bending Stiffness and Load-Deflection Response Prediction of Mass Timber Panel-Concrete Composite Floor System with Mechanical Connectors

by Md Abdul Hamid Mirdad, Ying Hei Chui, Douglas Tomlinson and Yuxiang Chen

Submitted to a journal and under review

Abstract:

Mass Timber Panel-Concrete (MTPC) composite floor systems, a preferred choice by the designers in modern multi-storey mass timber construction are generally designed using the Gamma method. The Gamma method has limitations and cannot predict the effective bending stiffness of the composite floor system for widely spaced discrete connectors in the presence of a soft insulation layer between the timber and concrete for acoustic and/or thermal purposes. An analytical model for one way acting composite panels has been developed that considers the elastic-plastic behaviour of interlayer connectors and the presence of a soft layer between timber and concrete, to accurately predict the bending stiffness and load-deflection response of MTPC composite floor system. Composite floor panels in one-way action were tested under four-point bending with different configurations to validate the developed stiffness prediction model and investigate the influence of different parameters. The experiment shows that the model is capable of predicting the stiffness of the MTPC composite system within the range of -15% to +10% of the bending test values, while the Gamma method was found to over-estimate the bending stiffness on average by 43%. This developed bending stiffness prediction model for MTPC composite floors will facilitate the design and use of MTPC in mass timber construction.

6.1 Introduction

In the construction of modern multi-storey mass timber buildings, a composite floor system commonly specified by structural engineers is the MTP-Concrete (MTPC) composite system where, a Mass Timber Panel (MTP) is connected to a concrete slab or topping with mechanical shear connectors and a sound insulation layer sandwiched between the MTP and concrete slab. MTPC systems have higher strength and stiffness to weight ratios, in-plane rigidity, and better acoustics, thermal and fire performances than conventional timber only systems (Ceccotti, 2002) (Yeoh, et al., 2011) (Lukaszewska, et al., 2008). In between MTP and concrete slab, a sandwiched insulation layer is usually provided to enhance thermal and acoustic performance. However, due to the flexibility of the insulation material used, this layer has an adverse impact on the connection strength and stiffness (Mirdad & Chui, 2019). Self-Tapping Screws (STS) are extensively used modern dowel-type fasteners which were developed as an improved threaded fastener for mass timber construction, including timber-concrete composite systems. It was also experimentally (Mirdad & Chui, 2019), and later analytically (Mirdad & Chui, 2020a) (Mirdad & Chui, 2020b) proven that there is a significant increase in the stiffness and strength of concrete-timber connection with inclined STS when the screws are inserted at 30° angle to the timber surface compared to 45° angle.

Serviceability performance requirements such as deflection and vibration often govern the allowable maximum span for MTPC composite type floor system. Therefore, the effective bending stiffness of the MTPC system is an important property to consider in structural design. For the semi-rigid behavior of the mechanical shear connector, relative slip happens between the bottom fibre of concrete slab and the top fibre of MTP under shear transfer which disrupts the first Euler-Bernoulli assumption of “plane sections remain plane”. Therefore, the method of the transformed section which is commonly used for steel-concrete is not applicable to MTPC composite system. The majority of timber standards around the world do not address the design of MTPC composite system, with the exception of Eurocode 5 (EN 1995-1-1, 2009), where the so-called Gamma method (Ceccotti, 2002) is adopted. This method can predict elastic bending stiffness more accurately for stiff notched timber, mechanical, and glued connections (COST, 2018). In the case of flexible connections, such as those utilizing STS and interlayer insulation, the

Gamma method is shown inappropriate (COST, 2018). Also, the Gamma method cannot predict the ultimate capacity and complete load-deflection response due to onset of inherent elasto-plastic behaviour of the interlayer connection even at relatively low load levels.

According to the Gamma method (Ceccotti, 2002) which is mostly linked to Mohler's model (Mohler, 1956) for partial composite systems, the effective bending stiffness of a timber-concrete composite system can be calculated as,

$$(EI)_{eff} = E_c I_c + \gamma E_c A_c a_c^2 + E_t I_t + E_t A_t a_t^2 \quad [1]$$

With shear coefficient gamma (γ) and distances a_m given by,

$$\gamma = \frac{1}{1 + \frac{\pi^2 E_c A_c s}{n_s k L^2}} \; ; \quad a_c = \frac{h_c + h_t + 2h_i}{2} - a_t \; ; \quad a_t = \frac{\gamma E_c A_c (h_c + h_t + 2h_i)}{2(\gamma E_c A_c + E_t A_t)} \quad [2]$$

where, *h*, *A*, *I* and *E* refers to the depth, area, moment of inertia and modulus of elasticity of the components with subscript *c*, *i* and *t* representing concrete slab, insulation and MTP. *L* is the span, *s* is the spacing of connector, n_s is the number of connector rows over the width of the beam, *k* is the linear-elastic stiffness of interlayer connection. The γ coefficient equal to 1 for full composite and 0 for no composite action by stiffness.

To better predict the effective bending stiffness and load-deflection response, Zhang (Zhang, 2013) developed a model for timber-concrete composite (T) beam considering linear-elastic perfectly plastic load-slip relationship of the connection based on progressive yielding under increasingly applied load where, soft insulation layer was not considered. Also, for timber-concrete composite (T) beam, a nonlinear model was developed by Cuerrier-Auclair (Cuerrier-Auclair, et al., 2016) by extending the model of a beam on an elastic foundation and composite beam theory. In that model, there are different levels of calculation to generate the load-deflection responses of composite beams directly from the component's material properties. Initially, the moment-curvature relationship is drawn from the dowel's uniaxial stress-strain relationship. Then the shear force-slip relationship is drawn for the dowel considering the properties of concrete and timber from moment-curvature relation. Therefore, the structural load-deflection response of the composite beam can be drawn but, this method is complicated for general use and limited to only

laterally loaded dowel's inserted at 90° angle. In this paper, an analytical model for effective bending stiffness was developed as well as user-friendly nonlinear load-deflection response prediction by extending Zhang's model (Zhang, 2013), to consider the soft sandwich insulation layer with inclined connectors and to better predict the bending stiffness of MTPC composite floor system. The stiffness model was validated by test data from four-point static bending tests on MTPC composite floor strip panels containing STS and an insulation layer with different construction parameters (e.g., MTP, concrete thickness, insulation thickness, span, STS angle and spacing). The model was also compared with the Gamma method to check its efficiency. Also, the full predicted load-deflection response was compared with actual load-deflection response from bending test. From this research, the bending stiffness of MTPC composite system at the presence of insulation layer can be predicted as insulation significantly reduces the stiffness of the connection (Mirdad & Chui, 2019) followed by the system. Also, the non-linear load-deflection response of MTPC composite at the presence of insulation can be generated and these two outcomes will be a significant contribution towards the composite design.

6.2 Analytical Model

The structural system for the analytical model is characterized by the following conditions: a) the panel is simply-supported and bending via one-way action, b) the panel cross-section consists of MTP below and concrete slab at the top, c) possible presence of soft insulation layer between MTP and concrete slab, d) uncracked concrete slab and MTP exhibits linear-elastic behavior for simplification and are connected via the shear connectors, and e) the horizontal load transfer between MTP and concrete slab is entirely by the linear-elastic perfectly plastic mechanical connectors which are arranged symmetrically about mid-span and in the vertical direction the connection is assumed rigid.

A cross-section of the structural system considered in this study is shown in *Figure 6.1*. The primary material and geometric parameters are specified as, *h:* depth, *A:* cross-sectional area, *I:* moment of inertia, *E:* modulus of elasticity, and *b*: width of the cross-section of concrete slab, insulation and MTP with the subscript *c*, *i* and *t* respectively. Initially, the connector behaviour is analyzed assuming linear-elastic behaviour from which the initial effective bending stiffness of the system can be found. Then the

connector behavior is extended for the case of elastic-perfectly plastic behaviour to produce the composite system load-deflection response.

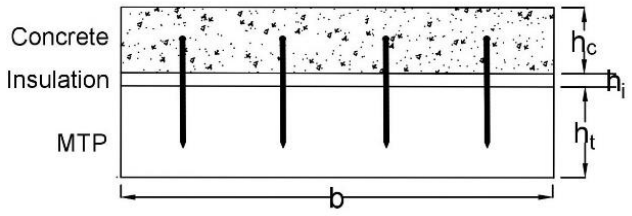

Figure 6.1: Cross-section of MTPC composite system considered.

6.2.1 Effective Bending Stiffness

In this analytical approach, superposition and compatibility conditions are applied to determine the redundant shear forces in the connectors and thereafter, the composite system's effective bending stiffness. Based on the superposition method, the simply supported panel is subdivided into two Sub-Systems under uniform load. In Sub-System 1, the connection is released, and the unconnected (i.e. fully non-composite) panel is under a uniform applied load. In Sub-System 2, the connectors are replaced by redundant shear force that acts opposite to the slip caused by the first Sub-System. The unknown shear force of connectors being transferred between concrete and MTP is found by applying the compatibility condition when the two Sub-Systems are combined. The simplified compatibility condition for MTPC composite systems are, 1) the curvature of concrete and timber must be equal at any cross section although, both the components might not deform together in the presence of soft insulation layer and, 2) the longitudinal interfacial slip at any connector cross-section must sum to zero at equilibrium. The Sub-Systems are shown in *Figure 6.2*. Here, a uniform load *w* is applied over span *L* and *n* is the distance between the connector.

For Sub-System 1, the initial slip due to the bending at the connector location between timber and concrete can be written as,

$$\delta_{1,0} = \frac{h_c + h_i + h_t}{2(E_c I_c + E_t I_t)} \int_{(L/2)-(n/2)}^{L/2} M(x)dx \qquad [3]$$

And for Sub-System 2, the relative slip at the connector location can be calculated as follows,

$$\delta_{1,1} = \left(\frac{1}{E_c A_c} + \frac{e_c h_c}{2E_c I_c} + \frac{1}{E_t A_t} + \frac{e_t h_t}{2E_t I_t}\right).\frac{n}{2} \qquad [4]$$

In the case of a soft insulation, E_iI_i is small compared with those of concrete and timber and can be ignored. According to the second compatibility condition, the unknown shear force X_1 in the connector can be solved based on the following equation,

$$\delta_{1,0} + (\delta_{1,1} + f)X_1 = 0 \quad [5]$$

Here, Flexibility of the connection, $f = 1/k$ and redundant force X_1. k is the stiffness of the shear connector which can be calculated from stiffness model (Mirdad & Chui, 2020b). The unknown redundant force X_1 for one pair of shear connectors can be calculated using equation [5].

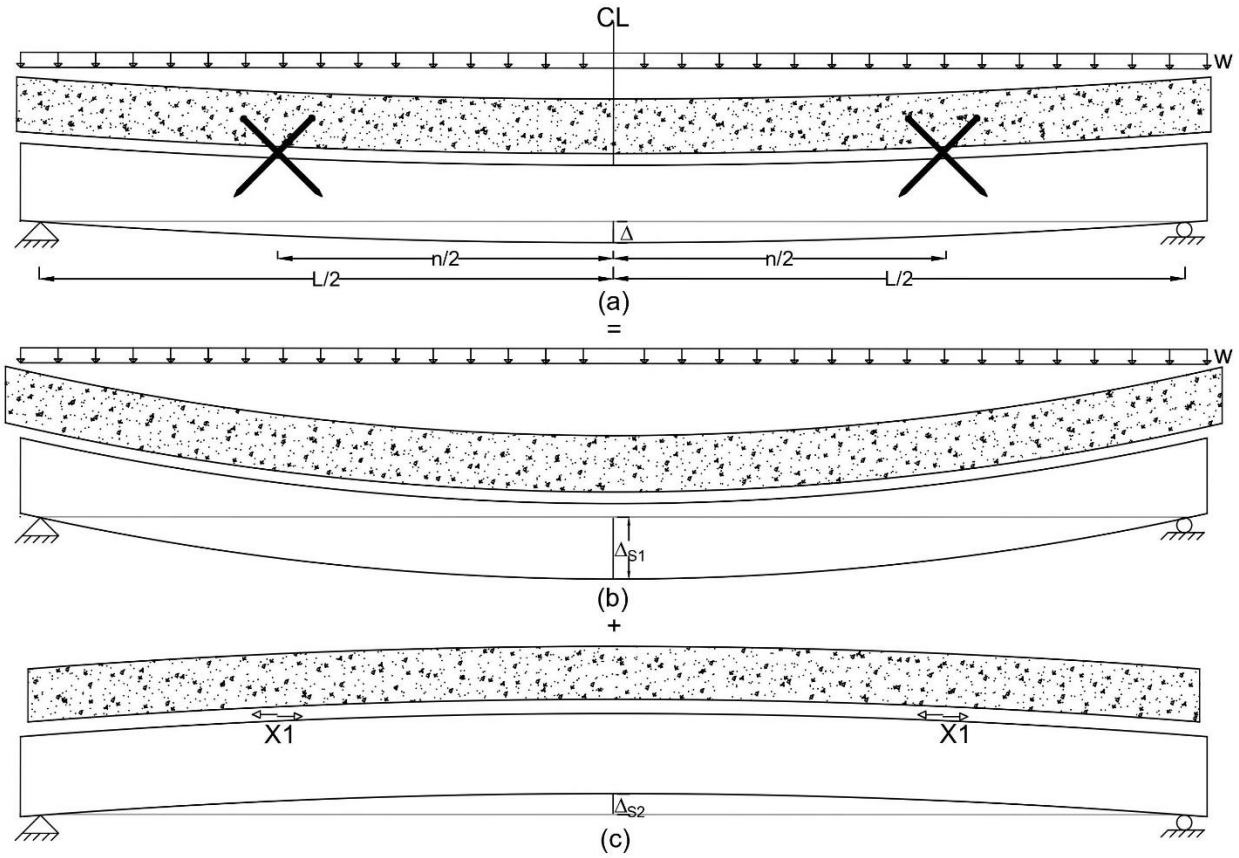

Figure 6.2: System response; a) Primary system with uniform load, b) Sub-System 1 with released connection and c) Sub-System 2 with unknown redundant force

For more than one pair of connectors, assume that there are r pair of shear connectors arranged symmetrically about the mid-span in a span L. The outermost connector pair can be referred as index 1 and the index will increase with the decrease of the connector distance from the mid-span. With r number

of connector rows, the unknown redundant shear forces will be X_r, which can be calculated based on the following matrix expression following an extension of equation [5].

$$\begin{Bmatrix}\delta_{1,0}\\ \delta_{2,0}\\ \vdots\\ \delta_{r,0}\end{Bmatrix}+\left[\begin{pmatrix}\delta_{1,1} & \delta_{1,2} & \dots & \delta_{1,r}\\ \delta_{2,1} & \delta_{2,2} & \dots & \delta_{2,r}\\ \vdots & \vdots & \ddots & \vdots\\ \delta_{r,1} & \delta_{r,2} & \dots & \delta_{r,r}\end{pmatrix}+\begin{pmatrix}f & 0 & \dots & 0\\ 0 & f & \dots & 0\\ \vdots & \vdots & \ddots & \vdots\\ 0 & 0 & \dots & f\end{pmatrix}\right]\begin{Bmatrix}X_1\\ X_2\\ \vdots\\ X_r\end{Bmatrix}=0 \quad [6]$$

where, $\delta_{i,0}$ for Sub-System 1 can be calculated from equation [3] and $\delta_{i,r}$ for Sub-System 2 can be calculated from equation [4]. From equation [6], unknown redundant forces, X_r in each connector can be calculated.

The vertical deflection at mid-span due to the applied load w can be calculated using the superposition method after obtaining the connector forces.

In Sub-System 1 (*Figure 6.2(b)*), the midspan deflection of the unconnected (i.e. fully non-composite) panel imposed to a uniformly distributed load w_r at simply supported condition can be written as,

$$\Delta_{S1}=\frac{5wL^4}{384(E_cI_c+E_iI_i+E_tI_t)} \quad [7]$$

In Sub-System 2 (*Figure 6.2(c)*), the eccentric axial loads generated by the shear forces of the connection prompt a midspan deflection, Δ_{S2}, opposing the initial one, Δ_{S1}, and can be derived by using the virtual work method as,

$$\Delta_{S2}=-X_r n_r\frac{L(h_c+h_t+2h_i)}{16(E_cI_c+E_iI_i+E_tI_t)} \quad [8]$$

Here, r is the number of connector rows. Therefore, the total deflection can be expressed as,

$$\Delta_r=\Delta_{S1}+\Delta_{S2} \quad [9]$$

Finally, effective bending stiffness of the MTPC composite system considering the mid-span deflection before yielding of the first connector can be written as,

$$EI_{eff}=\frac{5w_1L^4}{384\Delta_1} \quad [10]$$

6.2.2 Load-Deflection Response

To generate the load-deflection response of MTPC composite, the equations presented in the previous section are expanded to the case of linear-elastic perfectly plastic behaviour of connectors based on (Zhang, 2013). Due to the external applied load, the interface shear force must be carried by all

connectors between the support and midspan. Therefore, the connectors near the support will reach their yield strength first due to the high shear forces (Tommola & Jutila, 2001). Once the connector near the support yields, the load will be redistributed to the remaining elastic connectors until the next connector yields. This redistribution process of shear forces can be considered as a progressive yield mechanism which will lead to the elastic-plastic analysis for the entire system. The redistribution due to the yielding of each connector will affect the structural behavior by reducing the system bending stiffness and increasing stresses in the members. The progressive yielding mechanism is shown in *Figure 6.3*. As per *Figure 6.3*, the concrete and MTP are connected by three pairs of symmetric STS shear connectors at cross-pair arrangement. The load-slip response of a connector is elastic-perfectly plastic. The connection yield strength F_y can be calculated from the connection strength model (Mirdad & Chui, 2020a) and connection stiffness, *k,* can be calculated from the connection stiffness model (Mirdad & Chui, 2020b) where, the contribution from insulation gap in the shear behavior of connection was considered. A consistently increasing uniform load, *w,* is applied to the composite panel. Here, w_i refers to the load corresponding to the commencement of yielding in connector *i*.

A yielded connector does not contribute to resisting load greater than its yield load, which serves the basis for an incremental method to calculate the shear force in the concrete-MTP connection (Tommola & Jutila, 2001). The analysis procedure for the incremental method is illustrated in the following for a panel with six connectors under uniform load. $F_i(w)$ is the force in connector *i* when load *w* is applied to the panel counting for the yielding of any connectors. $X_i^{(r)}(w)$ is the force in connector *i* when load *w* is applied to the panel calculated based on equation [6]. The superscript *(r)* refers to the increment numbers used in the model for the calculation.

The calculation for connection force is shown in the following equations,

1) For $w_1 < w \leq w_2$ in *Figure 6.3(a)*,

$$F_1(w) = X_1^{(0)}(w_1) = F_y; \quad F_2(w) = X_2^{(0)}(w_1) < F_y; \quad F_3(w) = X_3^{(0)}(w_1) < F_y \qquad [11]$$

Here, the forces $X_i^{(0)}(w_1)$ is the solution of the system with three linear equations and three unknowns. Here, first connector 1L yielded for w_1 which can be called as w_e for the first yielding. Now, deflection after first connector yield Δ_e can be calculated based on equation [9] and effective bending stiffness based on

equation [10]. The stiffness at this point will be the effective bending stiffness of the system as after this point, the system load-deflection behaviour is no longer linear elastic.

2) For $w_2 < w \leq w_3$ in *Figure 6.3(b*), as connectors 1L have already yielded, therefore system of two linear equations with two unknowns can be solved for the load increment of $\Delta w_1 = (w\text{-}w_2)$ which will yield connector 2L. The deflection Δ_{11} can be calculated from equation [9] and therefore, $\Delta_1 = (\Delta_{11} - \Delta_e)$

$$F_1(w) = X_1^{(0)}(w_1) + 0 = F_y$$

$$F_2(w) = X_2^{(0)}(w_1) + X_2^{(1)}(\Delta w_1) = F_y$$

$$F_3(w) = X_3^{(0)}(w_1) + X_3^{(1)}(\Delta w_1) < F_y \qquad [12]$$

3) For $w_3 < w$ in *Figure 6.3(c)*, as connectors 1L, and 2L have yielded, a system with one linear equation and 1 unknown can be solved for the load increment of $\Delta w_2 = (w\text{-}w_3)$ which will yield connector 3L. The deflection Δ_{22} can be calculated from equation [9] and therefore, $\Delta_2 = (\Delta_{22} - \Delta_{11})$.

$$F_1(w) = X_1^{(0)}(w_1) + 0 + 0 = F_y$$

$$F_2(w) = X_2^{(0)}(w_1) + X_2^{(1)}(\Delta w_1) + 0 = F_y$$

$$F_3(w) = X_3^{(0)}(w_1) + X_3^{(1)}(\Delta w_1) + X_3^{(2)}(\Delta w_2) = F_y \qquad [13]$$

In equations [11] – [13], each of the connection force components is obtained by solving the system of linear equations. Therefore, combining the linear calculation with incremental load, the non-linear calculation for the connector force can be performed. When all connectors have yielded, the total load in MTPC composite system is obtained by summing all the load increments,

$$w_u = w_e + \sum_{i=1}^{a} \Delta w_i \qquad [14]$$

Similarly, the total deflection at the above total load can be written as,

$$\Delta_u = \Delta_e + \sum_{i=1}^{a} \Delta_i \qquad [15]$$

where, *a* is the number of load increments until total load.

From the above discussed incremental method, the nonlinear load-deflection response of the MTPC composite system can be generated as illustrated *Figure 6.3*. The grayed-out connectors in *Figure 6.3*

has been yielded and therefore, in plastic state. The effective bending stiffness of the MTPC composite system can be found from the load-deflection curve in the elastic stage using equation [10]. Similarly, stiffness after yielding of each connector can also be calculated which will gradually decrease. After yielding of each connector, the stresses in concrete and timber are checked to determine if either of them fails before yielding of the next connector. This approach allows designers to determine if the design ultimate limit state is either first yielding of connector or material failure in either the concrete or wood. In the load-deflection curve, the ultimate load and deflection can be found using equation [14] and [15]. In Appendix B, a calculation for effective bending stiffness and load-deflection response are shown.

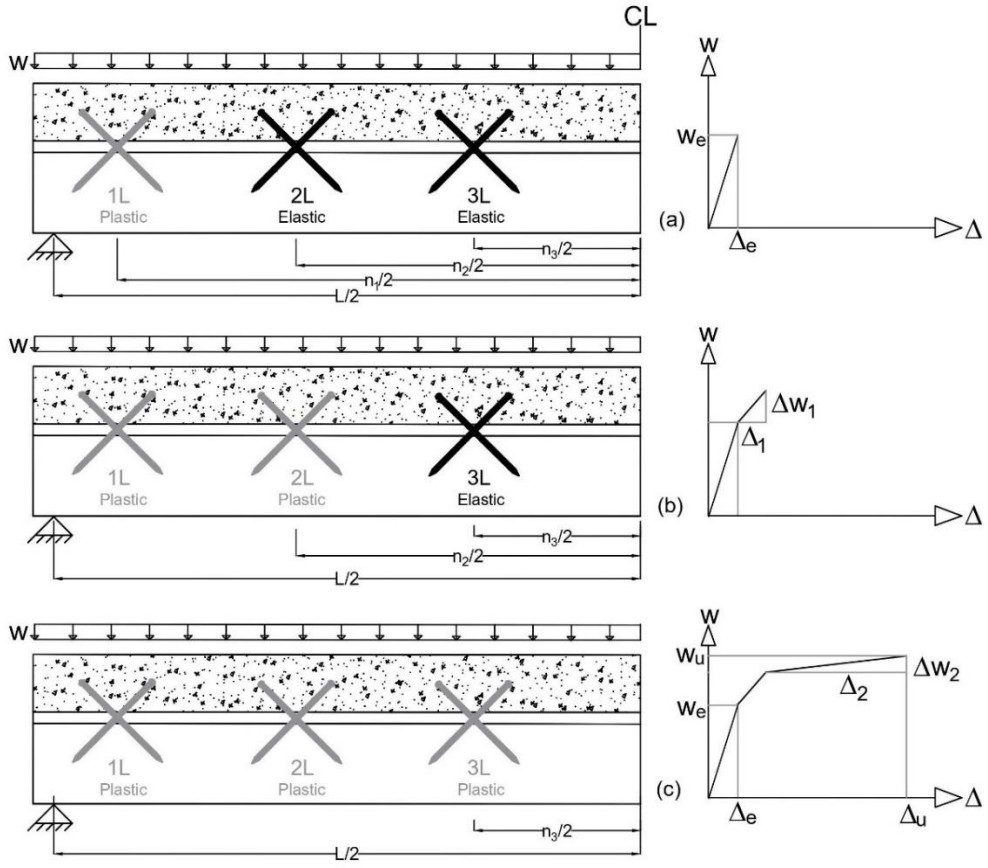

Figure 6.3: Load-deflection response from progressive yielding of connectors

6.3 Verification Test Program

A test program was conducted to verify the developed model presented above. In total, 12 MTPC strip panel specimens with different configurations were tested using static four-point bending testing procedures.

6.3.1 Materials

6.3.1.1 Mass Timber Panel (MTP):

Two types of Mass Timber Panel (MTP), namely Glue Laminated Timber (GLT) and Cross Laminated Timber (CLT) were used in the bending tests. Standard profile GLT (Western Archrib, 2019) of 130 mm thickness was used in this research, which was made of No. 2 grade Spruce-Pine-Fir (S-P-F) lumber. The mean wood density measured on the test date, was 455 kg/m^3 with modulus of elasticity of 9,500 MPa. The 3-ply E1 grade CLT thickness was 105 mm, which has 1950F$_b$-1.7E grade S-P-F lumber in longitudinal and No. 3/Stud S-P-F lumber in transverse layer (Nordic Structures, 2019). The measured average density at test date was 504 kg/m^3 with a modulus of elasticity of 11,700 MPa for the longitudinal layer.

6.3.1.2 Self-Tapping Screw

Fully threaded self-tapping screws (Rothoblaas, 2019b) with an 11 mm nominal diameter were used in this research. The screws have countersunk heads and self-drilling tip and are made of carbon steel with white galvanic zinc coating. Screws were all 200 mm long and inserted 100 mm into the MTP. In the timber-concrete composite application, fully threaded screw with wide countersank head is favorable as full thread provides higher load transfer in timber and better bonding with concrete, while the countersank head allows pullout resistance in concrete (Mirdad & Chui, 2019).

6.3.1.3 Acoustic material

A sound-proofing layer (RothoBlaas, 2019a) made of polyester felt and elasto-plastomer bitumen is used in this study, which is specially designed as an acoustic insulating material for absorbing noise and vibrations in timber-concrete composite application. The 5 mm thick acoustic material creates an elastic separation between stiff elements of the floor and dampening vibrations due to foot traffic. The acoustic material has a dynamic stiffness value of 7 MN/m^3 and this material can absorb vibrations from impact noise up to 26 dB (RothoBlaas, 2019a).

6.3.1.4 Concrete

Normal density ready-mix concrete with 13 mm nominal aggregate size was used. The concrete was reinforced with smooth welded steel wire reinforcement with 6.35 mm diameter and 100 mm x 100 mm grid size was used at concrete mid-depth to limit crack propagation in concrete due to shrinkage and temperature changes. Cylinder tests of concrete showed that the compressive strength on the test date was 55.8 MPa on average with modulus of elasticity of 23.5 GPa and Poisson's ratio of 0.14. Cylinder tests were performed according to ASTM C39/C39M-18 (ASTM, 2018) and ASTM C469/C469M-14 (ASTM, 2014).

6.3.2 Test Specimens

The CLT and GLT panels had lengths varying between 4.5 m to 6 m with 600 mm constant width. 75 mm and 100 mm concrete thicknesses were included. Studied insulation thicknesses were 0 mm (no insulation), 5 mm and 15 mm. Plastic sheets were used between the concrete slab and MTP to prevent any bond at the interface when there was no insulation. One screw diameter (11 mm) with two insertion angles relative to timber grain (30° and 45°) was tested at 250 mm and 500 mm spacing in cross-pairs. The self-tapping screw spacing in longitudinal and lateral direction of MTP was based on European Technical Approval ETA (ETA-Danmark, 2016) to prevent group effect. Acoustic insulation layer was inserted between concrete slab and MTP. A total of 12 specimens with different configurations were tested. The construction parameters that were changed for CLT and GLT were: concrete thickness (h_c), insulation thickness (h_i), screw angle and screw spacing (s). Two cross-pairs of screw (2 in shear-tension and 2 in shear-compression) were used in the transverse direction of 600 mm width specimen. Screws were located 75 mm from the edge and spaced 150 mm in the width direction. The construction details of all bending specimens with different configurations are shown in *Table 6.1*.

The specimens were prepared by first placing the acoustic layer over MTP and drilling the self-tapping screws into the MTP with appropriate specifications shown in Table 6.1. Formwork was installed to the side of the MTP to ensure the appropriate concrete thickness was achieved. The next step was to cast concrete on top of the MTP. The specimens were kept in normal shop temperature after casting the concrete and covered with plastic sheets for 7 days. Then the specimens were stacked outside and wrapped with tarps for a minimum of 28 days before bringing them in the structure's laboratory for testing.

Table 6.1: Construction details of bending test specimens

Specimen #	Specimen Code	MTP	Length, m	Concrete Thickness, mm	Insulation Thickness, mm	Screw Angle	Longitudinal Screw Spacing, mm	Screw #
1	GLT6-C100-I0-45°-S250	GLT	6	100	0	45°	250	96
2	GLT6-C75-I0-30°-S500	GLT	6	75	0	30°	500	48
3	GLT6-C75-I5-30°-S500	GLT	6	75	5	30°	500	48
4	GLT6-C75-I15-30°-S250	GLT	6	75	15	30°	250	96
5	CLT6-C75-I5-45°-S500	CLT	6	75	5	45°	500	48
6	CLT6-C75-I15-30°-S500	CLT	6	75	15	30°	500	48
7	GLT4.5-C100-I5-45°-S500	GLT	4.5	100	5	45°	500	36
8	GLT4.5-C100-I15-45°-S250	GLT	4.5	100	15	45°	250	72
9	GLT4.5-C100-I5-30°-S250	GLT	4.5	100	5	30°	250	72
10	GLT4.5-C75-I15-45°-S500	GLT	4.5	75	15	45°	500	36
11	CLT4.5-C100-I5-45°-S250	CLT	4.5	100	5	45°	250	72
12	CLT4.5-C100-I0-30°-S250	CLT	4.5	100	0	30°	250	72

6.3.3 Bending Tests

The specimens were tested to determine both their ultimate load and bending stiffness. The bending test setup is shown schematically in *Figure 6.4* and a typical test setup of a specimen is shown in *Figure 6.5*. As a four-point bending test, the distance between support and loading points was 1400 mm and 1900 mm respectively for 4.5 m and 6 m specimens. One end of the support was a roller over a pivot while the other support was allowed to rotate but not sliding. For loading, a steel spreader beam with a design capacity of 420 kN was connected with horizontal needle roller bearing and placed over the concrete at the one-third positions. Four horizontal Linear Variable Displacement Transducers (LVDT's) were placed at four corners of the specimen to measure the relative slip between MTP and concrete as shown in *Figure 6.5*. In the mid-span, two cable transducers were placed to measure the midspan displacement and can be seen in *Figure 6.5*. Load from hydraulic actuator was applied over the steel spreader beam and recorded using a calibrated load cell. The constant loading rate was 5 mm/minute until failure. The loading was stopped just after the specimen failed with a significant drop in the measured load. The effective bending stiffness of the specimens for four-point bending test were calculated based on ASTM D198-15 (ASTM , 2015) as follows,

$$EI_{eff} = \left(\frac{P}{\Delta}\right)\frac{23L^3}{1296} \quad [16]$$

Here, (P/Δ) is the slope of the load-deflection response in the linear range from 10-40% or 0-30% of P_{max} whichever is applicable, where, P_{max} is the maximum load at failure and L is the test span.

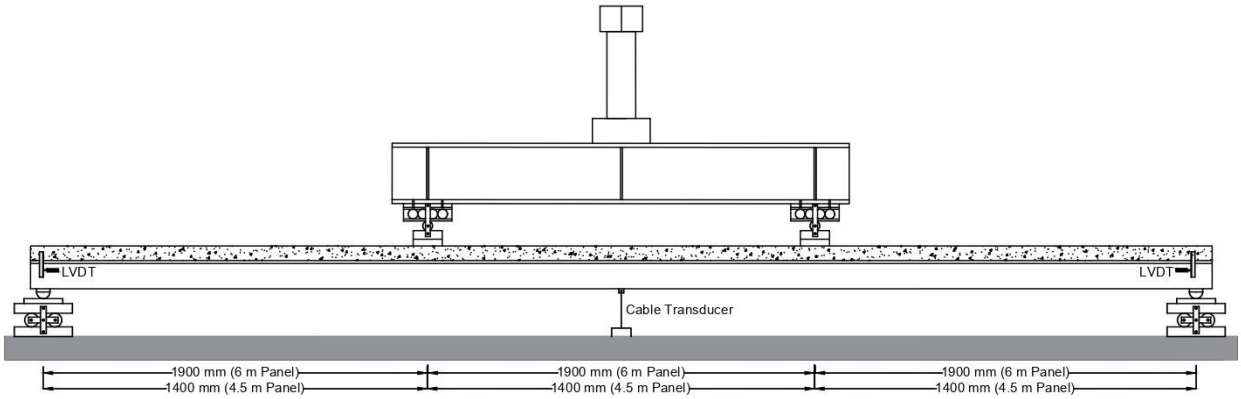

Figure 6.4: Bending test setup and instrumentation

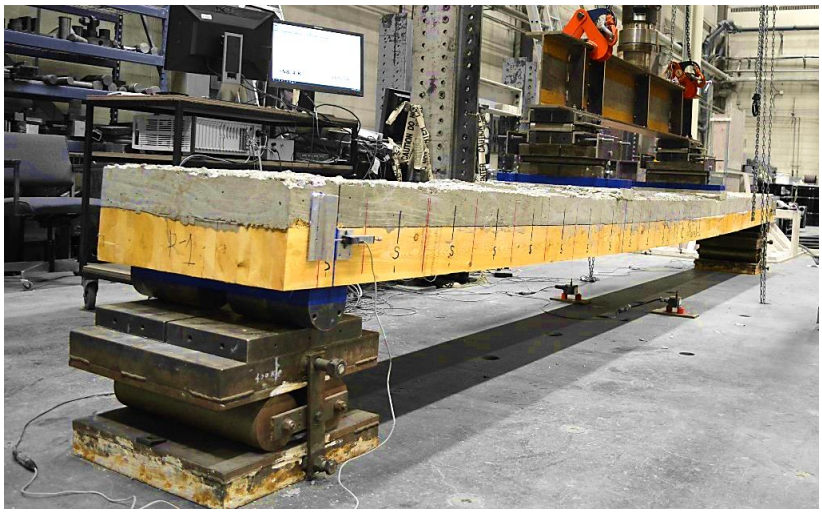

Figure 6.5: Typical bending test setup of a specimen

6.4 Model Validation

6.4.1 Effective Bending Stiffness

The load-slip responses were obtained by taking the average slip near the ends of the panel from LVDT's and applied load on the specimen which was recorded by the calibrated load cell and is presented in *Figure 6.6* for 6 m long specimens and in *Figure 6.7* for 4.5 m long specimens. In the bending test, the slip on each side was found nearly similar due to the cross-pair screw mechanism, which is the reason for using average slip in this study. The test vs prediction result from the models are presented in *Figure 6.8*. Besides, the load-deflection responses were obtained by taking the average mid-span deflection from two

cable transducers and applied load on the specimen and is presented in *Figure 6.9, 6.10 & 6.11* for all specimens. In *Figure 6.9*, the load-deflection response of test vs prediction of 6 m long GLT specimens are shown while in *Figure 6.10*, it is for 4.5 m long GLT specimens and in *Figure 6.11*, for all CLT specimens.

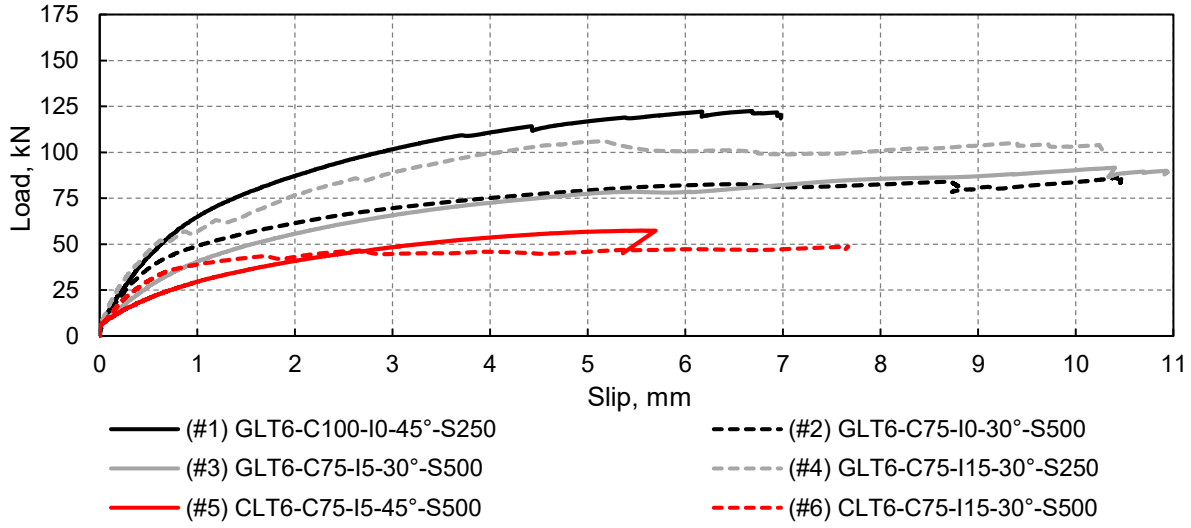

Figure 6.6: Load-slip responses of 6.0 m long specimens

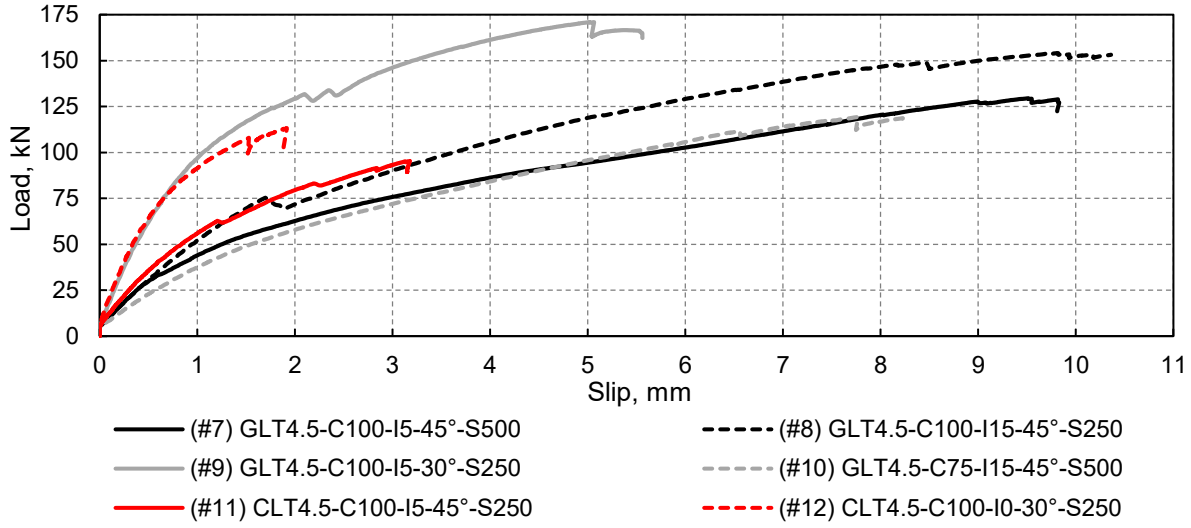

Figure 6.7: Load-slip responses of 4.5 m long specimens

The test vs prediction from model data are presented in *Table 6.2* where, the values for effective stiffness during each test were calculated using equation [16] from load-deflection measurements. In the equation [16], (P/Δ) was taken as the slope of the load-deflection response in the linear range from 10-40% or 0-30% of ultimate load based on the load-deflection curve. The slope within the range of 0-30% of ultimate

load was found applicable in the linear range in *Figures 6.10* for 4.5 m specimens. In this bending stiffness model, tested connection stiffness (Mirdad & Chui, 2019) were not used because it is not appropriate as the connection details were not the same in the bending and connection tests reported in (Mirdad & Chui, 2019). Here, connection stiffness was calculated based on the connection stiffness model (Mirdad & Chui, 2020b) where the predictions were within 18% of the connection test results with CoV of 26%. In the comparison, (+ve) denotes over-prediction while (-ve) denotes under-predictions with the bending test values as the reference.

Table 6.2: Bending test results comparison with prediction

#	Specimen	Moisture Content	Relative Slip, mm	Bending Stiffness (10^3), kN.m^2			Error	
				Test	Prediction	Gamma	Prediction	Gamma
1	GLT6-C100-I0-45°-S250	8.0 %	7.82	2.78	2.62	5.12	-6%	46%
2	GLT6-C75-I0-30°-S500	10.5 %	10.47	2.22	2.04	3.95	-9%	44%
3	GLT6-C75-I5-30°-S500	8.3 %	10.94	1.87	2.02	3.71	7%	49%
4	GLT6-C75-I15-30°-S250	7.5 %	10.53	2.12	1.85	4.10	-15%	48%
5	CLT6-C75-I5-45°-S500	7.0 %	5.69	1.30	1.44	2.34	9%	44%
6	CLT6-C75-I15-30°-S500	6.3 %	7.67	1.39	1.52	2.36	8%	41%
7	GLT4.5-C100-I5-45°-S500	6.5 %	10.81	2.54	2.71	3.46	6%	27%
8	GLT4.5-C100-I15-45°-S250	7.5 %	10.36	2.47	2.59	4.65	5%	47%
9	GLT4.5-C100-I5-30°-S250	8.5 %	5.56	2.94	2.71	5.18	-9%	43%
10	GLT4.5-C75-I15-45°-S500	7.5 %	8.23	1.88	2.01	2.68	7%	30%
11	CLT4.5-C100-I5-45°-S250	6.3 %	3.18	1.91	2.12	3.49	10%	45%
12	CLT4.5-C100-I0-30°-S250	6.3 %	1.92	2.31	2.20	4.49	-5%	48%

It can be seen that the model is able to predict the bending stiffness of 6 m long specimens to within -15% to +9% of test results. For 4.5 m long specimens, the stiffness prediction is within -9% to +10% of test results. Stiffness of 6 m specimens were found within an absolute average value of 9% to the test results with some predicted stiffness higher while others being lower the test values. On the other hand, for 4.5 m specimens, the predictions were within an absolute average value of 7% to the test results. In 6 m long specimens, the concrete thickness was 75 mm except for specimen (#1) GLT6-C100-I0-45°-S250. On the other side, the concrete thickness for 4.5 m long specimens was 100 mm except for the specimen (#10) GLT4.5-C100-I15-45°-S250. The higher thickness of concrete might be a reason for higher stiffness in 4.5

m long specimens compared to 6 m long specimens. All the specimens with 30° angled screws showed under predictions except for specimen (#4) GLT6-C75-I15-30°-S250 and (#6) CLT6-C75-I15-30°-S500. The stiffness prediction varied with test results when there were insulation layers. This is because, after pouring the concrete, the soft insulation layer squeezed and therefore, the insulation thickness was reduced and the concrete thickness increased from the actual assumed one in the model. If we assume the insulation squeeze around 25% for the insulation, then the revised predicted stiffness comes within 4% of test results. Also, all the specimens without insulation were found to underestimate the bending stiffness slightly by about 6% (see specimen (#1) GLT6-C100-I0-45°-S250, (#2) GLT6-C75-I0-30°-S500 and (#12) CLT4.5-C100-I0-30°-S250). In the model, the used material properties were not tested and extracted from the more reliable in-grade lumber test data (Barrett & Lau, 1994) which might be another reason for the discrepancy in the prediction.

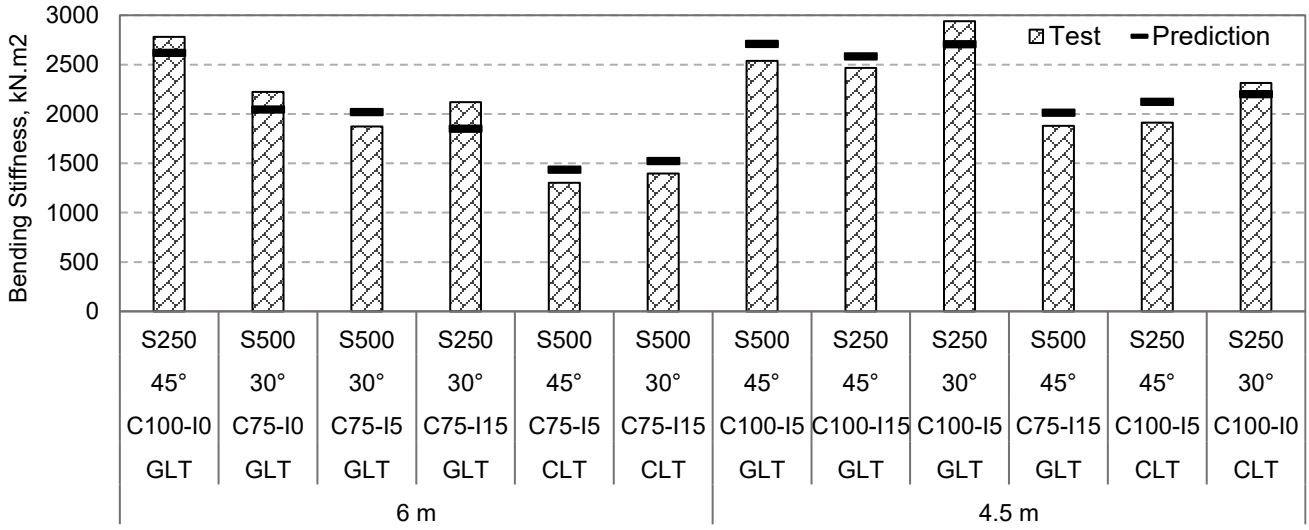

Figure 6.8: Test bending stiffness compared to predicted stiffness for each specimen

From the previous connection tests (Mirdad & Chui, 2019), it was found that 30° angled screw had higher stiffness compared to 45° angled screws and in the bending test, the trend matches well as all the specimens with 45° angled screw showed lower stiffness except specimen (#1) GLT6-C100-I0-45°-S250 without insulation. Also, the bending stiffness trend matches well with the connection test result (Mirdad & Chui, 2019) as there was a significant drop in stiffness due to the presence of insulation layers and can be seen in specimen (#1) GLT6-C100-I0-45°-S250 and (#2) GLT6-C75-I0-30°-S500. Closely spaced

screw contributes to the bending stiffness significantly. Therefore, the reduction of bending stiffness due to the presence of insulation layer can be mitigated by using closely spaced screws which can be seen in specimen (#8) GLT4.5-C100-I15-45°-S250 and (#10) GLT4.5-C75-I15-45°-S500. The specimens with CLT showed lower bending stiffness compared to the specimens with GLT because of the rolling shear failure at early stage except for the specimen (#12) CLT4.5-C100-I0-30°-S250, where there was no insulation. Concrete thickness was found to influence the bending stiffness of MTPC composite system. Besides, the bending stiffness in 6 m and 4.5 m long specimens varies with different parameters.

When equation [1] was used to calculate the bending stiffness (*Table 6.2*), it was found that Gamma method overestimates the stiffness on average by 43% which raises questions about its suitability for predicting stiffness properties of MTPC composite systems with semi-rigid connections. This finding matches well with previous research (Gerber, 2016). In *Table 6.2, Figure 6.6* and *Figure 6.7*, the relative slip values at ultimate load level are shown. The relative slip at ultimate load can be seen much higher when there was an insulation layer and less screws except for the CLT specimens. The CLT specimens (#5) CLT6-C75-I5-45°-S500, (#6) CLT6-C75-I15-30°-S500, (#11) CLT4.5-C100-I5-45°-S250 and (#12) CLT4.5-C100-I0-30°-S250 failed in rolling shear at early stage of test and therefore, and the relative slip at ultimate load was found to be less compared to other GLT specimens. Overall, the test vs prediction result from the models are presented in *Figure 6.8*. The bending stiffness measured from tests can vary significantly even between seemingly similar specimens. This is because it is a property that is very sensitive to specimen fabrication, friction between components, variation in concrete thickness and deflection measuring device alignment, etc. The predictions using the model are within a reasonable range of -15% to +10% with an average of 8% of bending test values although concrete cracking behaviour was not considered in the model. Therefore, this model can be a potential basis for predicting effective bending stiffness as Gamma method is only an approximate method with underlying assumptions about loading and uniform slip along the beam. Moreover, Gamma method is not appropriate for MTPC composite system that contains widely spaced discrete connectors and MTP.

6.4.2 Load-Deflection Response

The full load-deflection response predictions are compared with the tested response and shown in *Figure 6.9, 6.10* and *6.11* for 6 m GLT specimen, 4.5 m GLT specimens and all CLT specimens respectively. In *Figure 6.9, 6.10 and 6.11*, solid line denotes test response and dotted line denotes predicted response. The predictive bending stiffness was extracted from linear stage before the first connector yields. After yielding of first connector, the nonlinear part starts which finally ends at the predicted peak load. As discussed in the previous section for the effective bending stiffness, the load-deflection response of specimen with an insulation showed some variance which might be because, after pouring concrete over insulation, the thickness reduces in practice due to the soft nature of the insulation but, the model considers the actual insulation thickness. The predicted response does not follow the test response exactly also because of the higher predictions of total load due to not considering the cracking behaviour of concrete. Usually, beyond the elastic range, concrete cracking governs the performance of the composite system and therefore, the predicted post elastic behaviour was always found stiffer than the test response. Another reason for the variance in the load-deflection responses might be due to the ignorance of vertical load in the connection model which might additionally bend the screw and affect the connection properties. The tested load-deflection response of 4.5 m long specimen (*Figure 6.10)* can be seen stiffer than the response of 6 m long specimen (*Figure 6.9)* and the predicted response follow the trends.

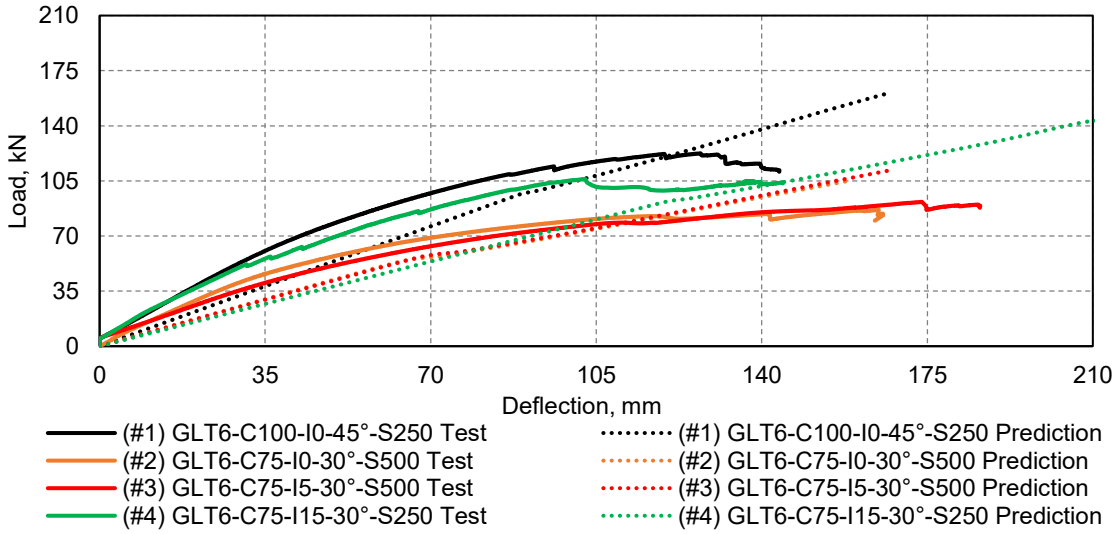

Figure 6.9: Load-deflection responses of 6.0 m GLT specimens

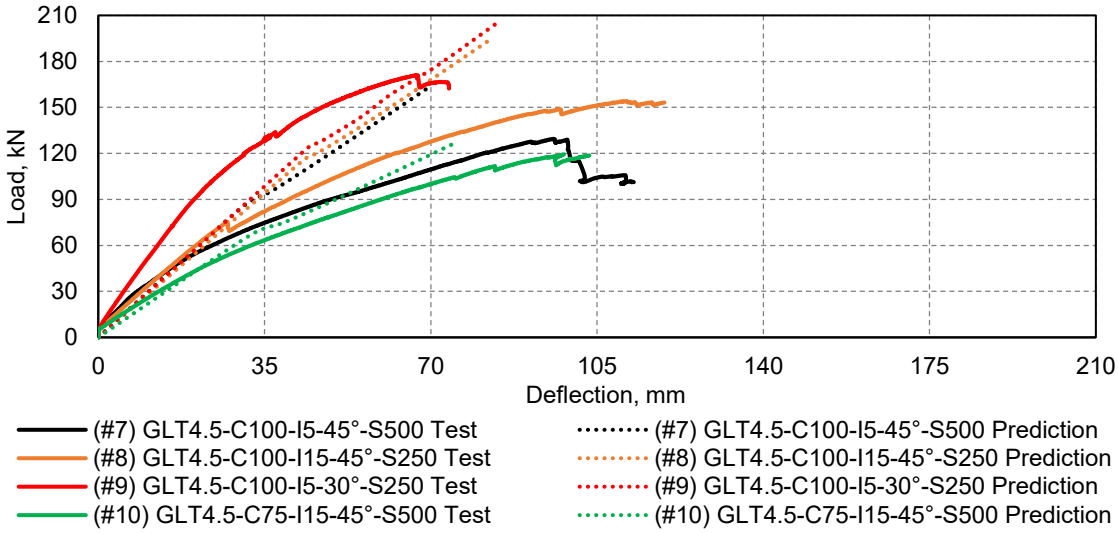

Figure 6.10: Load-deflection responses of 4.5 m GLT specimens

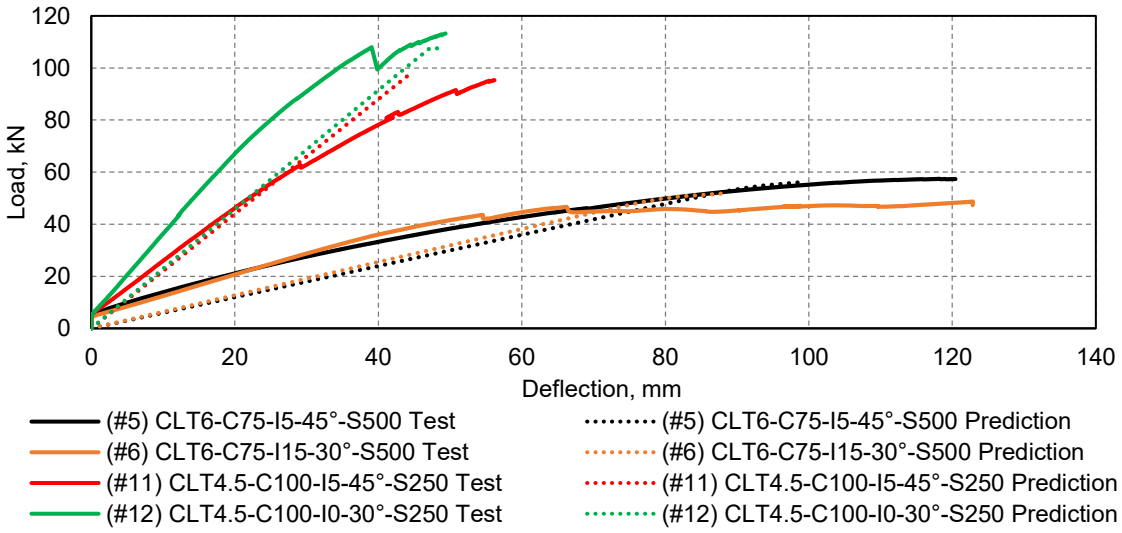

Figure 6.11: Load- deflection responses of all CLT specimens

The predicted responses for CLT specimens are found to be the best match to the corresponding test responses and can be seen in *Figure 6.11*. This is because, all the CLT specimen failed dramatically in rolling shear during the linear stage which can be seen from the tested load-deflection response in *Figure 6.11*. The predicted load-deflection response generated by this model also showed that the CLT specimens reached its total load when first or second connector yielded and therefore, follows the trend of test response. The input parameters into the model for generating the load-deflection response also vary from the actual parameters of the composite members. During the bending test, the distributed beam of 4.2 kN was placed over the MTPC specimens before recording the data. This is because the

distributed beam was not connected with the loading jack due to the test setup and therefore, all tested load-deflection response stated from 4.2 kN instead of zero in *Figure 6.9, 6.10 and 6.11*. It is always difficult to predict the exact non-linear load-deflection response of the partially composite timber-concrete panels specially at the presence of insulation layers. This developed model provides a user-friendly procedure to predict close enough load-deflection response to the test but, the predicted response can be significantly improved by considering the cracking behaviour of concrete.

6.5 Conclusions

The major aim of this study was to develop a rational analytical model to predict the effective bending stiffness and load-deflection response of MTPC composite system considering the strength, stiffness and plastic behaviour of the interlayer connection. MTPC composite panel test specimens with various construction parameters, including an insulation layer and inclined self-tapping screws, were tested under bending to validate the developed bending stiffness model. The developed model was also compared with the most widely used Gamma method for stiffness predictions.

An analytical model was developed in this study, by extending the model by Zhang (Zhang, 2013). The predictive capability of the developed model was evaluated by comparing the predictions with bending test results. It was found that on average, the developed model predicts composite bending stiffness within the range from -15% to +10% of bending test values. Also, the universally used Gamma method was found to over-predict bending stiffness on average by about 43% and not appropriate when there is widely spaced discrete connectors and MTP. Similar to the connection behaviour reported earlier (Mirdad & Chui, 2019), the effective bending stiffness of the composite panel is influenced significantly by the screw inclination and insulation thickness. The influence of screw spacing on system bending stiffness was found to be significant and can be used to mitigate the reduction in stiffness due to the presence of an insulation layer. On the other hand, the predicted load-deflection response was found stiffer in the post-elastic region due to the ignorance of concrete cracking behaviour. Therefore, the proposed model can mitigate the short-comings of the models that are based on the Gamma method.

Chapter 7. Conclusion

7.1 Research Summary

The major focus of this research was on the structural behavior of Mass Timber Panel-Concrete (MTPC) composite containing self-tapping screws inserted in an inclined orientation and an insulation layer between the components to propose the design method to facilitate the use of such a system in mass timber construction. Therefore, the behaviour of Self-Tapping Screw was initially investigated with wide range of parameters (e.g.; insulation thickness, screw insertion angle, screw embedment length, and MTP) through small-scale connection test and rational analytical models were proposed for predicting strength and stiffness of the connection at the presence of insulation gap. Once the connection behaviour was well understood, the design analytical models were proposed to predict capacity, effective bending stiffness, failure modes and load-deflection response of MTPC composite.

The connection properties were found heavily influenced by the insulation thickness compared to the screw insertion angle, screw embedment length, and MTP. The stiffness (65% reduction) of the connections appears to be strongly influenced by the insulation layer compared to the strength (35% reduction). The 30° angled screws relative to the timber grain showed higher strength and stiffness compared to 45° angled ones in concrete-timber joints which is one of the new findings in this research field. Also, a larger embedment length of screw into MTP showed a higher stiffness and strength but it was less significant in the presence of an insulation layer. Test values in terms of strength and stiffness were similar in all MTP.

Analytical models for predicting timber-to-concrete connection strength with inclined screws and an insulation gap were presented for solid and layered timber based on the extended Johansen's yield theory covering all possible failure modes. The predictive capability of the developed models was evaluated by comparing the predictions with connection test results. The predictions through the developed models were within 10% of tested connection strengths for solid timber and 12% for layered timber with proper failure modes.

Analytical models for predicting timber-to-concrete connection stiffness with inclined screws and an insulation gap were also presented for solid and layered timber considering the bending stiffness of the screw by applying a theoretically derived correction factor for the embedment stiffness modulus based on the beam on elastic foundation. Again, the predictive capability of the developed models were evaluated by comparing the predictions with connection test results. The predictions through the developed models were within 22% of tested connection stiffness for solid timber and 14% for layered timber with a significant contribution of interfacial friction at the absence of insulation layers.

Rational analytical model to predict the load-carrying capacity, effective bending stiffness, failure modes and load-deflection response of MTPC composite beam considering the strength, stiffness and plastic behaviour of the interlayer connection was developed extending the model of Zhang (Zhang, 2013) and validated with MTPC composite panel bending test specimens with various construction parameters. Although, the developed model has some limitations due to the ignorance of concrete cracking behaviour, it was able to predict composite panel capacity within 13% and effective bending stiffness within 8% of bending test values with proper failure modes. The universally used Gamma method was found to over-predict bending stiffness on average by about 43% and not appropriate when there are widely spaced discrete connectors, beside its inability of predicting system capacity. The influence of screw spacing on system capacity and bending stiffness was found to be significant and can be used to mitigate the reduction in capacity due to the presence of an insulation layer.

Overall, the entire procedure to design the MTPC composite system are shown below with a flowchart in *Figure 7.1*.

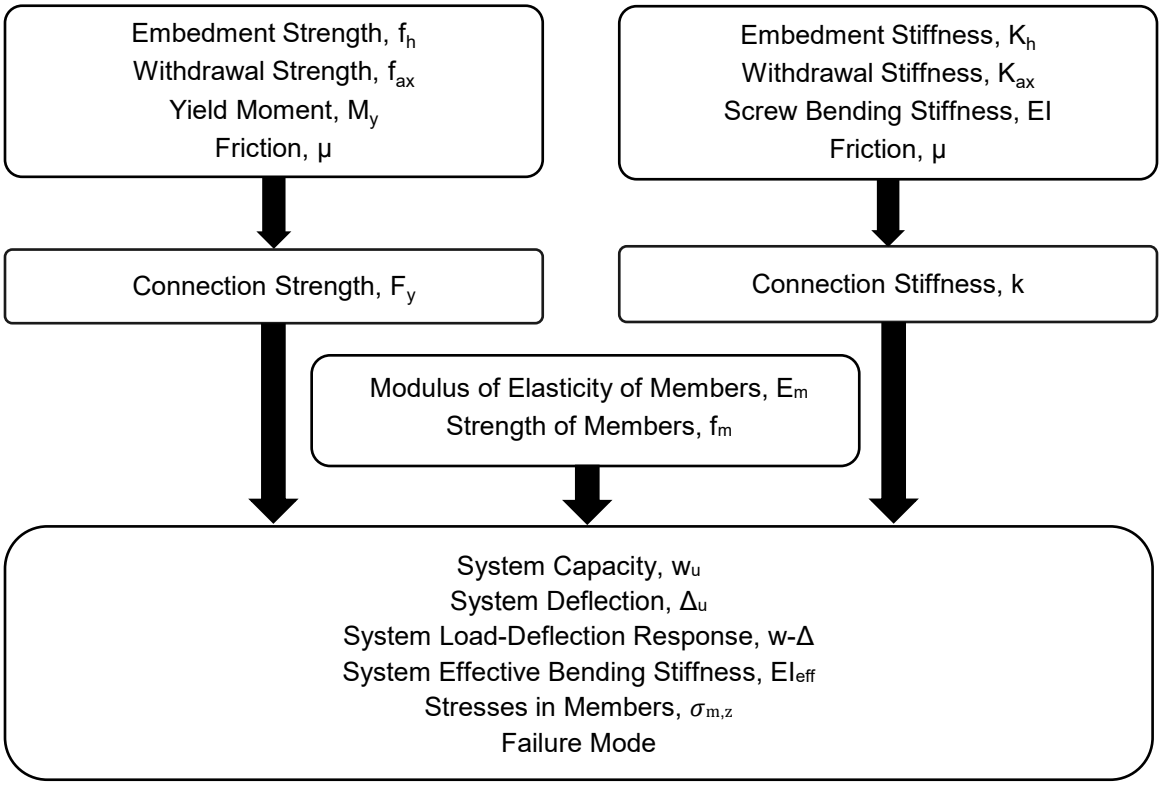

Figure 7.1: Flowchart of MTPC composite design procedure

7.2 Research Contributions

The original contributions of this research through the outcomes are,

1) 30° angled screws relative to the timber grain has higher strength and stiffness compared to 45° angled ones and performs better in timber-concrete joints.
2) Strength of the connection into solid and layered timber can be directly predicted by developed strength model containing inclined self-tapping screws and insulation layer with input parameter such as embedment strength, withdrawal strength and yield moment capacity of screws.
3) Stiffness of the connection into solid and layered timber can be directly predicted by the developed stiffness model containing inclined self-tapping screws and insulation layer with input parameter such as embedment stiffness, withdrawal stiffness of screws and friction in timber-concrete interface.
4) Capacity, effective bending stiffness, failure modes and load-deflection response of MTPC composite beam containing insulation layer can be predicted from the extended elastic-plastic

model with progressive connector yielding mechanism with input parameters from developed connection strength and stiffness model.

5) Structural design guidelines such as span-table for the MTPC composite floor system with insulation layers under one-way bending action can be extracted with construction details optimizing structural performance for various occupancy requirements (e.g., residential or commercial).

7.3 Future Recommendation

This research was limited to scope discussed above and can be further expanded to address the following,

1) Improve the connection model by including the compressive force normal to the shear plane of the connection. In the real application, this compressive force might affect the connection properties at the presence of insulation gap with additional bending of the screws.
2) Improve the system model by considering the cracking behaviour of the concrete. In the post elastic region, the concrete starts to crack under applied load. Therefore, ignoring concrete cracking behaviour might lead to a higher capacity and stiffer response at that region.
3) Extend the system model for different boundary conditions as in the real application, pure simply supported condition might not exist. Therefore, end-fixity factor can be developed to mitigate this problem. Also, the model can be extended for different loading conditions.

References

ACI, 1985. *Code requirements for nuclear safety related concrete structures: Appendix B- Steel embedemnts,* Farmington Hills, USA: Designation: 349-85, American Concrete Institute.

ACI, 2008. *Building code requirements for structural concrete and commentary,* Farmington Hills, USA: Designation: 318-08, American Concrete Institute.

ASTM , 2013. *Standard test method for evaluation dowel-bearing strength of wood and wood-based products,* West Conshohocken, USA: Designation: D5764-97a, ASTM International.

ASTM , 2014. *Standard test method for static and kinetic coefficients of friction of plastic film and sheeting,* West Conshohocken, USA: Designation: D1894-14, ASTM International.

ASTM , 2015. *Standard Test Methods of Static Tests of Lumber in Structural Sizes,* West Conshohocken, PA : Designation D198-15, ASTM International.

ASTM , 2016. *Standard test methods for tension testing of metallic materials,* West Conshohocken, USA: Designation: E8/E8M-16a, ASTM International.

ASTM , 2017. *Standard test method for determining bending yield moment of nails,* West Conshohocken, USA: Designation: F1575-17, ASTM International.

ASTM, 2014. *Standard Test Method for Static Modulus of Elasticity and Poisson's Ratio of Concrete in Compression,* West Conshohocken, PA: Designation C469/C469M-14, ASTM International.

ASTM, 2018. *Standard Test Method for Compressive Strength of Cylindrical Concrete Specimens,* West Conshohocken, PA: Designation C39/C39M-18, ASTM International.

ASTM, 2019. *Standard Specification for Establishing and Monitoring Structural Capacities of Prefabricated Wood I-Joists*, West Conshohocken, PA: Designation D5055-19e1, ASTM International.

Barrett, J. D. & Lau, W., 1994. *Canadian Lumber Properties.* Ottawa, Ontario, Canada: Canadian Wood Council.

Bejtka, I., 2005. *Verstärkung von bauteilen aus holz mit vollgewindeschrauben,* Karlsruhe, Germany: PhD Thesis, Universtität Karlsruhe.

Bejtka, I. & Blass, H., 2001. *Screws with continuous threads in timber connections,* Stuttgart: In:RILEM, Proceedings PRO 22, p. 193-202.

Bejtka, I. & Blass, H., 2002. *Joints with inclined screws.* In Meeting, 35 international council for building research studies and documentation, CIB W18 - timber Structures, Kyoto, Japan.

Blass, H., Bejtka, I. & Uibel, T., 2006. *Trägfähigkeit von verbindung mit selbst bohrenden holzschrauben mit vollgewinde. lehrstuhl für ingenieurholzbau und baukonstruktionen,* Karlsruhe, Germany: Universität Karlsruhe.

Carvalho, E. & Carrasco, E., 2010. Influence of Test Specimen on Experimental Characterization of Timber-Concrete Composite Joint. *Construction and Building Materials,* 24(2010) (doi:10.1016/j.conbuildmat.2009.12.036), p. 1313-1322.

Ceccotti, A., 2002. Composite concrete-timber structures. *Structural Engineering and Materials,* 2002(4) (https://doi.org/10.1002/pse.126), p. 264-275.

Closen, M., 2012. *Self-tapping screw assemblies under monotonic and reverse cyclic load,* Vancouver, Canada: M.A.Sc thesis, University of British Colombia.

COST, 2018. *Design of timber-concrete composite structures,* Aachen, Germany: COST, European Cooperation in Science and Technology.

CSA , 2014. *Design of concrete structures: Annex D- Anchorage,* Mississauga, Ontario: Designation: A23.3-14, Canadian Standards Association .

Cuerrier-Auclair, S., Sorelli, L. & Salenikovich, A., 2016. Simplified nonlinear model for timber-concrete composite beams. *International Journal of Mechanical Sciences,* 117 (http://dx.doi.org/10.1016/j.ijmecsci.2016.07.019), p. 30-42.

Deam, B., Fragiacomo, M. & Buchanan, A., 2008. Connections for composite concrete slab and LVL flooring systems. *Materials and Structures,* 41(3) (doi: 10.1617/s11527-007-9261-x), p. 495–507.

Dias, A., 2005. *Mechanical behaviour of timber-concrete joints,* Delft. The Netherlands: Ph.D. thesis, Delft University of Technology.

Dias, A., 2012. Analysis of Nonlinear Behavior of Timber-Concrete Connections. *Journal of Structural Engineering,* 138(9) (doi: 10.1061/(ASCE)ST.1943-), p. 1128-1137.

Dias, A., Cruz, H., Lopes, S. & van der Kuilen, J., 2010. The stiffness of dowel-type fasteners in timber-concrete joints. *Structures and Buildings,* 163(4) (doi: 10.1680/stbu.2010.163.4.257), p. 257–266.

Dias, A. & Jorge, L., 2011. The Effect of Ductile Connectors on the Behaviour of Timber-Concrete Composite Beam. *Engineering Structures,* 33(2011) (doi:10.1016/j.engstruct.2011.05.014), p. 3033-3042.

Dias, A., Lopes, S., Van de Kuilen, J. & Cruz, H., 2007. Load-carrying capacity of timber-concrete joints with dowel-type fasteners. *Journal of Structural Engineering,* 133(5) (doi: 10.1061/(ASCE)0733-9445(2007)133:5(720)), p. 720–727.

Dietsch P., B. R., 2015. Self-tapping screw and threaded rods as reinforcement for structural timber element- A state of the art reports. *Construction and Building Materials,* 97 (2015) (http://dx.doi.org/10.1016/j.conbuildmat.2015.04.028), p. 78–89.

EN 1382, 1999. *Timber structures- test methods- withdrawal capacity of timber fasteners,* Brussels, Belgium: European Committee for Standardization, CEN.

EN 1995-1-1, 2009. *Eurocode 5: Design of timber structures part 1-1: General-common rules and rules for buildings,* Brussels, Belgium: European Committee for Standardization, CEN.

EN 26891, 1991. *Timber structures - Joints made with mechanical fasteners - General principles for the determination of strength and deformation characteristics,* Brussels, Belgium: European Committee for Standardization, CEN.

ETA-Danmark, 2016. *Rothoblaas self-tapping screws,* Danmark: European Technical Assessment ETA-11/0030 of 2016-04-07.

Frangi, A. & Fontana, M., 2003. Elasto-plastic model for timber-concrete composite beams with ductile connection. *Structural Engineering International,* 13(https://doi.org/10.2749/101686603777964856), p. 47.

Gelfi, P., Giuriani, E. & Marini, A., 2002. Stud shear connection design for composite concrete slab and wood beams. *Journal of Structural Engineering,* 128(12) (doi: 10.1061/~ASCE!0733-9445~2002!128:12~1544!), p. 1544–1550.

Gerber, A., 2016. *Timber-concrete composite connectors in flat-plate engineered wood products.,* Vancouver, Canada: M.A.Sc. thesis, University of British Colombia.

Girhammar, U., Jacquier, N. & Källsner, B., 2017. Stiffness model for inclined screws in shear-tension mode in timber-timber joints. *Engineering Structures,* 136 (http://dx.doi.org/10.1016/j.engstruct.2017.01.022), p. 580-595.

Hetenyi, M., 1983. *Beams on elastic foundation.* Volume XVI. Michigan: University of Michigan.

Hlavicˇka, V. & Lublóy, E., 2018. Concrete cone failure of bonded anchors in thermally damaged concrete. *Construction and Building Materials,* 171 (https://doi.org/10.1016/j.conbuildmat.2018.03.148), p.588–597.

Jacquier, N., 2015. *Development and evaluation of mechanical joints for composite floor elements with cross laminated timber,* Sweden: Doctoral Thesis, Luleå University of Technology.

Jockwer, R., Steiger, R. & Frangi, A., 2014. Fully threaded self-tapping screws subjected to combined axial and lateral loading with different load to grain angles. *Materials and Joints in Timber Structures, RILEM,* 9 (doi: 10.1007/978-94-007-7811-5_25), p. 265-272.

Johansen, K., 1949. Theory of timber connection. *Bridge Structural Engineering,* Volume 9, p. 249-262.

Kavaliauskas, S., Kazimieras-Kvedaras, A. & Valiu¯nas, B., 2007. Mechanical behaviour of timber-to-concrete connections. *Journal of Civil Engineering and Management,* 13:3 (http://dx.doi.org/10.1080/13923730.2007.9636437), p. 193-199.

Kennedy, S., 2014. *Withdrawal and embedding resistance of fasteners in timber and CLT panels,* Quebec, canada: M.Sc. Thesis, Laval University.

Kevarinmäki, A., 2002. *Joints with inclined screws.* In Meeting, 35 international council for building research studies and documentation, CIB W18 - timber Structures, Japan.

Khorsandnia, N., Valipour, H. & Crews, K., 2012. Experimental and analytical investigation of the short-term behaviour of LVL-concrete composite connections and beams. *Construction and Building Materials,* 37 (http://dx.doi.org/10.1016/j.conbuildmat.2012.07.022), p. 229-238.

Kremor, P. & Symmons, M., 2015. Mass-timber construction as an alternative to concrete and steel in the Australian building industry: a PESTL evaluation of the potential. *International Wood Products Journal,* 6(3) (https://doi.org/10.1179/2042645315Y.0000000010), p. 138-147.

Lukaszewka, E., 2009. *Development of prefabricated timber-concrete composite floors,* Sweden: Doctoral Thesis, Luleå University of Technology.

Lukaszewska, E., Johnsson, H. & Fragiacomo, M., 2008. Performance of connections for prefabricated timber-concrete composite floors. *Materials and Structures,* 41 (DOI 10.1617/s11527-007-9346-6), p. 1533–1550.

Marchi, L., Scotta, R. & Pozza, L., 2017. Experimental and Theoretical Evaluation of TCC Connections with Inclined Self-Tapping Screws. *Materials and Structures,* 50:180(doi: 10.1617/s11527-017-1047-1).

Mirdad, M. A. H. & Chui, Y. H., 2020a. Strength prediction of Mass Timber Panel-Concrete composite connection with inclined screws and a gap. *Journal of Structural Engineering,* 146(8): 04020140 (https://doi.org/10.1061/(ASCE)ST.1943-541X.0002678).

Mirdad, M. A. H. & Chui, Y. H., 2020b. Stiffness prediction of Mass Timber Panel-Concrete (MTPC) composite connection with inclined screws and a gap. *Engineering Structures,* 207: 110215 (https://doi.org/10.1016/j.engstruct.2020.110215).

Mirdad, M. A. H. & Chui, Y. H., 2019. Load-slip performance of Mass Timber Panel-Concrete (MTPC) composite connection with self-tapping screws and insulation layer. *Construction and Building Materials.,* vol. 213 (https://doi.org/10.1016/j.conbuildmat.2019.04.117), p. 696-708.

Mohler, K., 1956. *U¨ ber das Tragverhalten von Biegetra¨gern und Drucksta¨ben mit zusammengesetztem Querschnitt und nachgiebigen Verbindungsmitteln,* Karlsruhe, Germany: KTH.

Monteira, S., Dias, A. & Negrao, J., 2013. Assessment of Timber-Concrete Connections Made. *Society for Experimental Mechanics,* 37 (doi:10.1111/j.1747-1567.2011.00804.x), p. 50-65.

Moshiri, F., Shrestha, R. & Crews, K., 2014. The predictive model for stiffness of inclined screws as shear connection in timber-concrete composite floor. *Materials and Joints in Timber Structures, RILEM,* 9 (doi:10.1007/978-94-007-7811-5_40), p. 443-453.

Niederwestberg, J., Zhou, J. & Chui, Y. H., 2018. Mechanical Properties of Innovative, Multi-Layer Composite Laminated Panels. *Buildings,* 8(10) (https://doi.org/10.3390/buildings8100142), p. 142.

Nordic Structures, 2019. *Nordic X-Lam Cross laminated Timber.* [Online]
Available at: www.nordic.ca/en/products/nordic-x-lam-cross-laminated-timber-clt

Pirnbacher, G., Brandner, R. & Schickhofer, G., 2009. *Base Parameters of Self-Tapping Screws.* Duebendorf, Switzerland.

Ringhofer, A., 2017. *Axially loaded self-tapping screws in solid timber and laminated timber products,* Graz, Austria: Dissertation, Graz University of Technology.

RothoBlaas, 2019a. *Silent floor, soundproofing foils.* [Online]
Available at: www.rothoblaas.com/products/soundproofing/soundproofing-foils/silent-floor

Rothoblaas, 2019b. *VGS, Total thread connector with countershunk head.* [Online]
Available at: www.rothoblaas.com/products/fastening/screws/screws-structures/vgs

Shirvani, M., 1998. Statistical analysis and design recommendations. In: *Behavior of tensile anchors in concrete.* Austin, USA: University of Texas at Austin, p. 261-271.

Symons, D., Persaud, R. & Stanislaus, H., 2010. Slip modulus of inclined screws in timber–concrete floor. *Structures and Buildings,* 163(4) (doi: 10.1680/stbu.2010.163.4.245), p. 245–255.

Symons, D., Persaud, R. & Stanislaus, H., 2010. Strength of inclined screw shear connections for timber and concrete composite construction. *Structural Engineer,* Volume 88(1), p. 25–32.

Think Wood, 2019. *Mass Timber in North America; Expanding the Possibilities of Wood Building Design.* [Online] Available at: www.thinkwood.com/wp-content/uploads/2017/12/Think-Wood-CEU-Mass-Timber-in-North-America-2017.pdf

Timmerman, K. & Meierhofer, U., 1993. *Holz/Beton-Verbundkonstuktionen: Untersuchungen und Entwicklungen zum mechanischen Verbund von Holz und Beton,* Schweiz: EMPA.

Tomasi, R., Crosatti,, A. & Piazza, M., 2010. Theoretical and experimental analysis of timber-to-timber joints connected with inclined screws. *Construction and Building Materials,* Volume 24 (10.1016/j.conbuildmat.2010.03.007), p. 1560-1574.

Tommola, J. & Jutila, A., 2001. *Analysis of wood-concrete composite girder with discrete shear connectors.* Zurich, Switzerland.

Uibel, T. & Blaß, H. J., 2006. *Load carrying capacity of joints with dowel type fasteners in solid wood panels,* Florence, Italy: In: Proceedings. CIB-W18 Meeting.

Van der Linden, M., 1999. *Timber-concrete composite floor systems,* Delft, The Netherlands: Ph.D. thesis, Delft University of Technology.

Western Archrib, 2019. *Western Archrib Product, WESTDEK.* [Online]
Available at: http://www.westernarchrib.com/?page_id=193/#westdek

Yeoh, D., Fragiacomo, M., De Franceschi, M. & Boon, K., 2011. State of the art on timber-concrete composite structures: a Literature review. *Journal of Structural Engineering,* 137(10) (doi: 10.1061/(ASCE)ST.1943-541X.0000353.), p. 1085-1095.

Zhang, C., 2013. *Analysis of the timber-concrete composite systems with ductile connection,* Toronto, Canada: Masters Thesis, University of Toronto.

Appendices

Appendix A. Effect of the Flexibility of Screw

Using the theory of beam-on-elastic foundation proposed by Hetenyi (Hetenyi, 1983), the lateral deflection of the screw subjected to a concentrated shear force (F_{lat}) applied at the shear plane is given by,

$$\delta_{lat} = \frac{2F_{lat}}{k_h l}\frac{\omega l[\sinh(\omega l)\cosh(\omega l) - sin(\omega l)cos(\omega l)]}{sinh^2(\omega l) - sin^2(\omega l)} \quad [A1]$$

Here, $\omega = \sqrt[4]{[K_h d/(4EI)]} = \sqrt[4]{[16K_h d/(\pi E d^4)]}$ [A2]

where, k_h [N/mm^2] and K_h [N/mm^3] is the modulus of foundation, d is the outer diameter of screw, EI is the bending stiffness of the screw.

For a rigid screw when the bending stiffness of the screw tends to $EI \rightarrow \infty$ (infinity) or $\omega \rightarrow 0$, the slip is,

$$\lim_{\omega \to 0} \delta_{lat}(0) = \frac{4F_{lat}}{k_h l} \quad [A3]$$

If the load-slip relationship of the joint is written as $F_{lat} = k_h^{eq}\delta_{lat}(0)$, the equivalent embedment stiffness to account for flexibility of screw, $K_h^{eq} = \frac{k_h^{eq}}{dl}$, is then given by,

$$K_h^{eq} = (2K_h)\frac{sinh^2(\omega l) - sin^2(\omega l)}{\omega l[sinh(\omega l)\,cosh(\omega l) - sin(\omega l)cos(\omega l)]} \quad [A4]$$

where, d is the diameter of the screw and l is the embedment length of the screw in timber.

For rigid screw, when the bending stiffness of the screw tends to $EI \rightarrow \infty$ (infinity) or $\omega \rightarrow 0$, the equivalent embedment stiffness reduces to the embedment stiffness as defined earlier as,

$$K_h^{eq} = K_h \quad [A5]$$

Therefore, embedment stiffness used in this article can be replaced by the equivalent embedment stiffness according to equation [A4] to consider the effect of flexibility of the screw.

Appendix B. MTPC Composite Capacity and Effective Bending Stiffness Calculation

This appendix provides an example for calculating the capacity and effective bending stiffness of a MTPC composite panel according to the proposed analytical model. The numerical values of geometric and material properties are as follows,

1) Span and connector spacing: L = 4500 mm, n_1 = 4000 mm, n_2 = 3000 mm, n_3 = 2000 mm, n_4 = 1000 mm and n_5 = 0 mm.
2) Concrete properties: h_c = 100 mm, b_c = 600 mm, A_c = 60,000 mm^2, I_c = 50×10^6 mm^4, S_c = 1,000,000 mm^3, f_c = 55.8 MPa, E_c = 23,480 MPa.
3) Insulation thickness: h_i = 5 mm.
4) MTP properties: h_t = 130 mm, b_t = 600 mm, A_t = 78,000 mm^2, I_t = 110x 10^6 mm^4, S_t = 1,690,000 mm^3, f_t = 18.3 MPa, f_v = 1.3 MPa, E_t = 9,500 MPa.
5) Connector properties: Yield force, F_y =14.66 x 2 x 2 = 58.6 kN (2 cross-pair) (Mirdad & Chui, 2020a) and Elastic stiffness, k = 7.34 x 2 x 2 = 29.4 kN/mm (2 cross-pair) (Mirdad & Chui, 2020b)
6) Eccentricities: e_c = 63.5 mm and e_t = 56.5 mm.

Step 1: After incremental load to reach the connector yield strength of first connector, for w = 20.11 N/mm, assume that structure responds linear elastically to this load.

The compatibility equation will be a system of four linear equations with four unknowns,

$$\begin{Bmatrix}3.97\\3.45\\2.52\\1.33\end{Bmatrix}+\left[\begin{pmatrix}50.6 & 12.4 & 8.28 & 4.14\\12.4 & 46.5 & 8.28 & 4.14\\8.28 & 8.28 & 42.3 & 4.14\\4.14 & 4.14 & 4.14 & 38.2\end{pmatrix}*10^{-6}\right]\begin{Bmatrix}X_1{}^{(0)}\\X_2{}^{(0)}\\X_3{}^{(0)}\\X_4{}^{(0)}\end{Bmatrix}=0;\qquad \text{Therefore,}\begin{Bmatrix}X_1{}^{(0)}\\X_2{}^{(0)}\\X_3{}^{(0)}\\X_4{}^{(0)}\end{Bmatrix}=\begin{Bmatrix}-58.6\\-50.3\\-36.3\\-19.0\end{Bmatrix}\text{kN}$$

$\boldsymbol{F_1(w) = -58.6\ \text{kN} = Fy}$; $F_2(w) = -50.3$ kN; $F_3(w) = -36.3$ kN; $F_4(w) = -19.0$ kN

Therefore, $w_e = w_1$ = 20.11 N/mm as the first connector row yielded.

The deflection for the first connector yielding can be found as,

$\Delta_{S1} = 48.42$ mm; $\Delta_{S2} = -7.14$ mm and $\Delta_e = 41.28$ mm

Therefore, effective bending stiffness can be found as, $\boldsymbol{EI_{eff} = 2601.2\ \text{kN.m}^2}$

$N_t = N_c = 58.6$ kN and therefore,

$\sigma_{t,N} = 0.75$ MPa & $\sigma_{c,N} = -0.98$ MPa

$M = 10683437.5\ \text{N.mm}$ at first connector location,

$M_c = 5655980.9\ \text{N.mm}$ & $M_t = 5027456.6\ \text{N.mm}$

$\sigma_{t,B} = -1.02\ \text{MPa}$ & $\sigma_{c,B} = -1.93\ \text{MPa}$

The stresses in timber and concrete can be found as follows,

$\boldsymbol{\sigma_{c,t}} = -2.91\ \text{MPa},\quad \sigma_{c,B} = 0.95\ \text{MPa},\quad \sigma_{t,t} = -0.26\ \text{MPa}$ & $\boldsymbol{\sigma_{t,B}} = 1.77\ \text{MPa}$

$y_{t1} = 113.15\ \text{mm}$ & $\boldsymbol{\tau_{max}} = 0.94\ \text{MPa}$

Therefore, after yielding of first row screws, the stress in timber and concrete are within the limit.

Step 2: Calculate force in the connector for load w = 22.70 N/mm which is greater than w_1 = 20.11 N/mm. Therefore, calculate the forces in next 3 connector rows with an increment $\Delta w_1 = (w\text{-}w_1)$ = 2.59 kN. The compatibility equation will be three linear equations with three unknowns.

$$\begin{Bmatrix}0.45\\0.33\\0.17\end{Bmatrix} + \left[\begin{pmatrix}46.5 & 8.28 & 4.14\\8.28 & 42.3 & 4.14\\4.14 & 4.14 & 38.2\end{pmatrix} * 10^{-6}\right]\begin{Bmatrix}X_2{}^{(1)}\\X_3{}^{(1)}\\X_4{}^{(1)}\end{Bmatrix} = 0; \qquad \text{Therefore,} \begin{Bmatrix}X_2{}^{(1)}\\X_3{}^{(1)}\\X_4{}^{(1)}\end{Bmatrix} = \begin{Bmatrix}-8.3\\-5.8\\-3.0\end{Bmatrix}\text{kN}$$

$\boldsymbol{F_1(w) = (-58.6\ + 0)\ \text{kN} = -58.6\ \text{kN} = F_y}$

$\boldsymbol{F_2(w) = -50.3\ + X_2^{(1)}(2.59) = (-50.3\ - 8.3)\ \text{kN}\ =\ -58.6\ \text{kN} = F_y}$

$F_3(w) = -36.3\ + X_3^{(1)}(2.59) = (-36.3\ - 5.8)\ \text{kN}\ =\ -42.1\ \text{kN}\ < F_y$

$F_4(w) = -19.0\ + X_4^{(1)}(2.59) = (-19.0\ - 3.0)\ \text{kN}\ =\ -21.9\ \text{kN} < F_y$

Therefore, w_2 = 22.70 N/mm as the second connector row yielded for Δw_1 = 2.59 kN

The deflection as well as bending stiffness for second connector yielding is as follows,

$\Delta_{11} = 49.31\ \text{mm}$ Therefore, $\Delta_1 = (\Delta_{11} - \Delta_e) = 8.03\ \text{mm}$

The stresses in timber and concrete can be found as follows,

$\boldsymbol{\sigma_{c,t}} = -11.41\ \text{MPa},\quad \boldsymbol{\sigma_{t,b}} = 6.47\ \text{MPa}$ & $\boldsymbol{\tau_{max}} = 0.47\ \text{MPa}$

After yielding of second row screws, the stress in timber and concrete are within the limit.

Step 3: Calculate force in the connector for load w = 28.56 N/mm which is greater than w_2 = 22.70 N/mm. Therefore, calculate the forces in next 2 connector rows with an increment $\Delta w_2 = (w\text{-}w_2)$ = 5.86 kN. The compatibility equation will be two linear equations with two unknowns.

$$\begin{Bmatrix}0.74\\0.39\end{Bmatrix}+\left[\begin{pmatrix}42.3 & 4.14\\4.14 & 38.2\end{pmatrix}*10^{-6}\right]\begin{Bmatrix}X_3{}^{(2)}\\X_4{}^{(2)}\end{Bmatrix}=0; \qquad \text{Therefore,}\begin{Bmatrix}X_3{}^{(2)}\\X_4{}^{(2)}\end{Bmatrix}=\begin{Bmatrix}-16.5\\-8.4\end{Bmatrix}\text{kN}$$

$$\boldsymbol{F_1(w)=(-58.6\ +0+0)\ kN=-58.6\ kN=F_y}$$

$$\boldsymbol{F_2(w)=(-50.3\ -8.3\ +0)\ kN=\ -58.6\ kN=F_y}$$

$$\boldsymbol{F_3(w)=-36.3\ -5.8\ +X_3^{(2)}(5.86)\ =(-36.3\ -5.8\ -16.5)\ kN=\ -58.6\ kN\ =F_y}$$

$$F_4(w)=-19.0\ -3.0\ +X_4^{(2)}(5.86)=(-19.0\ -3.0\ -8.4)\ \text{kN}=\ -30.2\ \text{kN}<F_y$$

Therefore, w_3 = 28.56 N/mm as the third connector row yielded for Δw_2 = 5.86 kN

The deflection as well as bending stiffness for third connector yielding is as follows,

$\Delta_{22}=65.20$ mm Therefore, $\Delta_2=(\Delta_{22}-\Delta_{11})=15.89$ mm

The stresses in timber and concrete can be found as follows,

$\boldsymbol{\sigma_{c,t}}=-22.47$ MPa, $\boldsymbol{\sigma_{t,b}}=12.53$ MPa & $\boldsymbol{\tau_{max}}=0.36$ MPa

After yielding of third row screws, the stress in timber and concrete are still within the limit.

Step 4: Calculate force in the connector for load w = 38.82 N/mm which is greater than w_3 = 28.56 N/mm.

The compatibility equation will be one linear equation with one unknown with an increment $\Delta w_3 = (w-w_3)$ = 10.26 kN

$$\{0.68\}+[(38.2)*10^{-6}]\{X_4{}^{(3)}\}=0; \qquad \text{Therefore,}\{X_4{}^{(3)}\}=\{-17.7\}\text{kN}$$

$$\boldsymbol{F_1(w)=(-58.6\ +0+0+0)\ kN=-58.6\ kN=F_y}$$

$$\boldsymbol{F_2(w)=(-50.3\ -8.3\ +0+0)\ kN=\ -58.6\ kN=F_y}$$

$$\boldsymbol{F_3(w)=(-36.3\ -5.8\ -16.5+0)\ kN=\ -58.6\ kN\ =F_y}$$

$$F_4(w)=-19.0\ -3.0\ -8.4\ +X_4^{(3)}(10.26)=(-19.0\ -3.0\ -8.4-17.7)\ \text{kN}=\ -47.96\ \text{kN}<F_y$$

Therefore, w_4 = 38.82 N/mm as the third connector row yielded and fourth connector partially yielded for Δw_3 = 10.26 kN.

The deflection as well as bending stiffness for the ultimate capacity is,

$\Delta_{33}=92.01$ mm Therefore, $\Delta_3=(\Delta_{33}-\Delta_{22})=26.81$ mm

The stresses in timber and concrete are as follows,

$\boldsymbol{\sigma_{c,t}}=-38.97$ MPa, $\boldsymbol{\sigma_{t,b}=21.40\ MPa}$ & $\boldsymbol{\tau_{max}}=0.23$ MPa

After yielding of third row screws and with some increments, the bending stress of MTP reaches its tensile capacity of 21.40 MPa.

System capacity,

$w_u = w_e + (\Delta w_1 + \Delta w_2 + \Delta w_3)$ = (20.11 + 2.59 + 5.86 + 10.26) * 4500 = **174.70 kN**

Ultimate deflection,

$\Delta_u = \Delta_e + (\Delta_1 + \Delta_2 + \Delta_3)$ = (41.28 + 8.03 + 15.89+ 26.81) = **92.01 mm**

Effective Bending Stiffness = **2601.2 kN.m^2**

Failure mode of the specimen = **Timber fracture**

Load-deflection response can be generated based on the load, *w* and corresponding deflection, *Δ* from each step.

Appendix C. Connection and Material Test Curves

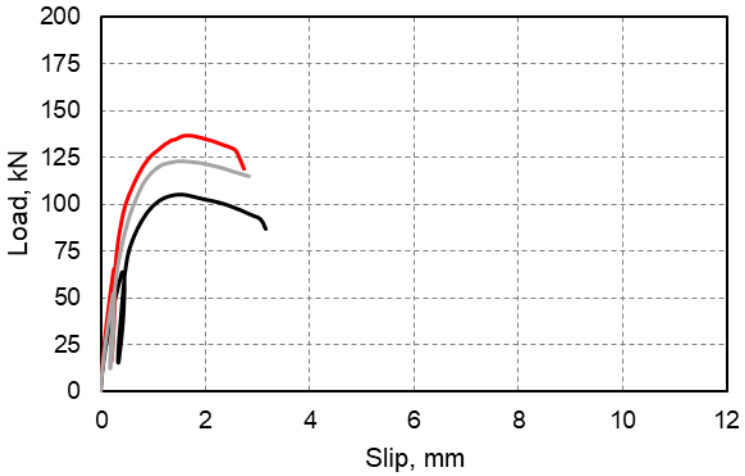

Figure 8.1: Load-slip performance of GLT-L80-I0-30°

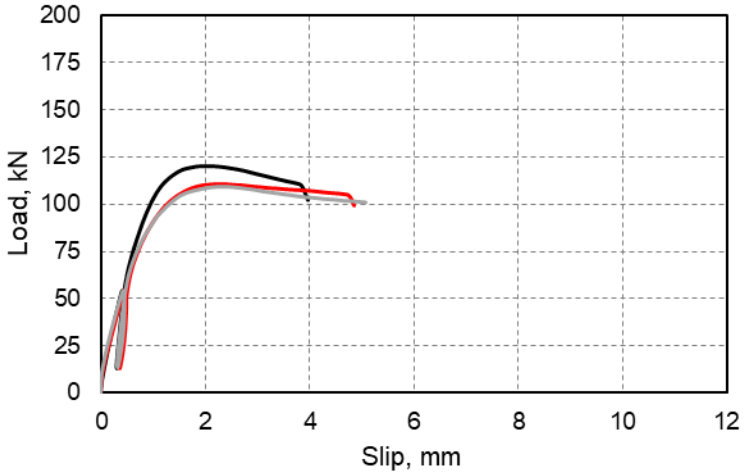

Figure 8.2: Load-slip performance of GLT-L80-I0-45°

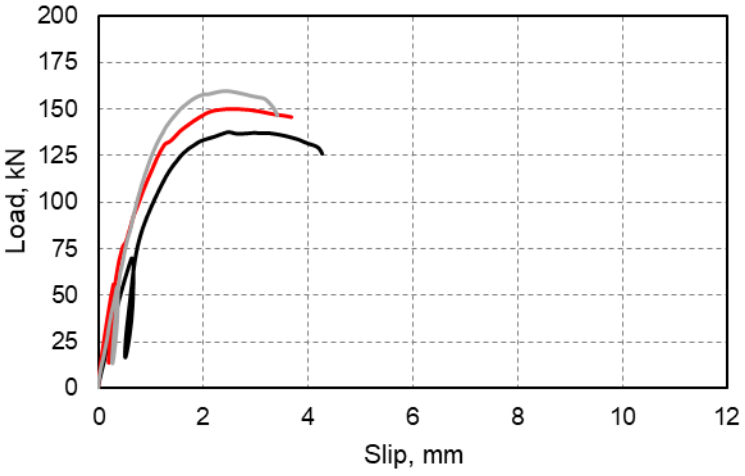

Figure 8.3: Load-slip performance of GLT-L100-I0-45°

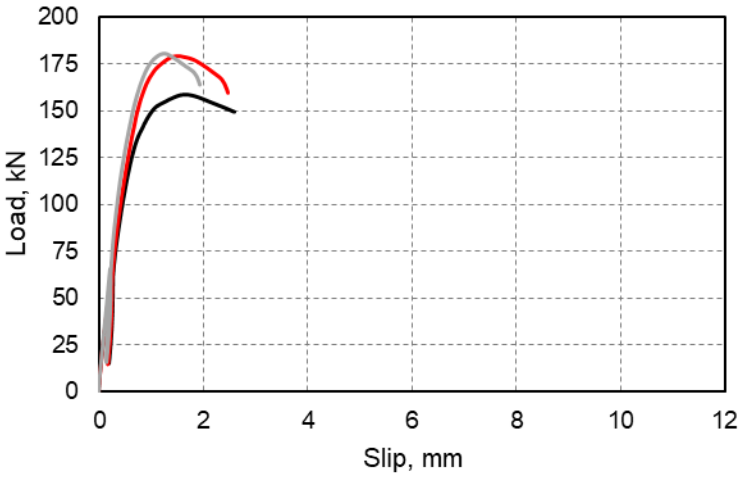

Figure 8.4: Load-slip performance of GLT-L100-I0-30°

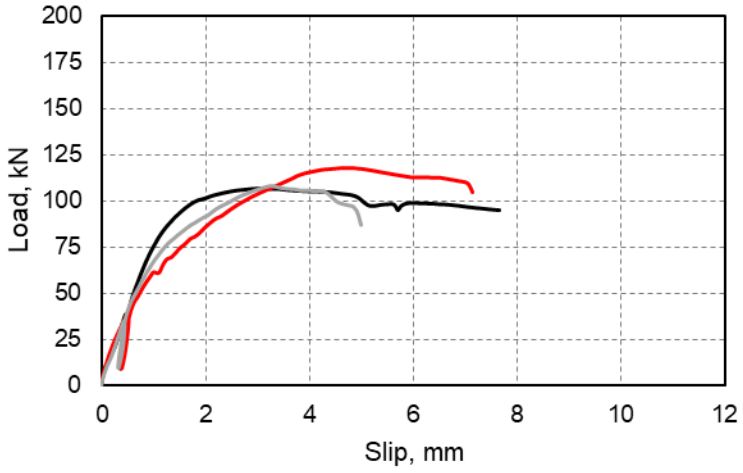

Figure 8.5: Load-slip performance of GLT-L80-I5-45°

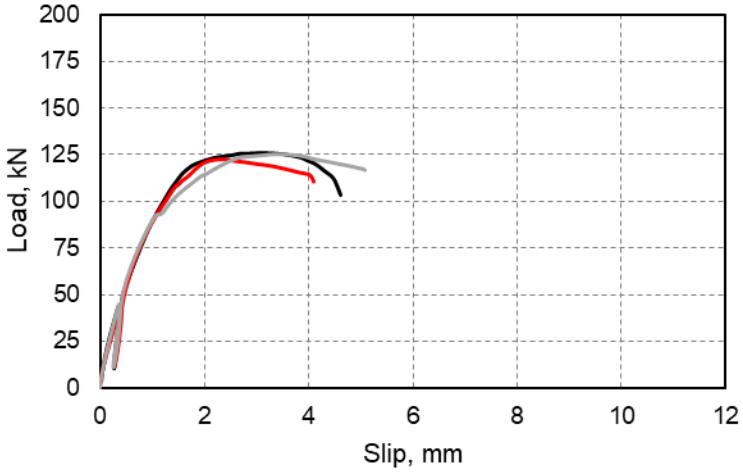

Figure 8.6: Load-slip performance of GLT-L80-I5-30°

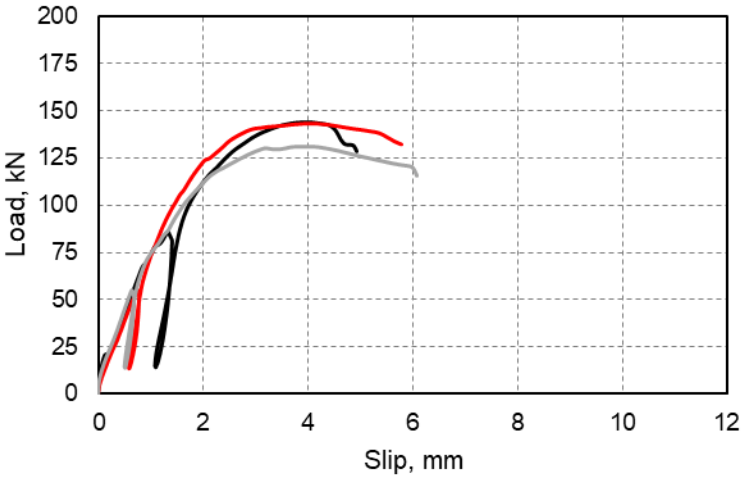

Figure 8.7: Load-slip performance of GLT-L100-I5-45°

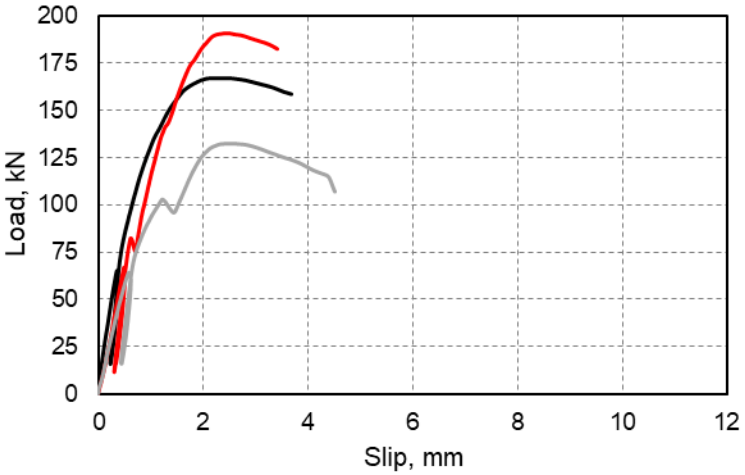

Figure 8.8: Load-slip performance of GLT-L100-I5-30°

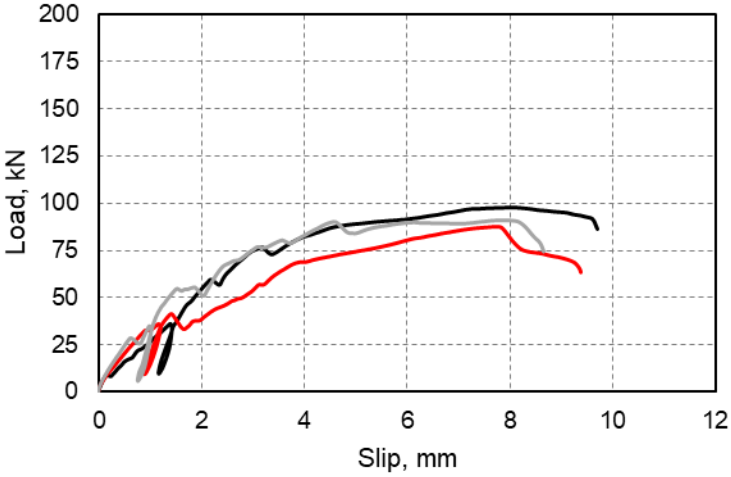

Figure 8.9: Load-slip performance of GLT-L80-I15-45°

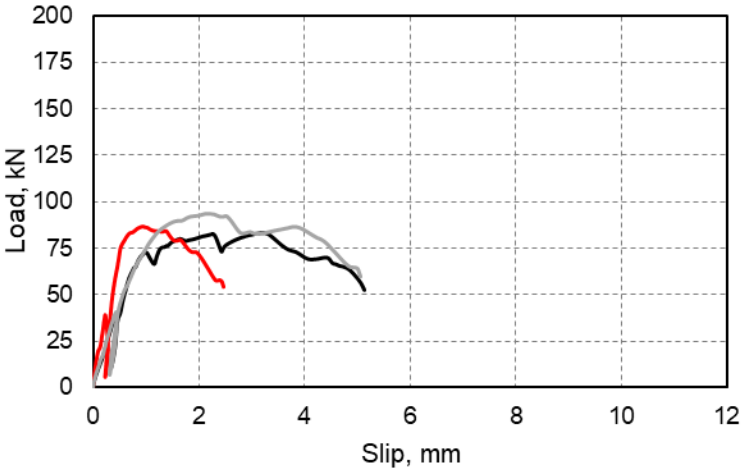

Figure 8.10: Load-slip performance of GLT-L80-I15-30°

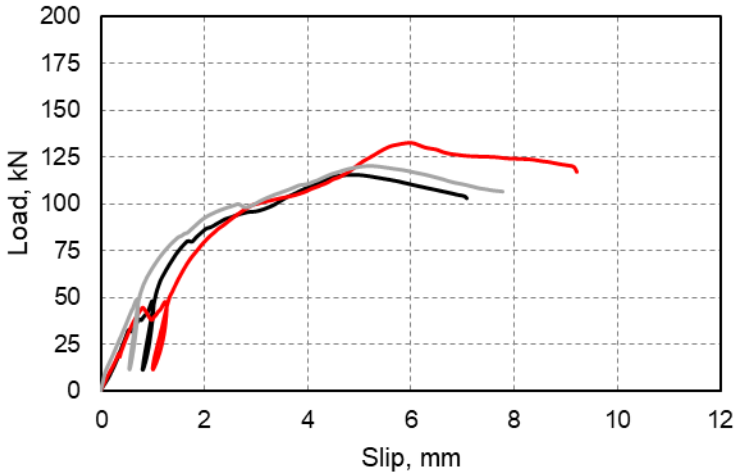

Figure 8.11: Load-slip performance of GLT-L100-I15-45°

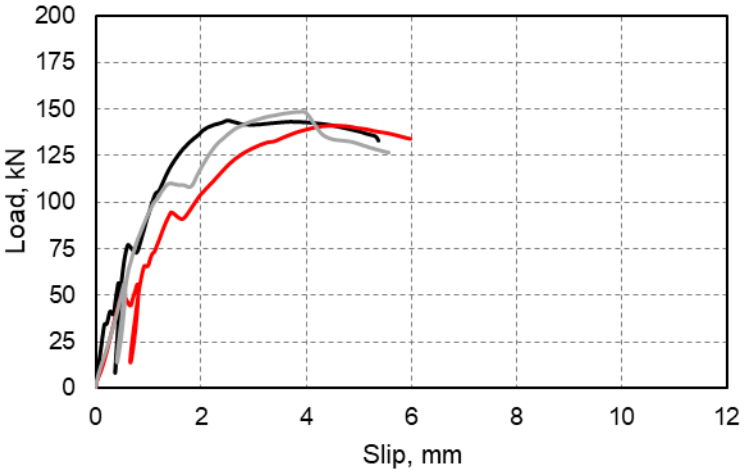

Figure 8.12: Load-slip performance of GLT-L100-I15-30°

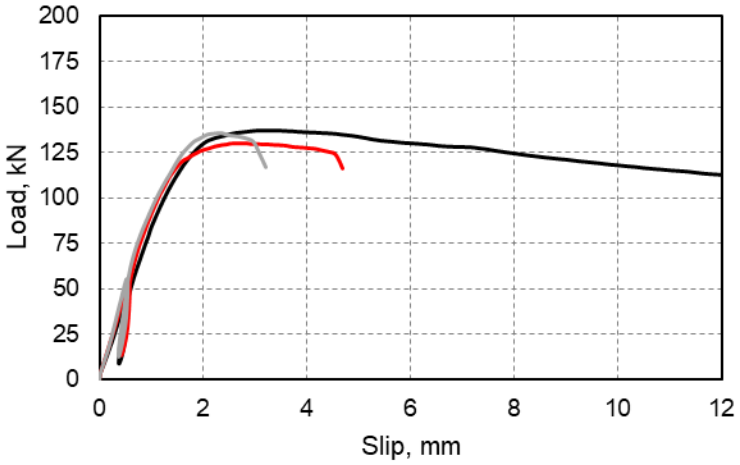

Figure 8.13: Load-slip performance of CLT-L80-I0-45°

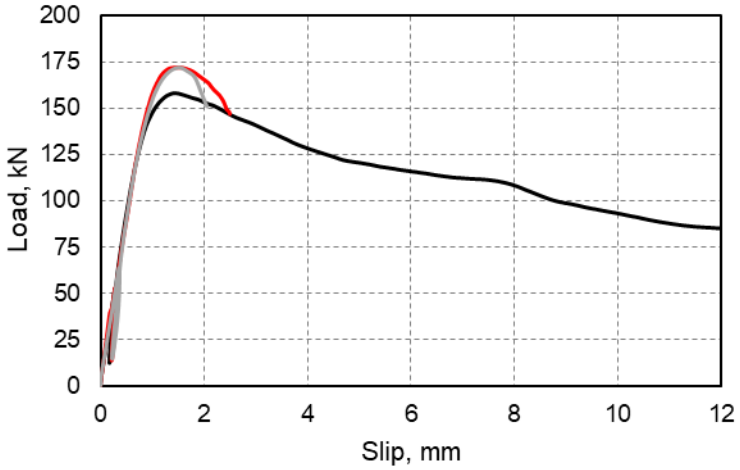

Figure 8.14: Load-slip performance of CLT-L80-I0-30°

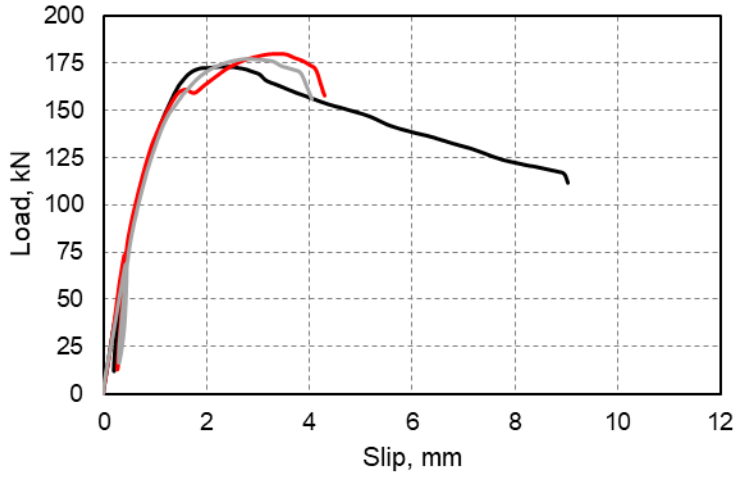

Figure 8.15: Load-slip performance of CLT-L100-I0-45°

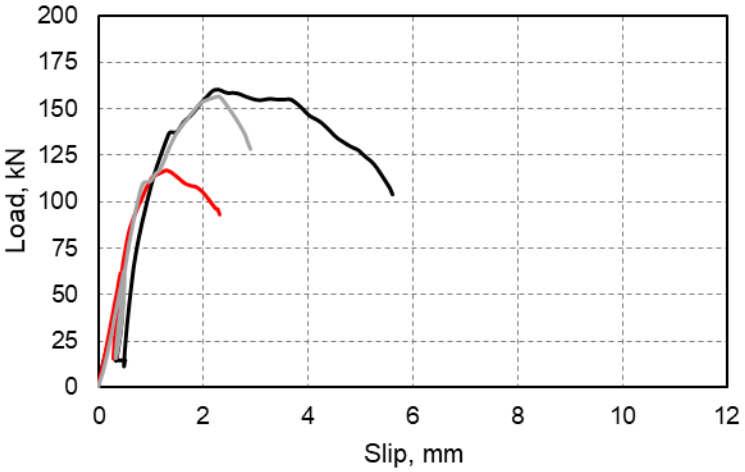

Figure 8.16: Load-slip performance of CLT-L100-I0-30°

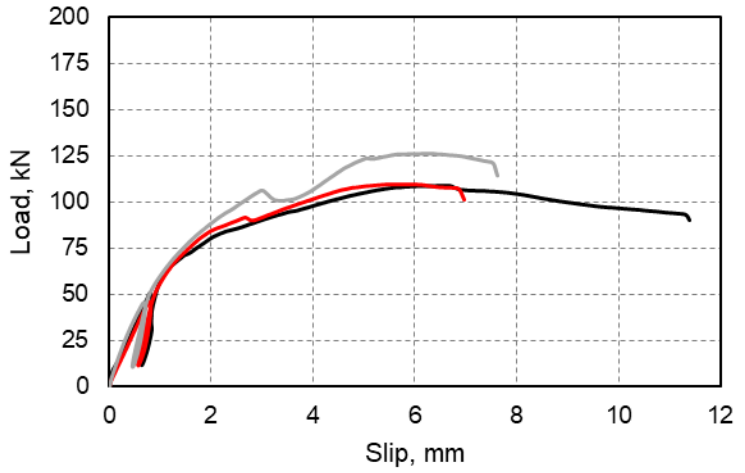

Figure 8.17: Load-slip performance of CLT-L80-I5-45°

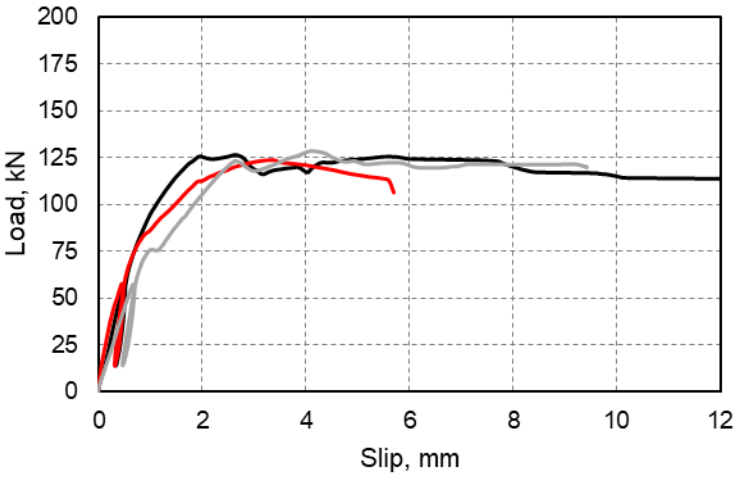

Figure 8.18: Load-slip performance of CLT-L80-I5-30°

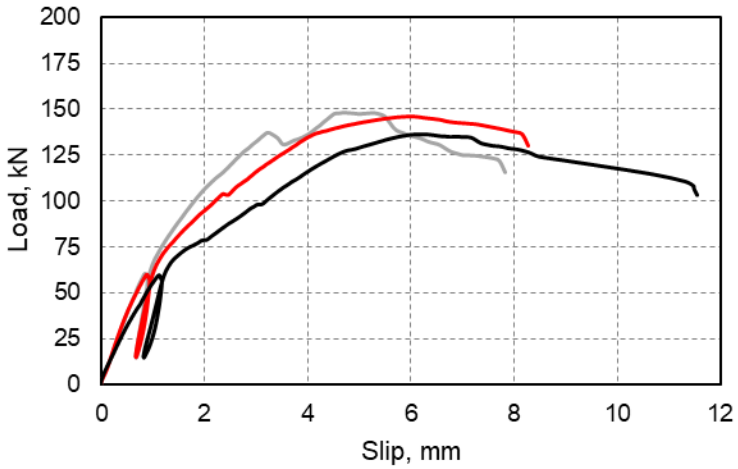

Figure 8.19: Load-slip performance of CLT-L100-I5-45°

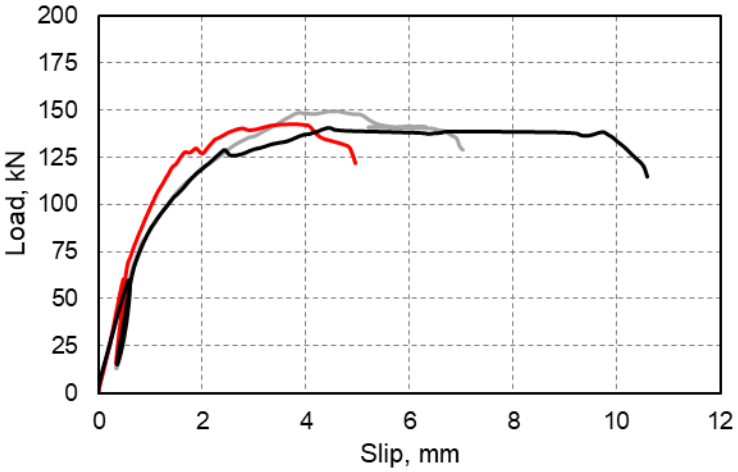

Figure 8.20: Load-slip performance of CLT-L100-I5-30°

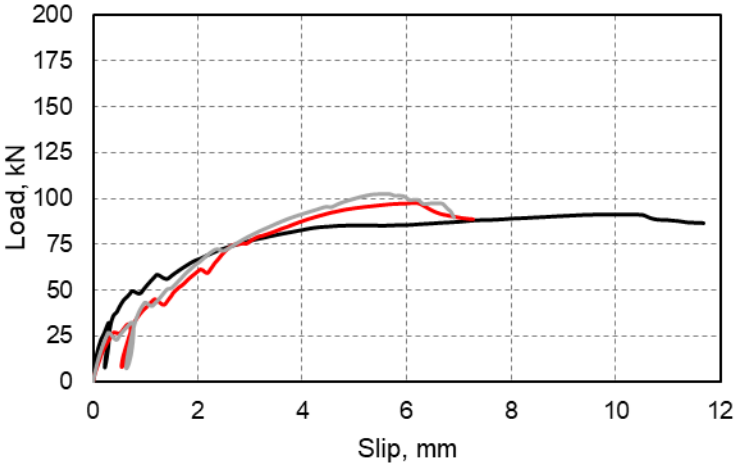

Figure 8.21: Load-slip performance of CLT-L80-I15-45°

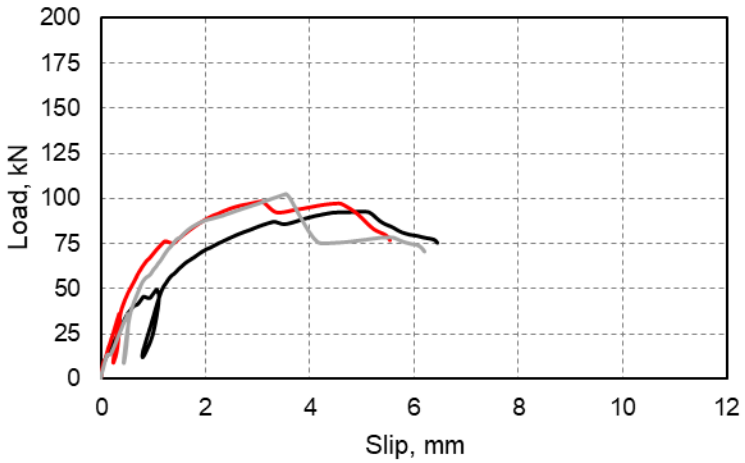

Figure 8.22: Load-slip performance of CLT-L80-I15-30°

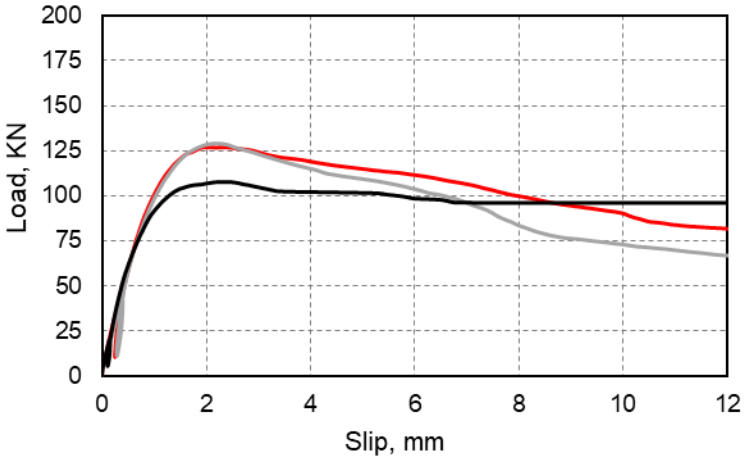

Figure 8.23: Load-slip performance of CLP-L80-I0-45°

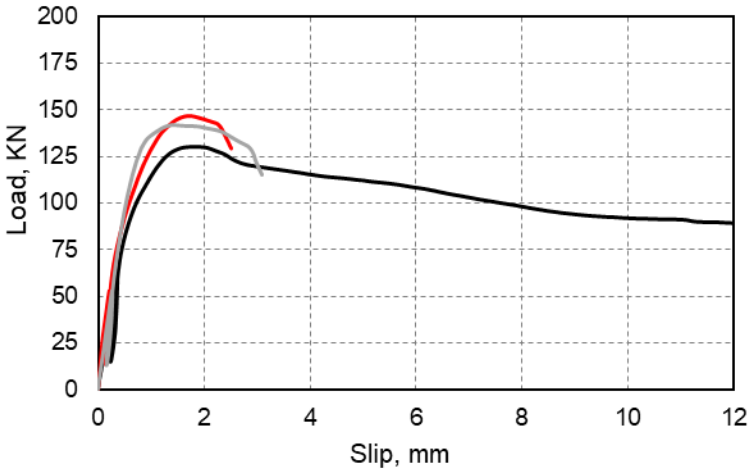

Figure 8.24: Load-slip performance of CLP-L80-I0-30°

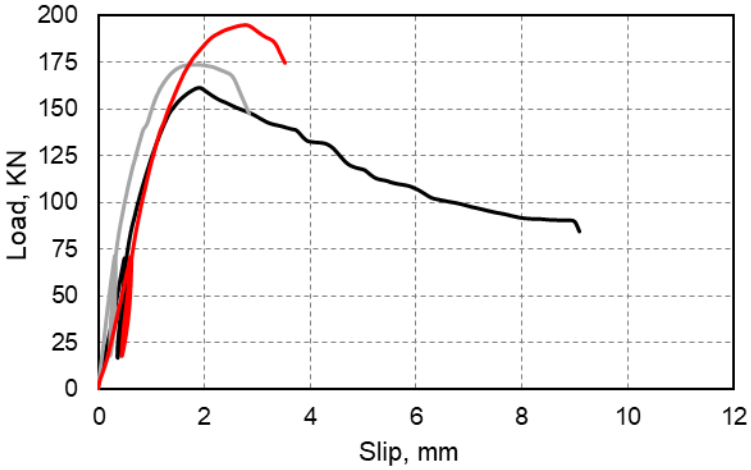

Figure 8.25: Load-slip performance of CLP-L100-I0-45°

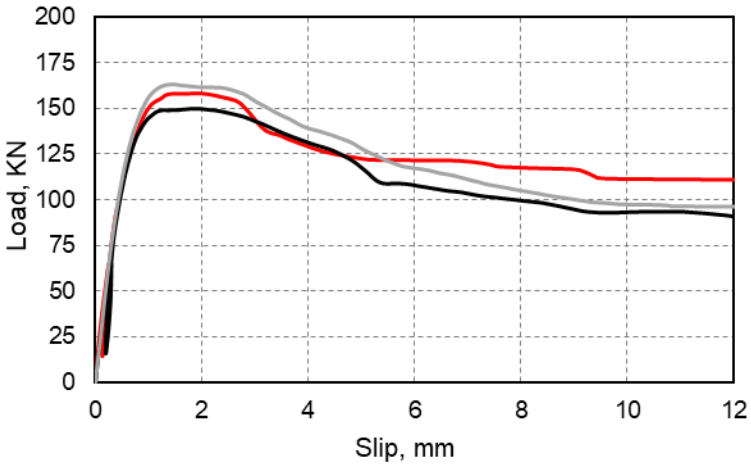

Figure 8.26: Load-slip performance of CLP-L100-I0-30°

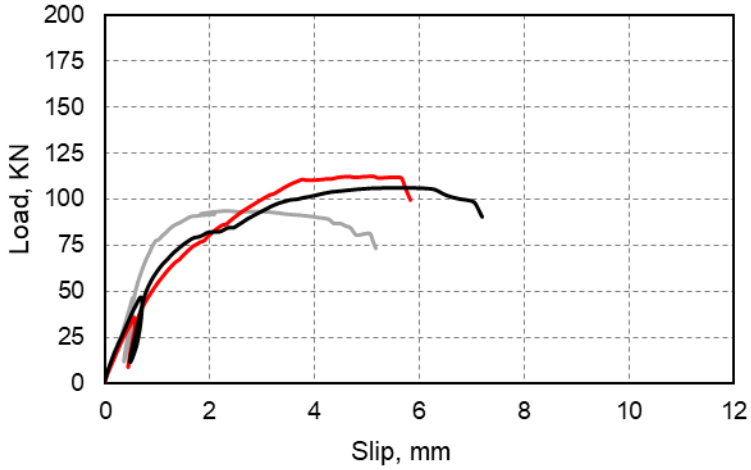

Figure 8.27: Load-slip performance of CLP-L80-I5-45°

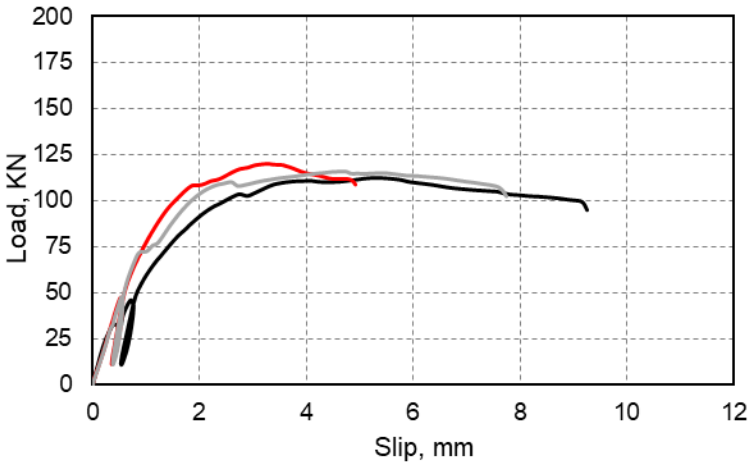

Figure 8.28: Load-slip performance of CLP-L80-I5-30°

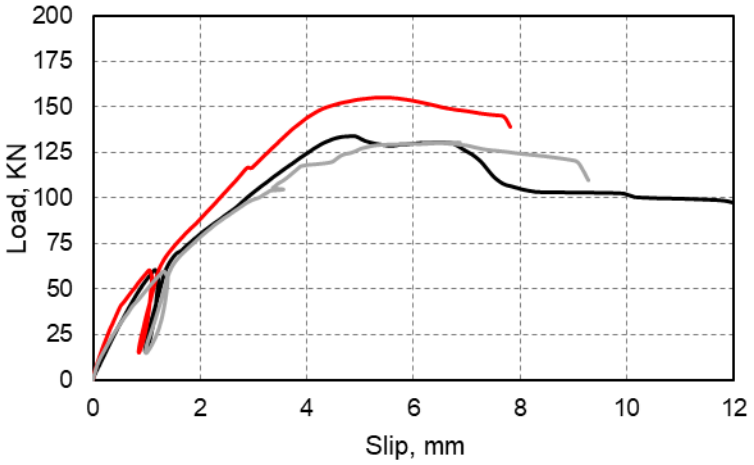

Figure 8.29: Load-slip performance of CLP-L100-I5-45°

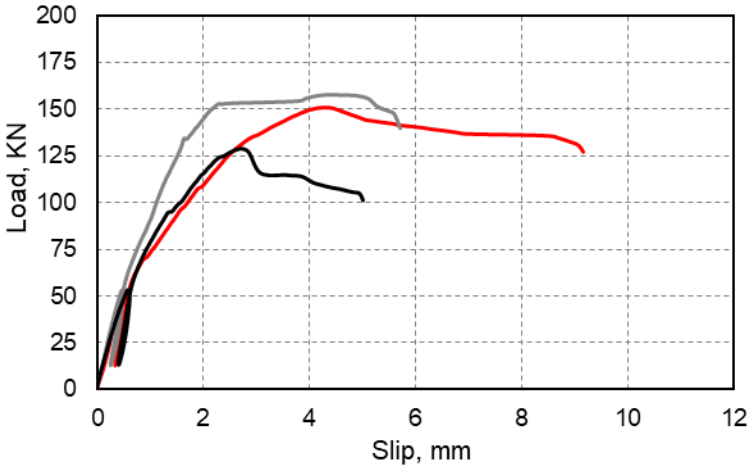

Figure 8.30: Load-slip performance of CLP-L100-I5-30°

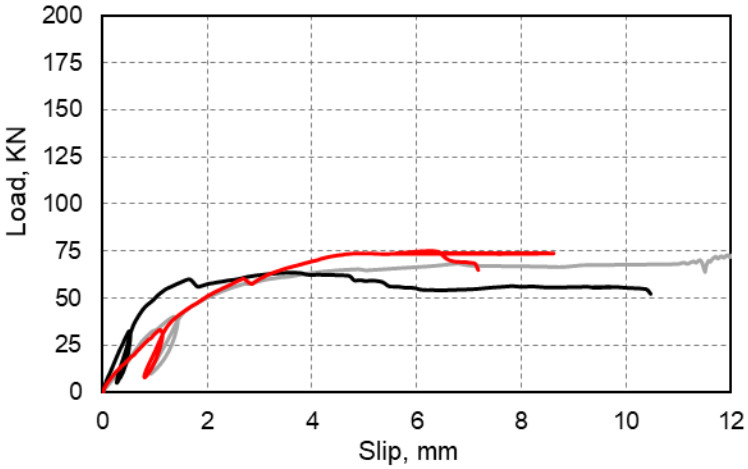

Figure 8.31: Load-slip performance of CLP-L80-I15-45°

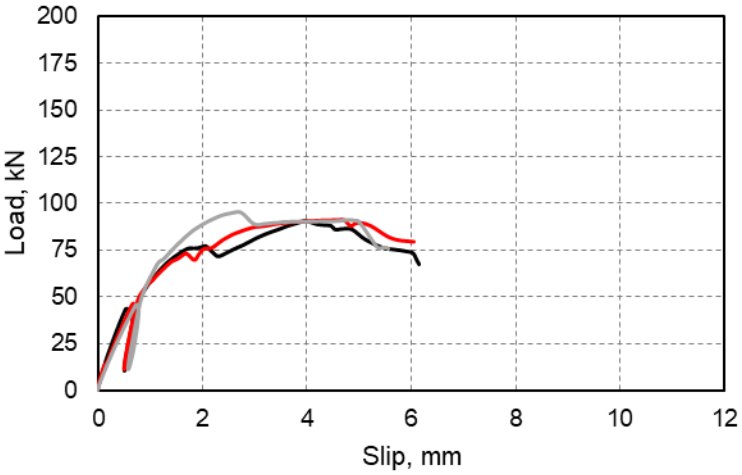

Figure 8.32: Load-slip performance of CLP-L80-I15-30°

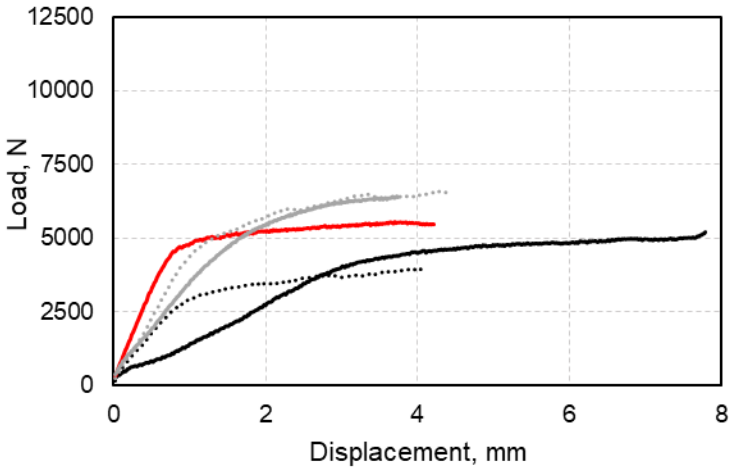

Figure 8.33: Embedment of 11 mm diameter screw at 0° angle

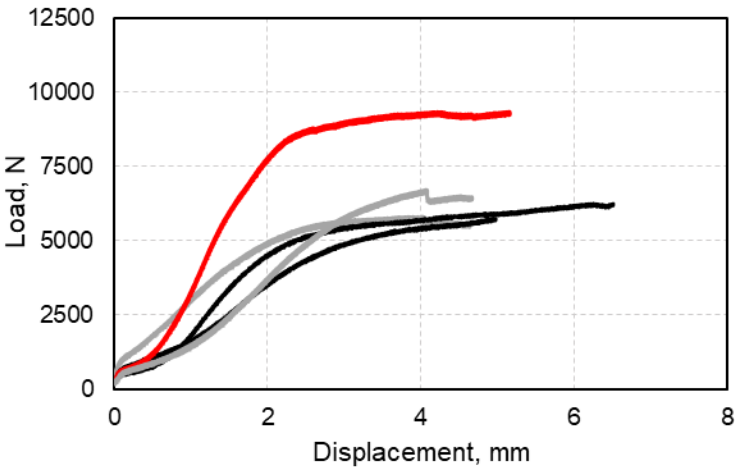

Figure 8.34: Embedment of 11 mm diameter screw at 30° angle

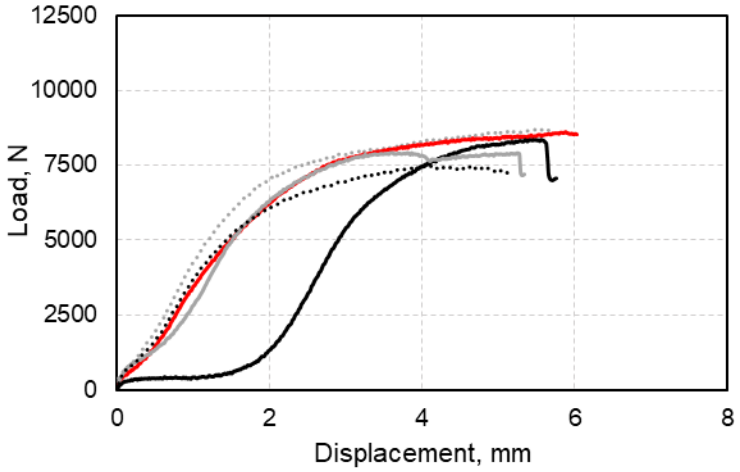

Figure 8.35: Embedment of 11 mm diameter screw at 45° angle

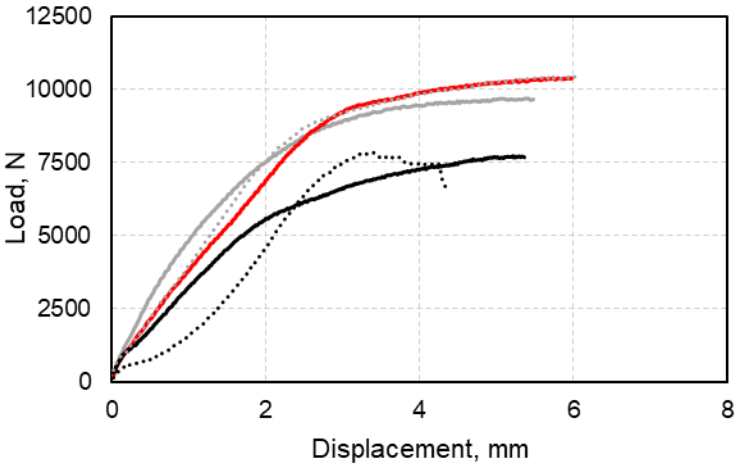

Figure 8.36: Embedment of 11 mm diameter screw at 60° angle

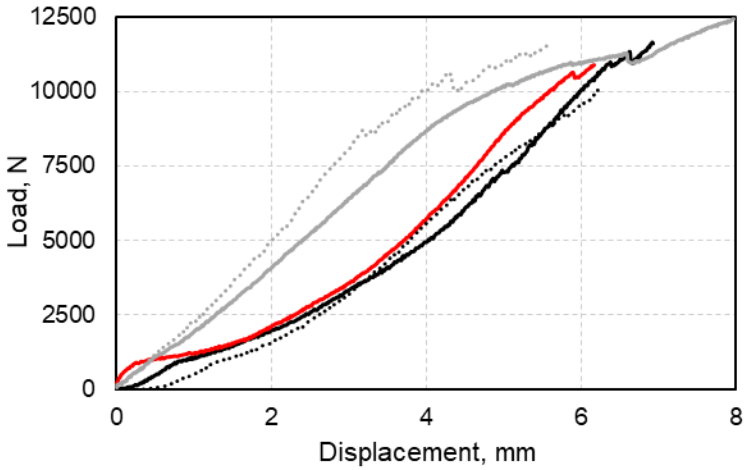

Figure 8.37: Embedment of 11 mm diameter screw at 90° angle

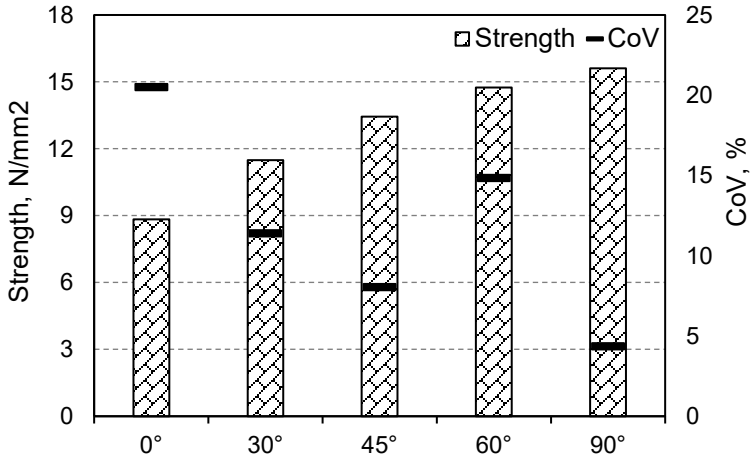

Figure 8.38: Embedment strength of 11 mm diameter screw at different angle

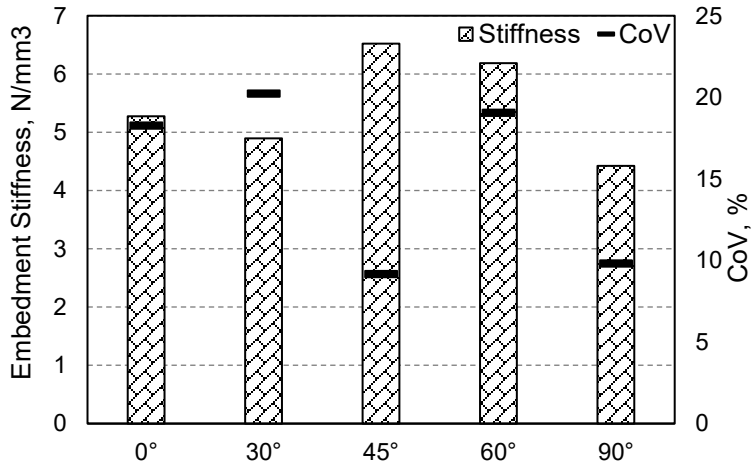

Figure 8.39: Embedment stiffness of 11 mm diameter screw at different angle

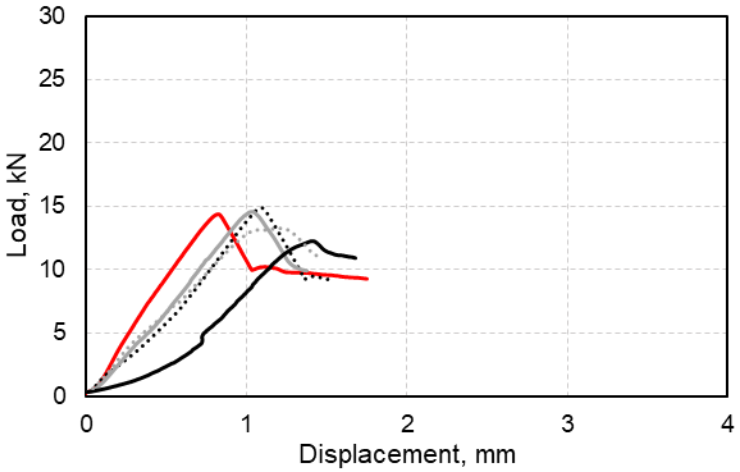

Figure 8.40: Withdrawal of 11 mm diameter screw at 0° angle and 80 mm penetration

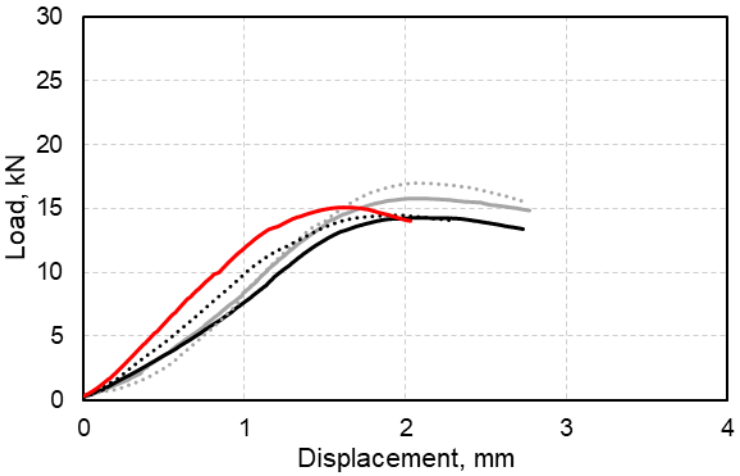

Figure 8.41: Withdrawal of 11 mm diameter screw at 30° angle and 80 mm penetration

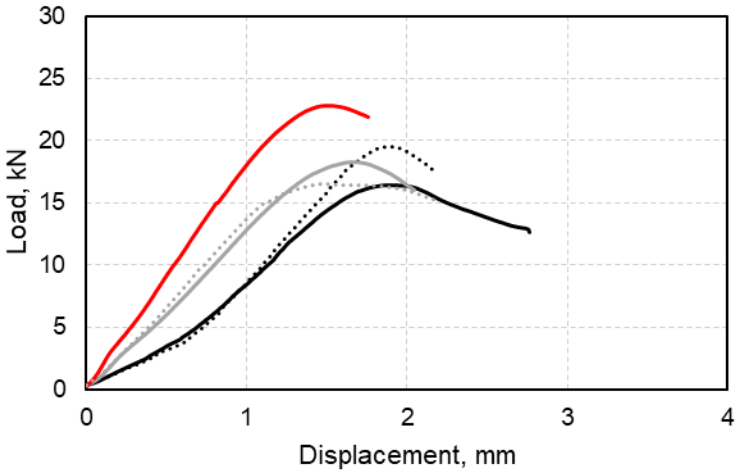

Figure 8.42: Withdrawal of 11 mm diameter screw at 45° angle and 80 mm penetration

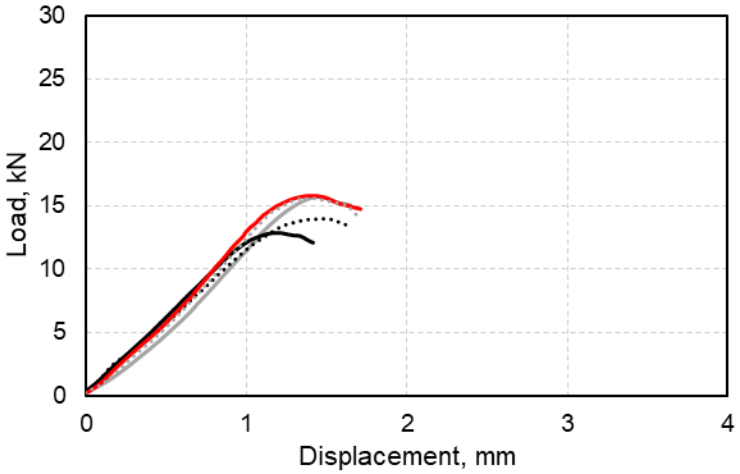

Figure 8.43: Withdrawal of 11 mm diameter screw at 60° angle and 80 mm penetration

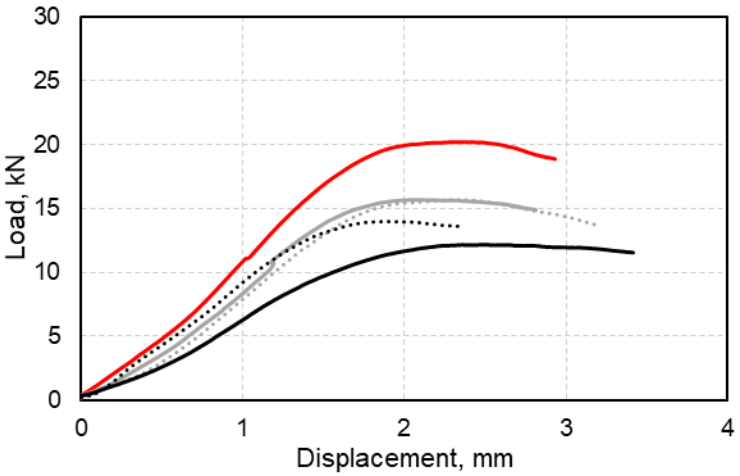

Figure 8.44: Withdrawal of 11 mm diameter screw at 90° angle and 80 mm penetration

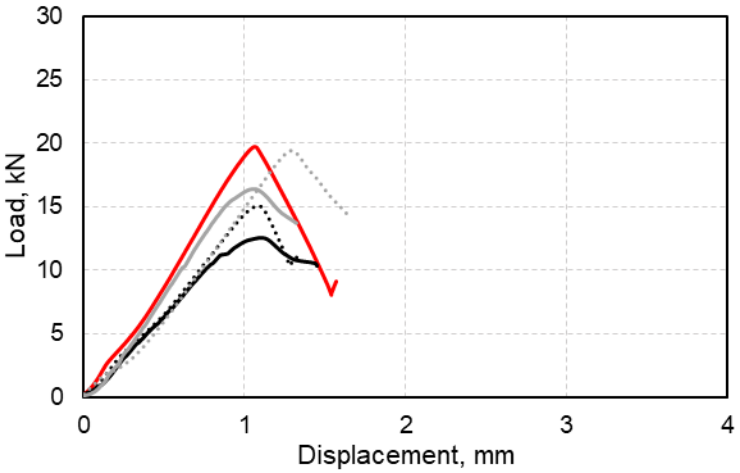

Figure 8.45: Withdrawal of 11 mm diameter screw at 0° angle and 100 mm penetration

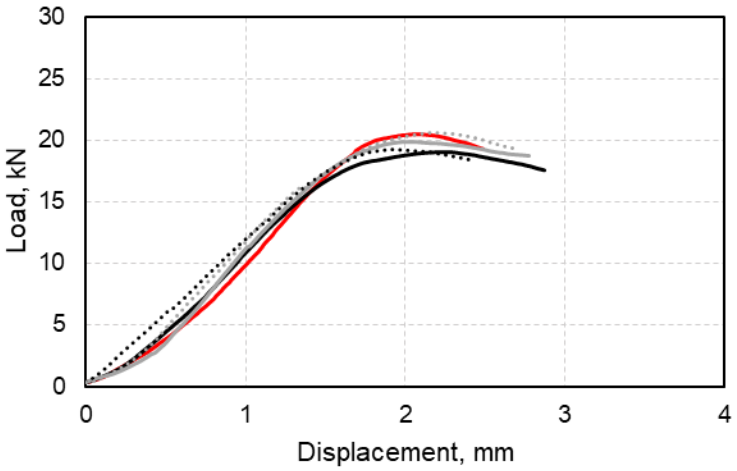

Figure 8.46: Withdrawal of 11 mm diameter screw at 30° angle and 100 mm penetration

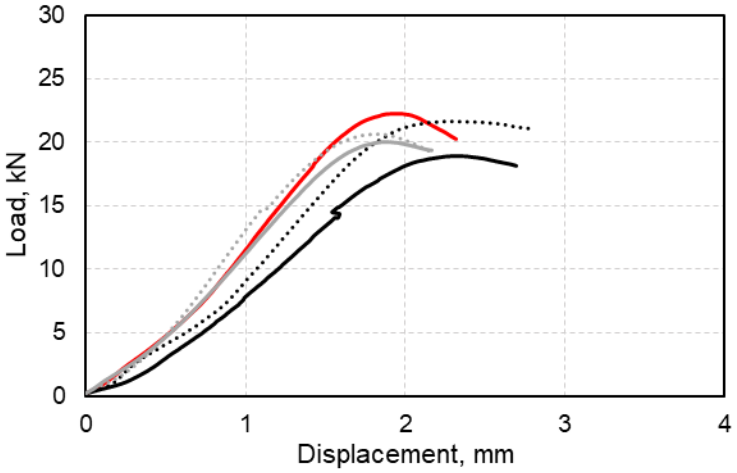

Figure 8.47: Withdrawal of 11 mm diameter screw at 45° angle and 100 mm penetration

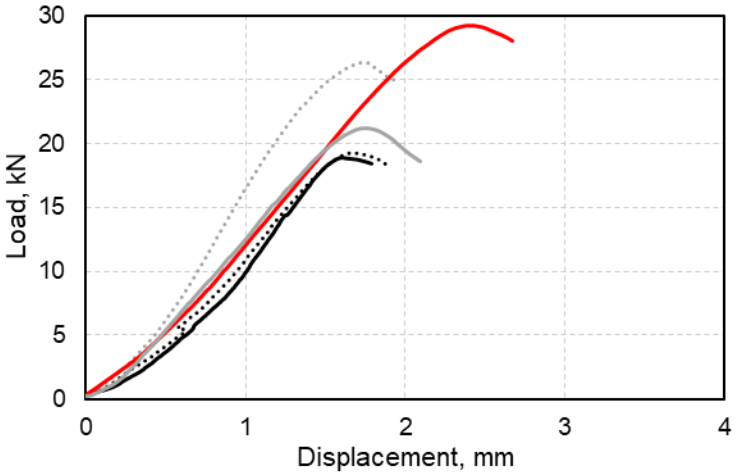

Figure 8.48: Withdrawal of 11 mm diameter screw at 60° angle and 100 mm penetration

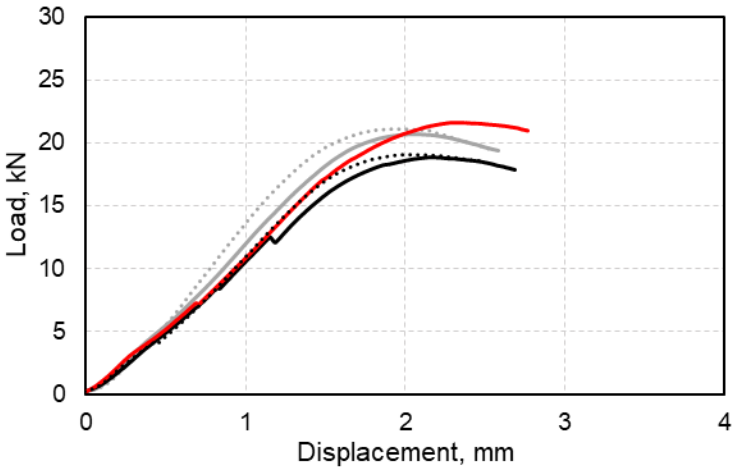

Figure 8.49: Withdrawal of 11 mm diameter screw at 90° angle and 100 mm penetration

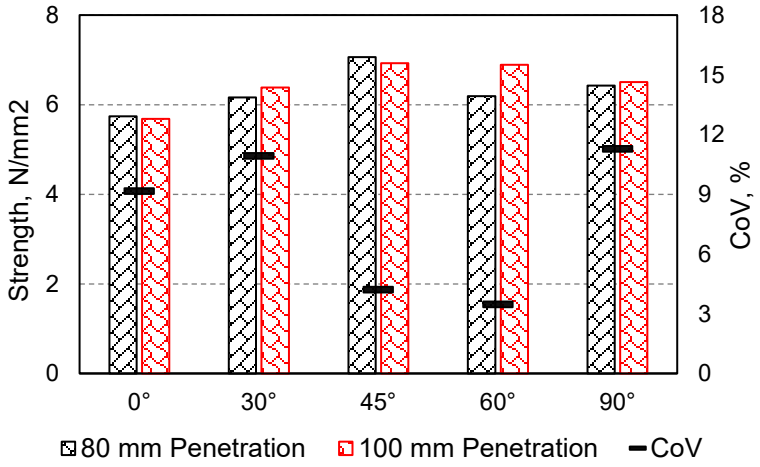

Figure 8.50: Withdrawal strength of 11 mm diameter screw at different angle and penetration

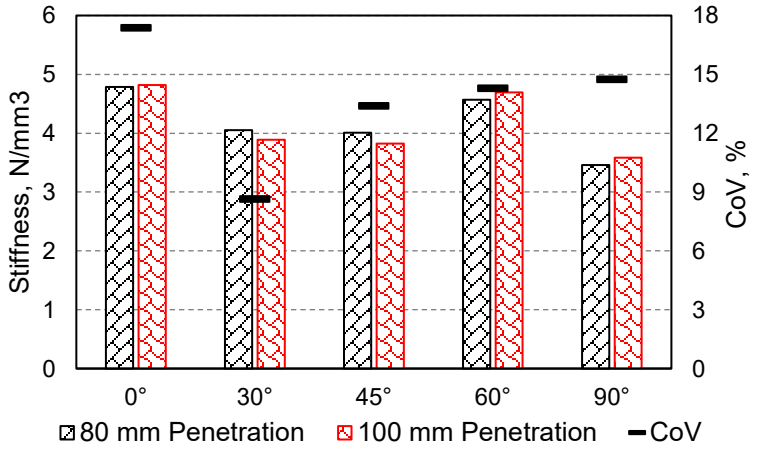

Figure 8.51: Withdrawal stiffness of 11 mm diameter screw at different angle and penetration

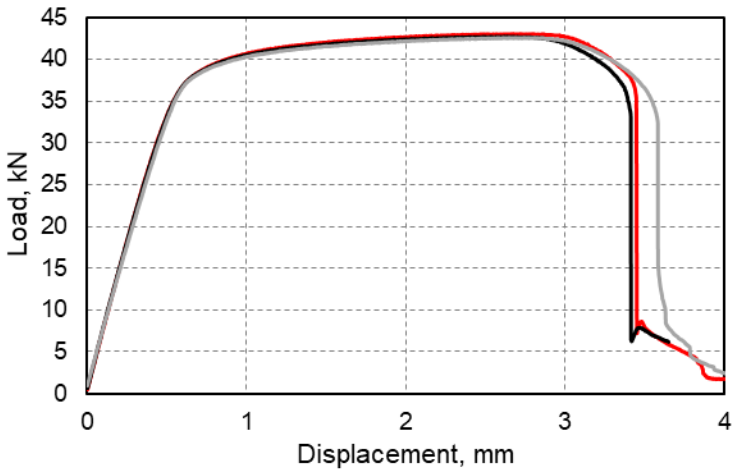

Figure 8.52: Load-displacement curve of tensile test of 11 mm diameter screw

Appendix D. Specifications of MTPC Composite Panels

Specimen #1: GLT6-C100-I0-45°-S250

Concrete properties: h_c = 100 mm, b_c = 600 mm, f_c = 55.8 MPa, E_c = 23,480 MPa.

Insulation thickness: h_i = 0 mm.

MTP properties: h_t = 130 mm, b_t = 600 mm, f_t = 21.4 MPa, f_v = 1.3 MPa, E_t = 9,500 MPa.

Connector properties: Diameter, d = 11 mm, Penetration length, l = 100 mm, Insertion angle, α = 45°,

Yield force, F_y = 15.34 x 2 x 2 = 61.36 kN (2 cross-pair) (Mirdad & Chui, 2020a), Elastic stiffness, k = 15.24 x 2 x 2 = 60.96 kN/mm (2 cross-pair) (Mirdad & Chui, 2020b) and Friction, μ = 0.45

Span and connector spacing: L = 6000 mm, Span = 5700 mm , Spacing, s = 250 mm, Connector row = 12, n_1 = 5750 mm, n_2 = 5250 mm, n_3 = 4750 mm, n_4 = 4250 mm, n_5 = 3750 mm, n_6 = 3250 mm, n_7 = 2750 mm, n_8 = 2250 mm, n_9 = 1750 mm, n_{10} = 1250 mm, n_{11} = 750 mm and n_{12} = 250 mm.

Eccentricities: e_c = 60.9 mm and e_t = 54.1 mm.

Table 8.1: Predictions for specimen (#1) GLT6-C100-I0-45°-S250

Connector Row	Deflection, Δ, mm	Load, w, kN	Concrete Top Stress, $\sigma_{c,T}$, MPa	Timber Bottom Stress, $\sigma_{t,B}$, MPa
0	0	0.00	0	0
1	88.21	95.82	-0.54	0.52
2	91.93	98.33	-4.06	2.62
3	96.93	102.03	-7.52	4.68
4	103.02	106.76	-11.01	6.75
5	110.17	112.52	-14.59	8.88
6	118.40	119.30	-18.33	11.09
7	128.01	127.40	-22.31	13.42
8	139.43	137.20	-26.66	15.95
9	153.84	149.85	-31.80	18.89
10	**166.52**	**160.51**	**-36.17**	**21.40**

Capacity, w_u = 160.51 kN

Ultimate deflection, Δ_u = 166.52 mm

Effective Bending Stiffness, EI_{eff} = 2619.43 kN.m^2

Failure mode = Timber fracture

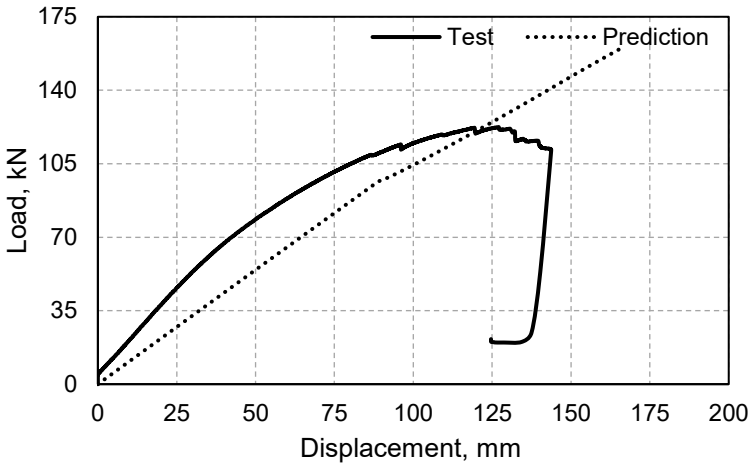

Figure 8.53: Load-deflection responses of specimen (#1) GLT6-C100-I0-45°-S250

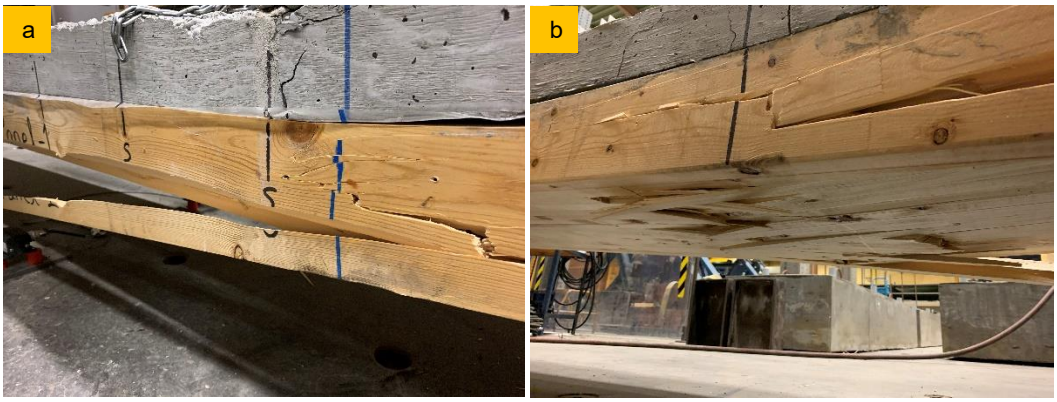

Figure 8.54: Timber fracture in specimen (#1) GLT6-C100-I0-45°-S250; a) side view and b) bottom view

Specimen #2: GLT6-C75-I0-30°-S500

Concrete properties: h_c = 75 mm, b_c = 600 mm, f_c = 55.8 MPa, E_c = 23,480 MPa.

Insulation thickness: h_i = 0 mm.

MTP properties: h_t = 130 mm, b_t = 600 mm, f_t = 21.4 MPa, f_v = 1.3 MPa, E_t = 9,500 MPa.

Connector properties: Diameter, d = 11 mm, Penetration length, l = 100 mm, Insertion angle, α = 30°,

Yield force, F_y = 17.67 x 2 x 2 = 70.68 kN (2 cross-pair) (Mirdad & Chui, 2020a), Elastic stiffness, k = 18.46 x 2 x 2 = 73.84 kN/mm (2 cross-pair) (Mirdad & Chui, 2020b) and Friction, μ = 0.45

Span and connector spacing: L = 6000 mm, Span = 5700 mm, Spacing, s = 500 mm, Connector row = 6, n_1 = 5500 mm, n_2 = 4500 mm, n_3 = 3500 mm, n_4 = 2500 mm, n_5 = 1500 mm and n_6 = 500 mm

Eccentricities: e_c = 33 mm and e_t = 69.5 mm.

Table 8.2: Predictions for specimen (#2) GLT6-C75-I0-30°-S500

Connector Row	Deflection, Δ, mm	Load, w, kN	Concrete Top Stress, $\sigma_{c,T}$, MPa	Timber Bottom Stress, $\sigma_{t,B}$, MPa
0	0	0	0	0
1	62.53	53.0	-1.21	0.66
2	71.913	57.1	-5.93	3.78
3	85.00	63.6	-10.85	7.04
4	102.77	73.13	-16.45	10.78
5	131.09	89.66	-24.28	16.08
6	**158.84**	**105.28**	**-31.99**	**21.40**

Capacity, w_u = 105.28 kN

Ultimate deflection, Δ_u = 158.84 mm

Effective Bending Stiffness, EI_{eff} = 2044.31 kN.m^2

Failure mode = Timber fracture

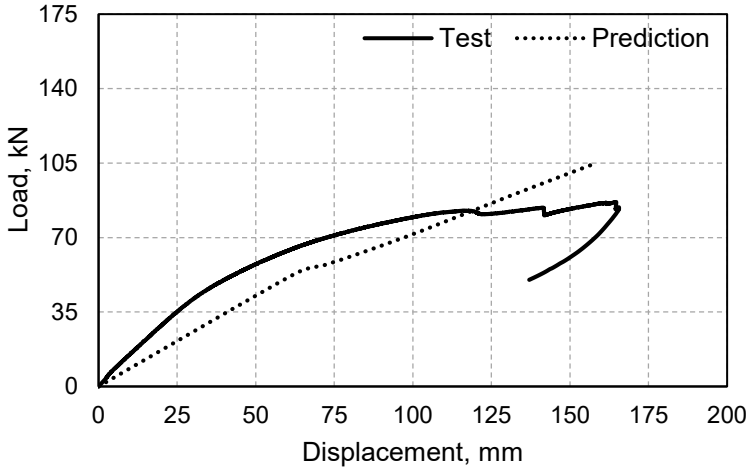

Figure 8.55: Load-deflection responses of specimen (#2) GLT6-C75-I0-30°-S500

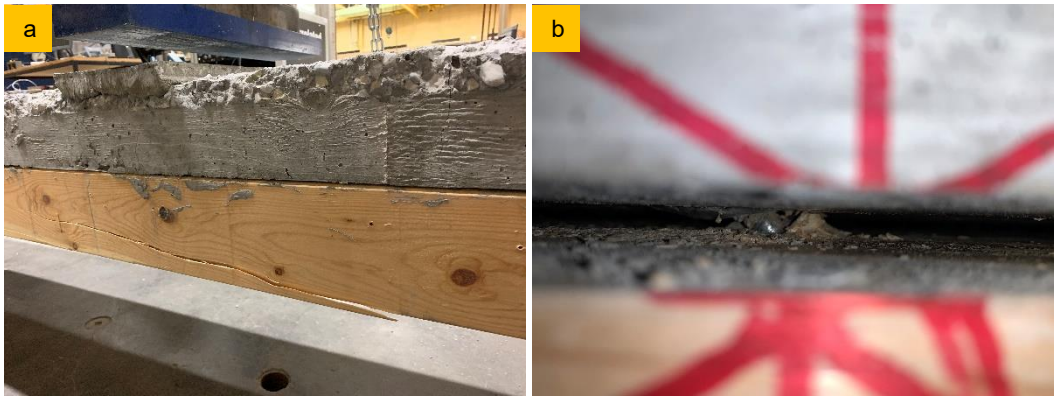

Figure 8.56: a) Timber fracture and b) screw withdrawal; in specimen (#2) GLT6-C75-I0-30°-S500

Specimen #3: GLT6-C75-I5-30°-S500

Concrete properties: h_c = 75 mm, b_c = 600 mm, f_c = 55.8 MPa, E_c = 23,480 MPa.

Insulation thickness: h_i = 5 mm.

MTP properties: h_t = 130 mm, b_t = 600 mm, f_t = 21.4 MPa, f_v = 1.3 MPa, E_t = 9,500 MPa.

Connector properties: Diameter, d = 11 mm, Penetration length, l = 100 mm, Insertion angle, α = 30°,

Yield force, F_y = 16.95 x 2 x 2 = 67.80 kN (2 cross-pair) (Mirdad & Chui, 2020a), Elastic stiffness, k = 12.50 x 2 x 2 = 50 kN/mm (2 cross-pair) (Mirdad & Chui, 2020b) and Friction, μ = 0

Span and connector spacing: L = 6000 mm, Span = 5700 mm, Spacing, s = 500 mm, Connector row = 6, n_1 = 5500 mm, n_2 = 4500 mm, n_3 = 3500 mm, n_4 = 2500 mm, n_5 = 1500 mm and n_6 = 500 mm

Eccentricities: e_c = 34.6 mm and e_t = 72.9 mm.

Table 8.3: Predictions for specimen (#3) GLT6-C75-I5-30°-S500

Connector Row	Deflection, Δ, mm	Load, w, kN	Concrete Top Stress, $\sigma_{c,T}$, MPa	Timber Bottom Stress, $\sigma_{t,B}$, MPa
0	0	0	0	0
1	66.48	55.7	-1.31	0.74
2	76.061	59.9	-6.29	4.05
3	89.95	66.9	-11.55	7.55
4	109.56	77.63	-17.73	11.71
5	143.08	97.58	-27.10	18.10
6	**167.94**	**112.20**	**-31.92**	**21.40**

Capacity, w_u = 112.20 kN

Ultimate deflection, Δ_u = 167.94 mm

Effective Bending Stiffness, EI_{eff} = 2020.08 kN.m^2

Failure mode = Timber fracture

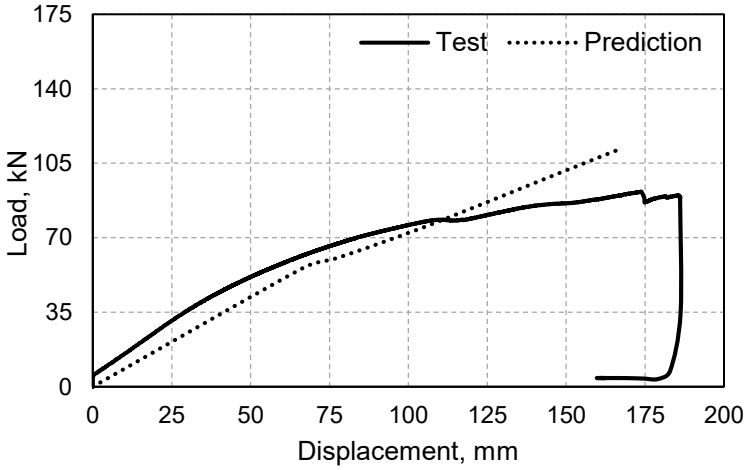

Figure 8.57: Load-deflection responses of specimen (#3) GLT6-C75-I5-30°-S500

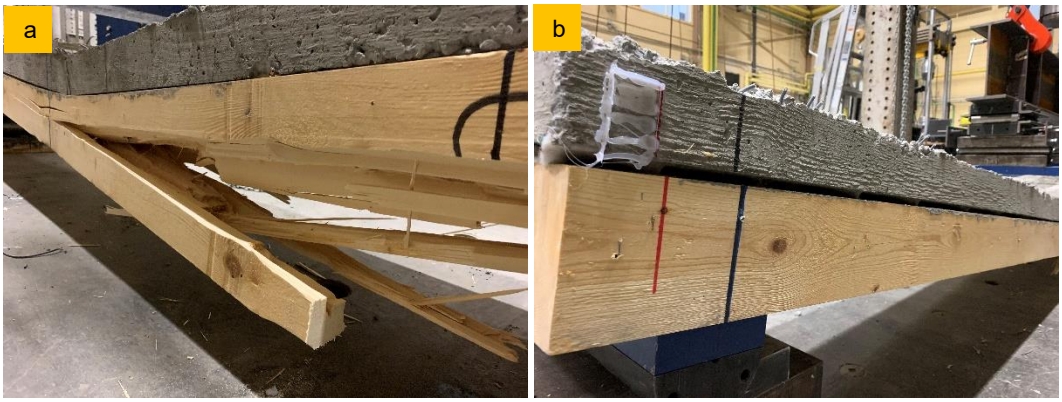

Figure 8.58: a) Timber fracture and b) gap opening; at the presence of 5 mm insulation in specimen (#3) GLT6-C75-I5-30°-S500

Specimen #4: GLT6-C75-I15-30°-S250

Concrete properties: h_c = 75 mm, b_c = 600 mm, f_c = 55.8 MPa, E_c = 23,480 MPa.

Insulation thickness: h_i = 15 mm.

MTP properties: h_t = 130 mm, b_t = 600 mm, f_t = 21.4 MPa, f_v = 1.3 MPa, E_t = 9,500 MPa.

Connector properties: Diameter, d = 11 mm, Penetration length, l = 100 mm, Insertion angle, α = 30°, Yield force, F_y = 15.98 x 2 x 2 = 63.92 kN (2 cross-pair) (Mirdad & Chui, 2020a), Elastic stiffness, k = 12.24 x 2 x 2 = 48.96 kN/mm (2 cross-pair) (Mirdad & Chui, 2020b) and Friction, μ = 0

Span and connector spacing: L = 6000 mm, Span = 5700 mm , Spacing, s = 250 mm, Connector row = 12, n_1 = 5750 mm, n_2 = 5250 mm, n_3 = 4750 mm, n_4 = 4250 mm, n_5 = 3750 mm, n_6 = 3250 mm, n_7 = 2750 mm, n_8 = 2250 mm, n_9 = 1750 mm, n_{10} = 1250 mm, n_{11} = 750 mm and n_{12} = 250 mm.

Eccentricities: e_c = 37.8 mm and e_t = 79.7 mm.

Table 8.4: Predictions for specimen (#4) GLT6-C75-I15-30°-S250

Connector Row	Deflection, Δ, mm	Load, w, kN	Concrete Top Stress, $\sigma_{c,T}$, MPa	Timber Bottom Stress, $\sigma_{t,B}$, MPa
0	0	0	0	0
1	118.86	91.14	-0.47	0.16
2	124.08	93.48	-4.01	2.47
3	131.34	97.19	-7.50	4.74
4	139.80	101.63	-10.99	7.02
5	149.71	107.05	-14.58	9.37
6	161.15	113.49	-18.34	11.83
7	174.42	121.13	-22.32	14.46
8	190.27	130.47	-26.73	17.37
9	208.43	142.44	-31.90	20.83
10	**214.27**	**143.24**	**-32.88**	**21.40**

Capacity, w_u = 143.24 kN

Ultimate deflection, Δ_u = 214.27 mm

Effective Bending Stiffness, EI_{eff} = 1849.08 kN.m^2

Failure mode = Timber fracture

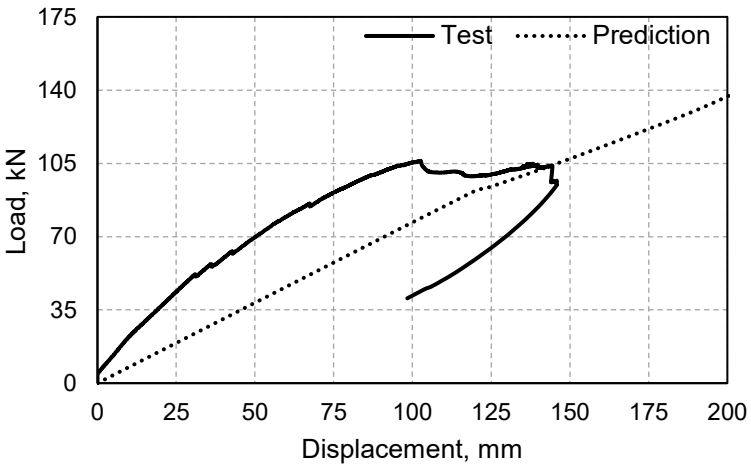

Figure 8.59: Load-deflection responses of specimen (#4) GLT6-C75-I15-30°-S250

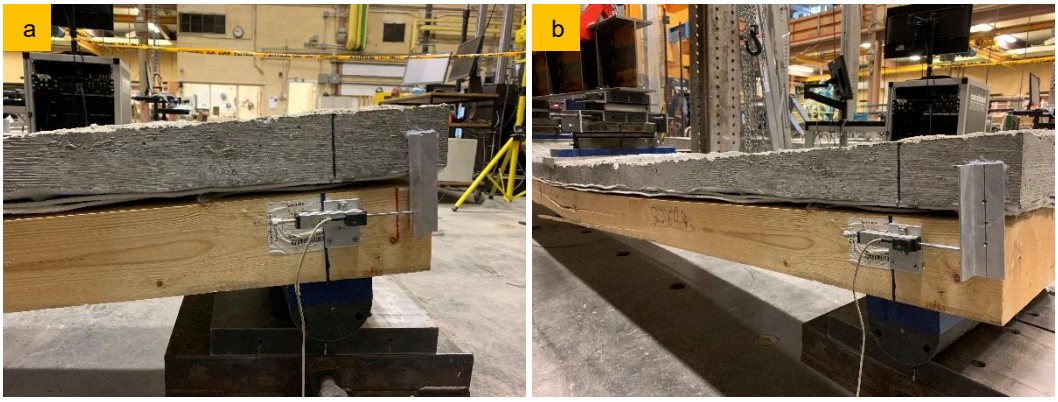

Figure 8.60: a) Relative slip at failure and b) large gap opening and timber fracture; at the presence of 15 mm insulation in specimen (#4) GLT6-C75-I15-30°-S250

Specimen #5: CLT6-C75-I5-45°-S500

Concrete properties: h_c = 75 mm, b_c = 600 mm, f'_c = 55.8 MPa, E_c = 23,480 MPa.

Insulation thickness: h_i = 5 mm.

MTP properties: h_t = 105 mm, b_t = 600 mm, f_t = 21.4 MPa, f_v = 1.3 MPa, E_t = 9,500 MPa.

Connector properties: Diameter, d = 11 mm, Penetration length, l = 100 mm, Insertion angle, α = 45°,

Yield force, F_y = 15.51 x 2 x 2 = 62.04 kN (2 cross-pair) (Mirdad & Chui, 2020a), Elastic stiffness, k = 7.03 x 2 x 2 = 28.12 kN/mm (2 cross-pair) (Mirdad & Chui, 2020b) and Friction, μ = 0

Span and connector spacing: L = 6000 mm, Span = 5700 mm, Spacing, s = 500 mm, Connector row = 6, n_1 = 5500 mm, n_2 = 4500 mm, n_3 = 3500 mm, n_4 = 2500 mm, n_5 = 1500 mm and n_6 = 500 mm

Eccentricities: e_c = 40.1 mm and e_t = 54.9 mm.

Table 8.5: Predictions for specimen (#5) CLT6-C75-I5-45°-S500

Connector Row	Deflection, Δ, mm	Load, w, kN	Concrete Top Stress, $\sigma c,T$, MPa	Timber Bottom Stress, $\sigma \tau, B$, MPa	Timber Shear Stress, τ_{max}, MPa
0	0	0	0	0	0
1	87.96	52.4	-1.91	1.35	0.59
2	**99.57**	**56.3**	**-8.49**	**5.97**	**0.75**

Capacity, w_u = 56.30 kN

Ultimate deflection, Δ_u = 99.57 mm

Effective Bending Stiffness, EI_{eff} = 1435.21 kN.m^2

Failure mode = Rolling shear

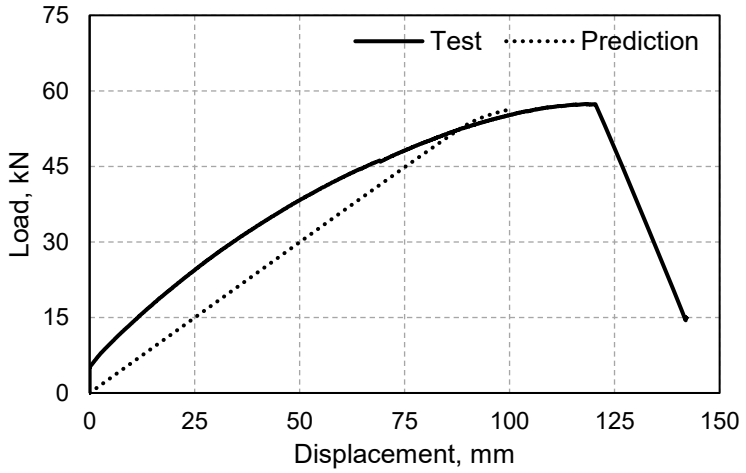

Figure 8.61: Load-deflection responses of specimen (#5) CLT6-C75-I5-45°-S500

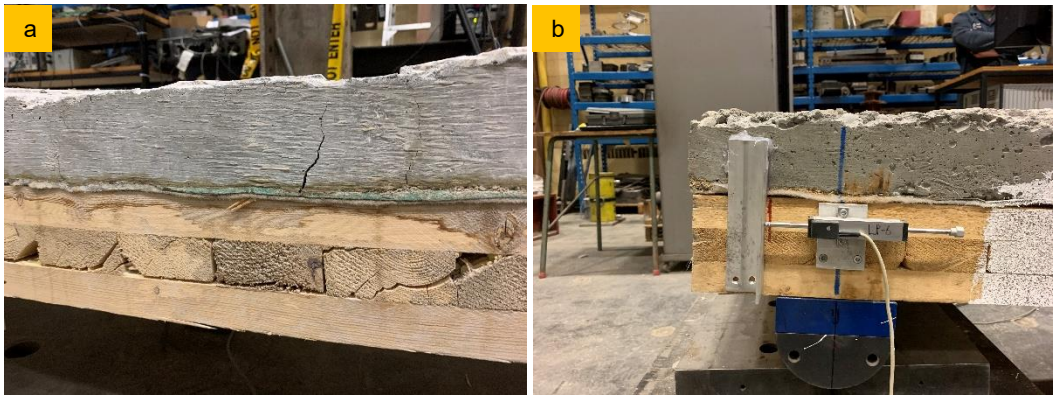

Figure 8.62: a) Rolling shear and b) small relative slip due to early rolling shear failure; in specimen (#5) CLT6-C75-I5-45°-S500

Specimen #6: CLT6-C75-I15-30°-S500

Concrete properties: h_c = 75 mm, b_c = 600 mm, f_c = 55.8 MPa, E_c = 23,480 MPa.

Insulation thickness: h_i = 15 mm.

MTP properties: h_t = 105 mm, b_t = 600 mm, f_t = 21.4 MPa, f_v = 1.3 MPa, E_t = 9,500 MPa.

Connector properties: Diameter, d = 11 mm, Penetration length, l = 100 mm, Insertion angle, α = 30°,

Yield force, F_y = 16.22x 2 x 2 = 64.88 kN (2 cross-pair) (Mirdad & Chui, 2020a), Elastic stiffness, k = 10.87 x 2 x 2 = 43.48 kN/mm (2 cross-pair) (Mirdad & Chui, 2020b) and Friction, μ = 0

Span and connector spacing: L = 6000 mm, Span = 5700 mm, Spacing, s = 500 mm, Connector row = 6, n_1 = 5500 mm, n_2 = 4500 mm, n_3 = 3500 mm, n_4 = 2500 mm, n_5 = 1500 mm and n_6 = 500 mm

Eccentricities: e_c = 44.4 mm and e_t = 60.6 mm.

Table 8.6: Predictions for specimen (#6) CLT6-C75-I15-30°-S500

Connector Row	Deflection, Δ, mm	Load, w, kN	Concrete Top Stress, $\sigma c,T$, MPa	Timber Bottom Stress, $\sigma t,B$, MPa	Timber Shear Stress, τ_{max}, MPa
0	0	0	0	0	0
1	76.15	48.1	-0.88	0.64	0.59
2	**87.78**	**51.8**	**-6.07**	**4.28**	**0.75**

Capacity, w_u = 51.80 kN

Ultimate deflection, Δ_u = 87.78 mm

Effective Bending Stiffness, EI_{eff} = 1523.29 kN.m^2

Failure mode = Rolling shear

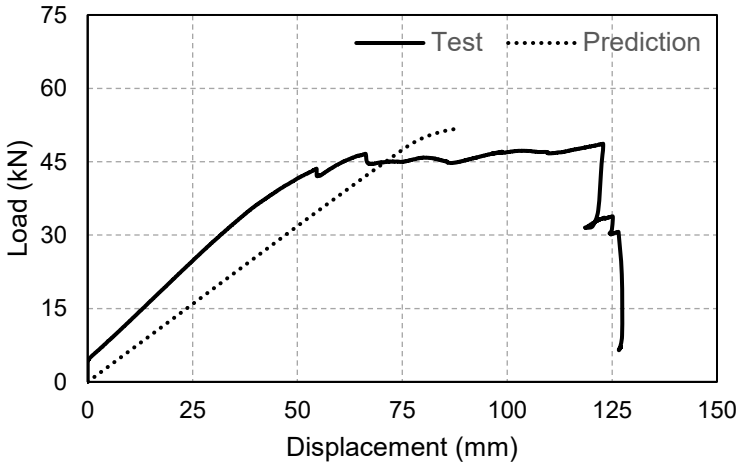

Figure 8.63: Load-deflection responses of specimen (#6) CLT6-C75-I15-30°-S500

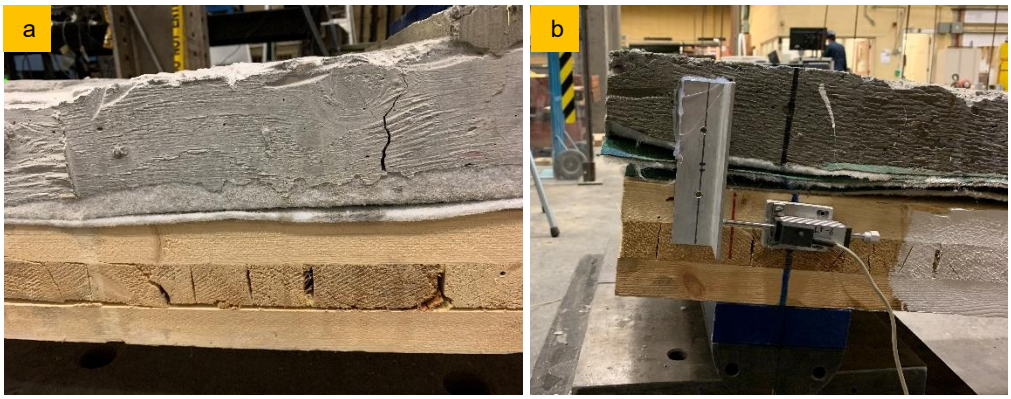

Figure 8.64: a) Rolling shear and b) large relative slip at the presence of 15 mm insulation in specimen (#6) CLT6-C75-I15-30°-S500

Specimen #7: GLT4.5-C100-I5-45°-S500

Concrete properties: h_c = 100 mm, b_c = 600 mm, f_c = 55.8 MPa, E_c = 23,480 MPa.

Insulation thickness: h_i = 5 mm.

MTP properties: h_t = 130 mm, b_t = 600 mm, f_t = 21.4 MPa, f_v = 1.3 MPa, E_t = 9,500 MPa.

Connector properties: Diameter, d = 11 mm, Penetration length, l = 100 mm, Insertion angle, α = 45°,

Yield force, F_y = 14.66 x 2 x 2 = 58.60 kN (2 cross-pair) (Mirdad & Chui, 2020a), Elastic stiffness, k = 7.34x 2 x 2 = 29.40 kN/mm (2 cross-pair) (Mirdad & Chui, 2020b) and Friction, μ = 0

Span and connector spacing: L = 4500 mm, Span = 4200 mm, Spacing, s = 500 mm, Connector row = 4, n_1 = 4000 mm, n_2 = 3000 mm, n_3 = 2000 mm and n_4 = 1000 mm

Eccentricities: e_c = 63.5 mm and e_t = 56.5 mm.

Table 8.7: Predictions for specimen (#7) GLT4.5-C100-I5-45°-S500

Connector Row	Deflection, Δ, mm	Load, w, kN	Concrete Top Stress, $\sigma_{c,T}$, MPa	Timber Bottom Stress, $\sigma_{t,B}$, MPa
0	0	0	0	0
1	30.08	84.5	-2.91	1.77
2	36.48	95.3	-11.41	6.47
3	48.85	120.0	-22.47	12.53
4	**69.56**	**163.0**	**-38.97**	**21.40**

Capacity, w_u = 163.0 kN

Ultimate deflection, Δ_u = 69.56 mm

Effective Bending Stiffness, EI_{eff} = 2709.01 kN.m^2

Failure mode = Timber fracture

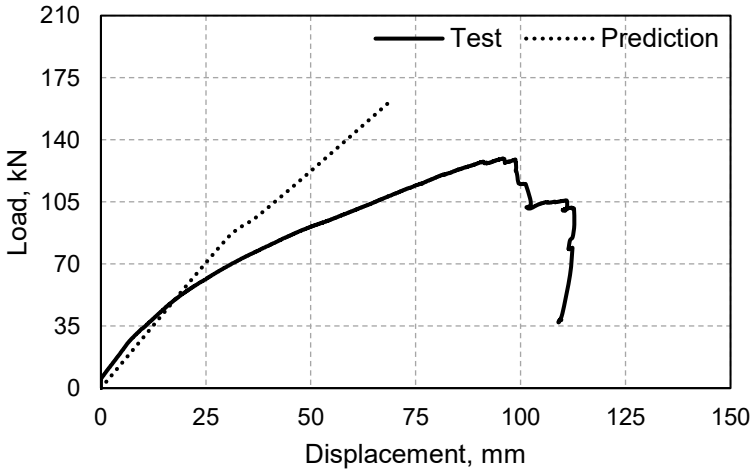

Figure 8.65: Load-deflection responses of specimen (#7) GLT4.5-C100-I5-45°-S500

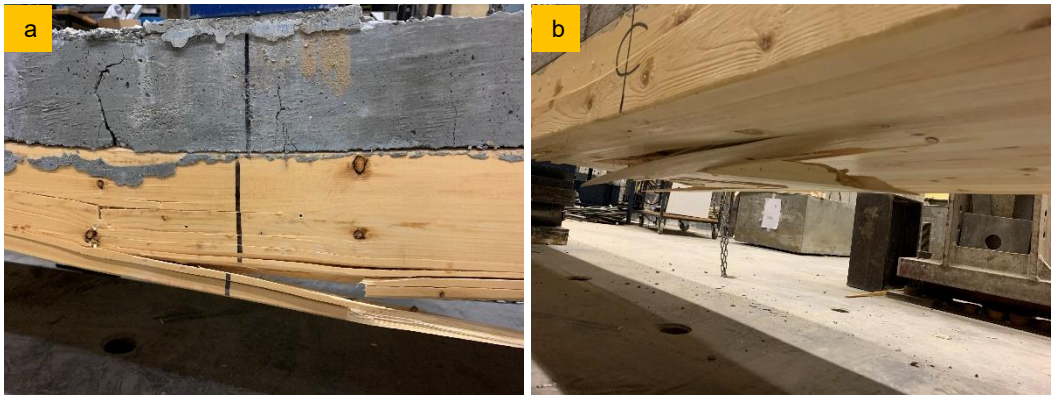

Figure 8.66: Timber fracture in specimen (#7) GLT4.5-C100-I5-45°-S500; a) side view with concrete crack in tension zone and b) bottom view

Specimen #8: GLT4.5-C100-I15-45°-S250

Concrete properties: h_c = 100 mm, b_c = 600 mm, f_c = 55.8 MPa, E_c = 23,480 MPa.

Insulation thickness: h_i = 15 mm.

MTP properties: h_t = 130 mm, b_t = 600 mm, f_t = 21.4 MPa, f_v = 1.3 MPa, E_t = 9,500 MPa.

Connector properties: Diameter, d = 11 mm, Penetration length, l = 100 mm, Insertion angle, α = 45°,

Yield force, F_y = 13.60 x 2 x 2 = 54.40 kN (2 cross-pair) (Mirdad & Chui, 2020a), Elastic stiffness, k = 7.13 x 2 x 2 = 28.52 kN/mm (2 cross-pair) (Mirdad & Chui, 2020b) and Friction, μ = 0

Span and connector spacing: L = 4500 mm, Span = 4200 mm , Spacing, s = 250 mm, Connector row = 9, n_1 = 4250 mm, n_2 = 3750 mm, n_3 = 3250 mm, n_4 = 2750 mm, n_5 = 2250 mm, n_6 = 1750 mm, n_7 = 1250 mm, n_8 = 750 mm and n_9 = 250 mm.

Eccentricities: e_c = 68.8 mm and e_t = 61.2 mm.

Table 8.8: Predictions for specimen (#8) GLT4.5-C100-I15-45°-S250

Connector Row	Deflection, Δ, mm	Load, w, kN	Concrete Top Stress, $\sigma_{c,T}$, MPa	Timber Bottom Stress, $\sigma_{t,B}$, MPa
0	0	0	0	0
1	43.03	115.29	-1.13	0.82
2	45.79	119.70	-5.98	3.59
3	49.64	126.63	-10.80	6.34
4	54.94	136.92	-16.00	9.30
5	61.82	150.78	-21.87	12.61
6	71.41	170.90	-29.23	16.70
7	**82.96**	**195.17**	**-37.78**	**21.40**

Capacity, w_u = 195.17 kN

Ultimate deflection, Δ_u = 82.96 mm

Effective Bending Stiffness, EI_{eff} = 2584.65 kN.m^2

Failure mode = Timber fracture

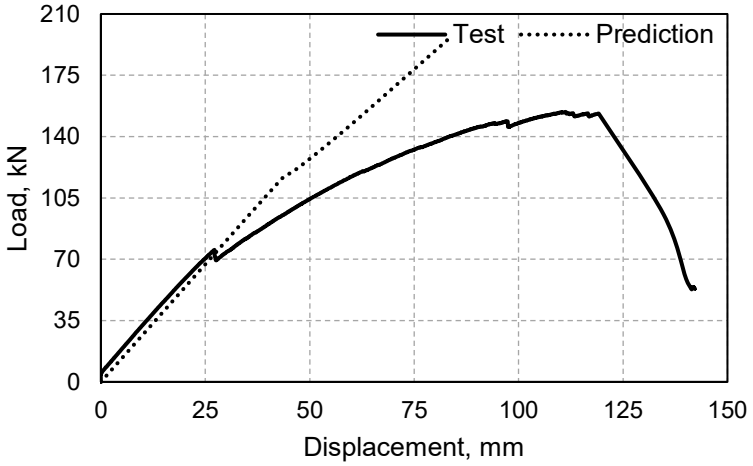

Figure 8.67: Load-deflection responses of specimen (#8) GLT4.5-C100-I15-45°-S250

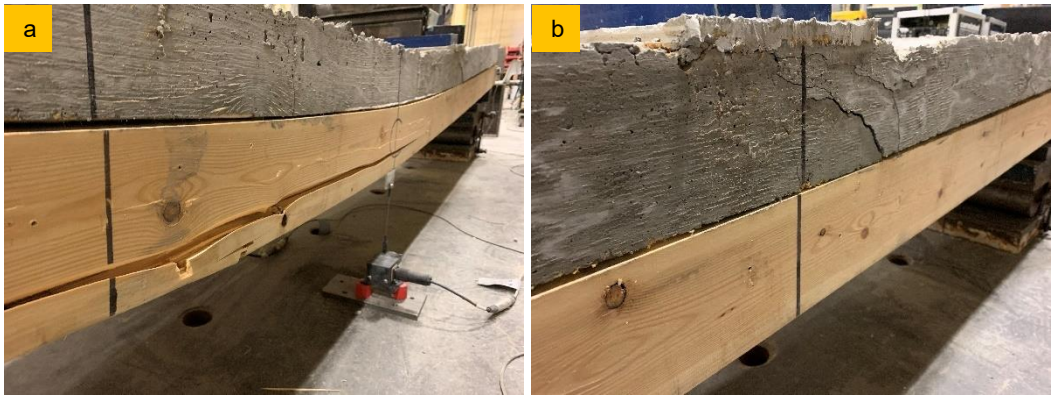

Figure 8.68: a) Timber fracture and b) concrete crack in the tension zone; in specimen (#8) GLT4.5-C100-I15-45°-S250

Specimen #9: GLT4.5-C100-I5-30°-S250

Concrete properties: h_c = 100 mm, b_c = 600 mm, f_c = 55.8 MPa, E_c = 23,480 MPa.

Insulation thickness: h_i = 5 mm.

MTP properties: h_t = 130 mm, b_t = 600 mm, f_t = 21.4 MPa, f_v = 1.3 MPa, E_t = 9,500 MPa.

Connector properties: Diameter, d = 11 mm, Penetration length, l = 100 mm, Insertion angle, α = 30°,

Yield force, F_y = 16.95 x 2 x 2 = 67.80 kN (2 cross-pair) (Mirdad & Chui, 2020a), Elastic stiffness, k = 12.5 x 2 x 2 = 50 kN/mm (2 cross-pair) (Mirdad & Chui, 2020b) and Friction, μ = 0

Span and connector spacing: L = 4500 mm, Span = 4200 mm , Spacing, s = 250 mm, Connector row = 9, n_1 = 4250 mm, n_2 = 3750 mm, n_3 = 3250 mm, n_4 = 2750 mm, n_5 = 2250 mm, n_6 = 1750 mm, n_7 = 1250 mm, n_8 = 750 mm and n_9 = 250 mm.

Eccentricities: e_c = 63.5 mm and e_t = 56.5 mm.

Table 8.9: Predictions for specimen (#9) GLT4.5-C100-I5-30°-S250

Connector Row	Deflection, Δ, mm	Load, w, kN	Concrete Top Stress, $\sigma_{c,T}$, MPa	Timber Bottom Stress, $\sigma_{t,B}$, MPa
0	0	0	0	0
1	43.70	122.64	-1.01	0.80
2	46.58	127.26	-5.85	3.61
3	50.64	134.69	-10.67	6.41
4	55.87	144.90	-15.73	9.34
5	61.61	158.55	-21.33	12.55
6	71.32	177.18	-27.97	16.31
7	**84.38**	**206.01**	**-37.14**	**21.40**

Capacity, w_u = 206.01 kN

Ultimate deflection, Δ_u = 84.38 mm

Effective Bending Stiffness, EI_{eff} = 2707.30 kN.m^2

Failure mode = Timber fracture

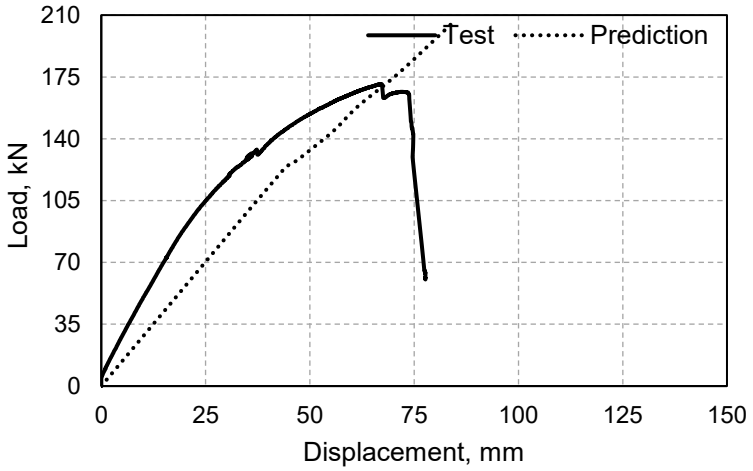

Figure 8.69: Load-deflection responses of specimen (#9) GLT4.5-C100-I5-30°-S250

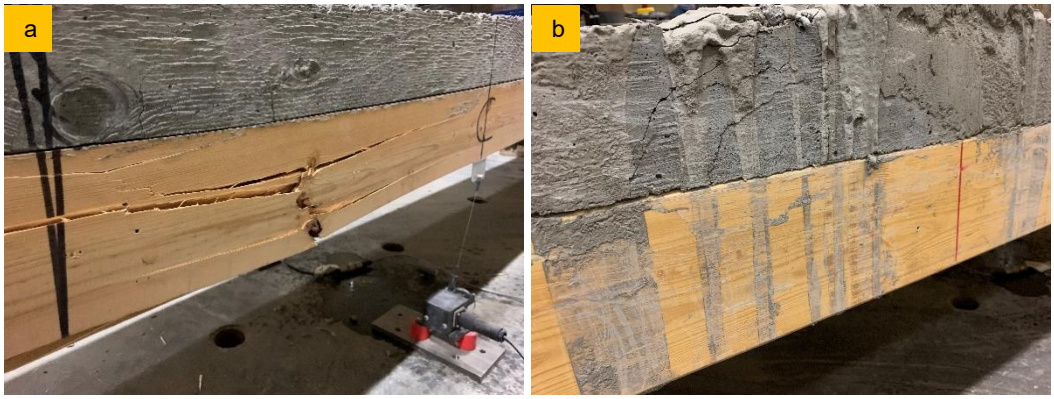

Figure 8.70: a) Timber fracture and b) concrete crack in tension zone; in specimen (#9) GLT4.5-C100-I5-30°-S250

Specimen #10: GLT4.5-C75-I15-45°-S500

Concrete properties: h_c = 75 mm, b_c = 600 mm, f_c = 55.8 MPa, E_c = 23,480 MPa.

Insulation thickness: h_i = 15 mm.

MTP properties: h_t = 130 mm, b_t = 600 mm, f_t = 21.4 MPa, f_v = 1.3 MPa, E_t = 9,500 MPa.

Connector properties: Diameter, d = 11 mm, Penetration length, l = 100 mm, Insertion angle, α = 45°,

Yield force, F_y = 13.60 x 2 x 2 = 54.40 kN (2 cross-pair) (Mirdad & Chui, 2020a), Elastic stiffness, k = 7.13 x 2 x 2 = 28.52 kN/mm (2 cross-pair) (Mirdad & Chui, 2020b) and Friction, μ = 0

Span and connector spacing: L = 4500 mm, Span = 4200 mm, Spacing, s = 500 mm, Connector row = 4, n_1 = 4000 mm, n_2 = 3000 mm, n_3 = 2000 mm and n_4 = 1000 mm

Eccentricities: e_c = 37.82 mm and e_t = 79.68 mm.

Table 8.10: Predictions for specimen (#10) GLT4.5-C75-I15-45°-S500

Connector Row	Deflection, Δ, mm	Load, w, kN	Concrete Top Stress, $\sigma_{c,T}$, MPa	Timber Bottom Stress, $\sigma_{t,B}$, MPa
0	0	0	0	0
1	31.79	66.3	-2.28	1.45
2	39.10	74.9	-9.14	6.12
3	52.55	93.6	-17.95	12.15
4	**75.50**	**127.3**	**-31.31**	**21.40**

Capacity, w_u = 127.3 kN

Ultimate deflection, Δ_u = 75.50 mm

Effective Bending Stiffness, EI_{eff} = 2012.47 kN.m^2

Failure mode = Timber fracture

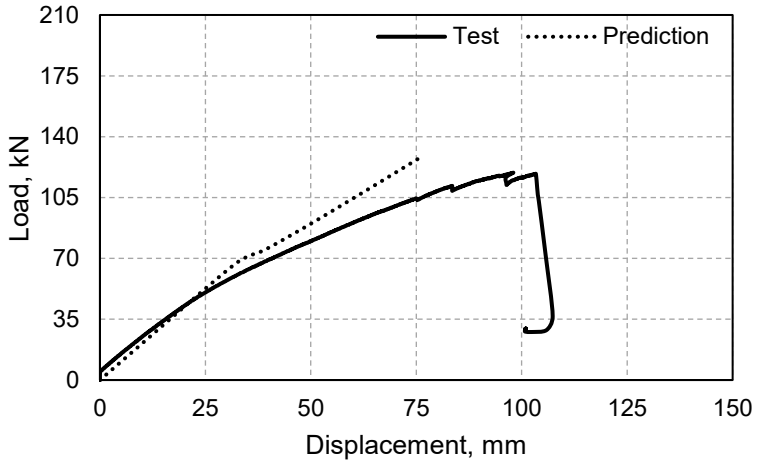

Figure 8.71: Load-deflection responses of specimen (#10) GLT4.5-C75-I15-45°-S500

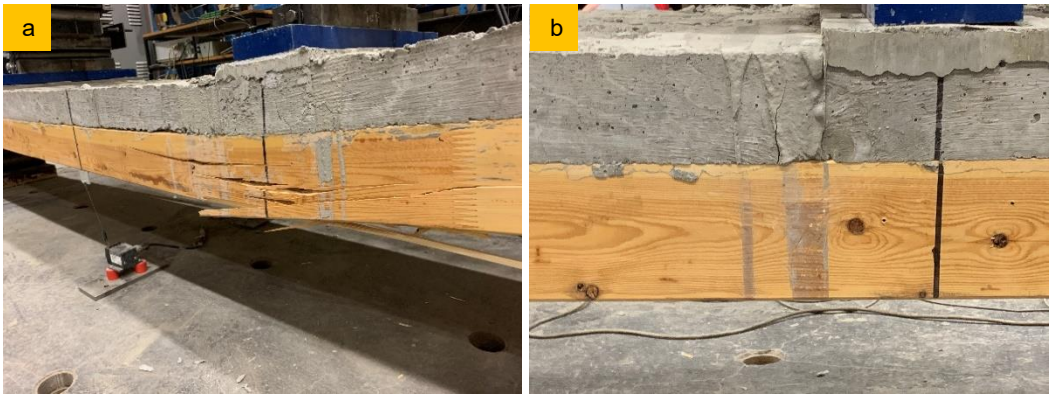

Figure 8.72: a) Timber fracture and b) concrete crack in tension zone; in specimen (#10) GLT4.5-C75-I15-45°-S500

Specimen #11: CLT4.5-C100-I5-45°-S250

Concrete properties: h_c = 100 mm, b_c = 600 mm, f_c = 55.8 MPa, E_c = 23,480 MPa.

Insulation thickness: h_i = 5 mm.

MTP properties: h_t = 105 mm, b_t = 600 mm, f_t = 21.4 MPa, f_v = 1.3 MPa, E_t = 9,500 MPa.

Connector properties: Diameter, d = 11 mm, Penetration length, l = 100 mm, Insertion angle, α = 45°, Yield force, F_y = 15.51 x 2 x 2 = 62.04 kN (2 cross-pair) (Mirdad & Chui, 2020a), Elastic stiffness, k = 7.03 x 2 x 2 = 28.12 kN/mm (2 cross-pair) (Mirdad & Chui, 2020b) and Friction, μ = 0

Span and connector spacing: L = 4500 mm, Span = 4200 mm , Spacing, s = 250 mm, Connector row = 9, n_1 = 4250 mm, n_2 = 3750 mm, n_3 = 3250 mm, n_4 = 2750 mm, n_5 = 2250 mm, n_6 = 1750 mm, n_7 = 1250 mm, n_8 = 750 mm and n_9 = 250 mm.

Eccentricities: e_c = 68.2 mm and e_t = 39.3 mm.

Table 8.11: Predictions for specimen (#11) CLT4.5-C100-I5-45°-S250

Connector Row	Deflection, Δ, mm	Load, w, kN	Concrete Top Stress, $\sigma_{c,T}$, MPa	Timber Bottom Stress, $\sigma_{t,B}$, MPa	Timber Shear Stress, τ_{max}, MPa
0	0	0	0	0	0
1	**44.69**	**98.28**	**-1.46**	**1.13**	**0.75**

Capacity, w_u = 98.28 kN

Ultimate deflection, Δ_u = 44.69 mm

Effective Bending Stiffness, EI_{eff} = 2121.53 kN.m^2

Failure mode = Rolling shear

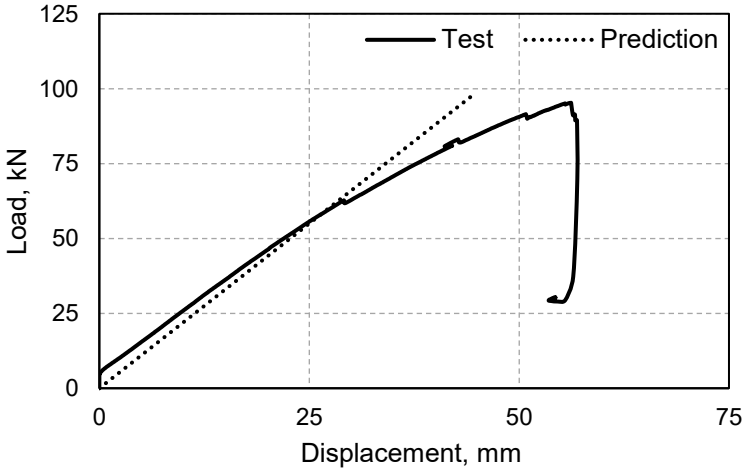

Figure 8.73: Load-deflection responses of specimen (#11) CLT4.5-C100-I5-45°-S250

Figure 8.74: Rolling shear in specimen (#11) CLT4.5-C100-I5-45°-S250

Specimen #12: CLT4.5-C100-I0-30°-S250

Concrete properties: h_c = 100 mm, b_c = 600 mm, f'_c = 55.8 MPa, E_c = 23,480 MPa.

Insulation thickness: h_i = 0 mm.

MTP properties: h_t = 105 mm, b_t = 600 mm, f_t = 21.4 MPa, f_v = 1.3 MPa, E_t = 9,500 MPa.

Connector properties: Diameter, d = 11 mm, Penetration length, l = 100 mm, Insertion angle, α = 30°,

Yield force, F_y = 17.92 x 2 x 2 = 71.68 kN (2 cross-pair) (Mirdad & Chui, 2020a), Elastic stiffness, k = 18.21 x 2 x 2 = 72.84 kN/mm (2 cross-pair) (Mirdad & Chui, 2020b) and Friction, μ = 0.45

Span and connector spacing: L = 4500 mm, Span = 4200 mm , Spacing, s = 250 mm, Connector row = 9, n_1 = 4250 mm, n_2 = 3750 mm, n_3 = 3250 mm, n_4 = 2750 mm, n_5 = 2250 mm, n_6 = 1750 mm, n_7 = 1250 mm, n_8 = 750 mm and n_9 = 250 mm.

Eccentricities: e_c = 65.0 mm and e_t = 37.5 mm.

Table 8.12: Predictions for specimen (#12) CLT4.5-C100-I0-30°-S250

Connector Row	Deflection, Δ, mm	Load, w, kN	Concrete Top Stress, $\sigma_{c,T}$, MPa	Timber Bottom Stress, $\sigma_{t,B}$, MPa	Timber Shear Stress, τ_{max}, MPa
0	0	0	0	0	0
1	47.00	107.18	-0.96	1.02	0.62
2	**48.48**	**107.31**	**-5.77**	**4.02**	**0.75**

Capacity, w_u = 107.31 kN

Ultimate deflection, Δ_u = 48.48 mm

Effective Bending Stiffness, EI_{eff} = 2200.06 kN.m^2

Failure mode = Rolling shear

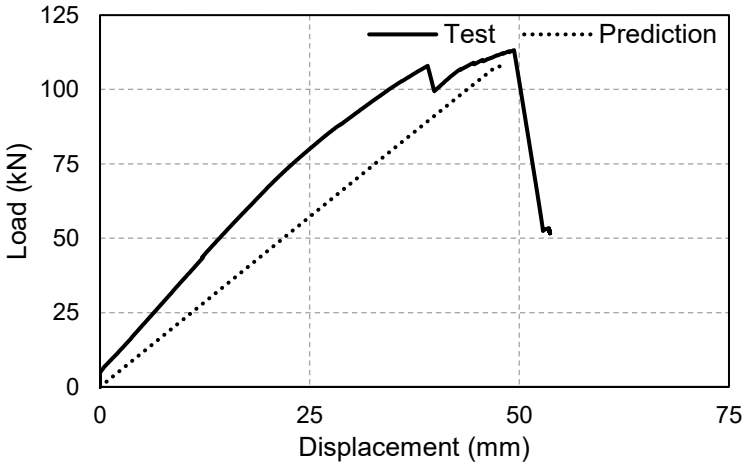

Figure 8.75: Load-deflection responses of specimen (#12) CLT4.5-C100-I0-30°-S250

Figure 8.76: Rolling shear in specimen (#12) CLT4.5-C100-I0-30°-S250

Appendix E. Test Pictures

Figure 8.77: Embedment test of the screw in timber at 0°, 30°, 45°, 60° and 90° angle respectively to the grain

Figure 8.78: Withdrawal test of screws at 0°, 30°, 45°, 60°, and 90° angle respectively to the timber grain

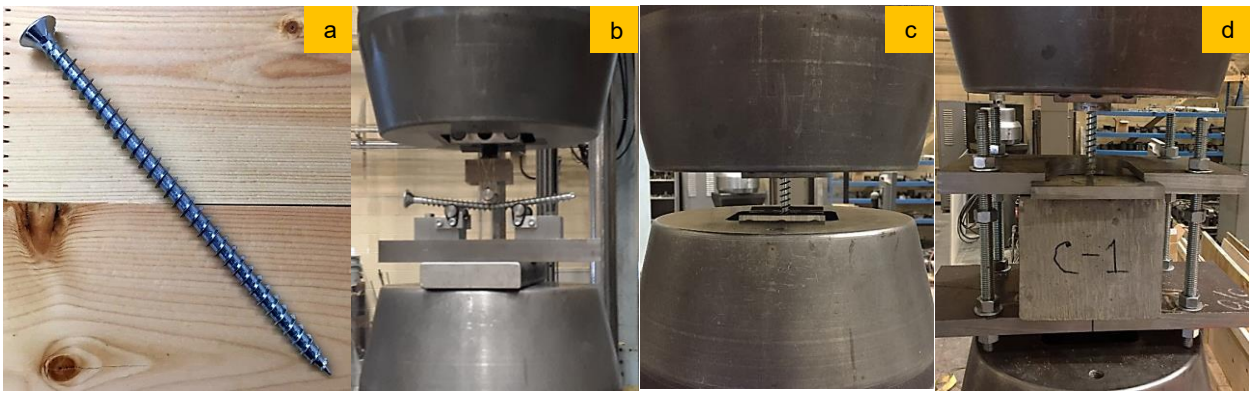

Figure 8.79: a) Fully threaded Self-Tapping Screw, b) screw yield moment test, c) screw tensile test and, d) screw withdrawal test in concrete

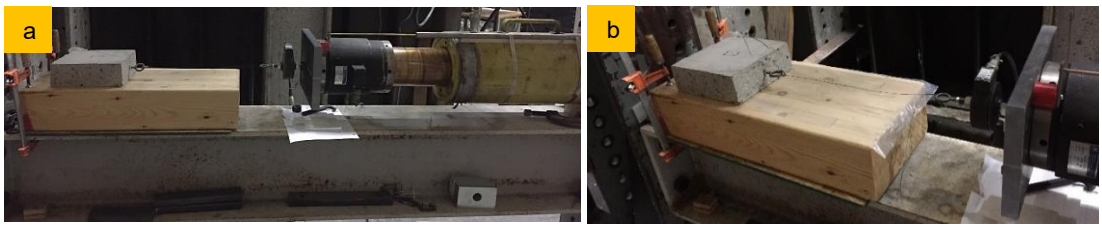

Figure 8.80: Friction test at concrete-timber interface; a) without plastic sheet and b) with plastic sheet

Figure 8.81: Specimen preparation; a) insertion of screw at 30° angle in horizontal cross-pair b) insertion of screw at 45° angle in vertical cross-pair, c) screwed MTP are ready for putting into forms, d) specimens are ready for casting, and e) specimens are ready for testing

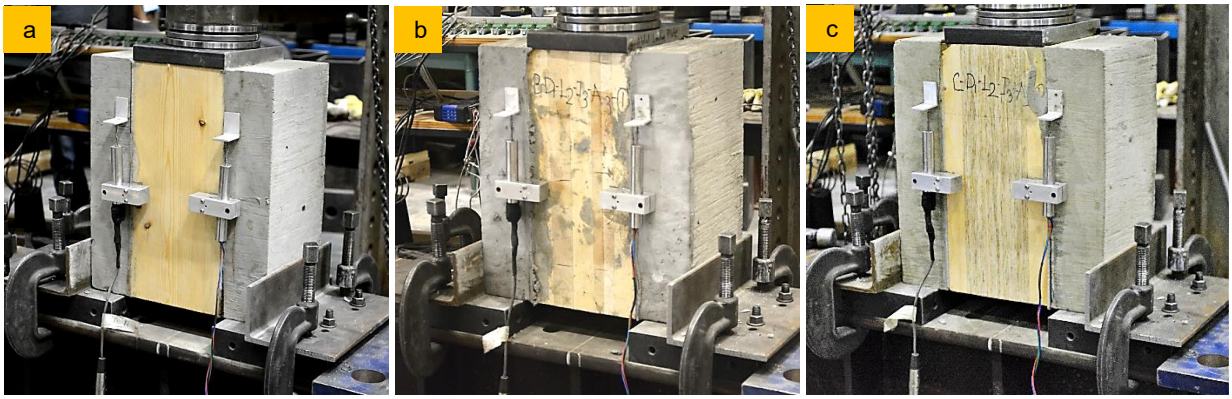

Figure 8.82: Typical connection test setup of a) GLT specimen, b) CLT specimen and c) CLP specimen

Figure 8.83: Bending test specimen preparation; a) insertion of cross-pair screw in the cross-section with wire mesh, b) specimens are ready for casting and, c) specimens are ready for testing

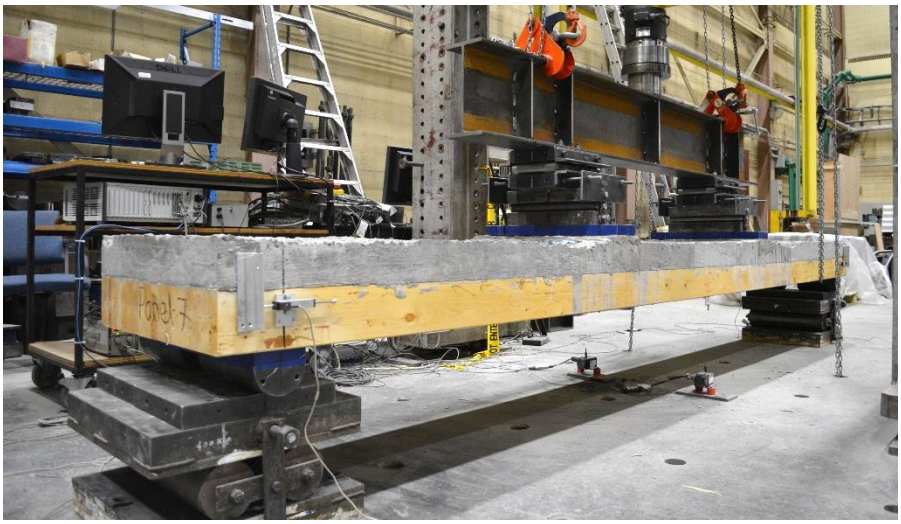

Figure 8.84: Typical bending test setup of a 4.5 m long GLT specimen

Figure 8.85: Typical bending test setup of a 6 m long CLT specimen